DESIGN AND MANUFACTURING OF A NEW TYPE MONORAIL CRANE, MOVING ON BOTH HORIZONTAL AND ANGULAR RAILS ALSO CLIMBING ON VERTICAL RAILS, BY USING FINITE ELEMENT ANALYSIS

YATAY VE AÇILI RAYLAR ÜZERİNDE HAREKET EDEBİLEN AYRICA DİKEY RAYLARA TIRMANABİLEN YENİ TİP BİR MONORAY VİNCİNİN SONLU ELEMANLAR METODU İLE TASARIMI VE ÜRETİMİ

GÜRBÜZ YILMAZ

PROF. DR. BORA YILDIRIM
Supervisor

Submitted to Institute of Sciences of Hacettepe University
as a Partial Fulfillment to the Requirements
for the Award of the Degree of Master of Science in Mechanical Engineering.

2014

This work named “Design of a New Type Monorail Crane Moving on Both Horizontal and Angular Rails Also Climbing on Vertical Rails By Using Finite Element Method” has been approved as a thesis for the Degree of MASTER OF SCİENCES IN MECHANICAL ENGINEERING by the below mentioned Examining Committee Members.

Yard. Doç. Dr. Benat KOÇKAR
Head – (Member) …………………………......

Prof. Dr. Bora YILDIRIM
Supervisor …………………………......

Yard.Doç. Dr. Hasan Basri ULAŞ
Member …………………………......

This thesis has been approved as a thesis for the Degree of MASTER OF SCIENCES IN MECHANICAL ENGINEERING by Board of Directors of the Institute for Graduate Studies in Science and Enginnering.

Prof. Dr. Fatma SEVİN DÜZ
Director of the Institute of
Graduate Studies in Science

ABSTRACT

DESIGN AND MANUFACTURING OF A NEW TYPE MONORAIL CRANE, MOVING ON BOTH HORIZONTAL AND ANGULAR RAILS ALSO CLIMBING ON VERTICAL RAILS, BY USING FINITE ELEMENT ANALYSIS

GÜRBÜZ YILMAZ

Graduate Science, Deparment of Mechanical Enginnering
Supervisor: Prof. Dr. BORA YILDIRIM

June 2014, 170 sayfa

This study has been prepared in cooperation University and Industry, 1505, with the support of TUBITAK. The reason why this project is needed, because buildings having curvilinear geometries is required to design a monorail crane moving not only on horizontal rails but also climbing on vertical and curvelinear rails. However, loads can be easily transformed or moved to a high point of a building only by means of curvilinear and vertical rails. At the beginning of design, firstly, the angle between rail and wheel has been optimized considering both isotropic half space assumption and Finite Element Method. After estimated the optimum angle between rail and wheel, the design of wheel has been examined by Finite Element Method. The section area and second moment of inertia of rails used has been optimized or designed in terms of the higher load that the monorail crane is able to remove and transform and stresses occurred on rail has been examined with the assumption of Hertz contact Stresses. Spur gears and worm – gear mechanism, driving the wheels of monorail crane, has been examined considering both AGMA Stress and Strength Equations and Finite Element Method. Lastly the shafts of monorail crane have been examined in terms of both classical mechanics and Finite Element Method.

Key words: Finite Element Method, Solid Mechanics, Fatigue, Contact Stresses, Horizontal – Vertical and Curved Rails, Wheels having angular shapes, Friction,

ÖZET

YATAY VE AÇILI RAYLAR ÜZERİNDE HAREKET EDEBİLEN AYRICA DİKEY RAYLARA TIRMANABİLEN YENİ TİP BİR MONORAY VİNCİNİN SONLU ELEMANLAR METODU İLE TASARIMI VE ÜRETİMİ

GÜRBÜZ YILMAZ

Yüksek Lisans, Makina Mühendisliği Bölümü
Danışman: Prof. Dr. BORA YILDIRIM
Haziran 2014, 170 sayfa

Bu çalışma, 1505 ÜNİVERSİTE SANAYİ İŞ BİRLİĞİ TÜBİTAK projesi desteğiyle hazırlanmıştır. Bu projeye ihtiyaç duyulmasının sebebi, günümüzdeki binaların dış yüzey geometrilerinin eğrisel olması, monoray vinç sistemlerinin sadece yatay ve dikey eksenlerde değil, aynı zamanda eğrisel eksenli yönlerde de hareket edebilme kabiliyetine sahip olmasını gerektirmiştir. Böylece istenilen yükler, yatay –dikey ve eğri rayların vasıtası ile bir binanın istenilen uzaklığına ve yüksekliğine kadar taşınabilecektir. Tasarım başlangıcında, ilk olarak ray ve tekerlek arasındaki açının değişimine göre temas gerilimleri ”isotropic half space metodu” ve “sonlu elemanlar metodu” ile incelenmiş olup, bu açı değeri optime edilmiştir. Bulunan optimum açı değerine gore tekerleğin analizi fem ile yapılmıştır. Rayın kesit alanı ve atalet momenti, vincin maksimum taşıyabileceği yüke göre optime edilmiş olup ray üzerinde oluşan temas gerilimlerinin hesaplanmasında Hertz Gerilim varsayımı yapılmış ve buna gore rayın analizi tamamlanmıştır. Tekerleklerin hareketini sağlayan düz dişlilerin ve sonsuz vida-karşılık dişli mekanizmasının tasarımı, hem Agma Gerilim ve Dayanım denklemlerine gore hemde fem kullanılarak analizleri yapılmıştır. Son olarak millerin analitik hesapları ve fem ile analizleri yapılmıştır.

Anahtar Kelimeler: Sonlu Elemanlar Metodu, Katı cisim mekaniği, Yorulma, Temas Gerilmeleri, Yatay – Dikey ve Açılı Raylar, Açılı çarklar, Sürtünme.

ETHICS

In this thesis study, prepared in accordance with the spelling rules of Institude of Graduate Studies in Science of Hacettepe University,

I declare that

- all the information and documents have been obtained in the base of the academic rules,
- all audio-visual and written information and results have been presented according to the rules of scientific ethics
- in case of using others Works, related studies have been cited in accordance with the scientific standards
- all cited studies have been fully referenced
- I did not do any distortion in the data set
- and any part of this thesis has not been presented as another thesis study at this or any other university.

…. / …. / 2014

Gürbüz YILMAZ

ACKNOWLEDGEMENTS

This thesis would not have been possible without the support of many people.

First of all I would like to thank my supervisior, Prof. Dr. Bora YILDIRIM, who offered guidance, encouragement, patience and all. I appreciate the time and energy she reserved for this study.

I also want to thank my thesis progress committee members Assistant Prof. Benat KOCKAR and Assistant Prof. Hasan Basri ULAS for their priceless advices at each step of this thesis.

I am indebted to my colleagues in the department, especially to Morteza Dousti, Morteza Yeganehpour and my family for him supports.

Lastly but not least, fond acknowledgement should go to my family and numerous friends who endured this long process with me, always offering support and love.

CONTENTS

Page

ABSTRACT i
ÖZET ii
ETHICS iii
ACKNOWLEDGEMENTS iv
CONTENTS v
LIST OF FİGURES vii
TABLES xi
LIST OF SYMBOLS xii
Finite Element Method 1
1.1.1 Introduction 1
1.1.2 The structural element and the structural system 2
1.1.3 Assembly and analysis of a structure 4
1.1.4 The boundary conditions 6
1.2 Plane stress and plane strain 7
1.2.1 Introduction 7
1.2.2 Element characteristics 8
1.2.2.1 Displacement functions 8
1.2.2.2 Strain (total) 9
1.2.2.3 Elasticity matrix 10
1.3. Three Dimensional Analysis 13
1.3.1 Introduction 13
1.3.2 Tetrahedral element characteristics 13
1.3.2.1 Strain Matrix 15
1.3.2.2 Elasticity Matrix 17
1.3.2.3 Stiffness, stress, and load matrices 17
1.4 Assumptions and Estimates of Monorail Crane Design 19
2.0 Wheel 29
2.1 Introduction to frictional contact with isotropic half-space assumption 29
2.1.1 Contact with Normal Loading 29
2.1.2 Contact with Tangential Loading 33
2.1.3 Conclusion 37
2.2 Wheel Analytical and Fem Results (45° Angle) 39
2.2.1 Wheel Contact Stress Results 39
2.2.2 Wheel Fem Results 42
2.2.3 Conclusion 48
3.0 Beams 49
3.1 Introduction 49
3.2 Rail materials 49
3.3 Rail Design and Fem Results 53
3.3.1 Horizontal Rail 53
3.3.1.1 Horizontal Rail Fem Results 56
3.3.1.2 Rail fem fatigue results 58
3.3.1.3 Fem results of the horizontal rail transporting two weights 60
3.3.1.4 Fatigue results of the horizontal rail transporting two weights 62

3.3.2 Vertical Rail 64
3.3.2.1 Vertical Rail Fem Results 64
3.3.2.2 Vertical Rail Fatigue Results 66
3.3.3 Curved Rail Analytical and Fem Results 68
3.3.3.1 S Rail Type 68
3.3.3.2 Bended Rail With 90° Curvature.. 71
3.3.3.3 Bended Rail With 75° Curvature.. 75
3.3.3.4 Bended Rail With 135° Curvature.. 79
3.4 Conclusion.. 82
4.0 Gears.. 84
4.1 Introduction.. 84
4.1.1 Gear Materials.. 84
4.2 Spur Gear Design.. 86
4.2.1 Spur Gear Design Analytical and Fem Results 86
4.2.1.1 Spur Gear Analytical Study, Gear tooth and Gear Mesh Parameters 86
4.2.1.2 Spur Gear Fem Results.. 99
4.2.2 Conclusion.. 106
4.3 Worm Gear 107
4.3.1 Design Of a Worm-Gear Mesh 108
4.3.2 Worm Gear Analytical and Fem Results.. 108
4.3.2.1 Worm Gear Analytical Results.. 108
4.3.2.2 Worm Gear Fem Results.. 114
4.3.3 Conclusion.. 121
5. Shaft Design.. 122
5.1 Introduction to Shaft Design 122
5.2 Shaft Analytical and Fem Results.. 123
5.2.1 Wheel Shaft Force and Stress Analysis 123
5.2.2 Wheel Shaft Fem Results.. 133
5.2.3 Pinion Shaft Analytical Results.. 138
5.2.4 Pinion Shaft Fem Results 141
5.3 Conclusion.. 146
Appendix (1) Contact results of wheel and rail in terms of different angles 147
References 160
Curriculum Vitae.. 162

LIST OF FIGURES

Page

Fig. 1.1.1 A typical structure built up from interconnected elements. 2

Fig. 1.2.1 An element of a continuum in plane stress or plane strain numbered in an anticlockwise order. 8

Fig. 1.3.1 A tetrahedral volume 13

Fig. 1.3.2 A systematic way of dividing a three-dimensional object into 'brick'-type elements. 18

Fig. 1.4.1 (a)Dynamic system (b)Lumped model (c)FBD 20

Fig. 1.4.2 Acceleration and Cable Force at Startup of Load-Lift 23
Fig. 1.4.3 Geometry of the wheel 25
Fig. 1.4.4 Geometry of the gears 26
Fig. 1.4.5 Geometry of worm - gear 27
Fig. 1.4.6 Motor 28
Fig. 2.1a) Two solids Ω_1 and Ω_2 b) The frictional indentation of a cone into a half space. 29
Fig. 2.2 Vertical Displacement variation of rail with different cone angles 35
Fig. 2.3 Total Displacement variation of rail with different cone angles 35
Fig. 2.4 Von Mises Stress variation of rail with different cone angles 36
Fig. 2.5 Contact Pressure variation of rail with different cone angles 36
Fig. 2.6 Max. Contact Stress variation of rail with different cone angles 37
Fig. 2.7 Mesh view of the wheel 42
Fig. 2.8 Directional deformation distribution of the wheel 42
Fig. 2.9 Total deformation distribution of the wheel 43
Fig. 2.10 Equivalent elastic strain distribution of the wheel 43
Fig. 2.11 Maximum Shear Stress distribution of the wheel 44
Fig. 2.12 Von Mises Stress distribution of the wheel 44
Fig. 2.13 Safety factor of the wheel 45
Fig. 2.14 Damage distribution of the wheel 45
Fig. 2.15 Mean biaxiliaty of the wheel 46
Fig. 2.16 Min. stress distribution of the wheel 46
Fig. 2.17 Max. stress distribution of the wheel 47

Fig. 2.18 Life of the wheel. 47

Fig. 3.2.1 Ultimate Tensile Strengths of Some Aluminum Alloys 50

Fig. 3.2.2 Tensile Test Stress-Strain Curves of Three Aluminum Alloys 51
Fig. 3.3.1 Two right circular cylinders held in contact by forces *F* uniformly distributed along cylinder length *l* and contact stress has an elliptical distribution across the contact zone width 2*b* 53
Fig. 3.3.2 Cylinder on a flat plate; a flat plate is a cylinder with an infinitely large radius 54
Fig. 3.3.3 Section of Rail. 55
Fig. 3.3.4 Ellipse occuring between rail and wheel 55
Fig. 3.3.5 Mesh view of the rail 56
Fig. 3.3.6 Directional deformation distribution of the horizontal rail 57
Fig. 3.3.7 Total deformation distribution of the horizontal rail 57
Fig. 3.3.8 Equivalent elastic strain distribution of the horizontal rail 57

Fig. 3.3.9 Maximum Shear Stress distribution of the horizontal rail 58
Fig. 3.3.10 Von Mises Stress distribution of the horizontal rail 58
Fig. 3.3.11 Mean biaxiality ratio of the horizontal rail... 58
Fig. 3.3.12 Damage distribution of the horizontal rail 59
Fig. 3.3.13 Max. stress distribution value of the horizontal rail 59
Fig. 3.3.14 Min. stress distribution value of the horizontal rail 59
Fig. 3.3.15 Life of the horizontal rail 60
Fig. 3.3.16 Mesh view of the rail with contact regions 60
Fig. 3.3.17 Directional deformation distribution of the rail transporting two weights .. 60
Fig. 3.3.18 Total deformation distribution of the rail transporting two weights 61
Fig. 3.3.19 Equivalent elastic strain distribution of the rail transporting two weights . 61
Fig. 3.3.20 Von Mises Stress distribution of the rail transporting two weights 61
Fig. 3.3.21 Damage distribution of the rail transporting two weights 62
Fig. 3.3.22 Mean biaxiliaty ratiodistribution of the rail transporting two weights 62
Fig. 3.3.23 Min. stress distribution of the rail transporting two weights...................... 62
Fig. 3.3.24 Max. stress distribution of the rail transporting two weights..................... 63
Fig. 3.3.25 Life of the rail transporting two weights. 63
Fig. 3.3.26 a) Front view of vertical rail (b) Back view of the vertical rail. 64
Fig. 3.3.27 Directional deformation distribution of the vertical rail 64
Fig. 3.3.28 Total deformation distribution of the vertical rail 65
Fig. 3.3.29 Equivalent elastic strain distribution of the vertical rail............................. 65
Fig. 3.3.30 Maximum Shear Stress distribution of the vertical rail 65
Fig. 3.3.31 Von Mises Stress distribution of the vertical rail 66
Fig. 3.3.32 Damage distribution of the vertical rail.. 66
Fig. 3.3.33 Mean biaxiliaty ratio distribution of the vertical rail 66
Fig. 3.3.34 Max. stress distribution of the vertical rail 67
Fig. 3.3.35 Min. stress distribution of the vertical rail 67
Fig. 3.3.36 Life of the vertical rail.. 67
Fig. 3.3.37 Mesh view of the S rail 68
Fig. 3.3.38 Directional deformation distribution of the S rail 68
Fig. 3.3.39 Total deformation distribution of the S rail 68
Fig. 3.3.40 Equivalent elastic strain distribution of the S rail 69
Fig. 3.3.41 Maximum Shear Stress distribution of the S rail...................................... 69
Fig. 3.3.42 Von Mises Stress distribution of the S rail 69
Fig. 3.3.43 Damage distribution of the S rail... 70
Fig. 3.3.44 Mean biaxiliaty ratio distribution of the S rail 70
Fig. 3.3.45 Min. stress distribution of the S rail... 70
Fig. 3.3.46 Max. stress distribution of the S rail.. 71
Fig. 3.3.47 Life of the S rail... 71
Fig. 3.3.48 Mesh view of the 90° curvature rail 71
Fig. 3.3.49 Directional deformation distribution of the 90° curvature rail 72
Fig. 3.3.50 Total deformation distribution of the 90° curvature rail 72
Fig. 3.3.51 Equivalent elastic strain distribution of the 90° curvature rail................... 72
Fig. 3.3.52 Maximum Shear Stress distribution of the 90° curvature rail 73
Fig. 3.3.53 Von Mises Stress distribution of the 90° curvature rail 73
Fig. 3.3.54 Damage distribution of the 90° curvature rail... 73
Fig. 3.3.55 Mean biaxiliaty ratio distribution of the 90° curvature rail......................... 74
Fig. 3.3.56 Min. stress distribution of the 90° curvature rail 74
Fig. 3.3.57 Max. Stress of the 90° curvature rail... 74

Fig. 3.3.58 Life of the 90° curvature rail........75
Fig. 3.3.59 Mesh view of the 75° curvature rail........75
Fig. 3.3.60 Directional deformation distribution of the 75° curvature rail........75
Fig. 3.3.61 Total deformation distribution of the 75° curvature rail........76
Fig. 3.3.62 Equivalent elastic strain distribution of the 75° curvature rail........76
Fig. 3.3.63 Maximum Shear Stress distribution of the 75° curvature rail........76
Fig. 3.3.64 Von Mises Stress distribution of the 75° curvature rail........77
Fig. 3.3.65 Damage distribution of the 75° curvature rail........77
Fig. 3.3.66 Mean biaxiliaty ratio distribution of the 75° curvature rail........77
Fig. 3.3.67 Min. stress of the 75° curvature rail........78
Fig. 3.3.68 Max. stress of the 75° curvature rail........78
Fig. 3.3.69 Life of the 75° curvature rail........78
Fig. 3.3.70 Mesh view of the 135° curvature rail........79
Fig. 3.3.71 Directional deformation distribution of the 135° curvature rail........79
Fig. 3.3.72 Total deformation distribution of the 135° curvature rail........79
Fig. 3.3.73 Equivalent elastic strain distribution of the 135° curvature rail........80
Fig. 3.3.74 Maximum Shear Stress distribution of the 135° curvature rail........80
Fig. 3.3.75 Von Mises Stress distribution of the 135° curvature rail........80
Fig. 3.3.76 Damage distribution of the 135° curvature rail........81
Fig. 3.3.77 Mean biaxiliaty ratio distribution of the 135° curvature rail........81
Fig. 3.3.78 Min. stress of the 135° curvature rail........81
Fig. 3.3.79 Max. stress of the 135° curvature rail........82
Fig. 3.3.80 Life of the 135° curvature rail........82
Fig. 4.1 Assembly view of the spur gears........86
Fig. 4.2 Mesh view of the gear – wheel and pinion........99
Fig. 4.3 Directional deformations of the gear – wheel and pinion........99
Fig. 4.4 Total deformations of the gear – wheel and pinion........100
Fig. 4.5 Equivalent elastic strain distribution of the gear – wheel and pinion........100
Fig. 4.6 Maximum shear stresses of the gear – wheel and pinion........101
Fig. 4.7 Von Mises Stress distribution of the gear – wheel and pinion........101
Fig. 4.8 Von Mises Stress distribution of the gear – wheel........102
Fig. 4.9 Von Mises Stress distribution of the pinion........102
Fig. 4.10 Safety factor of the gear – wheel and pinion........103
Fig. 4.11 Damage distribution of the gear – wheel and pinion........103
Fig. 4.12 Mean biaxiliaty ratio distribution of the gear – wheel and pinion........104
Fig. 4.13 Min stresses of the gear – wheel and pinion........104
Fig. 4.14 Max stresses of the gear – wheel and pinion........105
Fig. 4.15 Life of the gear – wheel and pinion........105
Fig. 4.16 Nomenclature of a single enveloping worm gearset........107
Fig. 4.17 Worm - Gear assembly view........109
Fig. 4.18 Worm - Gear mesh assembly view........115
Fig. 4.19 Directional deformation distribution of the worm – gear........115
Fig. 4.20 Total deformation distribution of the worm – gear........116
Fig. 4.21 Equivalent elastic strain distribution of the worm – gear........116
Fig. 4.22 Maximum Shear Stress distribution of the worm – gear........117
Fig. 4.23 Von Mises Stress distribution of the worm – gear........117
Fig. 4.24 Safety factor of the worm – gear........118
Fig. 4.25 Damage distribution of the worm – gear........118

Fig. 4.26 Mean biaxiliaty ratio distribution of the worm – gear 119
Fig. 4.27 Min. stress distribution of the worm – gear assembly view 119
Fig. 4.28 Max. stress distribution of the worm – gear assembly view 120
Fig. 4.29 Life of the worm – gear 120
Fig. 5.1 Gear forces 123
Fig. 5.2 Resultant forces on gear – wheel and shaft 124
Fig. 5.3a Force diagram 124
Fig. 5.3b Shear diagram 125
Fig. 5.3c Moment diagram 125
Fig. 5.4a Force diagram 126
Fig. 5.4b Shear diagram 126
Fig. 5.4c Moment diagram 126
Fig. 5.5 Wheel shaft 127
Fig. 5.6 Mesh view of the wheel shaft 133
Fig. 5.7 Directional deformation distribution of the wheel shaft. 133
Fig. 5.8 Total deformation distribution of the wheel shaft 134
Fig. 5.9 Von Mises Stress distribution of the wheel shaft 134
Fig. 5.10 Safety factor of the wheel shaft 135
Fig. 5.11 Damage distribution of the wheel shaft 135
Fig. 5.12 Mean biaxiliaty ratio distribution of the wheel shaft 136
Fig. 5.13 Max. stress distribution of the wheel shaft 136
Fig. 5.14 Min. stress distribution of the wheel shaft 137
Fig. 5.15 Life of the wheel shaft 137
Fig. 5.16 Pinion shaft 138
Fig. 5.17 Mesh view of the pinion shaft 141
Fig. 5.18 Directional deformation distribution of the pinion shaft 141
Fig. 5.19Total deformation distribution of the pinion shaft 142
Fig. 5.20 Von Mises Stress distribution of the pinion shaft 142
Fig. 5.21 Safety factor of the pinion shaft 143
Fig. 5.22 Damage distribution of the pinion shaft 143
Fig. 5.23 Mean biaxiliaty ratio distribution of the pinion shaft 144
Fig. 5.24 Max. stress distribution of the pinion shaft 144
Fig. 5.25 Min. stress distribution of the pinion shaft 145
Fig. 5.26 Life of the pinion shaft 145

TABLES

Table 2.1 Fem results of the Conical Contact System 38
Table 2.2 Wheel material properties 39
Table 3.1 Aluminum association designations of Aluminum Alloys 52
Table 3.2 Material properties of the rail 56
Table 4.1 Some metals and alloys for gears 85
Table 4.2 Material properties of the gear 114
Table 4.3 Material properties of the worm 114
Table 5.1 First Iteration Estimates for Stress-Concentration Factors K_t and K_{ts} 127

LIST OF SYMBOLS

A	area, area of cross section,
D	diameter
e	eccentricity, distance from the centtoidal axis to the neutral axis of a curved beam
E	Modulus of elasticity
F	concentrated force
F_x F_y F_z	body forces per unit volume
f	coefficient of friction
G	shear modulus
g	gravitational constant
h	dimension, depth of beam
I, I_y, I_z, I_{yz}	second-area moments (area moments of inertia) of a cross section
I_m, I_n	principal second-area moments of a cross section
I_1, I_2, I_3	stress invariants
K_f	fatigue stress concentration factor
K_t	static stress concentration factor» strain gage transverse sensitivity factor
L	length
M	applied or reaction concentrated bending moment (couple)
M_x M_y M_z	plate bending and twisting moments per unit length in rectangular coordinates
m	mass, modul
N	normal force number of cycles, shape functions
p	Pressure, pitch
Q	first-area moment of a partial area of a beam section
q	shear force per unit length, notch sensitivity factor
R	reaction force, radius
r_c	the distance from the center of curvature to the neutral axis of a curved beam
r_n	the distance from the center of curvature to the neutral axis of a curved beam
S_E	endurance strength
S_F	fatigue strength
S_Y	yield strength
S_{UT}	ultimate strength
T	torsional moment (couple)
V	net internal shear force
V	Linear velocity
α	angle, angular location of the neutral
v	Poisson's ratio
σ	Normal stress
σ_a, σ_m	alternating and mean stresses in fatigue applications
σ_1 σ_2 σ_3	principal stresses
σ_{vM}	Von Mises stress
τ	shear stress
ω	angular speed (rad/s)

1.1 FINITE ELEMENT METHOD

1.1.1 Introduction

The finite element method has emerged in the 21^{st} century and become a pivotal tool for the numerical solution of engineering problems. However, this method is used in many applications in the study of deformation, stress analysis, heat flux, fluid flow and other problems. With the advances in computer technology and CAD systems, the complex enginnering problems can be easily modeled. Even, many of the alternative configurations can be studied or tested on a computer before the first prototype is built. When it comes to why FEA is needed, because it helps designers, (The Finite Element Method, O.C. Zienkiewicz-R.L. Taylor)

- To reduce the amount of prototype testing,
- To simulate designs that are not suitable for prototype testing.

Finite Element Analysis determines the response of a design and simulates the response under loading conditions. The design is modeled using elements and each element has equations that describe the respond design under the influence of loads. The total response of all elements gives the full response of the design. The elements used in model have unknowns in finite number; hence the name is called finite elements. This method determines the total respond of design as approximate and at this point the real question arises that How good is the approximation?. Unfortunately, there is no easy answer for this question. For design, a complex region defining a continum is discretized into simple geometric shapes called finite elements. The material properties and the governing relationships are embedded in these elements and expressed in terms of unknown values at element corners. In design of fem of an assembly process, only considering the loading and constrain, results in ast of equations. By solving these equations, we can approximate the behaviour of the continuum model.

1.1.2 The structural element and the structural system

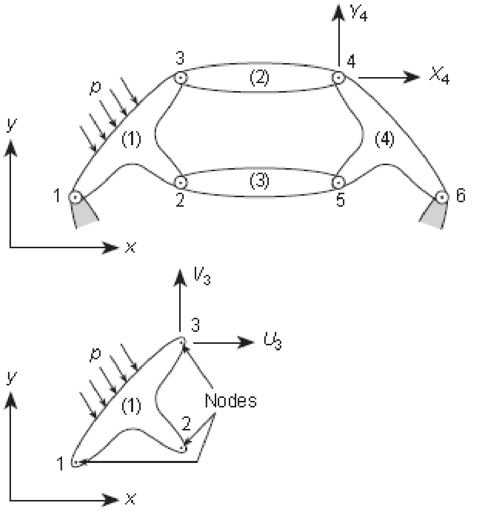

A typical element (1)

Fig. 1.1.1 A typical structure built up from interconnected elements.

(The Finite Element Method,O.C. Zienkiewicz-R.L. Taylor)

Fig. 1.1.1 shows that a two-dimensional structural assembly linked from distinct components and interconnected at the nodes numbered 1 to 6. If we know the characteristics of each elements, by labelling ang associating with nodes such as 1, 2, 3, we can calculate the forces acting at the nodes by defining the displacements, distributed loadings and initial strains of these nodes. The forces and the displacements of nodes are defined by suitable components in a coordinate system. As an example, by listing the forces acting on all the nodes of the element (1) we can write as a matrix eq. as

$$q^1 = \begin{Bmatrix} q_1^1 \\ q_2^1 \\ q_3^1 \end{Bmatrix} \quad q_1^1 = \begin{Bmatrix} U_1 \\ V_1 \end{Bmatrix} \qquad \text{etc.} \tag{1.1.1}$$

(The Finite Element Method,O.C. Zienkiewicz-R.L. Taylor)

We can write the following eq. considering also the corresponding nodal displacements

$$a^1 = \begin{Bmatrix} a_1 \\ a_2 \\ a_3 \end{Bmatrix} \qquad a_1 = \begin{Bmatrix} u_1 \\ v_1 \end{Bmatrix} \tag{1.1.2}$$

(The Finite Element Method,O.C. Zienkiewicz-R.L. Taylor)

If we assume element as linear elastic, the characteristic relationship becomes in the form

$$q^1 = K^1 a^1 + f_p^1 + f_{\varepsilon_0}^1 \tag{1.1.3}$$

(The Finite Element Method,O.C. Zienkiewicz-R.L. Taylor)

In the above eq. the first of the terms corresponds to the forces triggered by displacement of the nodes and f_p^1 corresponds to the nodal forces which is required to balance any distributed loads acting on the element and $f_{\varepsilon_0}^1$ is the nodal forces required to balance any initial strains, if the nodes are not exposed to any displacement.

As a starting analysis or an experiment may be unique definition of stresses or internal reactions at a point of the element in terms of the nodal displacements. Thus we can write such stresses in matrix σ^1 definition as follows,

$$\sigma^l = Q^1 a^1 + \sigma_{\varepsilon_0}^1 \tag{1.1.4}$$

(The Finite Element Method,O.C. Zienkiewicz-R.L. Taylor)

In Eq.1.1.4, the two term gives the stresses due to the initial strains if there is no nodal displacement takes place. The matrix K^e is known as the element stiffness matrix and the matrix Q^e as the element stress matrix for an element (e).

If the joints in Fig. 1.1.1 were considered as rigid, the last of these corresponding to a moment and a rotation respectively.

For an element which is rigidly jointed, a structure three-dimensional the number of individual nodal components would be six. Thus we can write as

$$q^e = \begin{Bmatrix} q_1^e \\ q_2^e \\ . \\ . \\ \\ q_m^e \end{Bmatrix} and \begin{Bmatrix} a_1 \\ a_2 \\ . \\ . \\ \\ a_m \end{Bmatrix} \qquad (1.1.5)$$

(The Finite Element Method,O.C. Zienkiewicz-R.L. Taylor)

In eq. 1.1.5 q_i^e and a_i corresponds to the same number of components or degrees of freedom. And the stiffness matrices of the element would clearly be square as it is shown in below eq;

$$K^e = \begin{bmatrix} K_{ii}^e & K_{ij}^e & . & . & K_{im}^e \\ . & . & & & . \\ . & . & & & . \\ . & . & & & . \\ K_{mi}^e & . & . & . & K_{mm}^e \end{bmatrix} \qquad (1.1.6)$$

(The Finite Element Method,O.C. Zienkiewicz-R.L. Taylor)

in which K_{ii}^e are submatrices which are in square and of the size *l x l,* where *l* is the number of force components to be considered at each node.

1.1.3 Assembly and analysis of a structure

To be able to obtain the total solution of Fig. 1.1.1, two conditions of displacement compatibility and equilibrium have to be satisfied.

Any system of nodal displacements can be listed in the following form, and for whole two dimensional structure satisfies the compatibility condition

$$a = \begin{Bmatrix} a \\ \cdot \\ \cdot \\ a_n \end{Bmatrix} \tag{1.1.7}$$

(The Finite Element Method,O.C. Zienkiewicz-R.L. Taylor)

Since the conditions of the whole equilibrium have been satisfied, the equilibrium equaitons needs to be satisfied and the resulting equations of each element contains unknowns in terms of displacements, we can determine the behaviour of structural element. When it comes to how we can determine the resulting equations, we can calculate the internal forces or the stresses easily by using eq. (1.1.4).

To clarify this, lets imagine a structure loaded by external forces r:

$$r = \begin{Bmatrix} r_1 \\ \cdot \\ \cdot \\ r_n \end{Bmatrix} \tag{1.1.8}$$

(The Finite Element Method,O.C. Zienkiewicz-R.L. Taylor)

and assuming that those forces applied on the nodes with the distributed loads on the elements. As an example, from Fig 1.1.1, as the joints were assumed to be pinned

$$r_i = \begin{Bmatrix} X_i \\ Y_i \end{Bmatrix} \tag{1.1.9}$$

(The Finite Element Method,O.C. Zienkiewicz-R.L. Taylor)

and considering all the force components we can write;

$$r_i = \sum_{e=1}^{m} q_i^e = q_i^1 + q_i^2 + \ldots\ldots \tag{1.1.10}$$

(The Finite Element Method,O.C. Zienkiewicz-R.L. Taylor)

Substituting the forces contributing to node i from the definition (1.1.3) and noting that nodal variables a$_i$, are common we can write

$$r_i = \left(\sum_{e=1}^{m} K_{i1}^{e}\right) a_1 + \left(\sum_{e=1}^{m} K_{i2}^{e}\right) a_2 + \ldots\ldots + \sum_{e=1}^{m} f_i^{e} \tag{1.1.11}$$

(The Finite Element Method,O.C. Zienkiewicz-R.L. Taylor)

$$f^{e} = f_{p}^{e} + f_{\varepsilon_0}^{e}$$

(The Finite Element Method,O.C. Zienkiewicz-R.L. Taylor)

The summation again only concerns the elements which contribute to node i. If all such equations are assembled we have simply

$$Ka = r - f \tag{1.1.12}$$

(The Finite Element Method,O.C. Zienkiewicz-R.L. Taylor)

In Eq. 1.1.12 we can write the submatrices as

$K_{ij} = \sum_{e=1}^{m} K_{ij}^{e}$ (The Finite Element Method,O.C. Zienkiewicz-R.L. Taylor)

(1.1.13)

$f_i = \sum_{e=1}^{m} f_i^{e}$ (The Finite Element Method,O.C. Zienkiewicz-R.L. Taylor)

1.1.4 The boundary conditions

The eq.'s of 1.1.12 can be solved by substituting the prescribed support displacements. In the example of Fig. 1.1.1, where both components of displacement of nodes 1 and 6 are zero, which means that the following

$a_1 = a_6 = \begin{Bmatrix} 0 \\ 0 \end{Bmatrix}$ (The Finite Element Method,O.C. Zienkiewicz-R.L. Taylor)

Clearly, above eq. is equivalent to reducing the number of equilibrium equations, we can reduce the sum of unknowm displacement components to eight by deleting the first and last pairs. It is, nevertheless, always convenient to assemble the equation according to relation (1.1.12) so as to include all the nodes. If all the equations of a system are assembled, we need to make summation as

$$K_{11}a_1 + K_{12}a_2 + ... = r_1 - f_1$$

(The Finite Element Method,O.C. Zienkiewicz-R.L. Taylor) (1.1.14)

$$K_{21}a_1 + K_{22}a_2 + ... = r_2 - f_2 \text{ etc.}$$

1.2 PLANE STRESS AND PLANE STRAİN

1.2.1 Introduction

In fem problems of plane stress and plane strain, the field of displacement is defined as u and v displacement in Cartesian coordinate system, being orthogonal x and y axes. The strains and stresses have three components in the xy plane. In plane stress assumption, all other components of stresses become zero and therefore do not affect internal work while in plane strain assumption the stress in a direction perpendicular to the cartesian coordinate system is not zero but the strain in that direction is zero, and this stress do not change the internal work. If it is required this could be explicitly evaluated from the three main stress components.

1.2.2 Element characteristics

1.2.2.1 Displacement functions

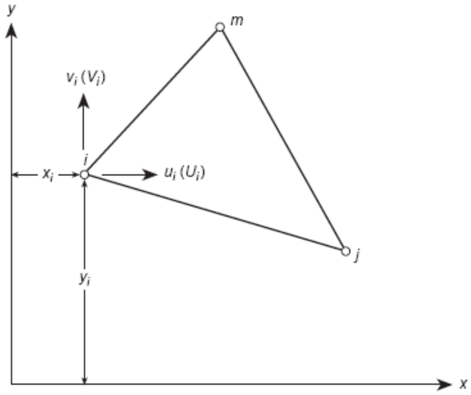

Fig. 1.2.1 An element of a continuum in plane stress or plane strain numbered in an anticlockwise order. (The Finite Element Method,O.C. Zienkiewicz-R.L. Taylor)

Fig. 1.2.1 shows a triangular element with nodes i, j, m and the displacements of a node have two components

$$a_i = \begin{Bmatrix} u_i \\ v_i \end{Bmatrix} \qquad (1.2.1)$$

(The Finite Element Method,O.C. Zienkiewicz-R.L. Taylor)

and the displacement of six components are listed as a vector

$$a^e = \begin{Bmatrix} a_i \\ a_j \\ a_m \end{Bmatrix} \qquad (1.2.2)$$

(The Finite Element Method,O.C. Zienkiewicz-R.L. Taylor)

In an element, the displacements can be defined by these six componenets. By defining two linear polynomials, we can represent the components as

$$u = \alpha_1 + \alpha_2 x + \alpha_3 y$$

(The Finite Element Method,O.C. Zienkiewicz-R.L. Taylor) (1.2.3)

$$v = \alpha_4 + \alpha_5 x + \alpha_6 y$$

(The Finite Element Method,O.C. Zienkiewicz-R.L. Taylor)

The six constants of two linear polynomials can be evaluated easily by solving the two sets of three simultaneous equations. But to be able evaluate those equations, the nodal coordinates has to be entered and the displacements equated to the appropriate nodal displacements. .

1.2.2.2 Strain (total)

Within any element, the total strain can be defined by its three components since they affects the internal work. Thus

$$\varepsilon = \begin{Bmatrix} \varepsilon_x \\ \varepsilon_y \\ \gamma_{xy} \end{Bmatrix} = \begin{bmatrix} \frac{\partial}{\partial_x} & 0 \\ 0 & \frac{\partial}{\partial_y} \\ \frac{\partial}{\partial_y} & \frac{\partial}{\partial_x} \end{bmatrix} \begin{Bmatrix} u \\ v \end{Bmatrix} = Su \tag{1.2.4}$$

(The Finite Element Method,O.C. Zienkiewicz-R.L. Taylor)

By substituting Eq. (1.2.7) we obtain the following eq.

$$\varepsilon = Ba^e = \left[B_i, B_j, B_m\right] \begin{Bmatrix} a_i \\ a_j \\ a_m \end{Bmatrix} \tag{1.2.5}$$

(The Finite Element Method,O.C. Zienkiewicz-R.L. Taylor)

with a typical matrix B_i given by, we can write;

$$B_i = SN_i = \begin{bmatrix} \frac{\partial N_i}{\partial x} & 0 \\ 0 & \frac{\partial N_i}{\partial y} \\ \frac{\partial N_i}{\partial y} & \frac{\partial N_i}{\partial x} \end{bmatrix} = \frac{1}{2\Delta} \begin{bmatrix} b_i, & 0 \\ 0, & c_i \\ c_i & b_i \end{bmatrix} \tag{1.2.6}$$

(The Finite Element Method,O.C. Zienkiewicz-R.L. Taylor)

1.2.2.3 Elasticity matrix

In general linear elastic behaviour and the relationship between stresses and strains is linear and given as

$$\sigma = D(\varepsilon - \varepsilon_0) + \sigma_0 \tag{1.2.7}$$

(The Finite Element Method,O.C. Zienkiewicz-R.L. Taylor)

The matrix form of above eq. can be written as follows and

$$\sigma = \begin{Bmatrix} \sigma_x \\ \sigma_y \\ \tau_{xy} \end{Bmatrix} = D\left(\begin{Bmatrix} \varepsilon_x \\ \varepsilon_y \\ \gamma_{xy} \end{Bmatrix} - \varepsilon_0 \right) \tag{1.2.8}$$

(The Finite Element Method,O.C. Zienkiewicz-R.L. Taylor)

can be explicitly stated for any material.

Plane stress - isotropic material

For plane stress in an isotropic material, the strain equations can be written in terms of stresses as

$$
\begin{aligned}
\varepsilon_x &= \frac{\sigma_x}{E} - \frac{v\sigma_y}{E} + \varepsilon_{x0} \\
\varepsilon_y &= -\frac{v\sigma_x}{E} + \frac{\sigma_y}{E} + \varepsilon_{y0} \\
\gamma_{xy} &= \frac{2(1+v)\tau_{xy}}{E} + \gamma_{xy0}
\end{aligned}
\tag{1.2.9}
$$

(The Finite Element Method,O.C. Zienkiewicz-R.L. Taylor)

By solving the above eq. for the stresses, we can write in matrix form as D matrix,

$$
D = \frac{E}{1-v^2}\begin{bmatrix} 1 & v & v \\ v & 1 & 0 \\ 0 & 0 & (1-v)/2 \end{bmatrix}
\tag{1.2.10}
$$

(The Finite Element Method,O.C. Zienkiewicz-R.L. Taylor)

and the initial strains can be writen as

$$
\varepsilon_0 = \begin{Bmatrix} \varepsilon_{x0} \\ \varepsilon_{x0} \\ \gamma_{xy0} \end{Bmatrix}
\tag{1.2.11}
$$

(The Finite Element Method,O.C. Zienkiewicz-R.L. Taylor)

in which E is the elastic modulus and v is Poisson’s ratio.

Plane strain - isotropic material

For plane strain assumption, in addition to plane stress components a normal stress σ_z exists. Then we can write the strain components in terms of stresses as

$$
\begin{aligned}
\varepsilon_x &= \frac{\sigma_x}{E} - \frac{v\sigma_y}{E} - \frac{v\sigma_z}{E} + \varepsilon_{x0} \\
\varepsilon_y &= -\frac{v\sigma_x}{E} + \frac{\sigma_y}{E} - \frac{v\sigma_z}{E} + \varepsilon_{y0} \\
\gamma_{xy} &= \frac{2(1+v)\tau_{xy}}{E} + \gamma_{xy0}
\end{aligned}
\tag{1.2.12}
$$

(The Finite Element Method,O.C. Zienkiewicz-R.L. Taylor)

and in addition to those components, the strain in z direction can be written

$$\varepsilon_z = -\frac{v\sigma_x}{E} - \frac{v\sigma_y}{E} + \frac{\sigma_z}{E} + \varepsilon_{z0} = 0$$

(The Finite Element Method,O.C. Zienkiewicz-R.L. Taylor)

And the stress in the z direction

$$\sigma_z = v(\sigma_x + \sigma_y) - E\varepsilon_{z0} = 0$$

(The Finite Element Method,O.C. Zienkiewicz-R.L. Taylor)

By eliminating σ_z and solving for the three remaining stresses the matrix D becomes as

$$D = \frac{E}{(1+v)(1-2v)}\begin{bmatrix} 1-v & v & 0 \\ v & 1-v & 0 \\ 0 & 0 & (1-2v)/2 \end{bmatrix} \tag{1.2.13}$$

(The Finite Element Method,O.C. Zienkiewicz-R.L. Taylor)

and the inital strains become in the form

$$\varepsilon_o = \begin{Bmatrix} \varepsilon_{x0} + v\varepsilon_{z0} \\ \varepsilon_{y0} + v\varepsilon_{z0} \\ \gamma_{xy0} \end{Bmatrix} \tag{1.2.14}$$

(The Finite Element Method,O.C. Zienkiewicz-R.L. Taylor)

1.3 THREE DIMENSIONAL ANALYSIS

1.3.1 Introduction

There is a difference between the elements of two dimensional and three dimensional problems in finite element method as it is emphasized previously. The simplest two-dimensional continuum element is a triangle, whereas, in three dimensions the continuum element is a tetrahedron, which is an element with four nodal corners. Tetrahedron element is one of ordering of the nodal numbers or is a suitable representation of a body divided into such elements.

1.3.2. Tetrahedral element characteristics

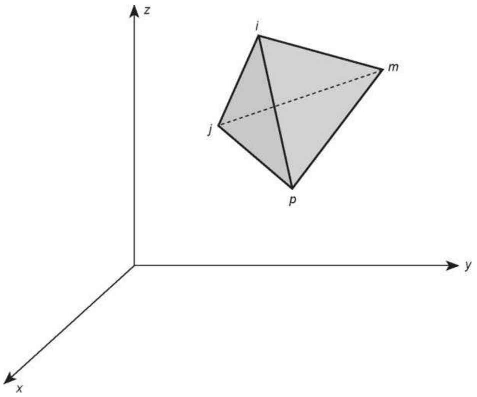

Fig. 1.3.1 A tetrahedral volume (The Finite Element Method,O.C. Zienkiewicz-R.L. Taylor)

Displacement functions of a tetrahedral volume can be written as

$$u = \begin{Bmatrix} u \\ v \\ w \end{Bmatrix} \tag{1.3.1}$$

(The Finite Element Method,O.C. Zienkiewicz-R.L. Taylor)

A linear variation can be defined by the four nodal values and we can write, for instance,

$$u = \alpha_1 + \alpha_2 x + \alpha_3 y + \alpha_4 z \qquad (1.3.2)$$

(The Finite Element Method,O.C. Zienkiewicz-R.L. Taylor)

By equating the displacement vslues at the nodes we obtain four equations in the form

$$u_i = \alpha_1 + \alpha_2 x_i + \alpha_3 y_i + \alpha_4 z_i \qquad (1.3.3)$$

(The Finite Element Method,O.C. Zienkiewicz-R.L. Taylor)

from which α_1 to α_4 can be evaluated. By using a determinant form, i.e.,

$$u = \frac{1}{6V}[(a_i + b_i x + c_i y + d_i z)u_i + (a_j + b_j x + c_j y + d_j z)u_j + (a_m + b_m x + c_m y + d_m z)u_m + \\ + (a_p + b_p x + c_p y + d_p z)u_p] \qquad (1.3.4)$$

(The Finite Element Method,O.C. Zienkiewicz-R.L. Taylor)

With

$$6V = \det \begin{vmatrix} 1 & x_i & y_i & z_i \\ 1 & x_j & y_j & z_j \\ 1 & x_m & y_m & z_m \\ 1 & x_p & y_p & z_p \end{vmatrix} \qquad (1.3.5)$$

(The Finite Element Method,O.C. Zienkiewicz-R.L. Taylor)

In eq.1.3.5 v represents the volume of the tetrahedron. By expanding the other relevant determinants into their cofactors we obtain the following coefficients

$$a_i = \det \begin{vmatrix} x_j & y_j & z_j \\ x_m & y_m & z_m \\ x_p & y_p & z_p \end{vmatrix} \quad b_i = -\det \begin{vmatrix} 1 & y_j & z_j \\ 1 & y_m & z_m \\ 1 & y_p & z_p \end{vmatrix} \qquad (1.3.6)$$

(The Finite Element Method,O.C. Zienkiewicz-R.L. Taylor)

$$c_i = -\det \begin{vmatrix} x_j & 1 & z_j \\ x_m & 1 & z_m \\ x_p & 1 & z_p \end{vmatrix} \quad d_i = -\det \begin{vmatrix} x_j & y_j & 1 \\ x_m & y_m & 1 \\ x_p & y_p & 1 \end{vmatrix} \qquad (1.3.7)$$

The state of displacement of a point is defined by three displacement components, u, v, and w, in the directions of the three coordinates x, y, and z. Thus

$$a^e = \begin{Bmatrix} a_i \\ a_j \\ a_m \\ a_p \end{Bmatrix} \quad \text{with} \quad a_i = \begin{Bmatrix} u_i \\ v_i \\ w_i \end{Bmatrix} \tag{1.3.8}$$

(The Finite Element Method,O.C. Zienkiewicz-R.L. Taylor)

At an arbitrary point, we can write the displacements as

$$u = \left[IN_i, IN_j, IN_m, IN_p \right] a^e = Na^e \tag{1.3.9}$$

(The Finite Element Method,O.C. Zienkiewicz-R.L. Taylor)

with shape functions as

$$N_i = \frac{a_i + b_i x + c_i y + d_i z}{6V} \tag{1.3.10}$$

(The Finite Element Method,O.C. Zienkiewicz-R.L. Taylor)

In eq.1.3.9 I is a three by three identity matrix.

1.3.2.1 Strain Matrix

Six strain components are relevant in full three-dimensional analysis. The strain matrix can be defined as in the form

$$\varepsilon = \begin{Bmatrix} \varepsilon_x \\ \varepsilon_y \\ \varepsilon_z \\ \gamma_{xy} \\ \gamma_{yz} \\ \gamma_{zx} \end{Bmatrix} = \begin{Bmatrix} \dfrac{\partial u}{\partial x} \\ \dfrac{\partial v}{\partial y} \\ \dfrac{\partial w}{\partial z} \\ \dfrac{\partial u}{\partial y} + \dfrac{\partial v}{\partial y} \\ \dfrac{\partial v}{\partial z} + \dfrac{\partial w}{\partial y} \\ \dfrac{\partial w}{\partial x} + \dfrac{\partial u}{\partial z} \end{Bmatrix} = Su \tag{1.3.11}$$

(The Finite Element Method,O.C. Zienkiewicz-R.L. Taylor)

Using Eqs (1.3.4)- (1.3.8) it can be shown that

$$\varepsilon = SNa^e = Ba^e = \left[B_i, B_j, B_m, B_p\right] a^e \tag{1.3.12}$$

(The Finite Element Method,O.C. Zienkiewicz-R.L. Taylor)

in which

$$B_i = \begin{bmatrix} \dfrac{\partial N_i}{\partial x}, & 0, & 0 \\ 0, & \dfrac{\partial N_i}{\partial y}, & 0 \\ 0, & 0, & \dfrac{\partial N_i}{\partial z} \\ \dfrac{\partial N_i}{\partial y}, & \dfrac{\partial N_i}{\partial x}, & 0 \\ 0, & \dfrac{\partial N_i}{\partial z}, & \dfrac{\partial N_i}{\partial y} \\ \dfrac{\partial N_i}{\partial z}, & 0, & \dfrac{\partial N_i}{\partial x} \end{bmatrix} = \frac{1}{6V} \begin{bmatrix} b_i, & 0, & 0 \\ 0, & c_i, & 0 \\ 0, & 0, & d_i \\ c_i, & b_i, & 0 \\ 0, & d_i, & c_i \\ d_i & 0, & b_i \end{bmatrix} \tag{1.3.13}$$

(The Finite Element Method,O.C. Zienkiewicz-R.L. Taylor)

1.3.2.2 Elasticity Matrix

The D matrix relating the six stress components to the strain components can contain 21 independent constants in a complete anisotropy. Thus,

$$\sigma = \begin{Bmatrix} \sigma_x \\ \sigma_y \\ \sigma_z \\ \tau_{xy} \\ \tau_{yz} \\ \tau_{zx} \end{Bmatrix} = D\left(\varepsilon - \varepsilon_0\right) + \sigma_0 \qquad (1.3.14)$$

(The Finite Element Method,O.C. Zienkiewicz-R.L. Taylor)

Although no difficulty presents itself in computation when dealing with such materials, it is convenient to recapitulate here the D matrix for an isotropic material. This, in terms of the usual elastic constants E (modulus) and v (Poisson's ratio), can be written as

$$D = \frac{E}{(1+v)(1-2v)} \begin{bmatrix} 1-v, & v, & v, & 0, & 0, & 0 \\ & 1-v, & v, & 0, & 0, & 0 \\ & & 1-v, & 0, & 0, & 0 \\ & & & (1-2v)/2, & 0, & 0 \\ & & & & (1-2v)/2 & 0 \\ & & & & & (1-2v)/2 \end{bmatrix} \qquad (1.3.15)$$

(The Finite Element Method,O.C. Zienkiewicz-R.L. Taylor)

1.3.2.3 Stiffness, stress, and load matrices

Since the strain and stress components are constant within the element, the stiffness matrix defined can be explicitly integrated. The general ij submatrix of the stiffness matrix will be a three by three matrix defined as in the form

$$K_{ij}^{e} = B_i^T D B_j V^e \tag{1.3.16}$$

(The Finite Element Method,O.C. Zienkiewicz-R.L. Taylor)

where V^e represents the volume of the elementary tetrahedron. The nodal forces due to the initial strain become,

$$f_i^e = -B_i^T D \varepsilon_0 V^e \tag{1.3.17}$$

(The Finite Element Method,O.C. Zienkiewicz-R.L. Taylor)

with a similar expression for forces due to initial stresses. Distributed body forces can once again be expressed in terms of their b_x, b_y, and b_z components or in terms of the body force potential.

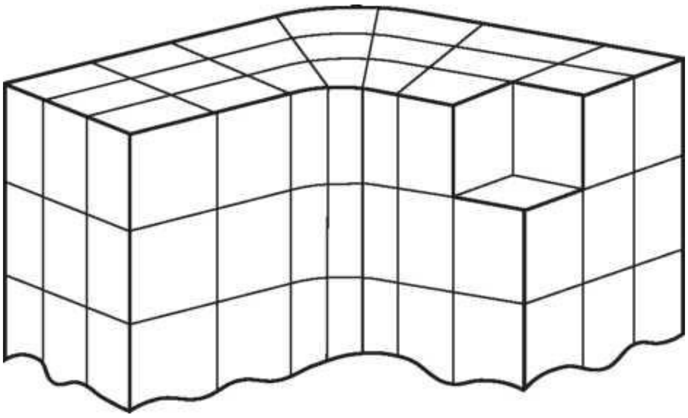

Fig. 1.3.2 A systematic way of dividing a three-dimensional object into 'brick'-type elements. (The Finite Element Method,O.C. Zienkiewicz-R.L. Taylor)

1.4 ASSUMPTIONS AND ESTIMATES OF MONORAİL CRANE DESİGN

In this study by considering or determining the force-time function in the lifting cable or wire, and the torque-time function acting on the shaft of the wheel during any one cycle, we can estimate gear ratio, power and torque requirements for the motor.

Assuming, the nominal load depends on the number of weights to be lifted at one time and the weight of any structure used to support the weights and assuming 100 weights from the truck, one at a time in 30 min, requires that the average weight rate be 100/30 = 3.3 weight/min, or approximately 18-sec average period per weight. Since some of this time must be used to return the empty lift to the ground, we can not use the entire 18 sec to lift the load. We must also allow some time for manual loading and unloading of the weights at top and bottom therefore we can assume that 1/3 of the period is used to load/unload, 1/3 to lift, and 1/3 to lower. This allows 6 sec per weight, if we lift only one weight at a time. The average velocity of the lift would then have to be 0.6 meter / 6 sec = 0.1 meter/sec.

The maximum load to be lifted on the machine is 500 kg. The dead-load is only the weight of the motors, reductors, rope, and any platform or structure used to support the weights. Since this structure has yet to be designed, its weight is unknown. We will assume that we can keep this deadweight under 75 kg. The total nominal load will then be 575 kg for the lift phase, and 75 kg for the lowering phase.

At steady state, the load on the rope may be the above that weights. However, at start-up, the load can be significantly higher due to the need to accelerate the load to its steady-state velocity and also due to the fact that there are both spring and mass in the system. A combination of spring and mass in a dynamic system allows oscillations to occur as the kinetic energy of the moving mass is transferred to potential energy in the elastic spring and vice versa. The rope is a spring. When the slack in the rope is suddenly taken up against the mass of the load, the rope will stretch, storing potential energy. When the force in the stretched rope becomes sufficient to move the load, it will accelerate the mass upward, increasing its velocity and transferring the springs potential energy to kinetic energy in the mass. If the mass accelerates sufficiently it will take the rope slack again. When the mass falls to take up the slack, the cycle repeats. Thus, as it starts up, the force in the rope can oscillate from zero to some value significantly greater than the steady-state nominal load. To calculate the dynamic loading requires writing and solving the differential equations of motion for the system. **Fig.1.4.1a** shows a simplified schematic of the portion of the dynamic system containing the lift mass and the rope spring. **Fig.1.4.1b** shows the system modeled as a lumped mass supported by a spring and a damper**.** **Fig.1.4.1c** shows a free-body diagram (FBD) of the mass acted upon by its weight W, the spring force F_s, and the damper force F_d

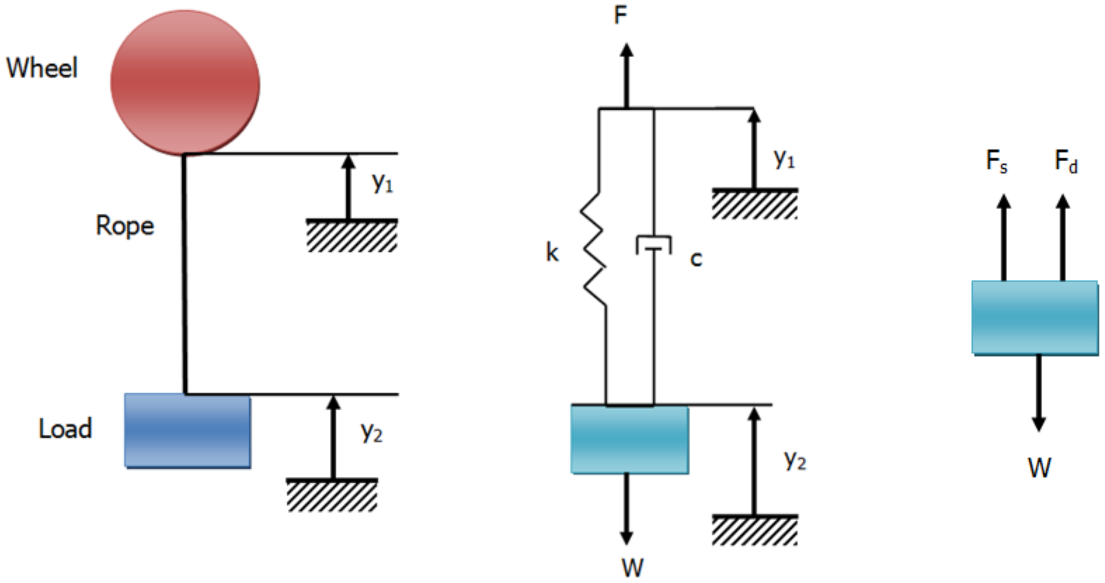

(a) Dynamic system (b) Lumped model (c) FBD

Fig.1.4.1

Writing Newton's 2nd law for this FBD gives;

$$\sum F = m\,a \qquad \text{(a)}$$

$$F_s + F_d - W = \frac{W}{g}\ddot{y}_2$$ where F_s and F_d is

$$\begin{aligned} F_s &= k \cdot (y_1 - y_2) \quad if\ y_1 > y_2\,, \quad else\,F_s = 0 \\ F_d &= c \cdot (y_1' - y_2') \quad if\ y_1 > y_2\,, \quad else\,F_d = 0 \end{aligned} \qquad \text{(b)}$$

$$F_s = k(y_1 - y_2) \qquad\qquad F_d = c(\dot{y}_1 - \dot{y}_2)$$

$$y' = \frac{d}{dt}y \qquad y'' = \frac{d^2}{dt^2}y \quad \mathbf{y_2} \qquad \text{(c)}$$

The initial conditions are: when t = 0: $y_1(0) = 0$, $y'_1(0) = 0$, $y_2(0) = 0$, $y'_2(0)=0$. From which $F_s(0) = 0$ and $F_d(0) = 0$. Solving equation a for y''

$$\mathbf{y_1} \quad \frac{1}{m}\cdot(F_s + F_d - W) \qquad \text{(d)}$$

↑

$$m\ddot{y}_2 = k(y_1 - y_2) + c(\dot{y}_1 - \dot{y}_2) - W$$

$$\ddot{y}_2 = \frac{1}{m}\left[k(y_1 - y_2) + c(\dot{y}_1 - \dot{y}_2) - W\right] \qquad \text{(e)}$$

In the above eq. we know that $\dot{y}_1 = v,\quad y_1 = v\,t$ and $y = y_2$; and assigning values for v, k, m and W and we estimated required speed of monorail crane as $v = 0.1\ m/s$

Payload weight is ; $W = 575N$ $\qquad m = \frac{W}{g} = \frac{575}{9{,}81} = 58.5\frac{kg\,sn^2}{m}$

Assuming deflection as 0.001 m in the rope and rope stiffness can be calculated as follows

$$F = k\,x \Rightarrow k = \frac{F}{x} = \frac{575}{0{,}001} = 575.10^3\,N/m$$

The critical damping c_c is easily calculated from the known mass and spring constant values. This system is only lightly damped by the ropes internal friction. Assuming that its ratio of actual damping to critical damping, z, is about 10% (ζ = 0.10) and using this to be able to calculate a damping value for equation (e), we find C_c and c as follows

$$c_c = 2m\sqrt{\frac{k}{m}} = 2x58,62x\sqrt{\frac{575x10^3}{58,62}} = 11611,46\frac{kg\sec}{m}$$

$$c = \zeta c_c = 0,1x11611,46 = 1161,1\ \frac{kg\sec}{m}$$

Equation (e) is a nonlinear, second-order differential equation that can only be solved by numerical methods. Therefore, we rewrite the second-order equation as two, first-order differential equations as

$$\frac{d^2}{dt^2}y = \frac{1}{m}\cdot\left(F_s + F_d - W\right)$$
$$\frac{d}{dt}\left(\frac{d}{dt}y\right) = \frac{1}{m}\cdot\left(F_s + F_d - W\right)$$

and taking derivatives as in the form

$$D_1 = \frac{d}{dt}y$$
$$D_2 = \frac{d}{dt}D_1 = \frac{d}{dt}\frac{d}{dt}y = \frac{1}{m}\cdot\left(F_s + F_d - W\right)$$

Or, in matrix form,

$$D = \begin{bmatrix} \frac{d}{dt}y \\ \frac{1}{m}\cdot\left(F_s + F_d - W\right) \end{bmatrix}$$

Matlab's differential equation solving functions (ode45) can solve this problem by creating a function that evaluates the D vector. By defining the initial conditions, where the first element is the initial value of y and the second is the initial value of y' and using Runge-Kutta solver, called ode45 in Matlab, to integrate function. The acceleration of the load over the first second of operation is shown in Fig. 1.4.2a. The periods of negative acceleration (at a limiting value of g) during which the load is in free-fall and the rope is slack with no tension. The force in the rope can also be calculated from the integration results. The force in the rope over the first second of operation is shown in Fig. 1.4.2b. From the below fig.s we can see that the tension force rises to over four times with the nominal load on the first oscillation and then drops to zero as the rope goes slack since it cannot support a compressive force. This pattern repeats for 3 cycles, at which point the damping has reduced the oscillations to the point that the rope is always in tension. After about 10 cycles, it has settled down to the value of the nominal load which is 575 kg.

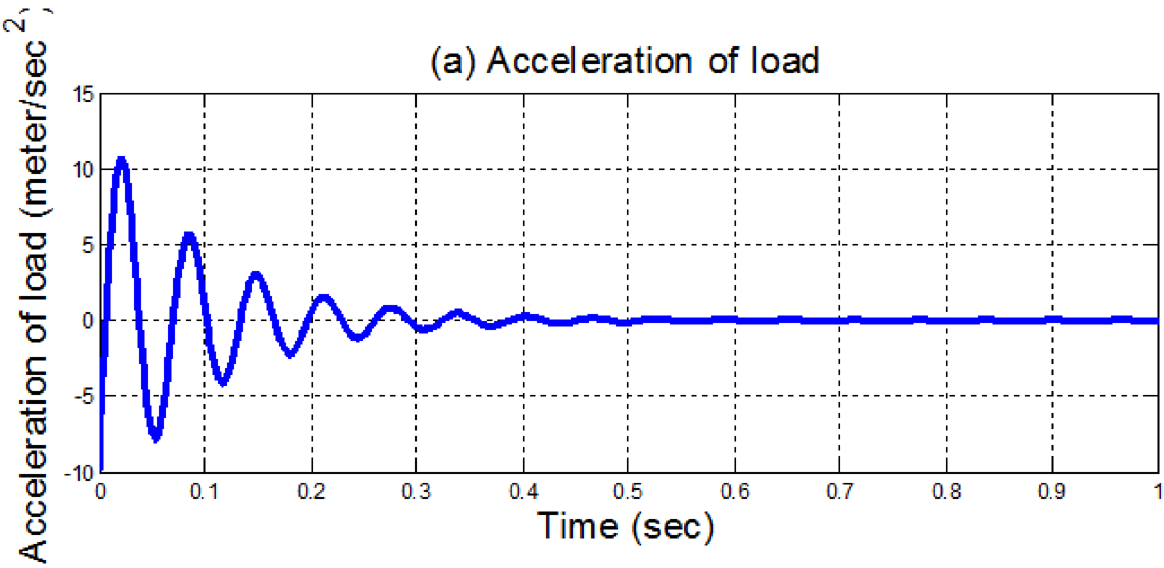

(a) Acceleration of load

(b) Dynamic force in cable

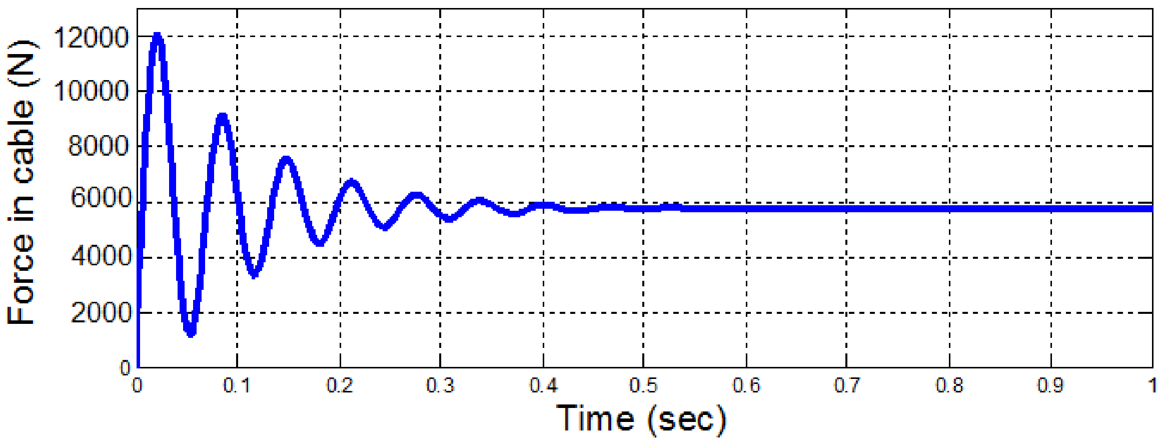

Fig. 1.4.2 Acceleration and Cable Force at Startup of Load-Lift

The torque required to drive the wheel shaft depend on the dynamic loads on the diameter of wheel selected. Too small a diameter will cause high stresses and wear on the rope. A large wheel diameter will increase the required torque and increase the package size. The torque required on the shaft is 10 times the tension in the rope and will have the same time variations as shown in Fig. 1.4.2. The average power required can be easily found from the change in potential energy over the time desired. To raise a 575 kg load to a high 0,6 m in 6 sec requires

$$P = \frac{Weight\, x\, height}{time}$$

$$P_{vertical} = FxV = \frac{(575\, x\, 9{,}81)\, x\, 0{,}6}{6} = 565W$$

Assuming a friction coefficient between the rail and wheel; the horizontal power can be calculated as follows;

$$P_{horizantal} = F_f xV = F_n x\mu xV = \frac{(575\, x\, 9{,}81x0{,}3)\, x\, 0{,}6}{6} = 169{,}25W$$

Since there will be losses in the gears, assumingthe efficiency as 0,85 we can calculate the last values of required power of motor as

$$P_{new,horizantal} = \frac{169{,}25}{0{,}85} \cong 200W \qquad P_{new,vertical} = \frac{565}{0{,}85} \cong 665W$$

When the motor types and powers are taken into account, it is desirable to keep it at or below this level since larger horsepower motors will require higher voltage than 110V. This average power is based on the nominal load. The peak load at startup requires more power. Rather than size the motor to accommodate the transient start-up load, another approach is to provide sufficient flywheel in the system to supply the transient pulse of energy to get it past the start-up phase. It is possible that the rotational inertia of the spur gears will supply enough flywheel effect assuming that the monorail crane is up to speed before the slack is first taken out of the rope. The average wheel angular velocity is determined from the required average linear velocity of the rope which is 0.1 m/sec.

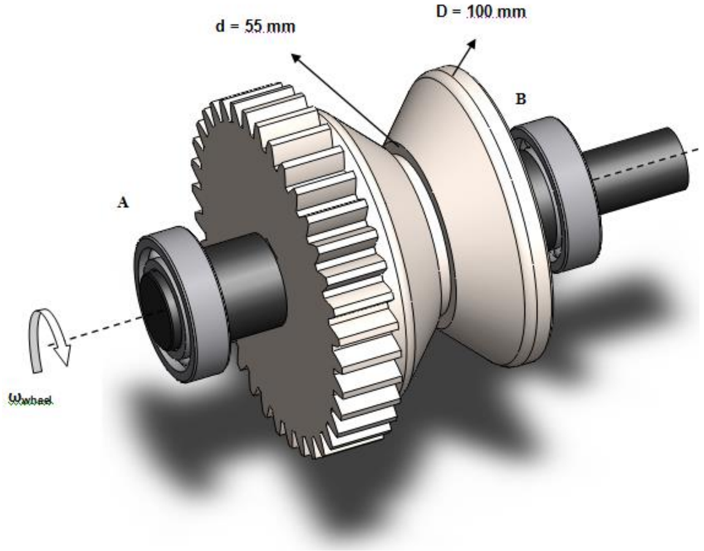

Fig. 1.4.3 Geometry of the wheel

$$D_{wheel,ort} = \frac{D+d}{2} = \frac{100+55}{2} = 77{,}5\,mm$$

$$\frac{D_{wheel,ort}}{2} x W_{wheel} = V_{wheel}$$

$$\frac{0{,}0775}{2} x W_{wheel} = \frac{6\,m}{dk} x \frac{1\,dk}{60\sec}$$

$$W_{wheel} \cong 2{,}6\,rad/\sec$$

Now that we find the angular velocity, the torque values can be calculated, in terms of both horizantal and vertical climbing conditions;

$$P_{wheel} = T_{wheel}\ x\ W_{wheel}$$

$$665 = \left(T_{wheel}\right)_{vert.}\ x 2{,}6 \qquad 200 = \left(T_{wheel}\right)_{hor.}\ x 2{,}6$$

$$\left(T_{wheel}\right)_{vert.} \cong 256\,N\,m \qquad \left(T_{wheel}\right)_{hor.} \cong 77\,N\,m$$

To be able to transfer power from motors to the wheel, it would be a good idea to use spur gears on the shafts. But, here there is an another good point to diminish in manufacturing time and to be able to obtain more rigid wheel, we would manufacture wheel and spur gear from the same cylindrical part as shown below.

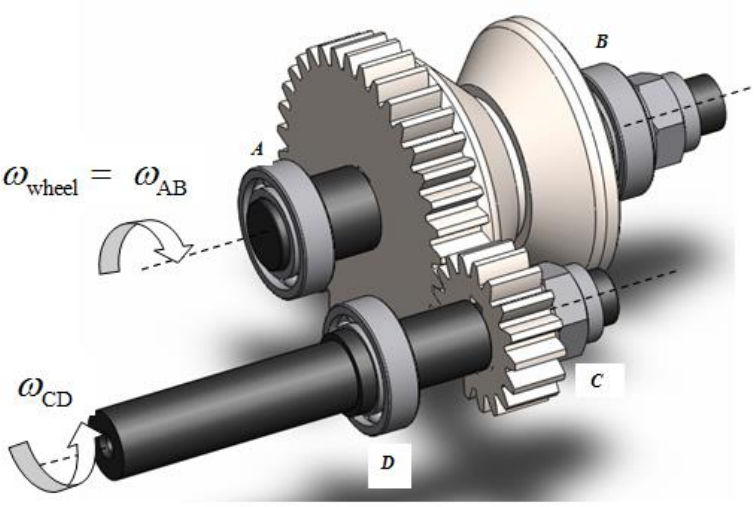

Fig. 1.4.4 Geometry of the gears

The tooth numbers for gear and pinion has been chosen as 36 and 17 respecticely. Then, we can calculate the angular velocity of the pinion as

$$i_1 = \frac{N_{gear,tooth}}{N_{pinion,tooth}} = \frac{36}{17} \cong 2{,}118$$

$$i_1 = \frac{\omega_{CD}}{\omega_{AB}} \Rightarrow \omega_{CD} = i_1\, x\, \omega_{AB} = 2{,}118\, x\, 2{,}6 = 5{,}5\, rad\,/\,sn$$

$$\omega_{CD} = N_{CD}\, x \frac{\pi}{30} \Rightarrow N_{CD} = \frac{30\, x\, 5{,}5}{\pi} = 52{,}5\, rpm$$

$$Assume;\eta_{\left(gear,pinion\right)_{\max}} \cong 0{,}60 \Rightarrow \frac{P_{gear}}{P_{pinion}} = \eta_{gear,pinion}$$

$$P_{pinion} = \frac{665}{0,6} \cong 1110W = P_{CD} = P_{EF}$$

Since CD shaft would take the required power from motor, before transfering the power, a reductor, in which has worm – gear mechanism, should be used.

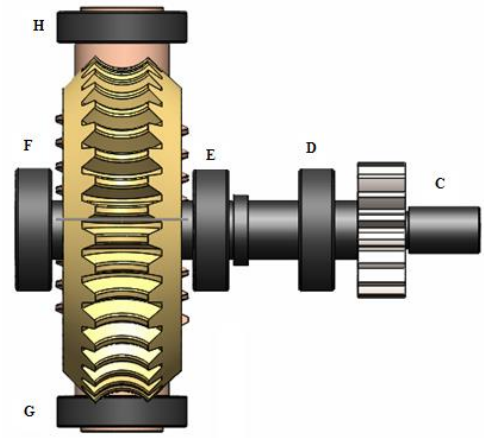

Fig. 1.4.5 Geometry of worm - gear

Since DC shaft is jointed to the FE shaft, W_{CD} equals to W_{FE}. W_{CD} = W_{CD} = 5,5 rad / sn corresponds to 52,5 rpm approximately. When it comes to the worm and gear features, lets assume a single thread worm and 33 tooth gear to be able to obtain the required velocity. $Assume; \eta_{(worm\,gear)_{\max}} = 30\,\%$

$$Since, \eta_{(worm\,gear)_{\max}} = \frac{P_{EF}}{P_{GH}} \Rightarrow P_{GH} = \frac{P_{EF}}{\eta_{(worm\,gear)_{\max}}} = \frac{1110}{0,3} \cong 3700W$$

$$P_{GH} = 3700W = P_{motor}$$

$$\omega_{CD} = \omega_{EF} = 5,5\,rad\,/\,sn$$

$$\dot{I}_2 = \frac{N_{gear,tooth}}{\dot{I}_{worm}} = \frac{33}{1} = 33$$

$$\dot{I}_2 = \frac{\omega_{GH}}{\omega_{EF}} \Rightarrow 33 = \frac{\omega_{GH}}{5,5} \Rightarrow \omega_{GH} = 181,5\,rad\,/\,sn$$

Electric motors are made in only a few standard rotational speeds, the most common of which are 1740 rpm and 3450 rpm.

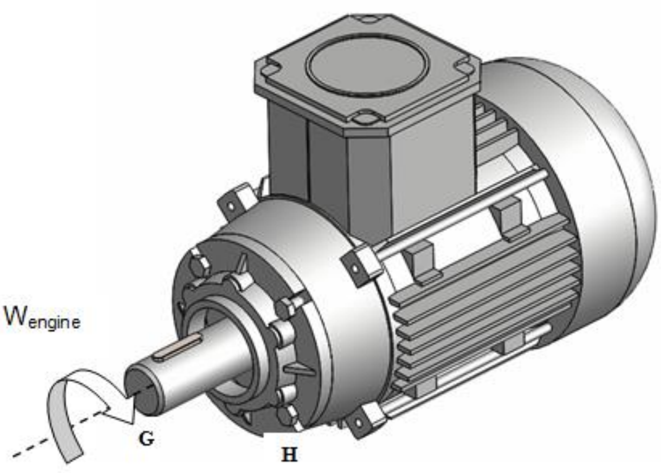

Fig. 1.4.6 Motor

$$W_{motor} = W_{GH} = 181{,}5 rad/sn = n_{motor}\ x \frac{\pi}{30} \Rightarrow n_{motor} \cong 1734\, rpm$$

The common type motor is 1740 rpm. Then if we use the 1740 rpm motor, frequency of the motor becomes;

$$f = \frac{n_{motor}}{60} = \frac{1740}{60} = 29\, Hz$$

To summarize the parameters determined from this preliminary design study, we are looking to design a system that has a 0,37 kW, and 1740 rpm, 230-400V AC electric motor, driving a 1:33 reduction worm-wheel set, that, in turn, drives a 100-mm-dia wheel at 52,5 rpm. These constitute a set of task specifications for our design.

2.0 WHEEL

2.1 Introduction to frictional contact with isotropic half-space assumption

There are two solids Ω_1 and Ω_2 in terms of contact system as seen below Fig.2.1a.

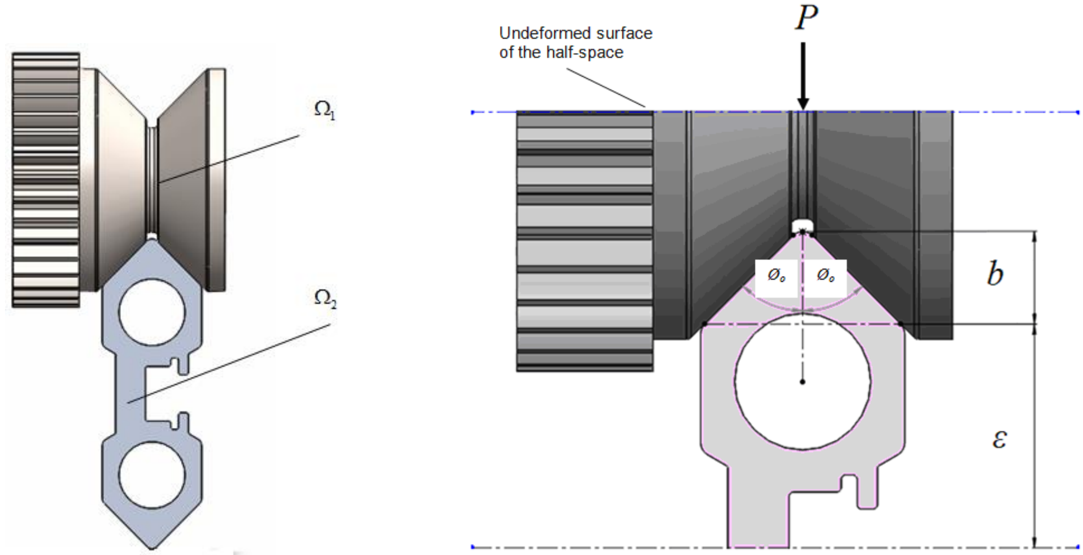

Fig. 2.1 a) Two solids Ω_1 and Ω_2 **b)** The frictional indentation of a cone into a half-pace.

As it can be seen from Fig. 2.1a, conical contact regions with a vertex angle of $2Ø_0$ exists between rail and wheel. Since the materials are isotropic for both type of materials, this corresponds to isotropic half-space assumption axisymmetrically about the central axis of the rail. The resultant force is P, which is along the cone axis and is perpendicular to the half-space surface. During the indentation, sliding with Coulomb friction occurs between the cone and space surfaces, except at the apex. With isotropic half-space asumption contact with normal loading and tangential loading equations are given as follows;

2.1.1 Contact with Normal Loading

The contact pressure is the same as an isotropic half-space (Sneddon, 1948; Elliott, 1949) and can be described as

$$\sigma_z(r,\alpha,0) = -\frac{P}{\pi a^2}\cosh^{-1}\left(\frac{a}{r}\right), \qquad 0 \le r \le a, \tag{2.1.1}$$

where a is the radius of the contact area which needs to be determined. To be able to obtain the displacements and stresses introduced by this pressure eq., we should replace “the concentrated force “N” eq. into “the half - space subjected to a normal force N Eq”. as follows;

The half - space subjected to a normal force N eq. is given by $\varphi_1(r,\alpha,z;r_0,\alpha_0) = H\,N\;\ln\left(R_1 + z_1\right)/(\alpha_1 - s_1)$

By replacing that equation with $[P\cos h^{-1}(a/r_0)/(\pi a)^2]\,r_0\,dr_0\,d\alpha_0$ integrating over the whole contact area $(0 \le r_0 \le a,\ 0 \le \alpha_0 \le 2\pi)$, the displacement functions can be found as follows;

$$\begin{aligned}
\varphi_1(r,\alpha,z) &= \frac{H\,P}{\pi a^2(\alpha_1 - s_1)}\Omega(r,\alpha,z_1)\\
\varphi_2(r,\alpha,z) &= \frac{H\,P}{\pi a^2(\alpha_2 - s_2)}\Omega(r,\alpha,z_2)\\
\varphi_3(r,\alpha,z) &= 0
\end{aligned} \tag{2.1.2}$$

where

$$\Omega(r,\alpha,z) = \int_0^{2\pi}\int_0^{a}\cosh^{-1}\left(\frac{a}{r_0}\right)\ln(R+z)\,r_0\,dr_0\,\alpha_0 \tag{2.1.3}$$

This integral can be expressed in terms of elementary functions as follows (Hanson, 1992a)

$$\Omega(r,\alpha,z) = 2\pi\left[\begin{array}{c} az\sin^{1}\left(\dfrac{l_1}{r}\right) + \dfrac{1}{4}(2a^2 + r^2 - 2z^2)\ln(l_2 + \sqrt{l_2^2 - r^2} + \dfrac{3zl_2(r^2 - 2l_1^2)}{4r\sqrt{r^2 - l_1^2}} \\ -\dfrac{3z\sqrt{r^2 + z^2}}{4} - \dfrac{1}{4}\left(r^2 - 2z^2\right)\ln(z + \sqrt{z^2 + r^2} \end{array}\right] \tag{2.1.4}$$

The displacements and stresses can then be derived by simple differentiations when using elastic equations

$$U = \frac{2HP}{a^2} e^{i\alpha} \sum_{j=1}^{2} \frac{1}{\alpha_j - s_j} \begin{bmatrix} \dfrac{rl_{2j} \;\; 2al_{1j}\sqrt{l_{2j}^2 - r^2}}{2r^2} + \dfrac{r}{2}\ln\left(l_{2j} + \sqrt{l_{2j}^2 - r^2}\right) \\ -\dfrac{z_j\sqrt{r^2 + z_j^2}}{2r} - \dfrac{r}{2}\ln\left(z_j + \sqrt{r^2 - z_j^2}\right) + \dfrac{a^2}{2r} \end{bmatrix} \quad (2.1.5a)$$

$$w = \frac{2HP}{a^2} \sum_{j=1}^{2} \frac{\alpha_j}{\alpha_j - s_j} \begin{bmatrix} a\sin^{-1}\left(\dfrac{l_{1j}}{r}\right) + \sqrt{l_{2j}^2 - a^2} - \sqrt{r^2 + z_j^2} \\ -z_j \ln\left(l_{2j} + \sqrt{l_{2j}^2 - r^2}\right) + z_j \ln\left(z_j + \sqrt{r^2 + z_j^2}\right) \end{bmatrix} \quad (2.1.5b)$$

$$\sigma_1 = -\frac{4HPc_{66}}{a^2} \sum_{j=1}^{2} \frac{k_{1j} - 1}{\alpha_j - s_j} \left[\ln\left(l_{2j} + \sqrt{l_{2j}^2 - r^2}\right) - \ln\left(z_j + \sqrt{r^2 + z_j^2}\right)\right] \quad (2.1.5c)$$

$$\sigma_2 = \frac{4HPc_{66}}{a^2} e^{i2\alpha} \sum_{j=1}^{2} \frac{1}{\alpha_j - s_j} \left[\frac{1}{ar^2}(2a^2 - l_{2j}^2)\sqrt{a^2 - l_{1j}^2} + \left(\frac{z_j + \sqrt{r^2 + z_j^2}}{r^2} - \frac{a^2}{r^2}\right)\right] \quad (2.1.5d)$$

$$\sigma_z = \frac{Ps_1s_2}{\pi a^2(s_2 - s_1)} \sum_{j=1}^{2} \frac{(-1)^j}{s_j} \left[\ln(l_{2j}^2 + \sqrt{l_{2j}^2 - r^2} - \ln\left(z_j + \sqrt{r^2 + z_j^2}\right)\right] \quad (2.1.5e)$$

$$\tau_z = \frac{Ps_1s_2}{\pi a^2(s_2 - s_1)} e^{i\alpha} \sum_{j=1}^{2} (-1)^{j+1} \left(\frac{1}{r}\sqrt{l_{2j}^2 - a^2} - \frac{\sqrt{r^2 + z_j^2}}{r}\right) \quad (2.1.5f)$$

The radius of the contact area, *a*, in these expressions can be determined by the compatibility of deformation (Hanson, 1992*a*). According to Fig. 2.1b, it is clear that the normal displacement at the half-space surface in the contact region can be written as

$$w = b + \varepsilon\left(1 - \frac{r}{a}\right), \qquad (0 \le r \le a) \quad (2.1.6)$$

where $\varepsilon = a\cot\phi_0$. However, Eq. (2.1.5*b*) specifies that at the surface,

$$w = \frac{2HP}{a^2}\left(\frac{\pi}{2}a - r\right) = \frac{2HP}{a}\left(\frac{\pi}{2} - 1\right) + \frac{2HP}{a}\left(1 - \frac{r}{a}\right), \qquad (0 \le r \le a) \tag{2.1.7}$$

Since the normal displacement at the contact interface must be continuous, the right hand sides of Eqs. (2.1.6) and (2.1.7) must be the same. This gives rise to

$$\varepsilon = \frac{2HP}{a}, \quad b = \varepsilon\left(\frac{\pi}{2} - 1\right) \tag{2.1.8}$$

When the resultant force *P* is known, the contact parameters shown in Fig. 2.1b can be determined from

$$a = \sqrt{2HP\tan\phi_0}\ , \qquad \varepsilon = \sqrt{2HP\cot\phi_0}\ ,\ b = \varepsilon\left(\frac{\pi}{2} - 1\right) \tag{2.1.9}$$

If, instead of the indentation force, the indentation depth to be $d_p = b + \varepsilon$ then the radius of contact area, *a*, and the indentation force, *P*, can be calculated by

$$a = \frac{2}{\pi}d_p\tan\phi_0, \quad P = \frac{2}{\pi^2 H}d_p^2\tan\phi_0 \tag{2.1.15}$$

If the half-space is isotropic, $H = (1 - v^2)/(\pi E)$ and the results reduce to those of Sneddon (1948) except for the incorrect definitions of two parameters, as pointed out by Hanson (1992*a*).

2.1.2 Contact with Tangential Loading

Now using,

$$\frac{Pf}{\pi a^2}\cosh^{-1}\left(\frac{a}{r_0}\right) r_0\, dr_0\, d\alpha_0 \tag{2.1.16}$$

to replace the concentrated tangential force Q, into a half-space subjected to tangential forces equations, and integrating over the contact area, $(0 \le r_0 \le a, 0 \le \alpha_0 \le 2\pi)$,we find the following displacement functions:

$$\begin{aligned}
\phi_1(r,\alpha,z) &= \frac{HP}{2\pi a^2 s_2(\alpha_1 - s_1)}\left(f\,\bar{\Delta} + \bar{f}\,\Delta \right)\left[z_1\Omega(r,\alpha,z_1) - \Gamma(r,\alpha,z_1)\right],\\
\phi_2(r,\alpha,z) &= \frac{HP}{2\pi a^2 s_2(\alpha_2 - s_2)}\left(f\,\bar{\Delta} + \bar{f}\,\Delta \right)\left[z_2\Omega(r,\alpha,z_2) - \Gamma(r,\alpha,z_2)\right],\\
\phi_3(r,\alpha,z) &= -i\frac{Ps_3}{4\pi^2 a^2 s_2\, c_{66}}\left(f\,\bar{\Delta} - \bar{f}\,\Delta \right)\left[z_3\Omega(r,\alpha,z_2) - \Gamma(r,\alpha,z_3)\right],
\end{aligned} \tag{2.1.17}$$

where $\Omega(r,\alpha,z_2)$ was given by Eq. (2.1.4) and $\Gamma(r,\alpha,z_2)$ is defined by (Hanson, 1992*a*)

$$\Gamma(r,\alpha,z) = \int_0^{2\pi}\int_0^{a} \cos h^{-1}\left(\frac{a}{r_0}\right) R r_0\, dr_0\, d\alpha_0 \text{ (2.1.4)}$$

$$= 2\pi\left[\begin{array}{l} \frac{a}{12}\left(2a^2 + 6z^2 3r^2\right)\sin^{-1}\left(\frac{l_1}{r}\right) + \frac{1}{3}z^3\ln\left(z + \sqrt{z^2 + r^2}\right) - \frac{1}{3}z^3\ln\left(l_2 + \sqrt{l_2^2 - r^2}\right) \\ -\frac{1}{9}(4z^2 + r^2)\sqrt{z^2 + r^2} + \frac{1}{36}(21l_1^2 + 16l_2^2 - 12r^2 - 10a^2)\sqrt{l_2^2 - a^2} \end{array}\right] \tag{2.1.18}$$

The displacements and stresses are correspondingly:

$$U = \frac{HP}{a^2 s_1 s_2}\sum_{j=1}^{2}\frac{s_j}{\alpha_j - s_j}\Bigg\{ f[-a\sin^{-1}\left(\frac{l_{1j}}{r}\right) - \sqrt{l_{2j}^2 - a^2} + z_j\ln\left(l_{2j} + \sqrt{l_{2j}^2 - r^2}\right) -$$

$$z_j\ln\left(z_j + \sqrt{r^2 + z_j^2}\right) + \sqrt{r^2 + z_j^2}] + \bar{f}\, e^{i2\alpha}[-\frac{a^2 z_j}{r^2} + \frac{\left(r^2 + z_j^2\right)^{3/2}}{3r^2} + \frac{4a^2 - 3l_{2j}^2 - l_{2j}^2}{3r^2}\sqrt{l_{2j}^2 - a^2}]\Bigg\}$$

$$-\frac{Ps_3}{2\pi a^2 c_{66}}\{f[-a\sin^{-1}\left(\frac{l_{132}}{r}\right)-\sqrt{l_{23}^2-a^2}+z_3\ln\left(l_{23}+\sqrt{l_{23}^2-r^2}\right)-z_3(z_3+\sqrt{r^2+z_3^2}+\sqrt{r^2+z_3^2}\,]$$

$$-\bar{f}\,e^{i2\alpha}[-\frac{a^2 z_3}{r^2}+\frac{\left(r^2+z_3^2\right)^{3/2}}{3r^2}+\frac{4a^2-3l_{13}^2-l_{23}^2}{3r^2}\sqrt{l_{23}^2-a^2}\Bigg]\Bigg\} \tag{2.1.19}$$

$$w=\frac{HP}{a^2 s_1 s_2}\left(\bar{f}\,e^{i\alpha}+f\,e^{-i\alpha}\right)\sum_{j=1}^{2}\frac{s_j\,\alpha_j}{\alpha_j-s_j}[\frac{r}{2}\ln(l_{2j}+\sqrt{l_{2j}^2-r^2})-\frac{r}{2}\ln\left(z_j+\sqrt{z_j^2+r^2}\right)+$$

(2.1.20)

$$+\frac{a^2}{2r}-\frac{z_j\sqrt{z_j^2+r^2}}{2r}+\frac{\left(rl_{2j}-2al_{1j}\right)\sqrt{l_{2j}^2-r^2}}{2r^2}.$$

$$\sigma_1=\frac{2HPc_{66}}{a^2 s_1 s_2}\left(\bar{f}\,e^{i\alpha}+f\,e^{-i\alpha}\right)\sum_{j=1}^{2}\frac{(k_{1j}-1)s_j}{\alpha_j-s_j}\left(\frac{\sqrt{l_{2j}^2-a^2}}{r}-\frac{\sqrt{r^2+z_j^2}}{r}\right) \tag{2.1.21}$$

$$\sigma_2=\frac{2HPc_{66}}{a^2 s_1 s_2}\sum_{j=1}^{2}\frac{s_j}{\alpha_j-s_j}\left(f\,e^{i\alpha}\left(\frac{\sqrt{r^2+z_j^2}}{r}-\frac{\sqrt{l_{2j}^2-a^2}}{r}\right)+\bar{f}\,e^{i3\alpha}\right.$$

$$\left.\left[(12l_{1j}^2+4l_{2j}^2-3r^2-16a^2)\frac{\sqrt{l_{2j}^2-a^2}}{3r^3}+\frac{4a^2 z_j}{r^3}-\frac{4z_j^4+r^4+5r^2 z_j^2}{3r^3\sqrt{r^2+z_j^2}}\right]\right)-\frac{Ps_3}{\pi a^2}[\,fe^{i\alpha}$$

$$\left(\frac{\sqrt{r^2+z_3^2}}{r}-\frac{\sqrt{l_{23}^2-a^2}}{r}\right)-\bar{f}\,e^{i3\alpha}\left[(12l_{23}^2-3r^2-16a^2)\frac{\sqrt{l_{23}^2-a^2}}{3r^3}+\frac{4a^2 z_3}{r^3}-\frac{4z_3^4+r^4+5r^2 z_3^2}{3r^3\sqrt{r^2+z_3^2}}\right]\Bigg]\Bigg\} \tag{2.1.22}$$

$$\sigma_z=\frac{P}{2\pi a^2(s_2-s_1)}\left(\bar{f}\,e^{i\alpha}+f\,e^{-i\alpha}\right)\sum_{j=1}^{2}(-1)^{j+1}\left(\frac{\sqrt{l_{2j}^2-a^2}}{r}-\frac{\sqrt{r^2+z_j^2}}{r}\right) \tag{2.1.23}$$

$$\tau_z=\frac{P}{2\pi a^2(s_2-s_1)}\sum_{j=1}^{2}(-1)^{j+1}\{f[\ln(l_{2j}+\sqrt{l_{2j}^2-r^2})-\ln\left(z_j+\sqrt{r^2+z_j^2}\right)]$$

$$+\bar{f}\, e^{i2\alpha}\left[\frac{\left(2a^2-l_{2j}^2\right)\sqrt{a^2-l_{1j}^2}}{ar^2}+\frac{z_j\sqrt{r^2+z_j^2}}{r^2}-\frac{a^2}{r^2}\right]\Bigg\}-\frac{P}{2\pi a^2}\Big\{f\left[\ln(l_{23}+\sqrt{l_{23}^2-r^2})-\ln\left(z_3+\sqrt{r^2+z_3^2}\right)\right]$$

$$-\bar{f}\, e^{i2\alpha}\left[\frac{\left(2a^2-l_{23}^2\right)\sqrt{a^2-l_{23}^2}}{ar^2}+\frac{z_3\sqrt{r^2+z_3^2}}{r^2}-\frac{a^2}{r^2}\right]\Bigg\} \tag{2.1.24}$$

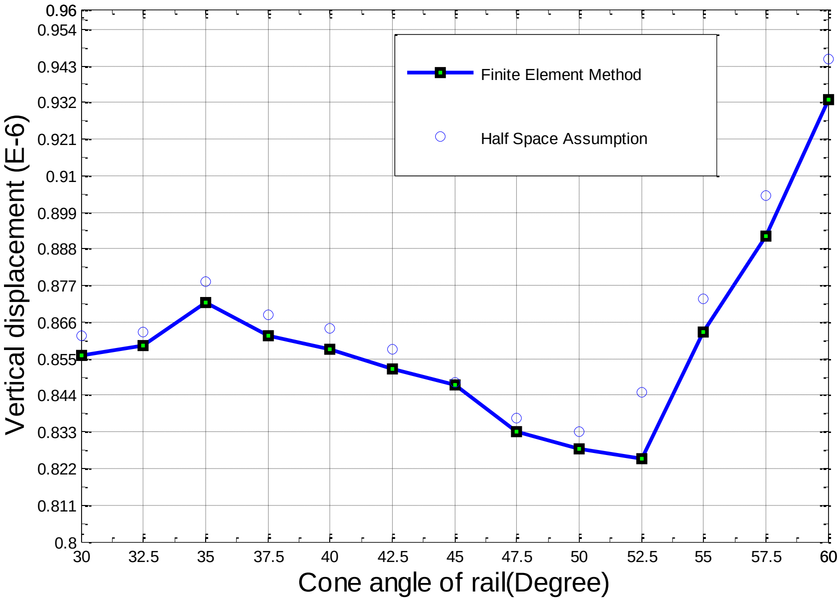

Fig. 2.2 Vertical Displacement variation of rail with different cone angles

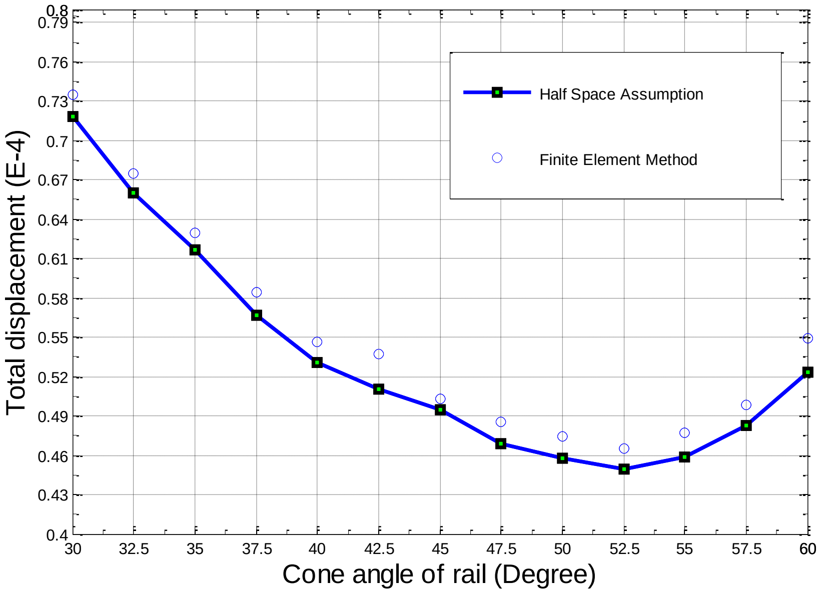

Fig. 2.3 Total Displacement variation of rail with different cone angles

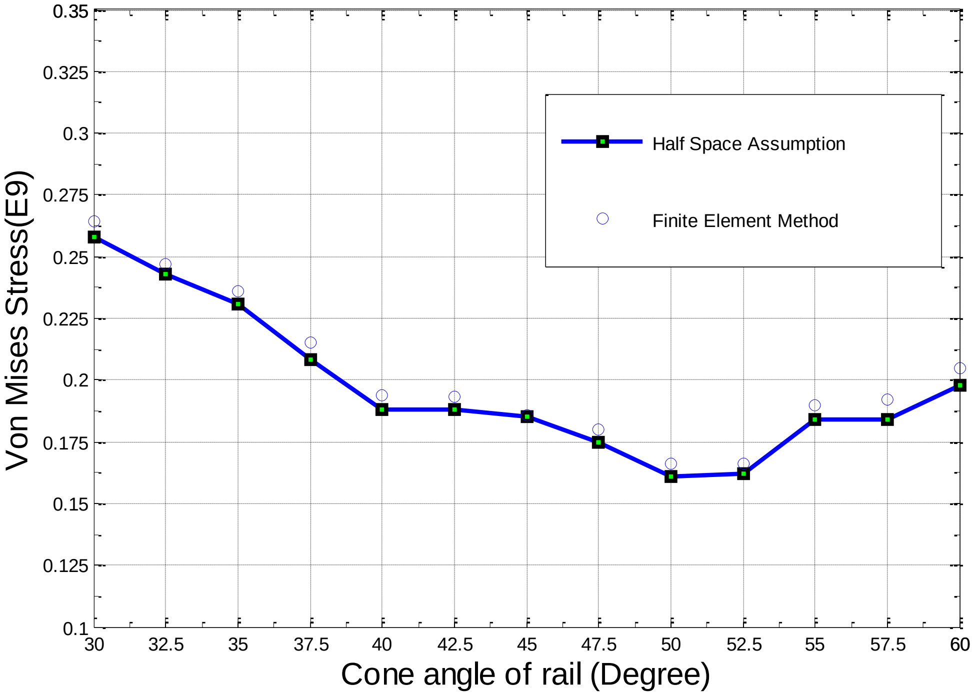

Fig. 2.4 Von Mises Stress variation of rail with different cone angles

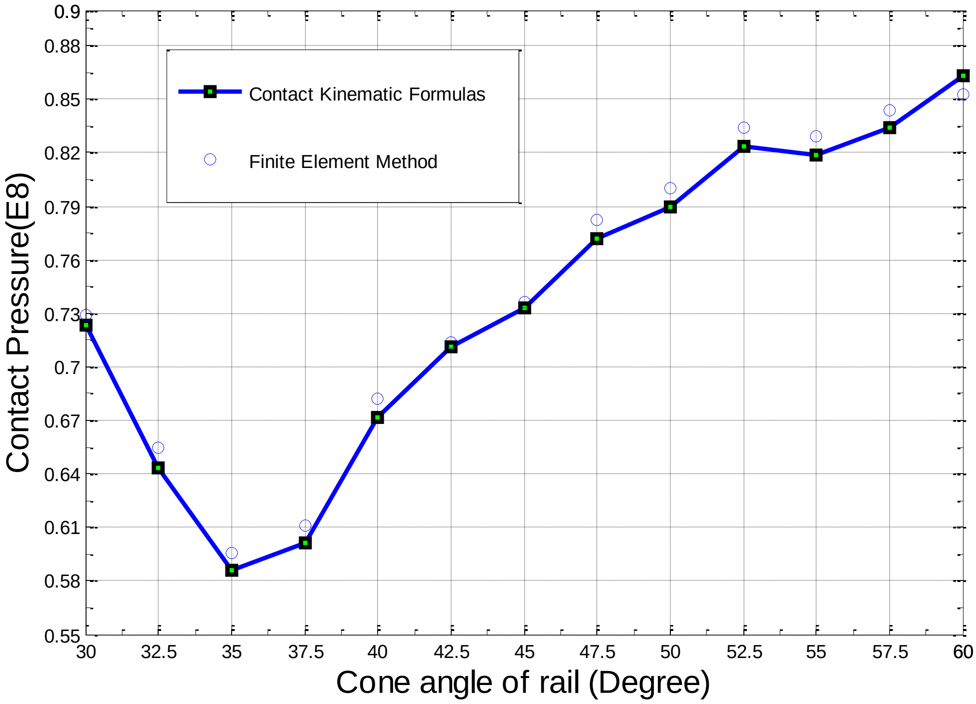

Fig. 2.5 Contact Pressure variation of rail with different cone angles

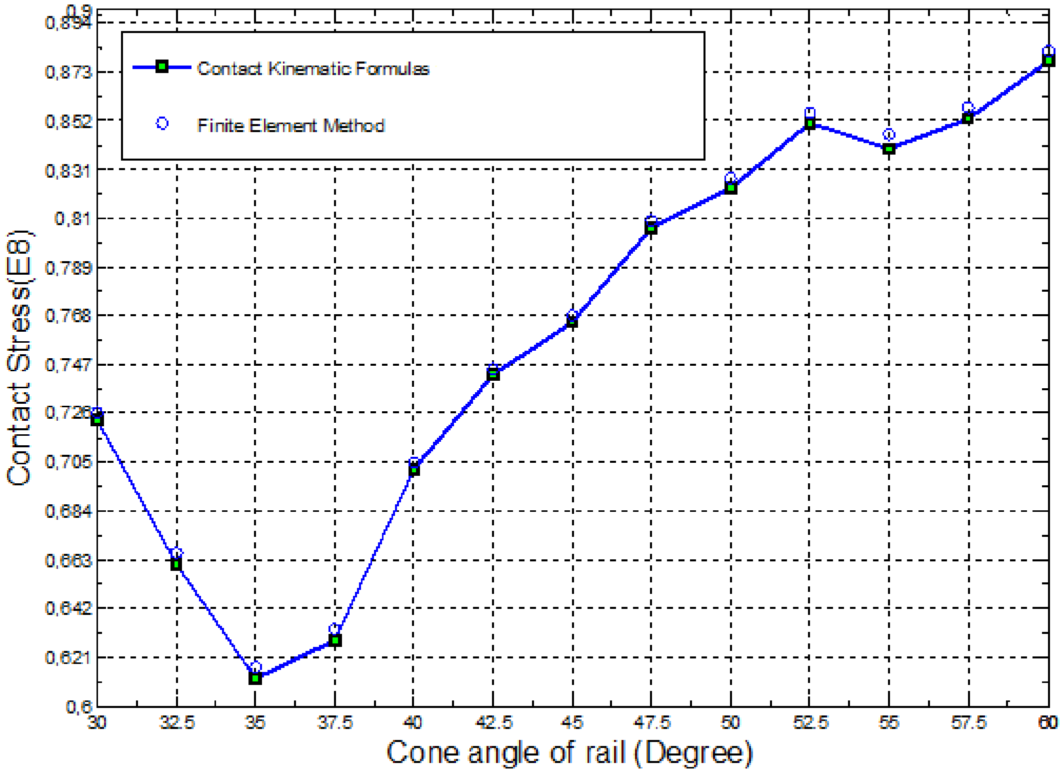

Fig. 2.6 Max. Contact Stress variation of rail with different cone angles

2.1.3 Conclusion

In this study, fem results of rail – wheel and the results of isotropic half space assumption has been examined. The fem results of the rail and wheel in assembly position are shown at the end of this study and given on the following page in the table 2.1. For both type of solution, different angles from 30 to 60 have been analyzed and it has been found that there is a good matching between the results obtained Isotropic Half Space Assumption and Finite Element Method. From the above figures, we can conclude that the following comments;

The vertical and total displacement results of rail found with fem and isotropic half space assumption gives good approximation on the rail angles between 30° and 50°.

Von Mises Stress results, found in found with fem and isotropic half space assumption, are nearly the same when the angle is 45°.

Contact Stress and Contact Pressure variation results found with fem and isotropic half space assumption, diverge between the angles at which from 30º to 40º converges from 40º to 50º and again starts to diverge from 50º to 60º. But at the cone angle of rail 45º, the most convergence values occur. However, it is appropriate for us to use 45º cone angle while designing a wheel.

FINITE ELEMENT RESULTS							
Cone Angle (Ø$_0$)	**Max. Vert. Displ. (E-6)**	**Max. Total Disp. (E-4)**	**Max. Von Mises Stress (E9)**	**Max. Cont. Press. e (E8)**	**Max. Cont Frict. Stress (E8)**	**Max. Cont. Total Stress (E8)**	**Max. Cont. Penetr. (E-5)**
30	0.856	0.718	0.258	0.723	0.217	0.723	0.396
32.5	0.859	0.660	0.243	0.643	0.189	0.661	0.339
35	0.872	0.617	0.231	0.586	0.172	0.612	0.288
37.5	0.862	0.567	0.208	0.601	0.180	0.628	0.314
40	0.858	0.531	0.188	0.672	0.201	0.702	0.327
42.5	0.852	0.510	0.188	0.711	0.212	0.743	0.357
45	0.847	0.495	0.185	0.733	0.220	0.765	0.387
47.5	0.833	0.469	0.175	0.772	0.229	0.806	0.395
50	0.828	0.458	0.161	0.790	0.226	0.823	0.420
52.5	0.825	0.449	0.162	0.824	0.205	0.851	0.430
55	0.863	0.459	0.184	0.819	0.187	0.840	0.444
57.5	0.892	0.483	0.184	0.834	0.179	0.853	0.464
60.	0.933	0.523	0.198	0.863	0.163	0.878	0.573

Table 2.1 Fem results of the Conical Contact System

2.2. WHEEL ANALYTICAL AND FEM RESULTS (45° ANGLE)

2.2.1 Wheel Contact Stress Results

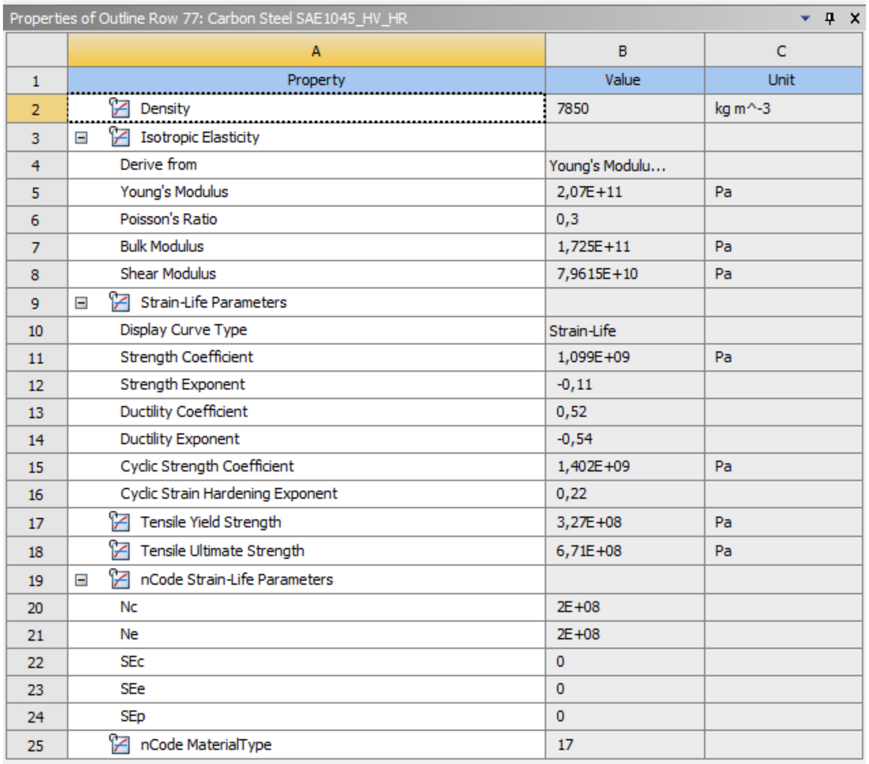

Properties of Outline Row 77: Carbon Steel SAE1045_HV_HR

	A	B	C
1	Property	Value	Unit
2	Density	7850	kg m^-3
3	Isotropic Elasticity		
4	Derive from	Young's Modulu...	
5	Young's Modulus	2,07E+11	Pa
6	Poisson's Ratio	0,3	
7	Bulk Modulus	1,725E+11	Pa
8	Shear Modulus	7,9615E+10	Pa
9	Strain-Life Parameters		
10	Display Curve Type	Strain-Life	
11	Strength Coefficient	1,099E+09	Pa
12	Strength Exponent	-0,11	
13	Ductility Coefficient	0,52	
14	Ductility Exponent	-0,54	
15	Cyclic Strength Coefficient	1,402E+09	Pa
16	Cyclic Strain Hardening Exponent	0,22	
17	Tensile Yield Strength	3,27E+08	Pa
18	Tensile Ultimate Strength	6,71E+08	Pa
19	nCode Strain-Life Parameters		
20	Nc	2E+08	
21	Ne	2E+08	
22	SEc	0	
23	SEe	0	
24	SEp	0	
25	nCode MaterialType	17	

Table. 2.2 Wheel material properties (Ansys ncode Material Library)

The contact-patch geometry, material constants, patch half-width, geometry const. and average and maximum contact pressures, principal stresses in the contact zone, tangential pressure and applied stress components can be calculated from Hertzian Contact Eq.s(See Hertzian Contact Eq.s) as follows;

The material constants;

$$m_1 = \frac{1-\nu_1^2}{E_1} = \frac{1-0,33^2}{68,9E9} = 1,24E-11$$

$$m_2 = \frac{1-\nu_2^2}{E_2} = \frac{1-0,3^2}{207E9} = 4,4E-12$$

Since our wheel contact region is conical, we should integrate the geometry const eq.

$$R_1 = \left(\frac{d_o - d_i}{2}\right)\left(h\,dr\right) = \left(\frac{100-55}{4}\right)\left(22,5+r\right) = \left(253,125+11,25r\right)$$

$$dB = \frac{1}{2\,dR_1} \Rightarrow \int_0^B dB = \frac{1}{2\int_{r_1}^{r_2}\left(253,125+11,25r\right)}$$

$$B = \frac{1}{2(253,125r + \frac{11,25}{2}r^2)\Big|_{r_1}^{r_2}} = \frac{1}{(506,25r + 11,25r^2)\Big|_{27,5}^{50}}$$

$$= \frac{1}{\left[506,25(0,05-0,0275)+11,25\left(0,05^2-0,0275^2\right)\right]} = 0,0876$$

The patch half-width can be calculated as,

$$a = \sqrt{\frac{2}{\pi}\,\frac{m_1+m_2}{B}\,\frac{F}{L}} = \sqrt{\frac{2}{\pi}\,\frac{((1,24E-11)+(4,4E-12))}{0,0876}\,\frac{(500x9,81/(2x\sin 45))}{0,03182}} = 3,65E-3$$

where a is the half-width of the contact patch. The rectangular contact-patch area is
then;

$$Area = 2\,x\,a\,x\,L = 2\,x\,3,65E-3\,x\,0,03182 = 2,32E-4$$

The average and maximum contact pressures can be found,

$$P_{avg} = \frac{F}{Area} = \frac{3468,36}{2.32E-4} = 14,95Mpa$$

$$p_{\max} = \frac{2\,x\,F}{\pi\,a\,L} = \frac{2\,x\,3468,36}{\pi\,x\,3,65E-3\,x\,0,03182} = 19,1Mpa$$

The tangential pressure is found,

$$f_{\max} = \mu\, p_{\max} = 0,3x19,1 = 5,7\, Mpa$$

With μ = 0.3, the principal stresses in the contact zone will be maximal on the surface (z = 0) at x = 0.3a from the centerline. The applied stress components can be found in tems of both the normal force the tangential forces as follows,

$$\sigma_{xn} = -p_{\max}\sqrt{1-\frac{x^2}{a^2}} = -p_{\max}\sqrt{1-\frac{(0,3a)^2}{a^2}} = -19,1x\sqrt{1-\frac{(0,3a)^2}{a^2}} = -18,22Mpa$$

$$\sigma_{xt} = -2 f_{\max}\frac{x}{a} = -2 f_{\max}\frac{0,3a}{a} = -0,6\, f_{\max} = -0,6x5,7 = -3,42\, Mpa$$

$$\sigma_{zn} = -p_{\max}\sqrt{1-\frac{x^2}{a^2}} = -p_{\max}\sqrt{1-\frac{(0,3a)^2}{a^2}} = -19,1x\sqrt{1-\frac{(0,3a)^2}{a^2}} = -18,22\, Mpa$$

$$\sigma_{zt} = 0 \qquad\qquad \tau_{xz_n} = 0$$

$$\tau_{xz_t} = -f_{\max}\sqrt{1-\frac{x^2}{a^2}} = -f_{\max}\sqrt{1-\frac{(0,3a)^2}{a^2}} = -5,7\sqrt{1-\frac{(0,3a)^2}{a^2}} = -5,44Mpa$$

Then we can solve for the total applied stresses along the x, y, and z axes.

$$\sigma_x = \sigma_{xn} + \sigma_{xt} = -18,22 - 3,44 = -21,66Mpa$$

$$\sigma_z = \sigma_{zn} + \sigma_{zt} = -18,22 + 0 = -18,22Mpa$$

$$\tau_{xz} = \tau_{xz_n} + \tau_{xz_t} = 0 - 5,44 = -5,44Mpa$$

Since the rollers are long, we expect a plane strain condition to exist. The stress in the third dimension is found from elasticity equations,

$$\sigma_y = \nu\left(\sigma_x + \sigma_z\right) = 0,3(-21,66 - 18,22) = -11,96$$

Unlike the pure rolling case, these stresses are not principal because of the applied shear stress. The principal stresses can be found by using a cubic root-finding solution as -11.96 Mpa, -14.225 Mpa and -25.655 Mpa. By using Tresca and Von-Mises yield equations; Tresca and Von Mises stresses have been found as 6.8475 Mpa and 12.72 Mpa respectively.

2.2.2 Wheel Fem Results

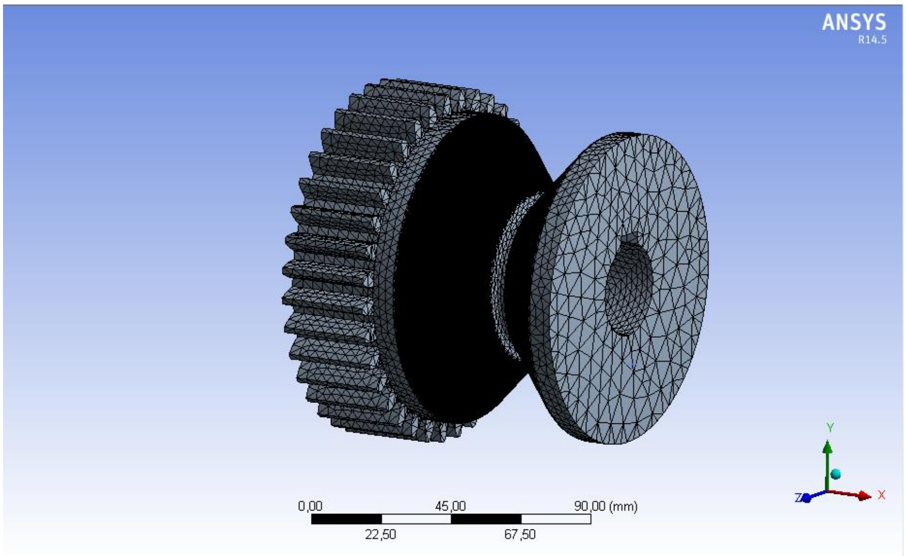
ANSYS
R14.5
0,00
45,00
90,00 (mm)
22,50
67,50
Y
Z
X

Fig. 2.7 Mesh view of the wheel

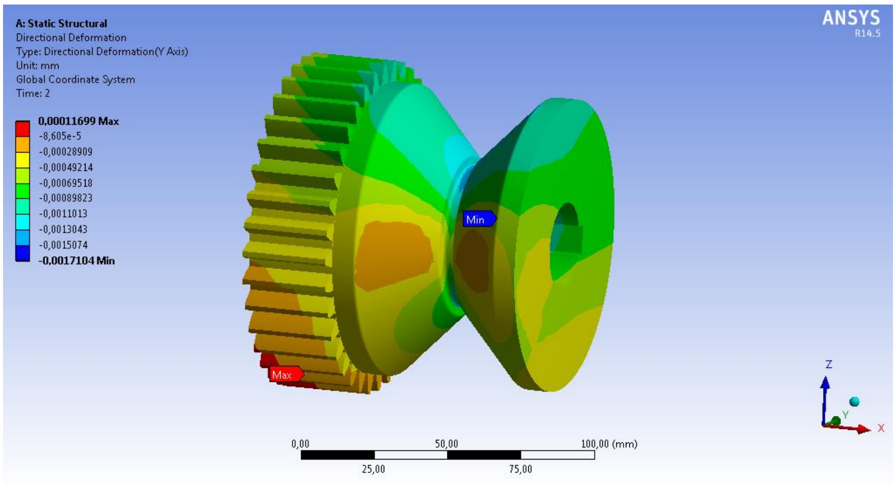
A: Static Structural
Directional Deformation
Type: Directional Deformation(Y Axis)
Unit: mm
Global Coordinate System
Time: 2
0,00011699 Max
-8,605e-5
-0,00028909
-0,00049214
-0,00069518
-0,00089823
-0,0011013
-0,0013043
-0,0015074
-0,0017104 Min
ANSYS
R14.5
Min
Max
0,00
50,00
100,00 (mm)
25,00
75,00
Z
Y
X

Fig. 2.8 Directional deformation distribution of the wheel

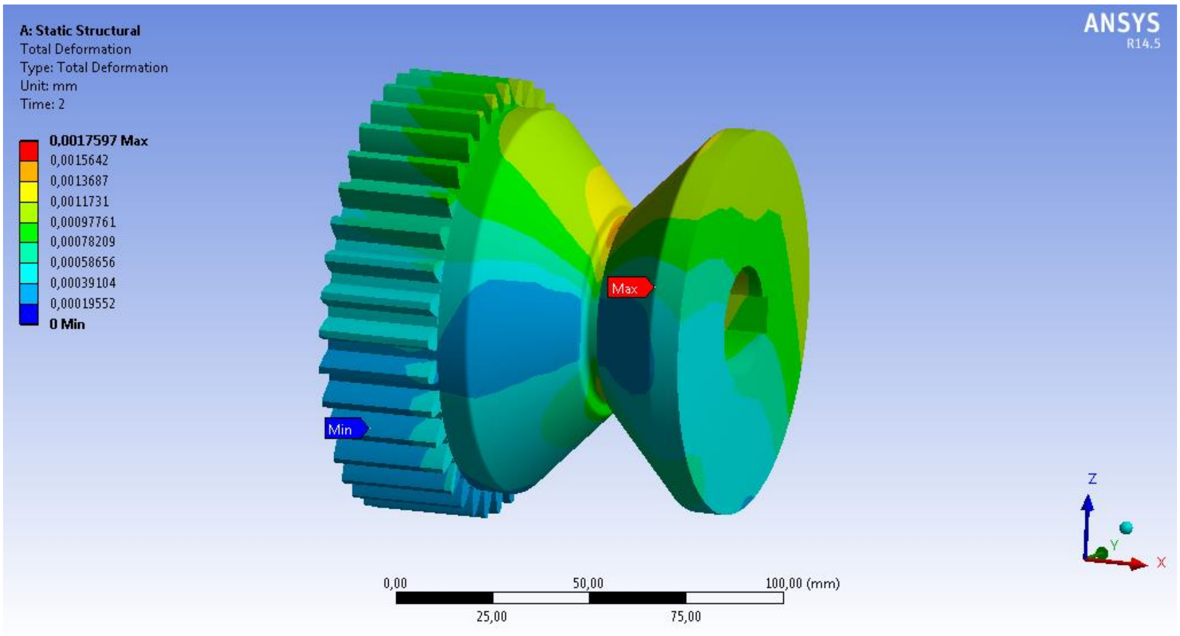
A: Static Structural
Total Deformation
Type: Total Deformation
Unit: mm
Time: 2
0,0017597 Max
0,0015642
0,0013687
0,0011731
0,00097761
0,00078209
0,00058656
0,00039104
0,00019552
0 Min
ANSYS
R14.5
Max
Min
Z
Y
X
0,00
50,00
100,00 (mm)
25,00
75,00

Fig. 2.9 Total deformation distribution of the wheel

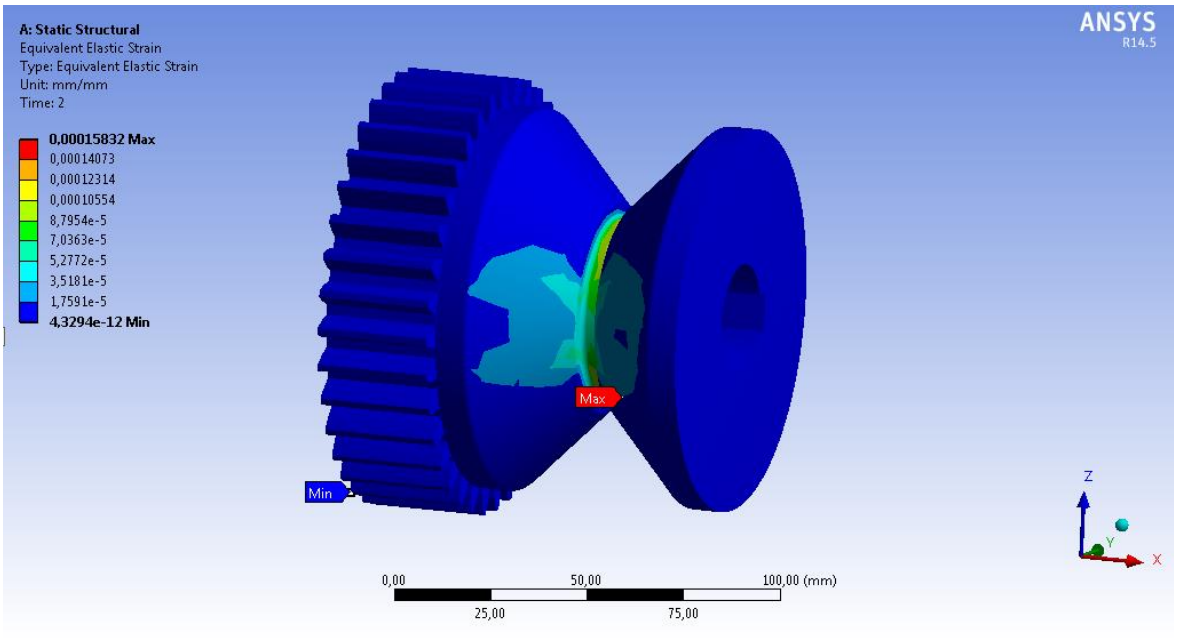
A: Static Structural
Equivalent Elastic Strain
Type: Equivalent Elastic Strain
Unit: mm/mm
Time: 2
0,00015832 Max
0,00014073
0,00012314
0,00010554
8,7954e-5
7,0363e-5
5,2772e-5
3,5181e-5
1,7591e-5
4,3294e-12 Min
ANSYS
R14.5
Max
Min
Z
Y
X
0,00
50,00
100,00 (mm)
25,00
75,00

Fig. 2.10 Equivalent elastic strain distribution of the wheel

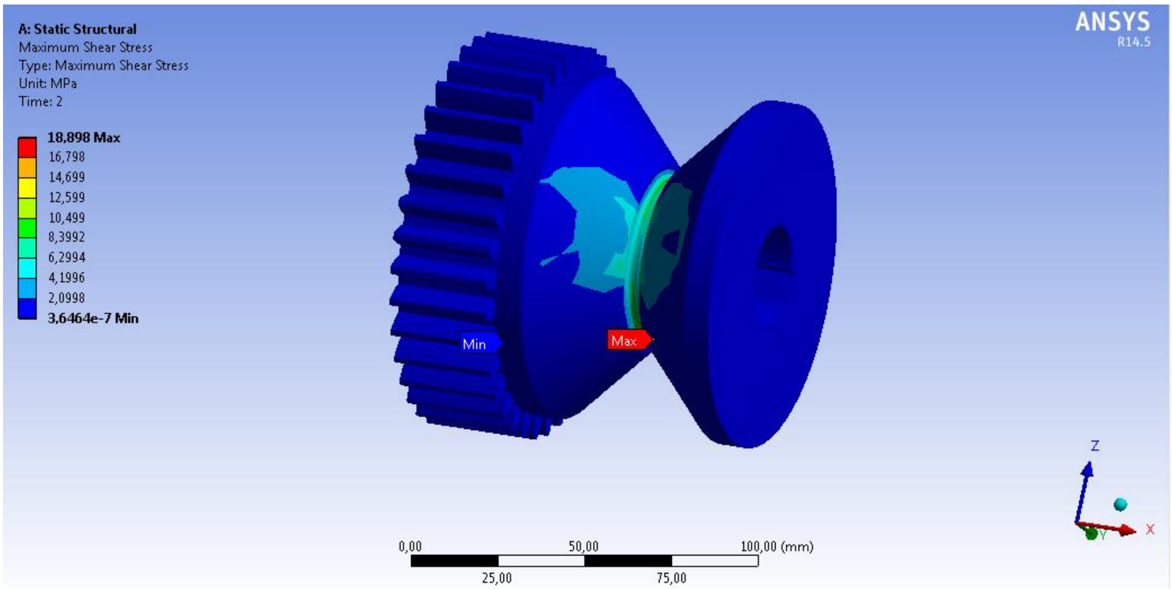
A: Static Structural
Maximum Shear Stress
Type: Maximum Shear Stress
Unit: MPa
Time: 2
18,898 Max
16,798
14,699
12,599
10,499
8,3992
6,2994
4,1996
2,0998
3,6464e-7 Min
ANSYS
R14.5
Min
Max
0,00
50,00
100,00 (mm)
25,00
75,00
Z
Y
X

Fig. 2.11 Maximum Shear Stress distribution of the wheel

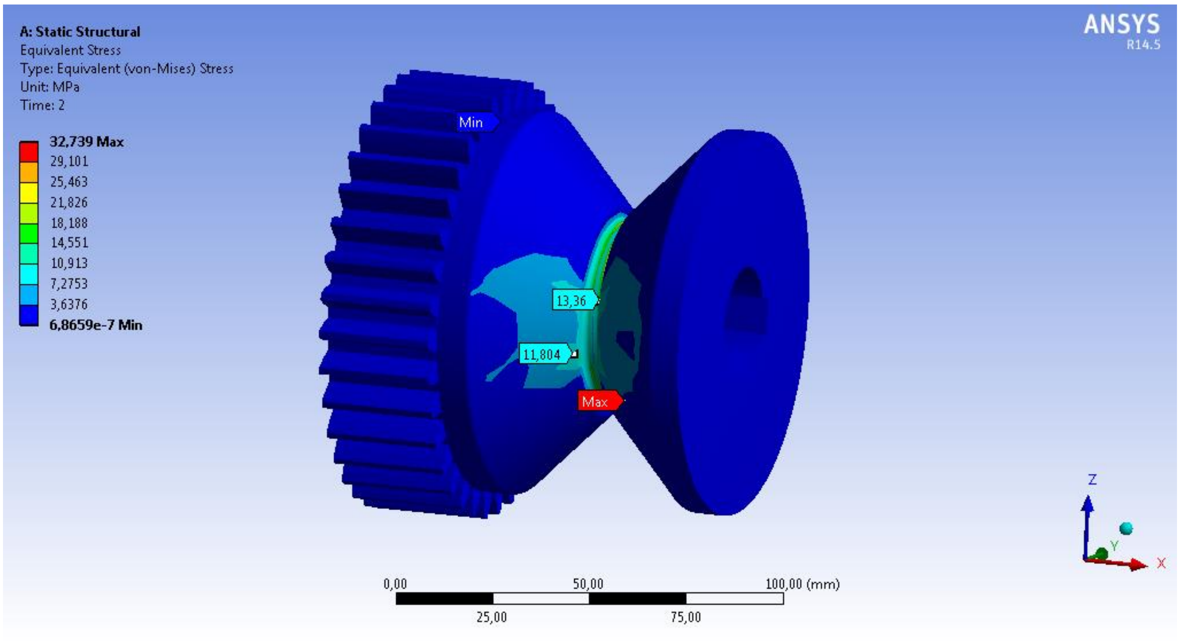
A: Static Structural
Equivalent Stress
Type: Equivalent (von-Mises) Stress
Unit: MPa
Time: 2
32,739 Max
29,101
25,463
21,826
18,188
14,551
10,913
7,2753
3,6376
6,8659e-7 Min
ANSYS
R14.5
Min
13,36
11,804
Max
0,00
50,00
100,00 (mm)
25,00
75,00
Z
Y
X

Fig. 2.12 Von Mises Stress distribution of the wheel

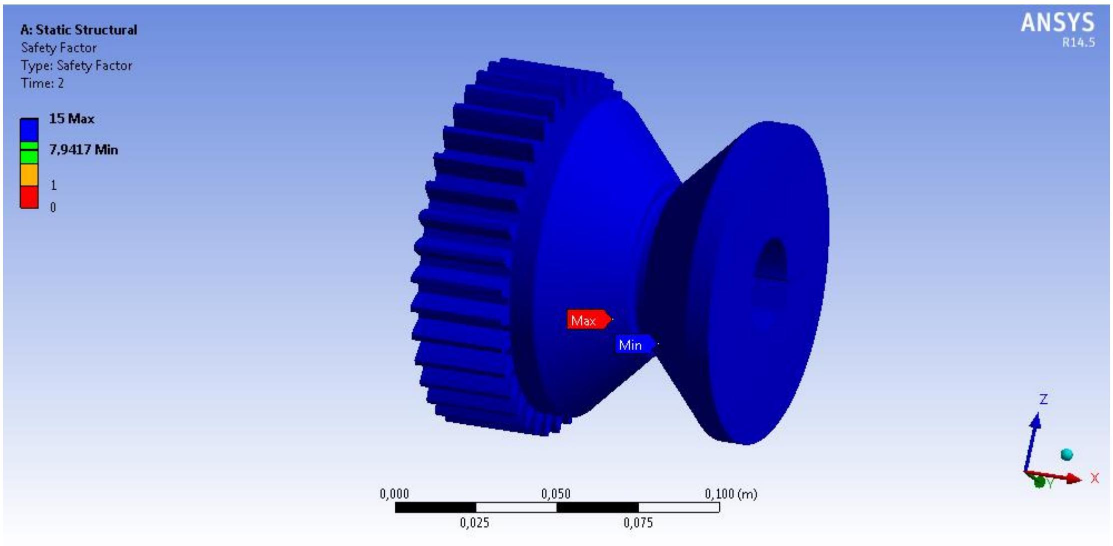
A: Static Structural
Safety Factor
Type: Safety Factor
Time: 2
15 Max
7,9417 Min
1
0
ANSYS
R14.5
Max
Min
0,000
0,050
0,100 (m)
0,025
0,075
Z
Y
X

Fig. 2.13 Safety factor of the wheel

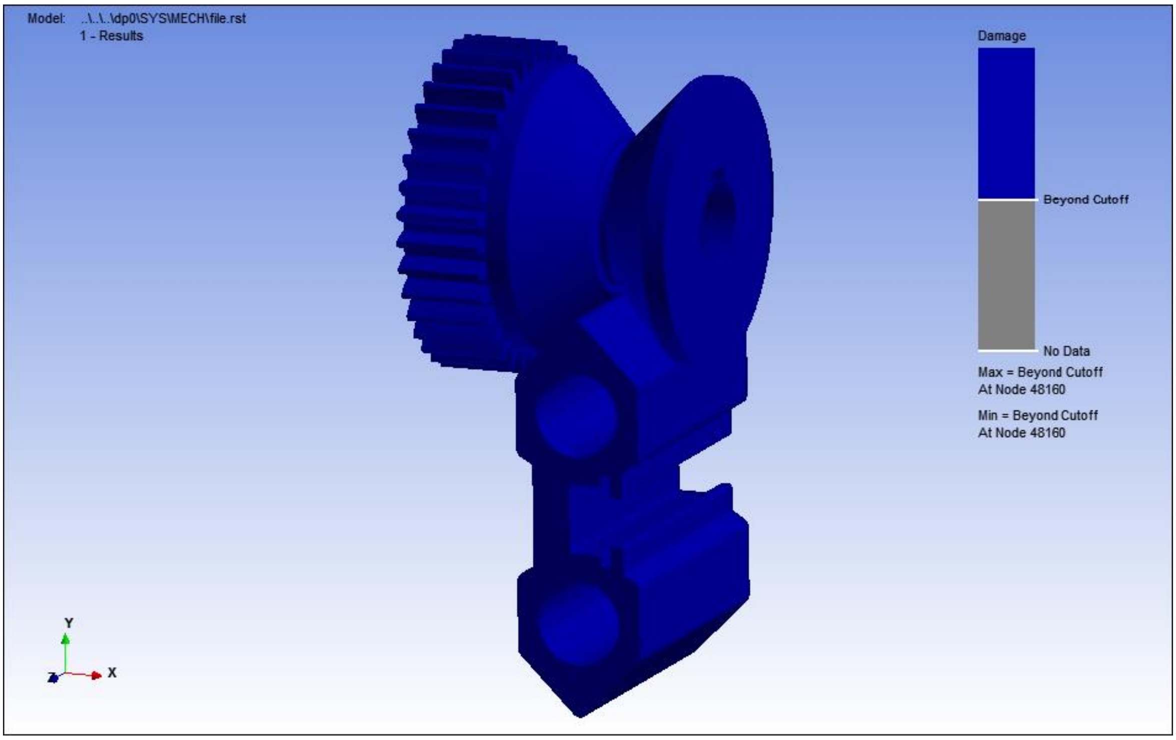
Model: ..\..\..\dp0\SYS\MECH\file.rst
1 - Results
Damage
Beyond Cutoff
No Data
Max = Beyond Cutoff
At Node 48160
Min = Beyond Cutoff
At Node 48160
Y
Z
X

Fig. 2.14 Damage distribution of the wheel

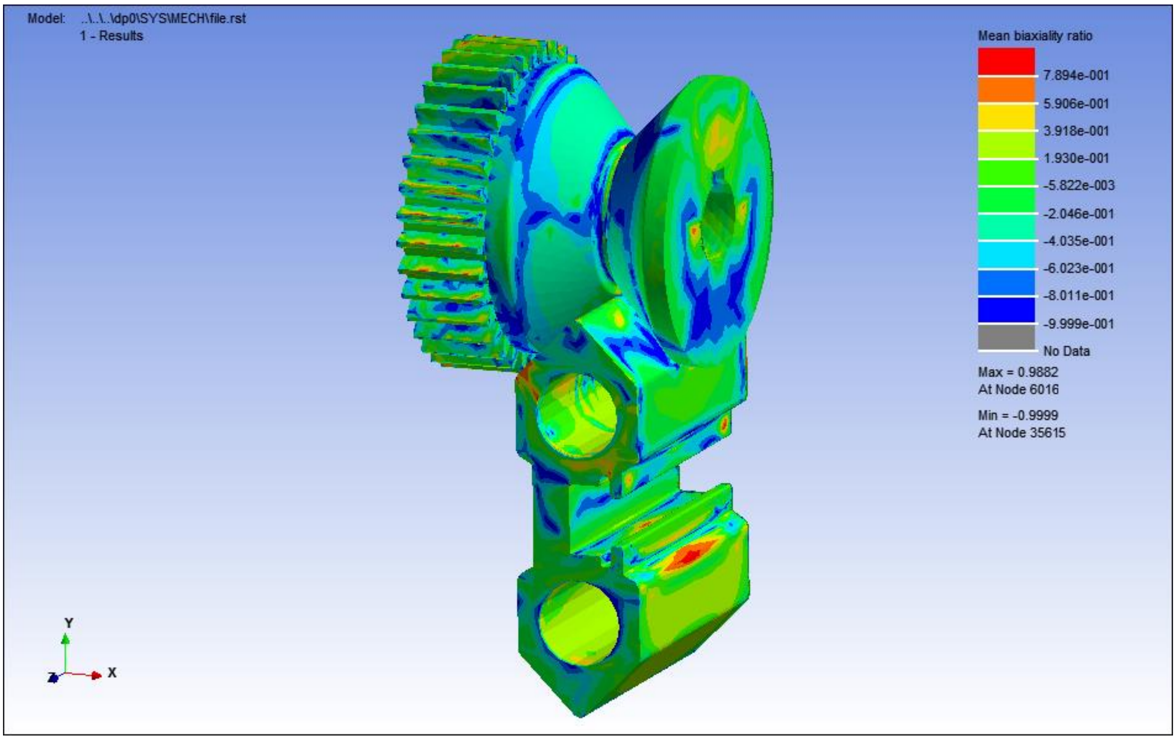
Model: ..\..\..\dp0\SYS\MECH\file.rst
1 - Results
Mean biaxiality ratio
7.894e-001
5.906e-001
3.918e-001
1.930e-001
-5.822e-003
-2.046e-001
-4.035e-001
-6.023e-001
-8.011e-001
-9.999e-001
No Data
Max = 0.9882
At Node 6016
Min = -0.9999
At Node 35615
Y
Z
X

Fig. 2.15 Mean biaxiliaty of the wheel

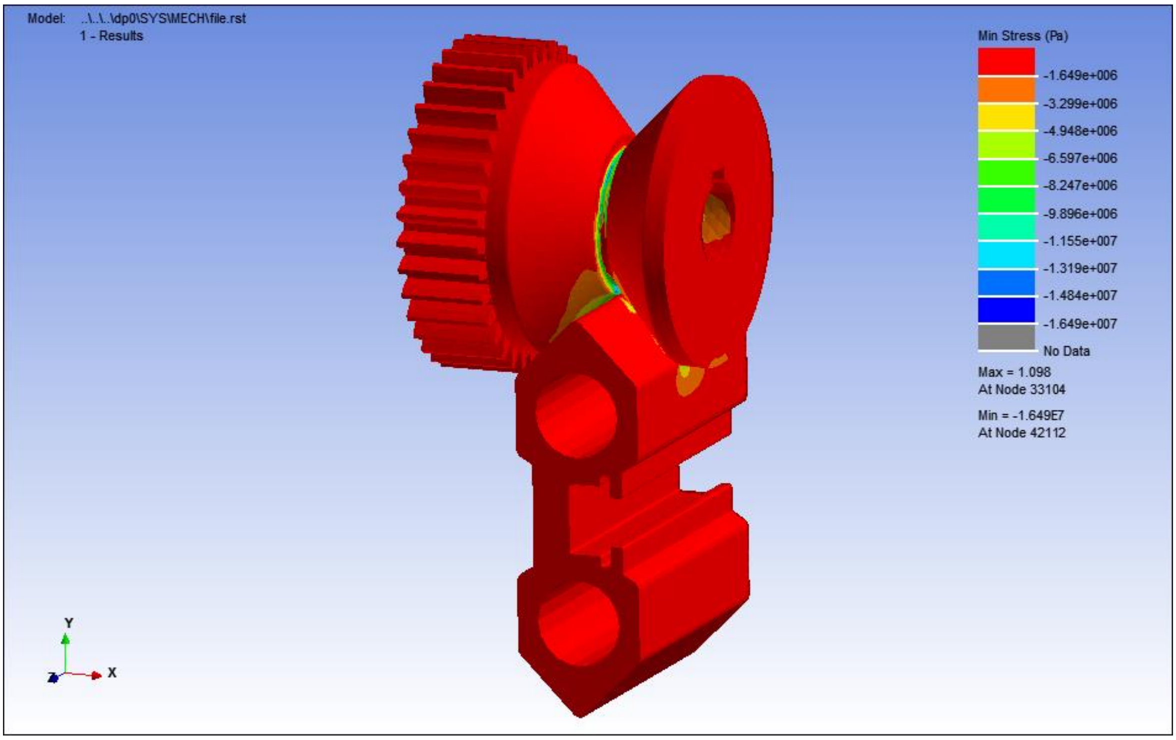
Model: ..\..\..\dp0\SYS\MECH\file.rst
1 - Results
Min Stress (Pa)
-1.649e+006
-3.299e+006
-4.948e+006
-6.597e+006
-8.247e+006
-9.896e+006
-1.155e+007
-1.319e+007
-1.484e+007
-1.649e+007
No Data
Max = 1.098
At Node 33104
Min = -1.649E7
At Node 42112
Y
Z
X

Fig. 2.16 Min. stress distribution of the wheel

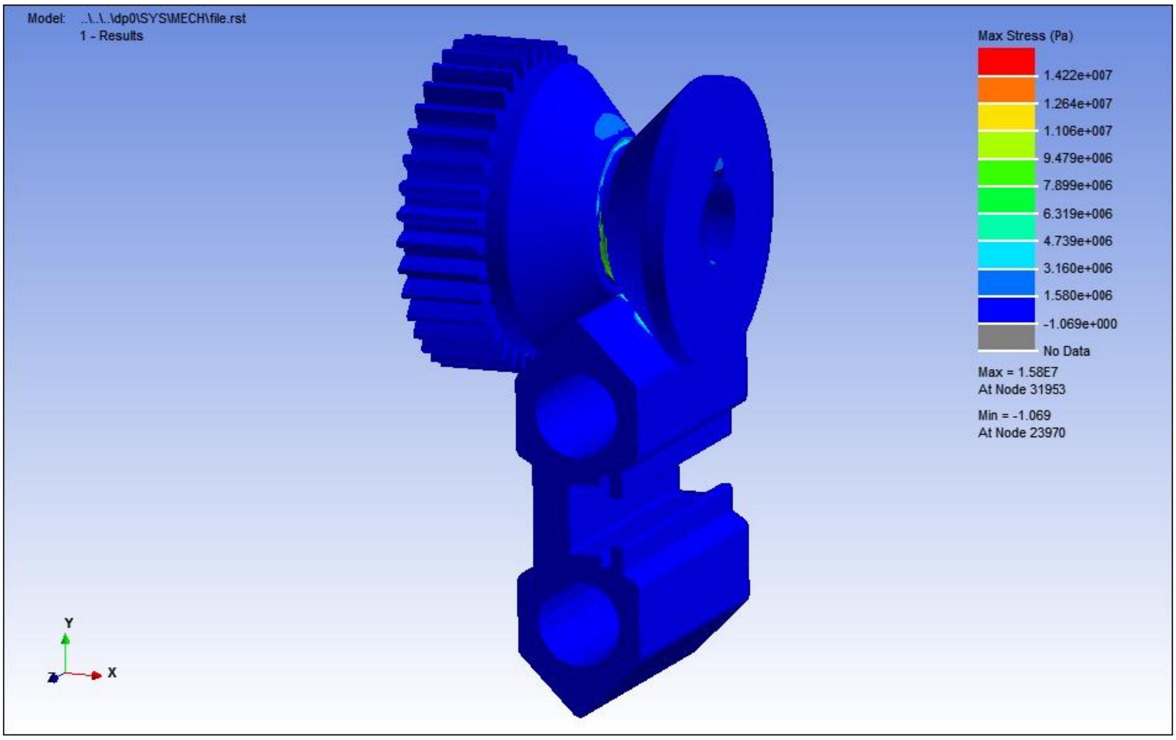
Model: ..\..\..\dp0\SYS\MECH\file.rst
1 - Results
Max Stress (Pa)
1.422e+007
1.264e+007
1.106e+007
9.479e+006
7.899e+006
6.319e+006
4.739e+006
3.160e+006
1.580e+006
-1.069e+000
No Data
Max = 1.58E7
At Node 31953
Min = -1.069
At Node 23970
Y
X
Z

Fig. 2.17 Max. stress distribution of the wheel

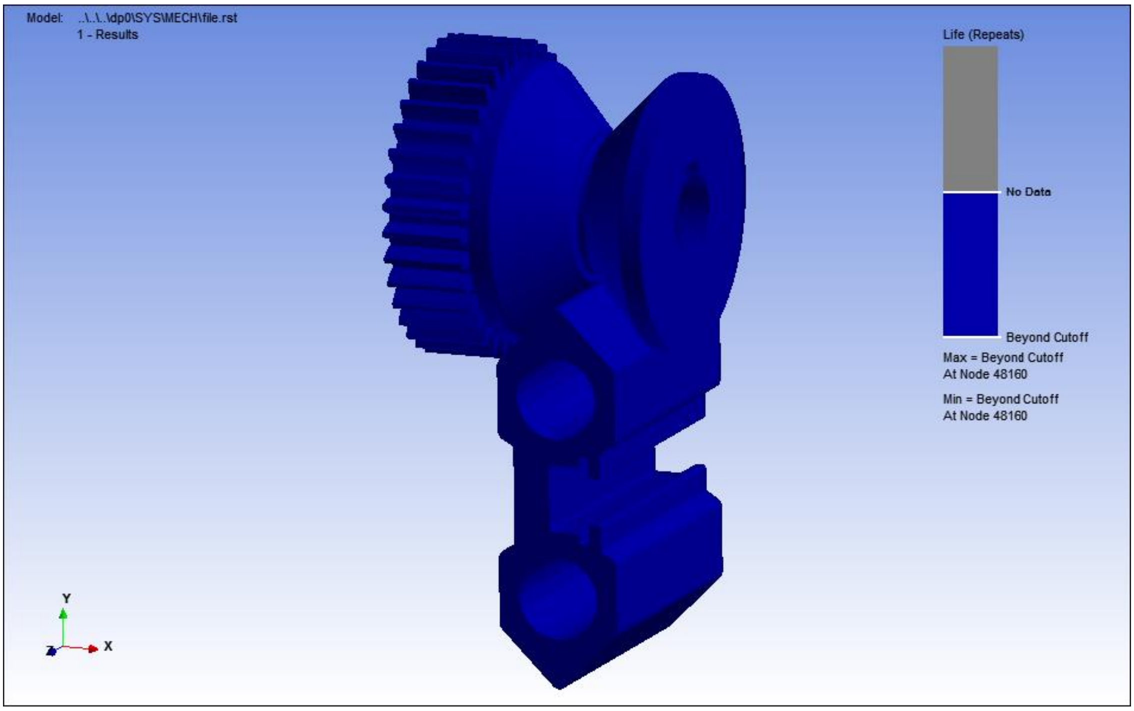
Model: ..\..\..\dp0\SYS\MECH\file.rst
1 - Results
Life (Repeats)
No Data
Beyond Cutoff
Max = Beyond Cutoff
At Node 48160
Min = Beyond Cutoff
At Node 48160
Y
X
Z

Fig. 2.18 Life of the wheel

2.2.3 Conclusion

In this study, a wheel having an angle of 45˚ has been examined. The hertz contact equations have been used to be able to estimate Von Mises stresses occurring on the wheel, assuming plane strain condition. By using fem, it has been found that Max. Von Mises stresses occurs in the middle of region of the wheel as 32, 739 Mpa. On the surface of the wheel, the Von Mises Stress have been found as 11,804 Mpa. Compared to the Von Mises Stresses found by hertz contact equations and fem a good matching have been observed.

Fatigue calculations of wheel have been calculated by fem-Ansys ncode. While the wheel moves on the rail, fluctuating stresses occur and therefore Constant amplitude, Proportional loading criteria have been considered.

Mean Biaxiliaty values have been found greater than 1 means that pure biaxial stress state occurs and smaller than -1 means that pure shear occurs on the wheel.

Damage and life results have been found by Ansys-ncode as Beyond Cutoff which means that wheel has infinite life. These results are very important in terms of fatigue calculations of any material in engineering applications.

3. BEAMS

3.1 Introduction

In general, beams are used in many structural applications. Any structural member exposed to loads transverse to its length behave as a beam. Some examples of beams are rails, machinery shafts, springs, and frames, which they may be under the influence of normal and shear stresses. For this reason, it is pivotal for enginneers to estimate how those stresses distribute within beams to be able to predict the right locations of the estimation of maximum stresses. In many applications beams are subjected to bending stresses, shear stresses or combination of those stresses.

3.2 Rail Materials

In this monorail crane design, the material used for rail is an aluminum alloy. The reason why aluminum material chosen in this study because aluminum can be easily extruded and extrusion is a basic manufacturing type that allows to produce inexpensive shapes of rails. Aluminum is produced in both “pure” and alloyed forms. The most common alloying elements used in aluminums are copper, silicon, magnesium, manganese, and zinc. There are many advantages of aluminum but the main advantages of aluminum are its low density, ductility, excellent workability, castability, and weldability, corrosion resistance, high conductivity, and reasonable cost. Compared to steel it is 1/3 as dense, about 1/3 as stiff, and generally less strong and compared in terms of the strengths of low-carbon steels and pure aluminum, the steel is about three times as strong. However, pure aluminum is rarely used in engineering applications because aluminum alloys provides us better specifications. For example aluminum is not only too soft but also weak. Besides those specifications, aluminum alloys have significantly greater strengths than pure aluminum.

The higher-strength aluminum alloys have tensile strengths in the 480 to 620 MPa range, and compared to yield strengths with mild steel strengths they are twice of mild steels. (See Mechanical Enginnering Design, R. G. Budynas and J. Keith Nisbett).

Aluminum competes successfully with steel in some applications, though few materials can beat steel if very high strength is needed. (See Fig. 3.2.1 for tensile strengths of some aluminum alloys). Fig. 3.2.2 shows tensile-test engineering stress-strain curves for three aluminum alloys. Aluminum's strength is reduced at low temperatures as well as at elevated temperatures. Hardenable property of some aluminum alloys can be increased by heat treatment, strain hardening or precipitation and aging.

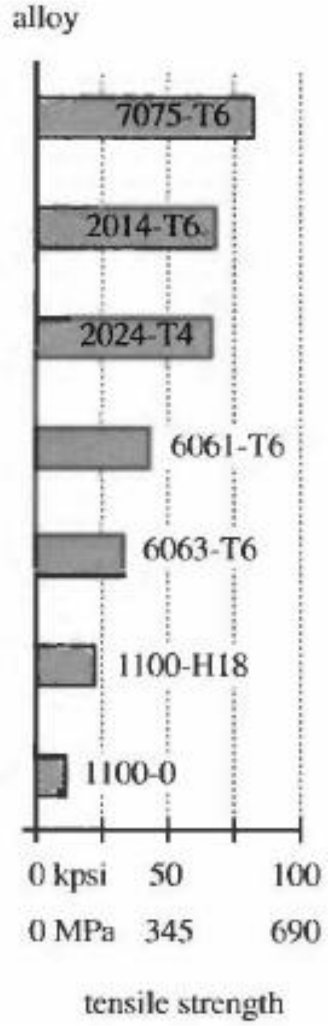

Fig. 3.2.1 Ultimate Tensile Strengths of Some Aluminum Alloys (From Fig. 2.20, p. 56, in Robert L. Norton, Machine Design,*)*

Aluminum alloys having high-strength are about 1.5 times harder than soft steel. With making good surface treatments such as *hard anodizing* can make the surface more harder than the hardest steel.

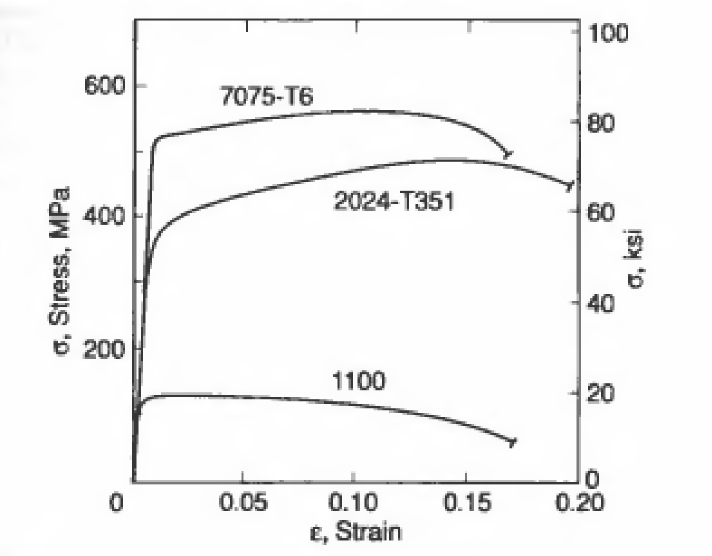

Fig. 3.2.2 Tensile Test Stress-Strain Curves of Three Aluminum Alloys (From Fig. 5.17, p. 160, in N. E. Dowling, *Mechanical Behavior of Materials,* Prentice-Hall, Englewood Cliffs, NJ., 1993)

In enginnering materials, aluminum is among the most easily worked, though it tends to work harden. Castability, machinebility, weldability, hot and cold formability of aluminums are good compared to many materials. In generally, aluminum alloys are classifed as either wrought or cast. Wrought aluminum alloys are produced with different shapes such as I-beams, angles, channels, bars, strip, sheet, rounds, and tubes.

“The Aluminum Association numbering system for alloys is shown in Table 3.1. The first digit indicates the principal alloying element and defines the series. Hardness is indicated by a suffix containing a letter and up to 3 numbers as defined in the table. The most commonly available and most-used aluminum alloys in machine-design applications are the 2000 and 6000 series.

The oldest aluminum alloy is 2024, which contains 4.5% copper, 1.5% magnesium, and 0.8% manganese. It is among the most machinable of the aluminum alloys and is heat treatable. In the higher tempers, such as -T3 and -T4, it has a tensile strength approaching 483 MPa, which also makes it one of the strongest of the aluminum alloys. It also has high fatigue strength. However, it has poor weldability and formability compared to the other aluminum alloys.

The 6061 alloy, used in the rails of monorail crane machine, contains 0.6% silicon, 0.27% copper, 1.0% manganese, and 0.2% chromium. “The aluminum 6061 alloys are widely used in structural applications because of its excellent weldability. Its strength is about 276 to 310 MPa in the higher tempers. It has lower fatigue strength than 2024 aluminum. It is easily machined and is a popular alloy for extrusion, which is a hot-forming process. The 7000 series is called aircraft aluminum and is used mostly in airframes. These are the strongest alloys of aluminum with tensile strengths up to 676 MPa and the highest fatigue strength of about 152 MPa@10^8 cycles. “(Richard G. Budynas & J. Keith Nisbett, Advanced Strength and Applied Stress Analysis, McGraw-Hill, 2006)

Table 3.1 Aluminum Association Designations of Aluminum Alloys

Series	Major Alloying Elements	Secondary Alloys
1xxx	Commercially pure (99%)	None
2xxx	Copper (Cu)	Mg, Mn, Si
3 xxx	Manganese (Mn)	Mg, Cu
4xxx	Silicon (Si)	None
5xxx	Magnesium (Mg)	Mn, Cr
6xxx	Magnesium and Silicon	Cu, Mn
7xxx	Zinc (Zn)	Mg, Cu, Cr
Hardness Designations		
xxxx-F	As fabricated	
xxxx-O	Annealed	
xxxx-Hyyy	Work hardened	
xxxx-Tyyy	Thermal/age hardened	

3.3 RAIL DESIGN AND FEM RESULTS

3.3.1 Horizontal Rail

While the wheel of monorail crane machine moves or climbs on rails, a contact area occurs between the rail and wheel. For this reason, we need to estimate the shape of this area in terms of contact mechanics. The difference between the classical mechanics and contact mechanics is the first one deals solely with bulk material properties, while the second one deals with bulk properties that consider surface and geometrical constraints. When two bodies having curved surfaces, as it is in rail and wheel, the stresses developed in the two bodies are threedimensional. Contact-stress problems arise in the contact of a wheel and a rail, in automotive valve cams and tappets, in mating gear teeth, and in the action of rolling bearings. Typical failures occuring by contact stresses are cracks, pits, or flaking in the surface of materials.

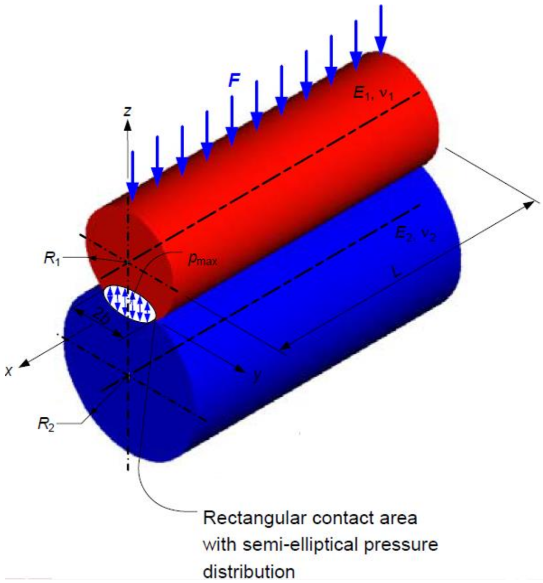

Rectangular contact area
with semi-elliptical pressure
distribution

Fig. 3.3.1 Two right circular cylinders held in contact by forces *F* uniformly distributed along cylinder length *l* and contact stress has an elliptical distribution across the contact zone width 2*b*. (Machine Design, Robert L. Norton)

The most general case of contact stress occurs when each contacting body has a double radius of curvature, that is, when the radius in the plane of rolling is different from the radius in a perpendicular plane, both planes taken through the axis of the contacting force. The equations for the area of contact, deformation, pressure distribution, and contact stresses on the centerline of two bodies with static loading were originally derived by Hertz in 1881. The presence of tangential sliding forces has a significant effect on the stresses compared to pure rolling. Figure 3.3.1 shows two cylinders of length *l* and diameters d_1 and d_2, the area of contact is a narrow rectangle of width 2*b* and length *l*, and the pressure distribution is elliptical. The half-width *b* is given by the following equation

$$b = \sqrt{\frac{2F}{\pi l} x \frac{\left(1-\nu_1^2\right)/E_1 + \left(1-\nu_2^2\right)/E_1}{1/d_1 + 1/d_2}}$$

The maximum pressure is; $p_{\max} = \dfrac{2F}{\pi b l}$

The equations above for two cylinders in contact are also valid for the following contact conditions.

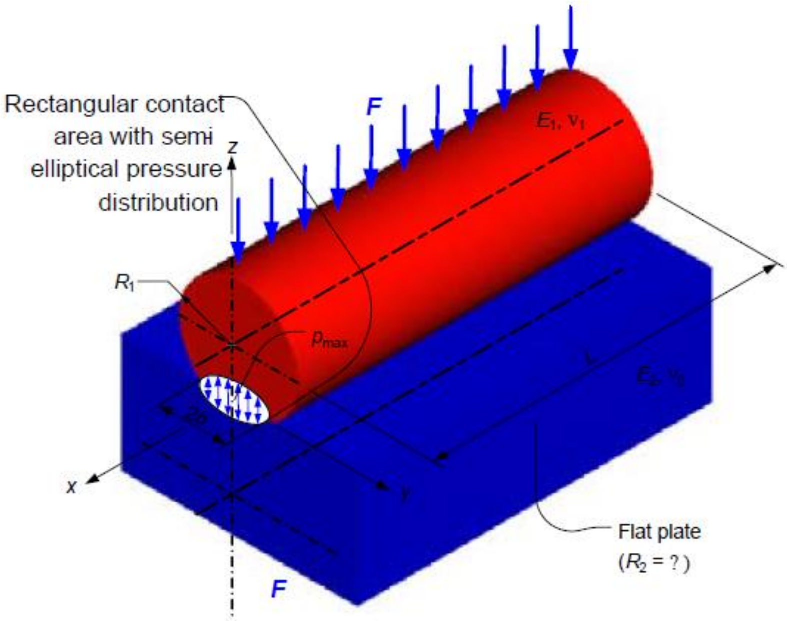

Fig. 3.3.2 Cylinder on a flat plate; a flat plate is a cylinder with an infinitely large radius (Machine Design, Robert L. Norton)

Since the rail and wheel contact condition is the same cylinder – flat plate contact condition, we can calculate the radius of ellipse on the rail as following;

$$b=\sqrt{\frac{2x2950}{\pi\left(27{,}577/1000\right)}\left[\frac{\left[\left(1-0{,}33^{2}\right)/68{,}9x10^{9}\right]+\left[\left(1-0{,}3^{2}\right)/200x10^{9}\right]}{\frac{1}{0{,}1}+\frac{1}{\infty}}\right]}=0{,}346\,mm$$

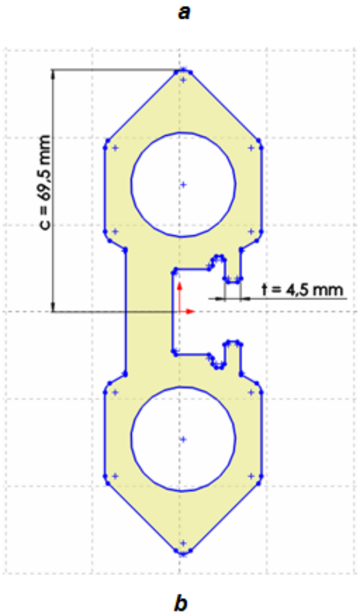
a
c = 69,5 mm
t = 4,5 mm
b

Fig. 3.3.3 Section of rail

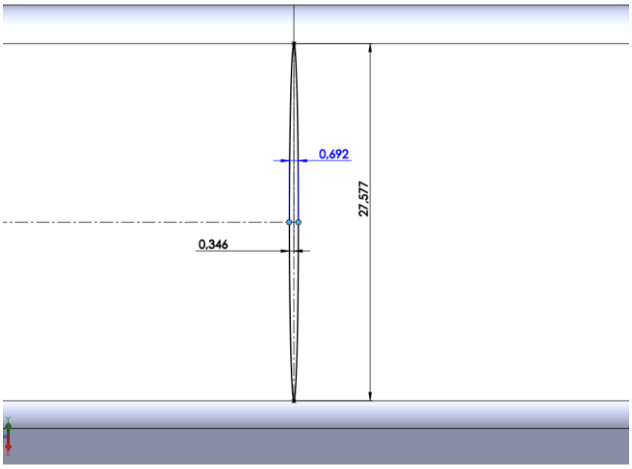
0,692
27,577
0,346

Fig. 3.3.4 Ellipse occuring between rail and wheel

The section of rail should be symmetric about its neutral axis. But there are some restrictions on rail section, which I mean since it will be linked to the wall, there should be a screw space on the rail used. Therefore design of rail should be symmetric about its one way but it is needless to make a symmetric section about other way as seen above fig.s.

3.3.1.1 Horizontal Rail Fem Results

The rail has been meshed with tetrahedron and used 73021 element and 349064 nodes.

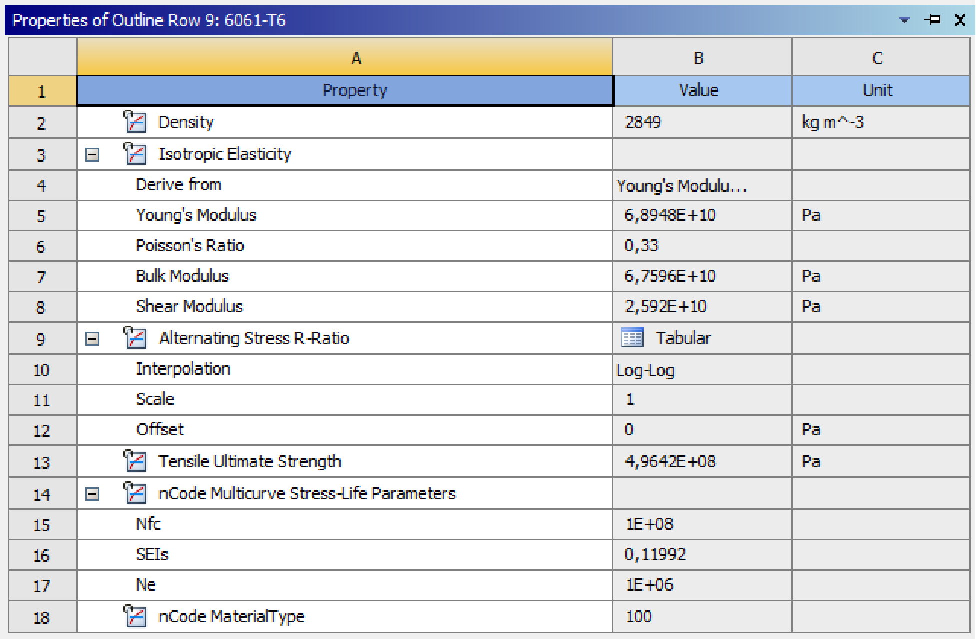

Properties of Outline Row 9: 6061-T6

	A	B	C
1	Property	Value	Unit
2	Density	2849	kg m^-3
3	⊟ Isotropic Elasticity		
4	Derive from	Young's Modulu...	
5	Young's Modulus	6,8948E+10	Pa
6	Poisson's Ratio	0,33	
7	Bulk Modulus	6,7596E+10	Pa
8	Shear Modulus	2,592E+10	Pa
9	⊟ Alternating Stress R-Ratio	Tabular	
10	Interpolation	Log-Log	
11	Scale	1	
12	Offset	0	Pa
13	Tensile Ultimate Strength	4,9642E+08	Pa
14	⊟ nCode Multicurve Stress-Life Parameters		
15	Nfc	1E+08	
16	SEIs	0,11992	
17	Ne	1E+06	
18	nCode MaterialType	100	

Table. 3.2 Material properties of the rail (Ansys ncode material prop.)

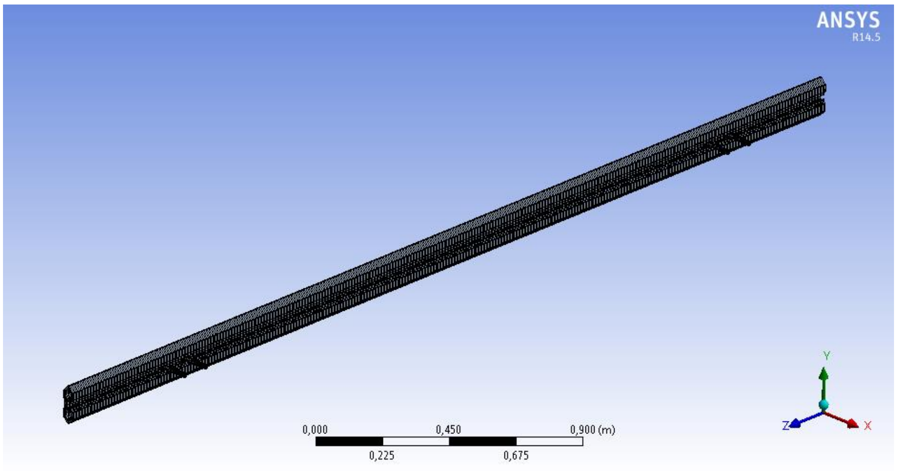

Fig. 3.3.5 Mesh view of the rail

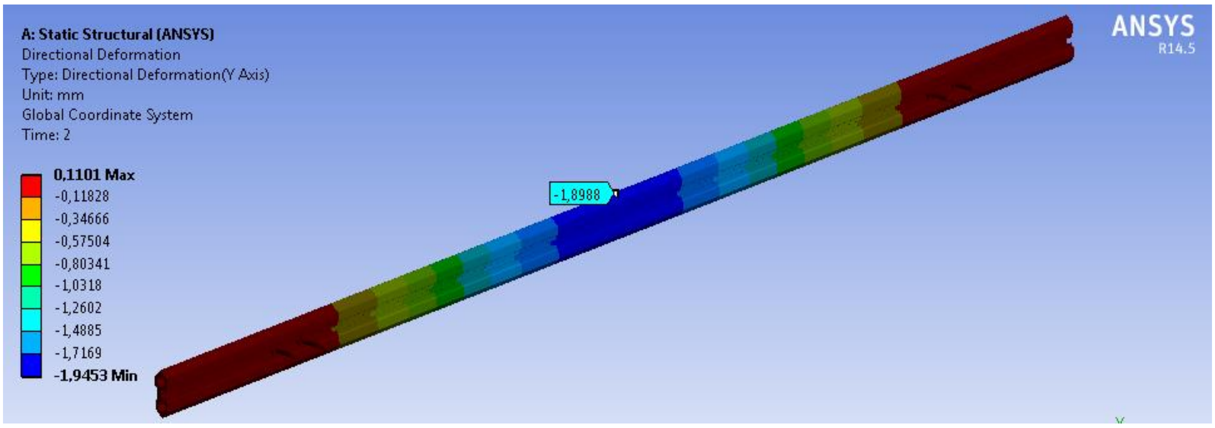
A: Static Structural (ANSYS)
Directional Deformation
Type: Directional Deformation(Y Axis)
Unit: mm
Global Coordinate System
Time: 2
0,1101 Max
-0,11828
-0,34666
-0,57504
-0,80341
-1,0318
-1,2602
-1,4885
-1,7169
-1,9453 Min
-1,8988
ANSYS
R14.5
Y

Fig. 3.3.6 Directional deformation distribution of the horizontal rail

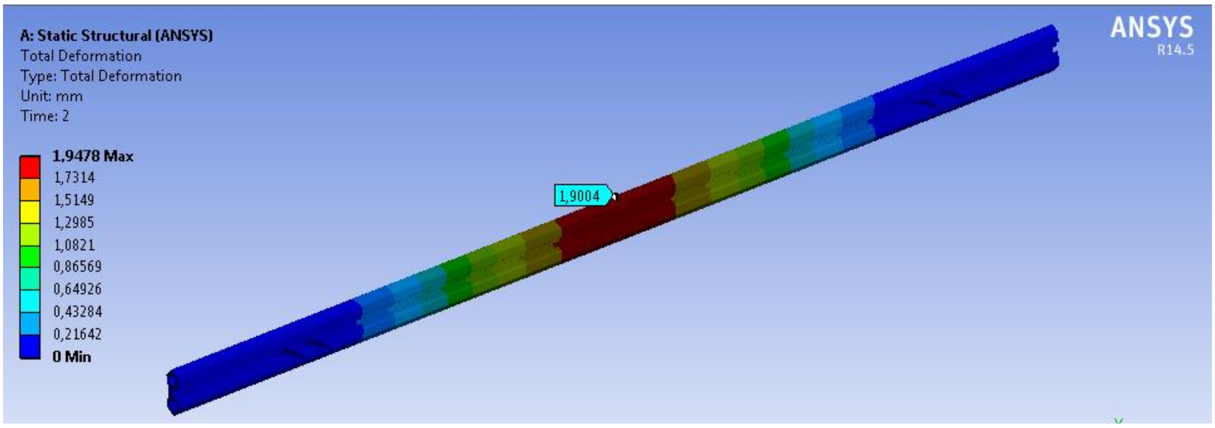
A: Static Structural (ANSYS)
Total Deformation
Type: Total Deformation
Unit: mm
Time: 2
1,9478 Max
1,7314
1,5149
1,2985
1,0821
0,86569
0,64926
0,43284
0,21642
0 Min
1,9004
ANSYS
R14.5
Y

Fig. 3.3.7 Total deformation distribution of the horizontal rail

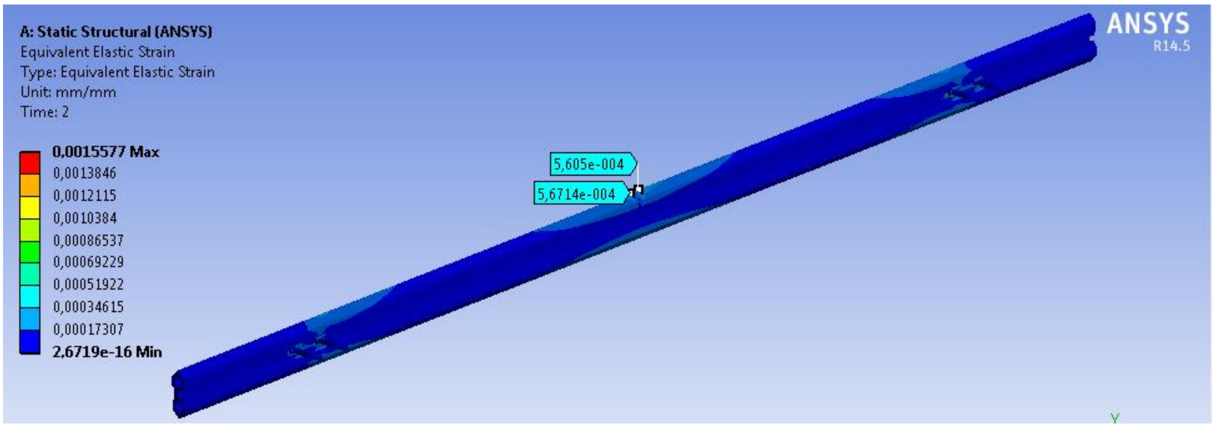
A: Static Structural (ANSYS)
Equivalent Elastic Strain
Type: Equivalent Elastic Strain
Unit: mm/mm
Time: 2
0,0015577 Max
0,0013846
0,0012115
0,0010384
0,00086537
0,00069229
0,00051922
0,00034615
0,00017307
2,6719e-16 Min
5,605e-004
5,6714e-004
ANSYS
R14.5
Y

Fig. 3.3.8 Equivalent elastic strain distribution of the horizontal rail

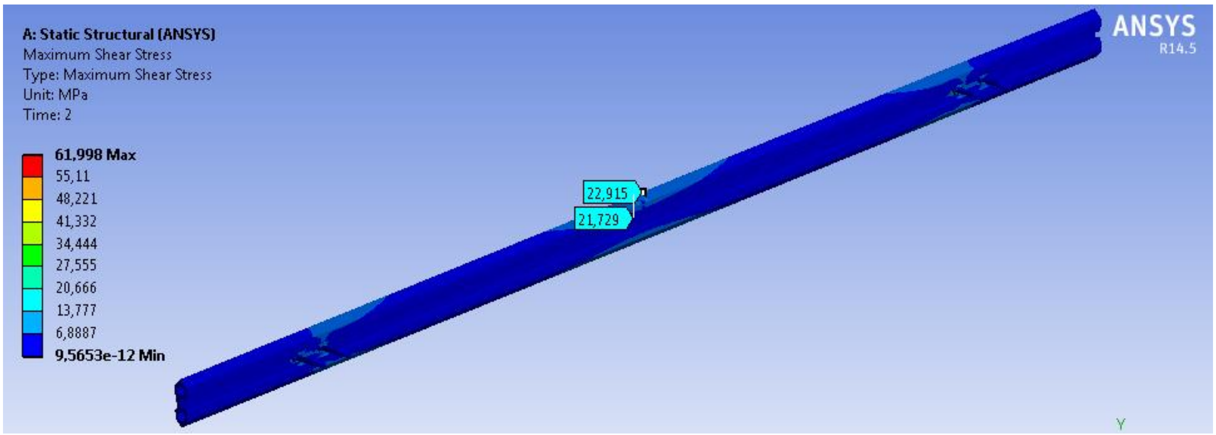
A: Static Structural (ANSYS)
Maximum Shear Stress
Type: Maximum Shear Stress
Unit: MPa
Time: 2
61,998 Max
55,11
48,221
41,332
34,444
27,555
20,666
13,777
6,8887
9,5653e-12 Min
22,915
21,729
ANSYS
R14.5
Y

Fig. 3.3.9 Maximum Shear Stress distribution of the horizontal rail

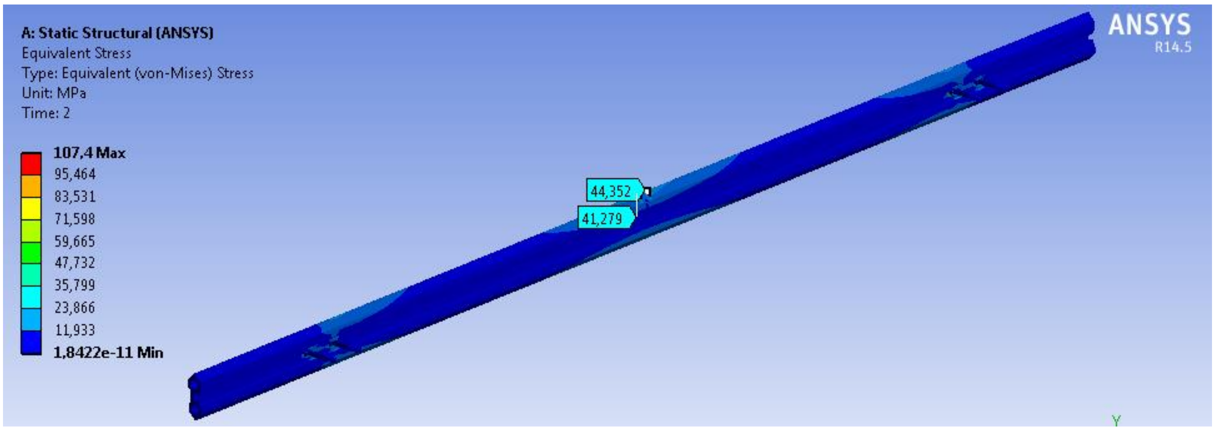
A: Static Structural (ANSYS)
Equivalent Stress
Type: Equivalent (von-Mises) Stress
Unit: MPa
Time: 2
107,4 Max
95,464
83,531
71,598
59,665
47,732
35,799
23,866
11,933
1,8422e-11 Min
44,352
41,279
ANSYS
R14.5
Y

Fig. 3.3.10 Von Mises Stress distribution of the horizontal rail

3.3.1.2 Rail fem fatigue results

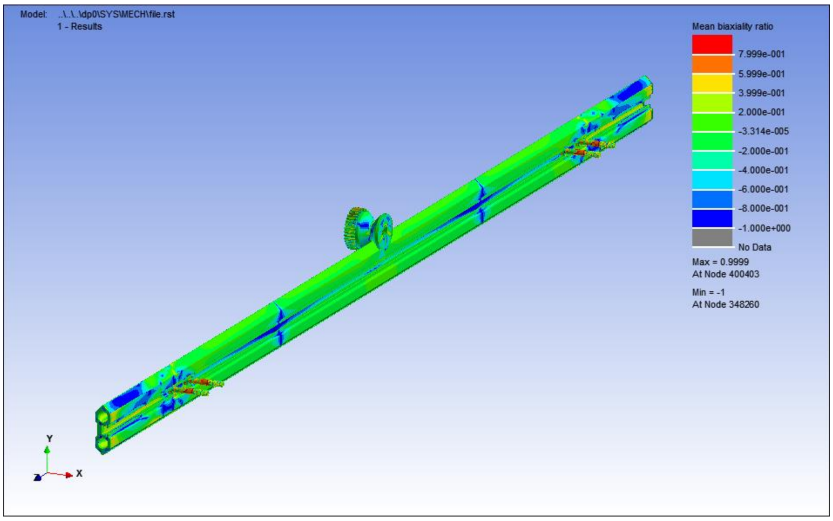
Model: ..\..\..\dp0\SYS\MECH\file.rst
1 - Results
Mean biaxiality ratio
7.999e-001
5.999e-001
3.999e-001
2.000e-001
-3.314e-005
-2.000e-001
-4.000e-001
-6.000e-001
-8.000e-001
-1.000e+000
No Data
Max = 0.9999
At Node 400403
Min = -1
At Node 348260
Y
X

Fig. 3.3.11 Mean biaxiality ratio of the horizontal rail

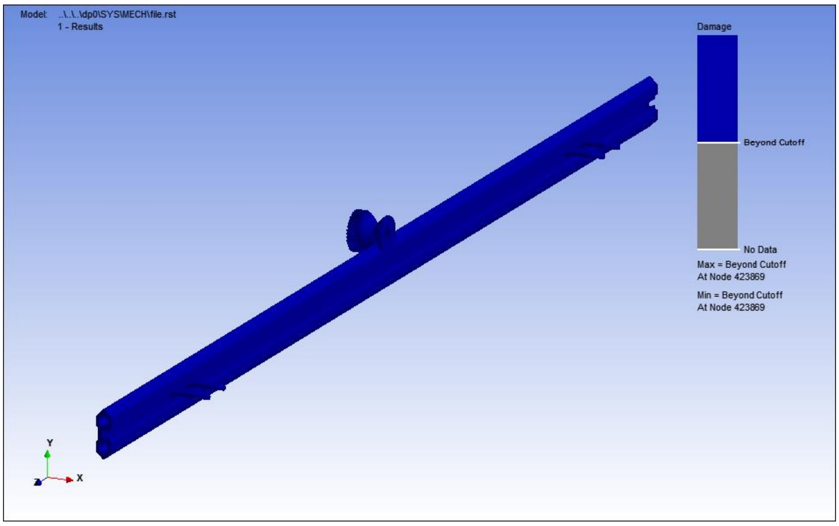
Model: ..\..\..\dp0\SYS\MECH\file.rst
1 - Results
Damage
Beyond Cutoff
No Data
Max = Beyond Cutoff
At Node 423869
Min = Beyond Cutoff
At Node 423869
Y
X

Fig. 3.3.12 Damage distribution of the horizontal rail

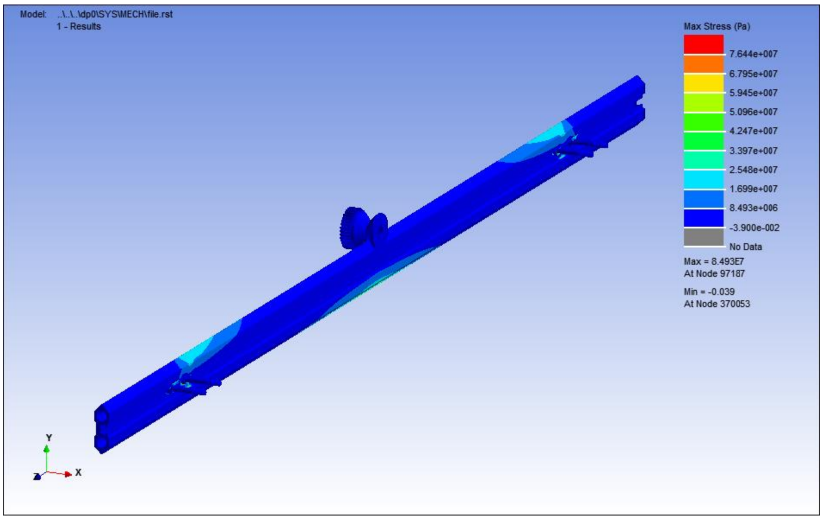
Model: ..\..\..\dp0\SYS\MECH\file.rst
1 - Results
Max Stress (Pa)
7.644e+007
6.795e+007
5.945e+007
5.096e+007
4.247e+007
3.397e+007
2.548e+007
1.699e+007
8.493e+006
-3.900e-002
No Data
Max = 8.493E7
At Node 97187
Min = -0.039
At Node 370053
Y
X

Fig. 3.3.13 Max. stress distribution value of the horizontal rail

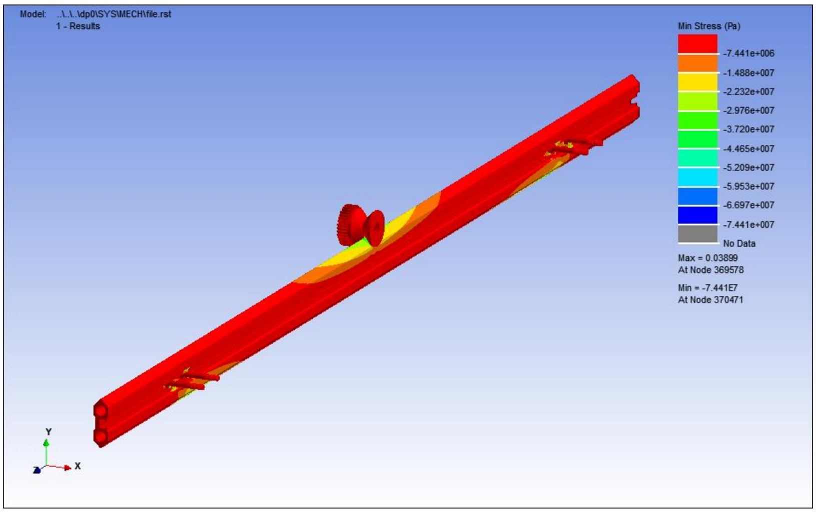
Model: ..\..\..\dp0\SYS\MECH\file.rst
1 - Results
Min Stress (Pa)
-7.441e+006
-1.488e+007
-2.232e+007
-2.976e+007
-3.720e+007
-4.465e+007
-5.209e+007
-5.953e+007
-6.697e+007
-7.441e+007
No Data
Max = 0.03899
At Node 369578
Min = -7.441E7
At Node 370471
Y
X

Fig. 3.3.14 Min. stress distribution value of the horizontal rail

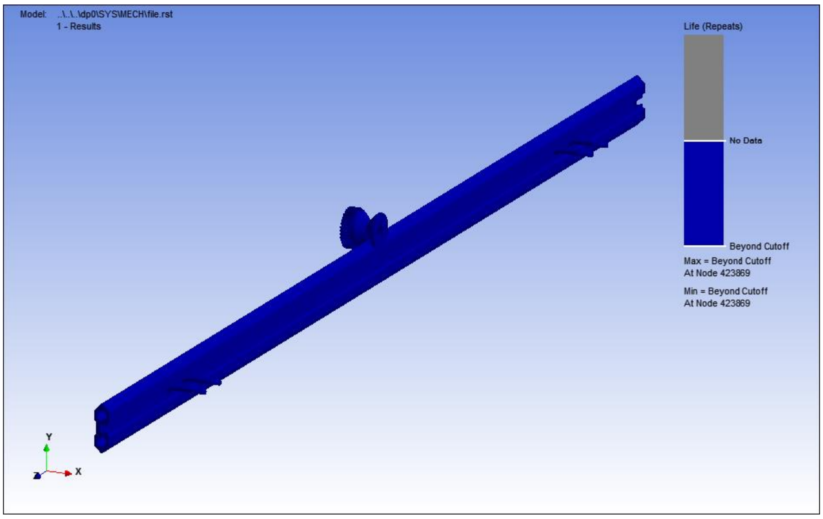
Model: ..\..\..\dp0\SYS\MECH\file.rst
1 - Results
Life (Repeats)
No Data
Beyond Cutoff
Max = Beyond Cutoff
At Node 423869
Min = Beyond Cutoff
At Node 423869
Y
X

Fig. 3.3.15 Life of the horizontal rail

3.3.1.3 Fem results of the horizontal rail transporting two weights

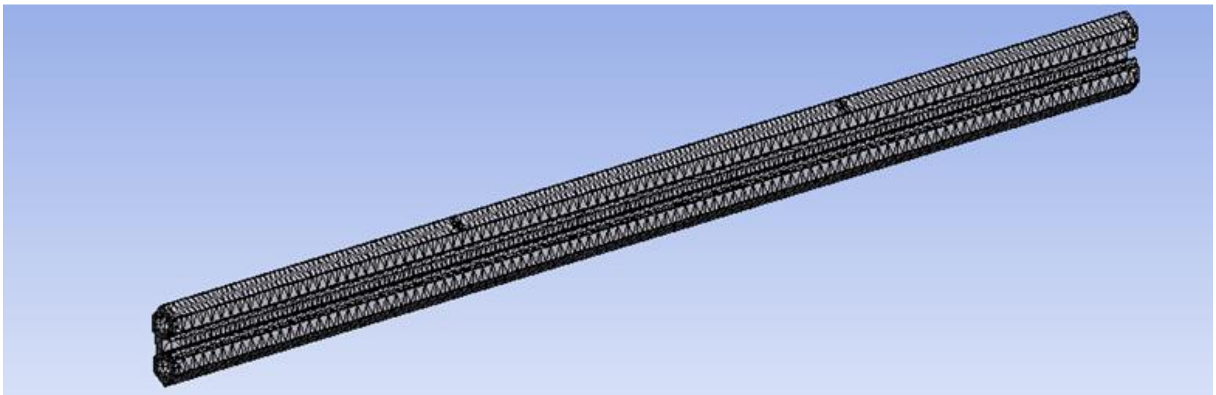

Fig. 3.3.16 Mesh view of the rail with contact regions

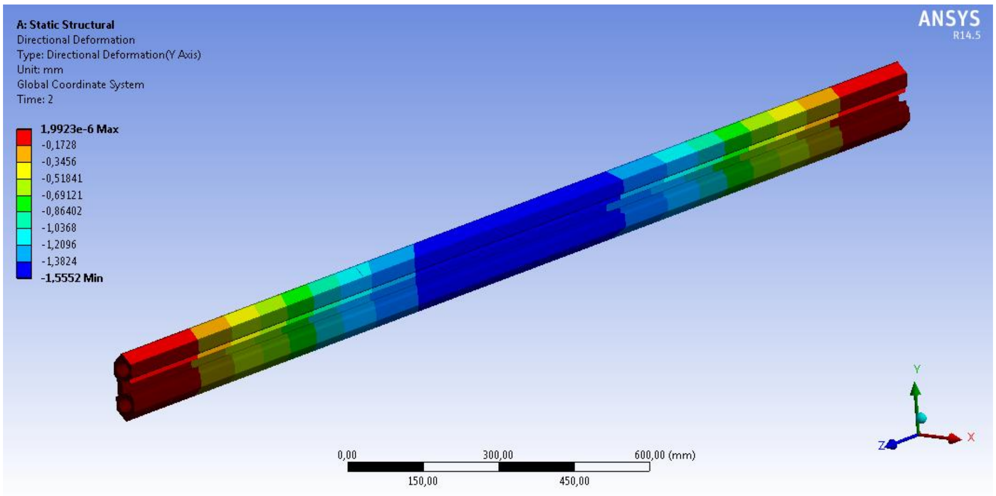
A: Static Structural
Directional Deformation
Type: Directional Deformation(Y Axis)
Unit: mm
Global Coordinate System
Time: 2
1,9923e-6 Max
-0,1728
-0,3456
-0,51841
-0,69121
-0,86402
-1,0368
-1,2096
-1,3824
-1,5552 Min
ANSYS
R14.5
0,00
300,00
600,00 (mm)
150,00
450,00
Y
Z
X

Fig. 3.3.17 Directional deformation distribution of the rail transporting two weights

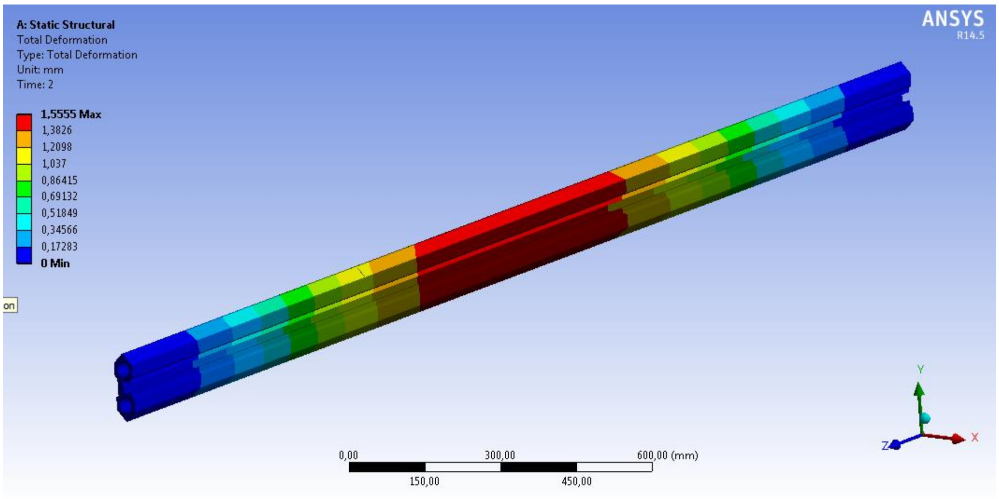
A: Static Structural
Total Deformation
Type: Total Deformation
Unit: mm
Time: 2
1,5555 Max
1,3826
1,2098
1,037
0,86415
0,69132
0,51849
0,34566
0,17283
0 Min
ANSYS
R14.5
0,00
300,00
600,00 (mm)
150,00
450,00
Y
X
Z

Fig. 3.3.18 Total deformation distribution of the rail transporting two weights

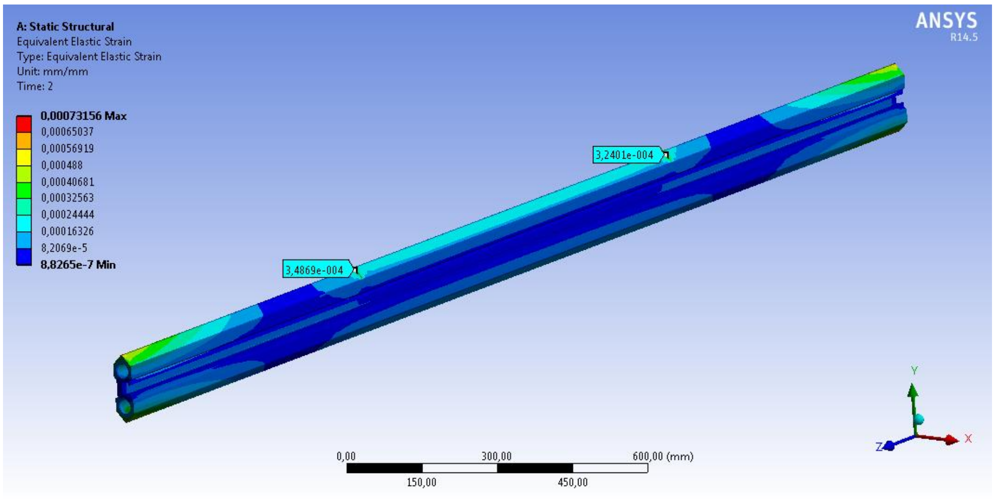
A: Static Structural
Equivalent Elastic Strain
Type: Equivalent Elastic Strain
Unit: mm/mm
Time: 2
0,00073156 Max
0,00065037
0,00056919
0,000488
0,00040681
0,00032563
0,00024444
0,00016326
8,2069e-5
8,8265e-7 Min
3,2401e-004
3,4869e-004
ANSYS
R14.5
0,00
300,00
600,00 (mm)
150,00
450,00
Y
X
Z

Fig. 3.3.19 Equivalent elastic strain distribution of the rail transporting two weights

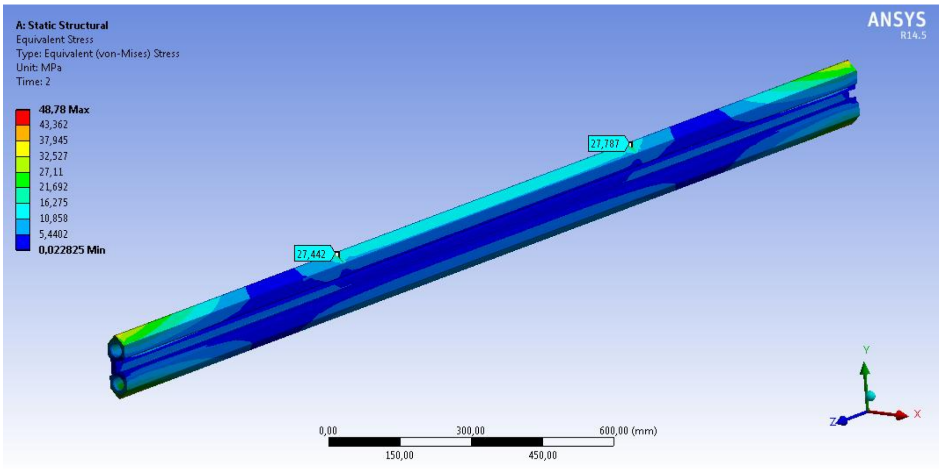
A: Static Structural
Equivalent Stress
Type: Equivalent (von-Mises) Stress
Unit: MPa
Time: 2
48,78 Max
43,362
37,945
32,527
27,11
21,692
16,275
10,858
5,4402
0,022825 Min
27,787
27,442
ANSYS
R14.5
0,00
300,00
600,00 (mm)
150,00
450,00
Y
X
Z

Fig. 3.3.20 Von Mises Stress distribution of the rail transporting two weights

3.3.1.4 Fatigue results of the horizontal rail transporting two weights

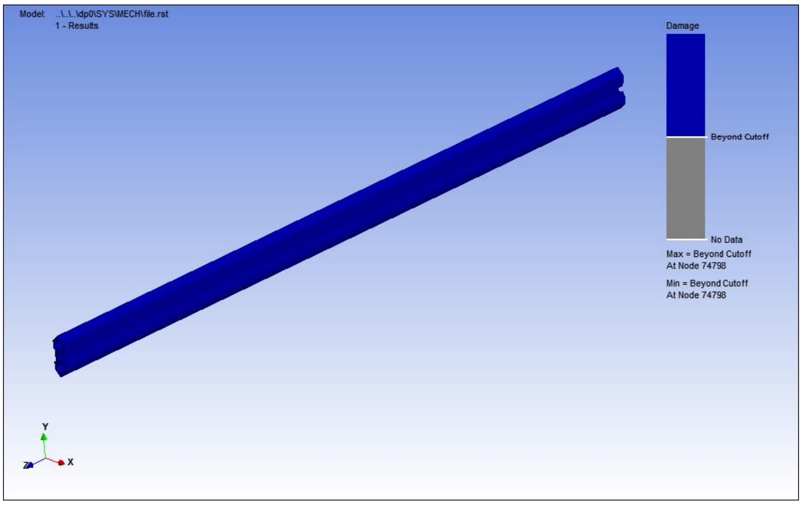
Model: ..\..\..\dp0\SYS\MECH\file.rst
1 - Results
Damage
Beyond Cutoff
No Data
Max = Beyond Cutoff
At Node 74798
Min = Beyond Cutoff
At Node 74798
Y
X
Z

Fig. 3.3.21 Damage distribution of the rail transporting two weights

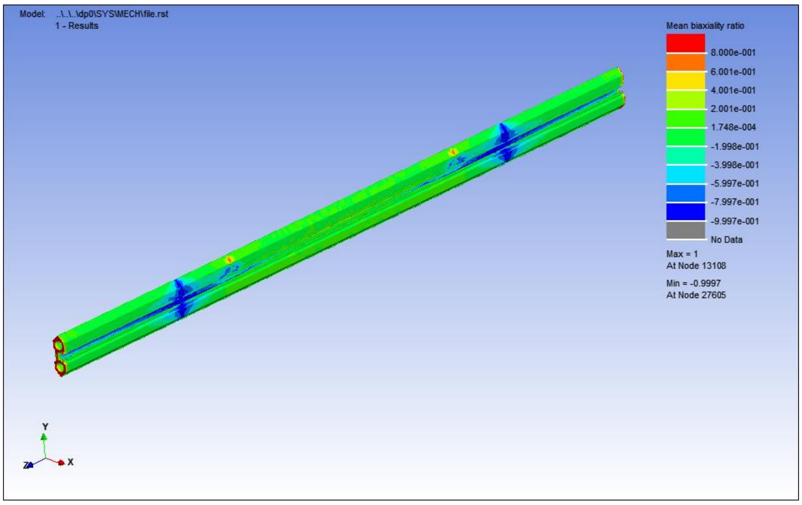
Model: ..\..\..\dp0\SYS\MECH\file.rst
1 - Results
Mean biaxiality ratio
8.000e-001
6.001e-001
4.001e-001
2.001e-001
1.748e-004
-1.998e-001
-3.998e-001
-5.997e-001
-7.997e-001
-9.997e-001
No Data
Max = 1
At Node 13108
Min = -0.9997
At Node 27605
Y
X
Z

Fig. 3.3.22 Mean biaxiliaty ratio distribution of the rail transporting two weights

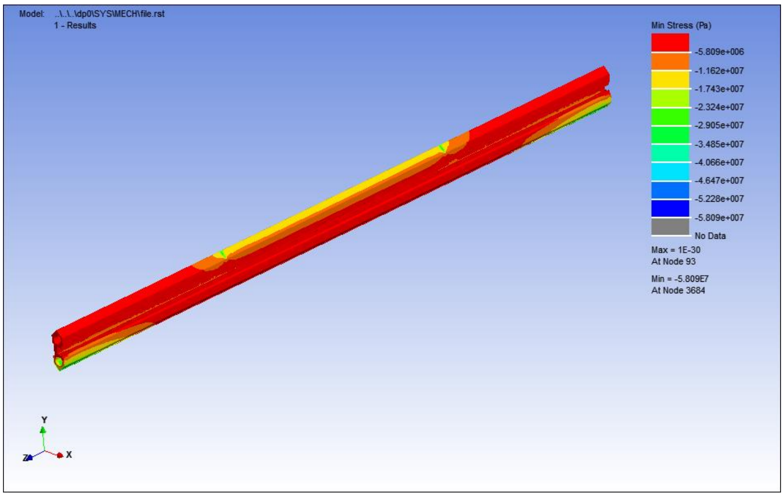
Model: ..\..\..\dp0\SYS\MECH\file.rst
1 - Results
Min Stress (Pa)
-5.809e+006
-1.162e+007
-1.743e+007
-2.324e+007
-2.905e+007
-3.485e+007
-4.066e+007
-4.647e+007
-5.228e+007
-5.809e+007
No Data
Max = 1E-30
At Node 93
Min = -5.809E7
At Node 3684
Y
X
Z

Fig. 3.3.23 Min. stress distribution of the rail transporting two weights

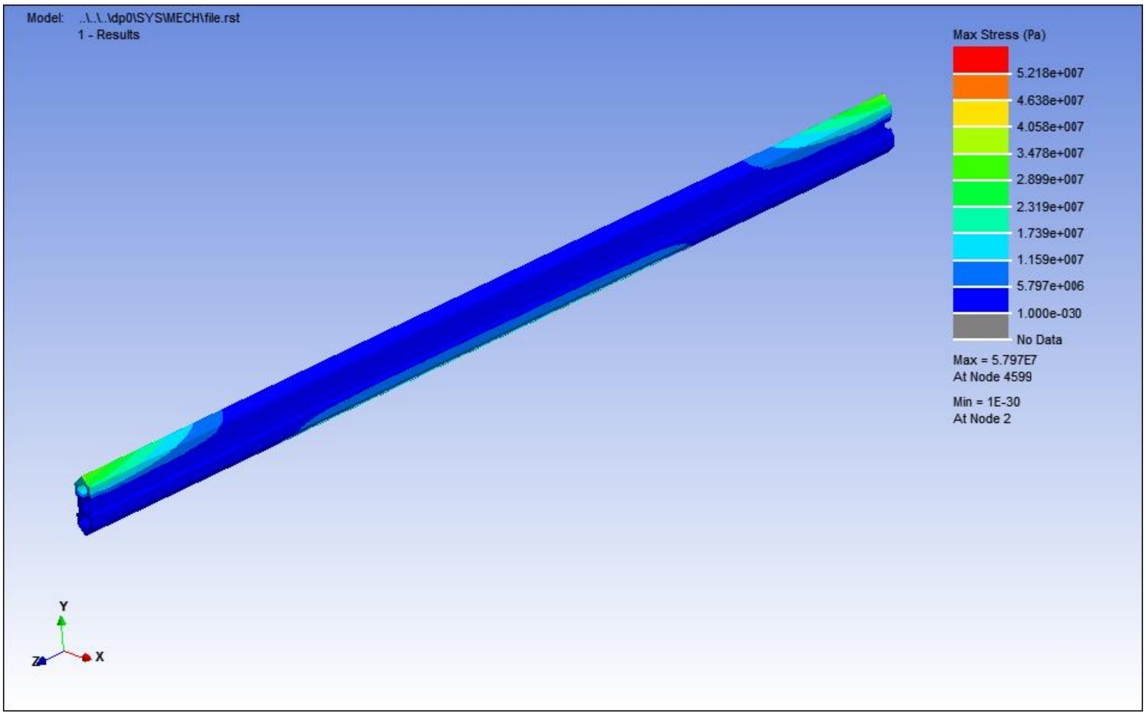
Model: ..\..\..\dp0\SYS\MECH\file.rst
1 - Results
Max Stress (Pa)
5.218e+007
4.638e+007
4.058e+007
3.478e+007
2.899e+007
2.319e+007
1.739e+007
1.159e+007
5.797e+006
1.000e-030
No Data
Max = 5.797E7
At Node 4599
Min = 1E-30
At Node 2
Y
Z
X

Fig. 3.3.24 Max. stress distribution of the rail transporting two weights

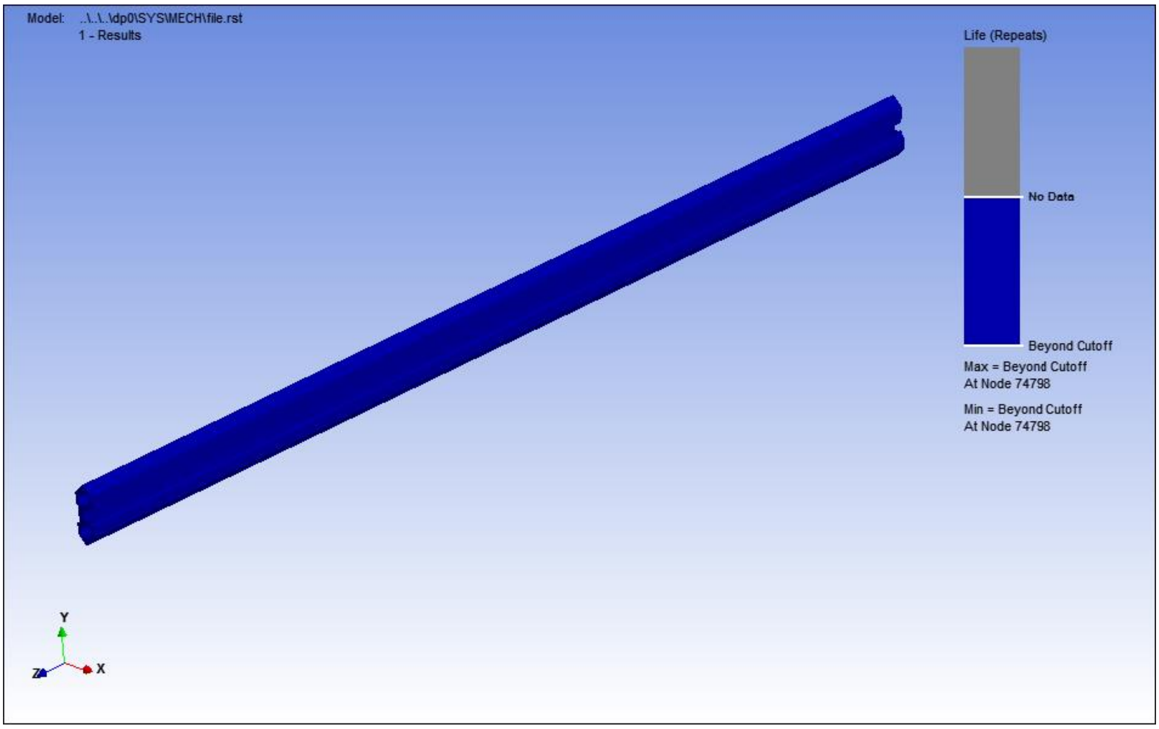
Model: ..\..\..\dp0\SYS\MECH\file.rst
1 - Results
Life (Repeats)
No Data
Beyond Cutoff
Max = Beyond Cutoff
At Node 74798
Min = Beyond Cutoff
At Node 74798
Y
Z
X

Fig. 3.3.25 Life of the rail transporting two weights

3.3.2 Vertical Rail

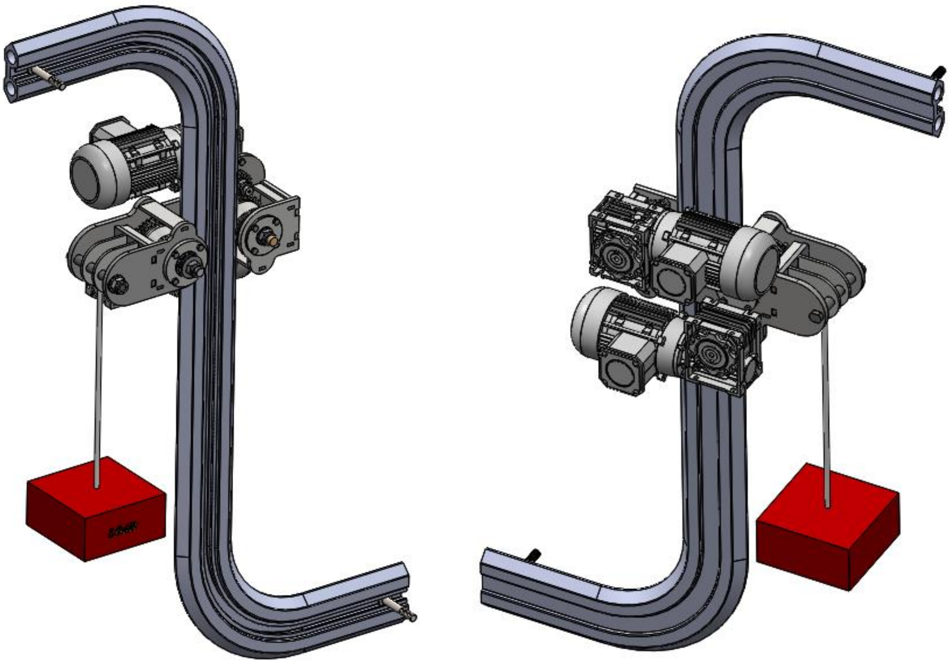

(a) **(b)**

Fig 3.3.26 (a) Front view of vertical rail **(b)** Back view of the vertical rail

3.3.2.1 Vertical Rail Fem Results

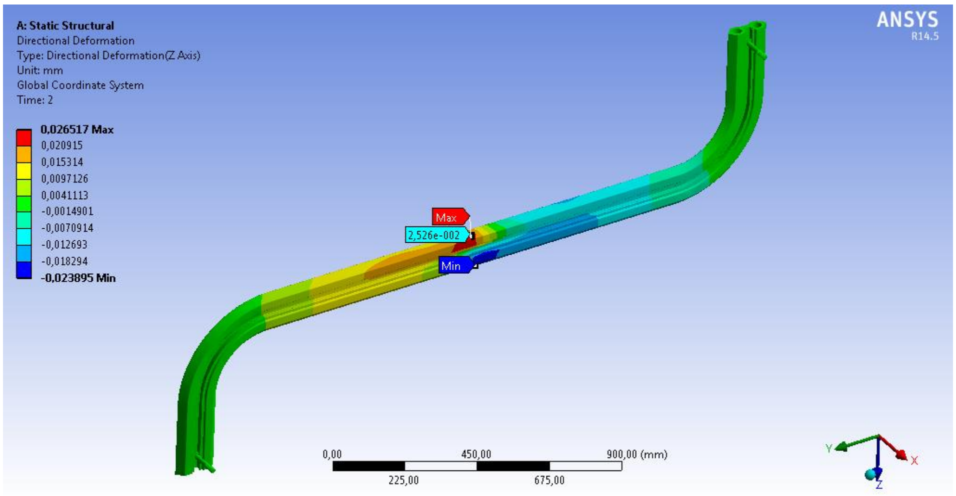
A: Static Structural
Directional Deformation
Type: Directional Deformation(Z Axis)
Unit: mm
Global Coordinate System
Time: 2
0,026517 Max
0,020915
0,015314
0,0097126
0,0041113
-0,0014901
-0,0070914
-0,012693
-0,018294
-0,023895 Min
Max
2,526e-002
Min
ANSYS
R14.5
0,00
450,00
900,00 (mm)
225,00
675,00
Y
X
Z

Fig. 3.3.27 Directional deformation distribution of the vertical rail

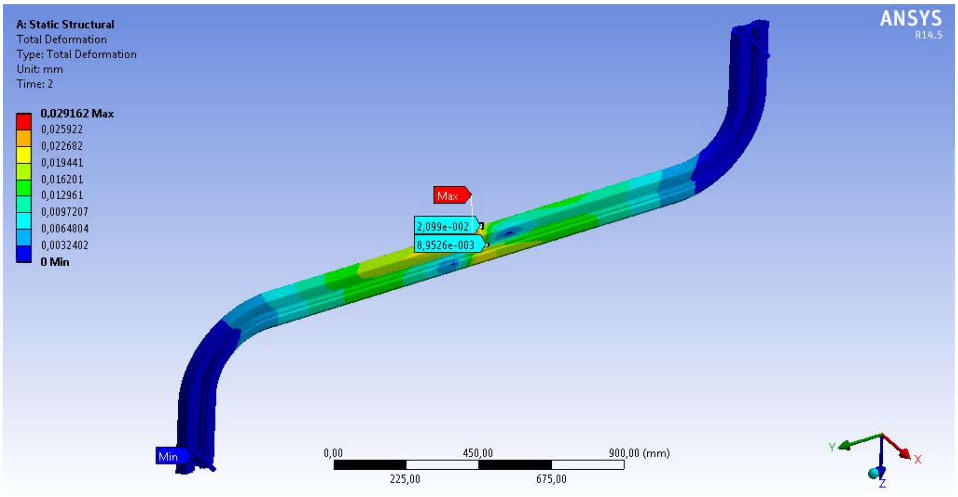
A: Static Structural
Total Deformation
Type: Total Deformation
Unit: mm
Time: 2
0,029162 Max
0,025922
0,022682
0,019441
0,016201
0,012961
0,0097207
0,0064804
0,0032402
0 Min
ANSYS
R14.5
Max
2,099e-002
8,9526e-003
Min
0,00
450,00
900,00 (mm)
225,00
675,00
Y
X
Z

Fig. 3.3.28 Total deformation distribution of the vertical rail

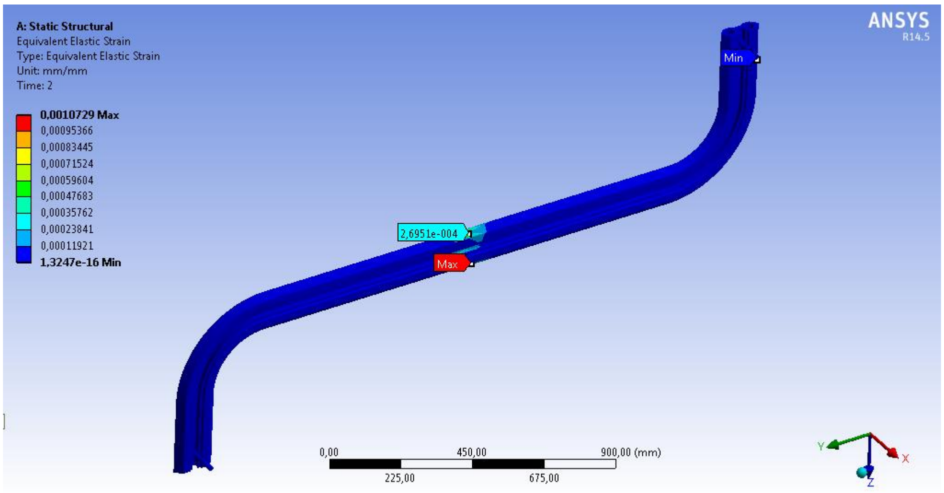
A: Static Structural
Equivalent Elastic Strain
Type: Equivalent Elastic Strain
Unit: mm/mm
Time: 2
0,0010729 Max
0,00095366
0,00083445
0,00071524
0,00059604
0,00047683
0,00035762
0,00023841
0,00011921
1,3247e-16 Min
ANSYS
R14.5
Min
2,6951e-004
Max
0,00
450,00
900,00 (mm)
225,00
675,00
Y
X
Z

Fig. 3.3.29 Equivalent elastic strain distribution of the vertical rail

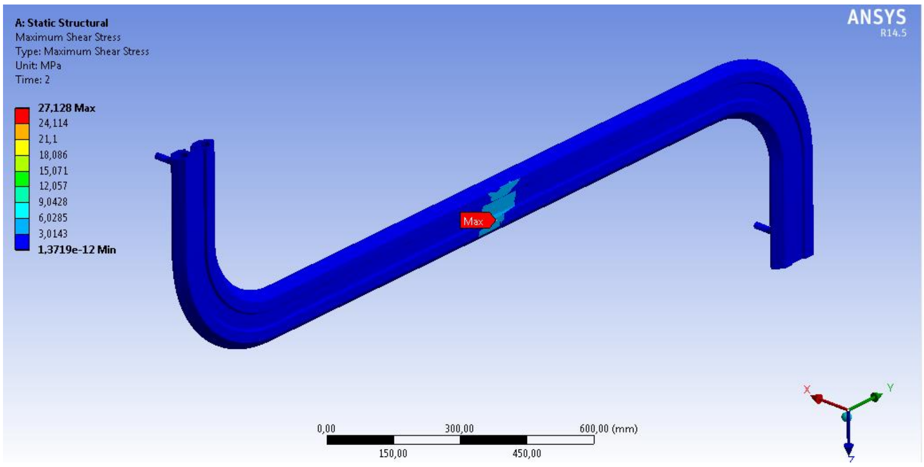
A: Static Structural
Maximum Shear Stress
Type: Maximum Shear Stress
Unit: MPa
Time: 2
27,128 Max
24,114
21,1
18,086
15,071
12,057
9,0428
6,0285
3,0143
1,3719e-12 Min
ANSYS
R14.5
Max
0,00
300,00
600,00 (mm)
150,00
450,00
X
Y
Z

Fig. 3.3.30 Maximum Shear Stress distribution of the vertical rail

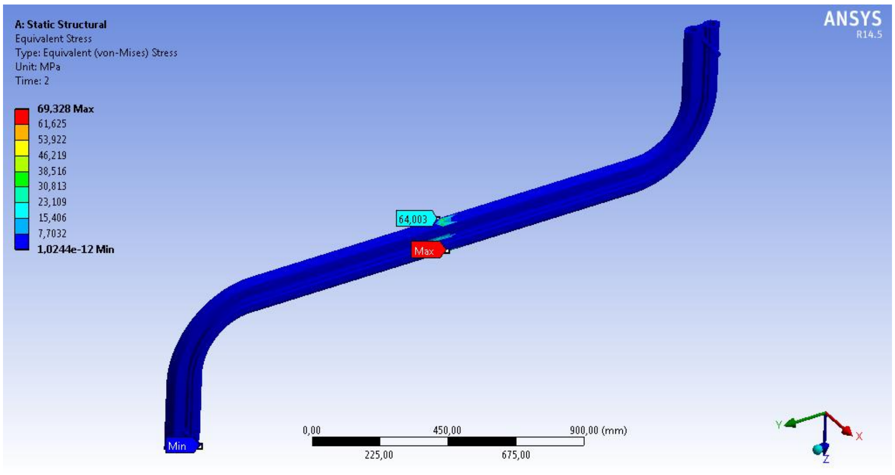
A: Static Structural
Equivalent Stress
Type: Equivalent (von-Mises) Stress
Unit: MPa
Time: 2
69,328 Max
61,625
53,922
46,219
38,516
30,813
23,109
15,406
7,7032
1,0244e-12 Min
ANSYS
R14.5
64,003
Max
Min
0,00
450,00
900,00 (mm)
225,00
675,00
Y
X
Z

Fig. 3.3.31 Von Mises Stress distribution of the vertical rail

3.3.2.2 Vertical Rail Fatigue Results

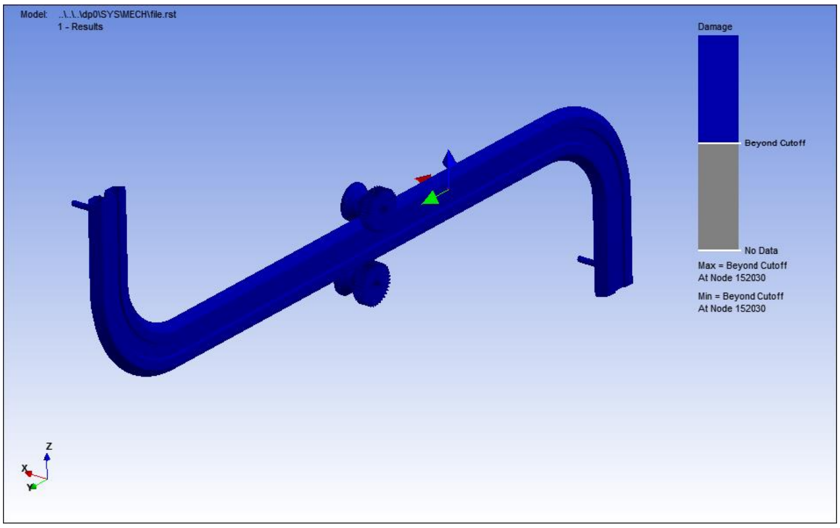
Model: ..\..\..\dp0\SYS\MECH\file.rst
1 - Results
Damage
Beyond Cutoff
No Data
Max = Beyond Cutoff
At Node 152030
Min = Beyond Cutoff
At Node 152030
Z
X
Y

Fig. 3.3.32 Damage distribution of the vertical rail

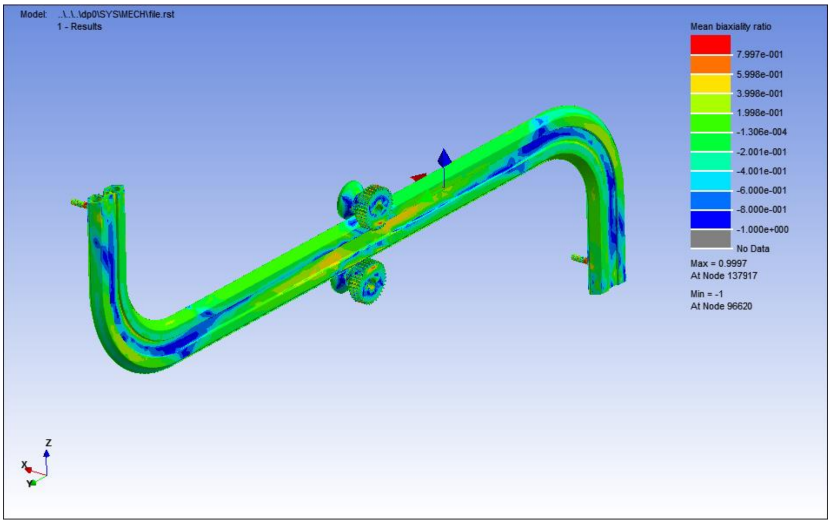
Model: ..\..\..\dp0\SYS\MECH\file.rst
1 - Results
Mean biaxiality ratio
7.997e-001
5.998e-001
3.998e-001
1.998e-001
-1.306e-004
-2.001e-001
-4.001e-001
-6.000e-001
-8.000e-001
-1.000e+000
No Data
Max = 0.9997
At Node 137917
Min = -1
At Node 96620
Z
X
Y

Fig. 3.3.33 Mean biaxiliaty ratio distribution of the vertical rail

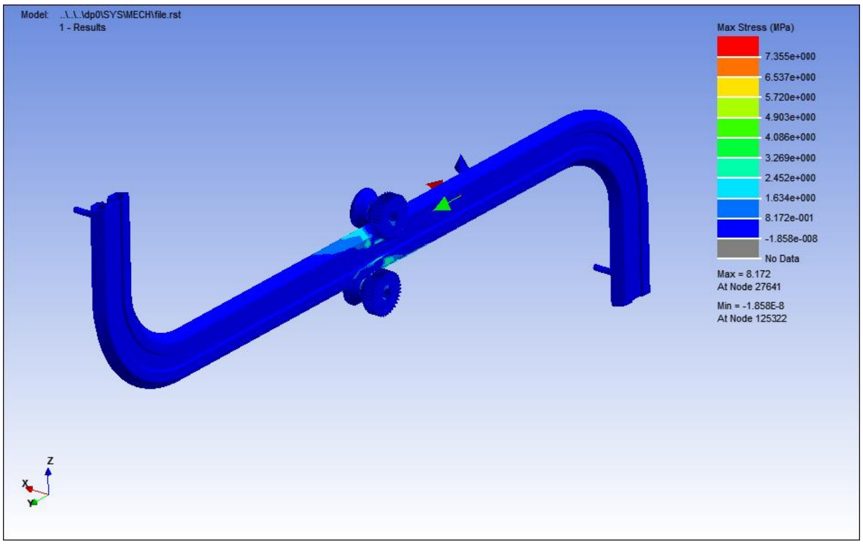
Model: ..\..\dp0\SYS\MECH\file.rst
1 - Results
Max Stress (MPa)
7.355e+000
6.537e+000
5.720e+000
4.903e+000
4.086e+000
3.269e+000
2.452e+000
1.634e+000
8.172e-001
-1.858e-008
No Data
Max = 8.172
At Node 27641
Min = -1.858E-8
At Node 125322
Z
X
Y

Fig. 3.3.34 Max. stress distribution of the vertical rail

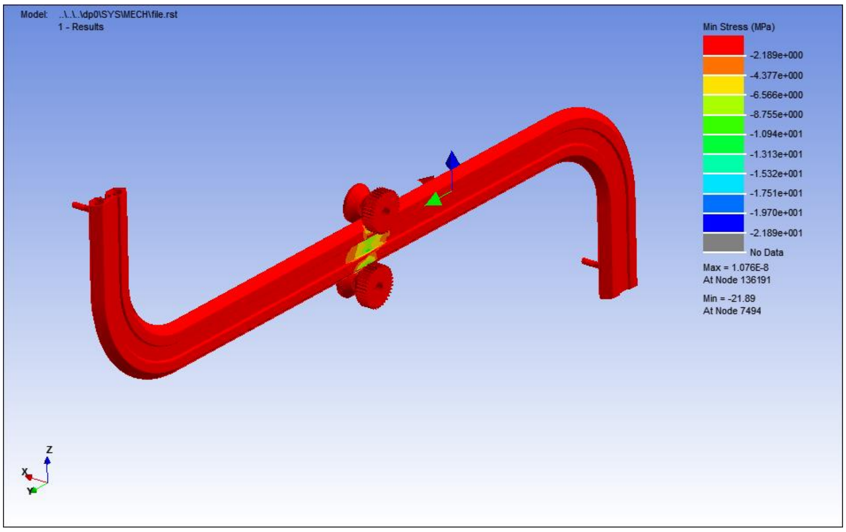
Model: ..\..\dp0\SYS\MECH\file.rst
1 - Results
Min Stress (MPa)
-2.189e+000
-4.377e+000
-6.566e+000
-8.755e+000
-1.094e+001
-1.313e+001
-1.532e+001
-1.751e+001
-1.970e+001
-2.189e+001
No Data
Max = 1.076E-8
At Node 136191
Min = -21.89
At Node 7494
Z
X
Y

Fig. 3.3.35 Min. stress distribution of the vertical rail

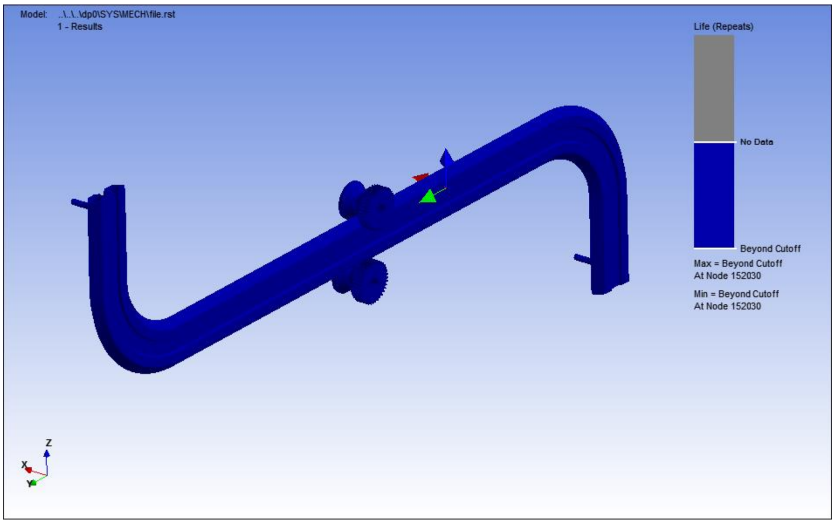
Model: ..\..\dp0\SYS\MECH\file.rst
1 - Results
Life (Repeats)
No Data
Beyond Cutoff
Max = Beyond Cutoff
At Node 152030
Min = Beyond Cutoff
At Node 152030
Z
X
Y

Fig. 3.3.36 Life of the vertical rail

3.3.3 Curved Rail Fem Results

3.3.3.1 S rail type

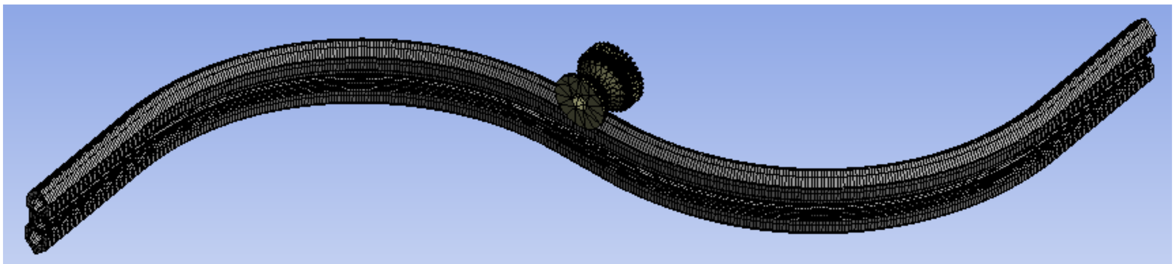

Fig. 3.3.37 Mesh view of the S rail

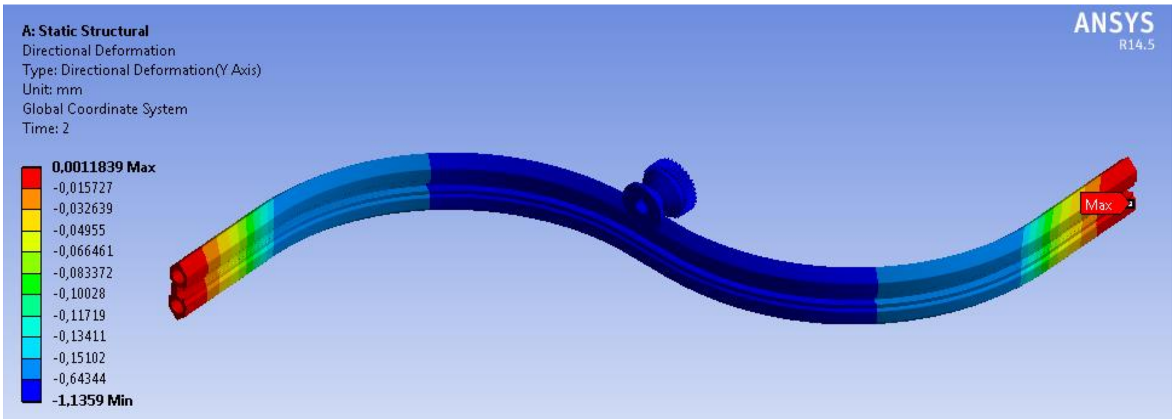
A: Static Structural
Directional Deformation
Type: Directional Deformation(Y Axis)
Unit: mm
Global Coordinate System
Time: 2
0,0011839 Max
-0,015727
-0,032639
-0,04955
-0,066461
-0,083372
-0,10028
-0,11719
-0,13411
-0,15102
-0,64344
-1,1359 Min
Max
ANSYS
R14.5

Fig. 3.3.38 Directional deformation distribution of the S rail

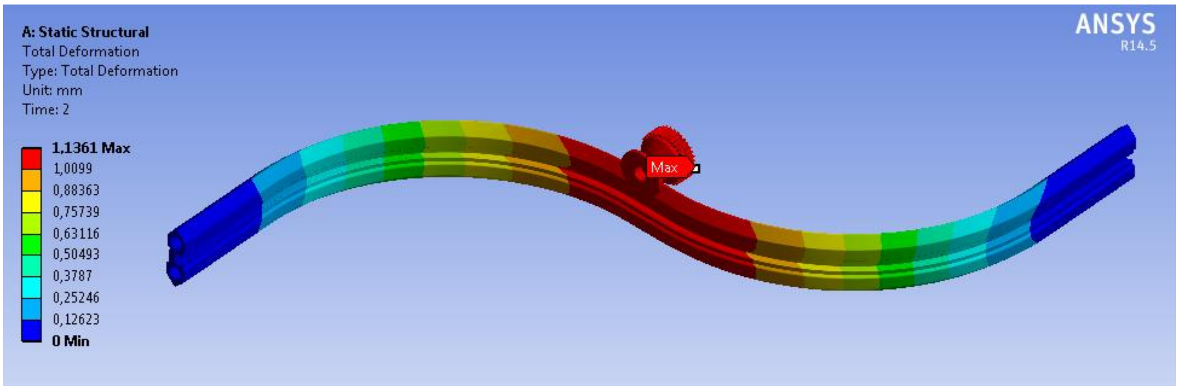
A: Static Structural
Total Deformation
Type: Total Deformation
Unit: mm
Time: 2
1,1361 Max
1,0099
0,88363
0,75739
0,63116
0,50493
0,3787
0,25246
0,12623
0 Min
Max
ANSYS
R14.5

Fig. 3.3.39 Total deformation distribution of the S rail

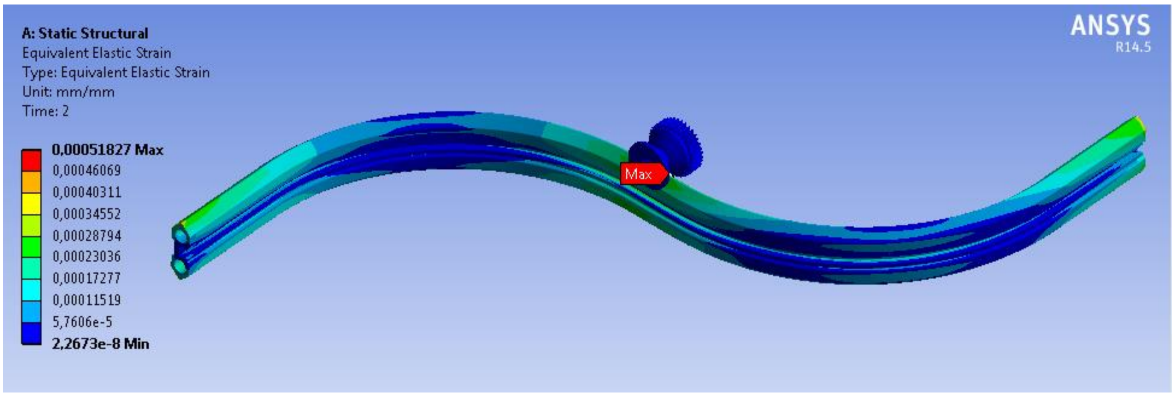
A: Static Structural
Equivalent Elastic Strain
Type: Equivalent Elastic Strain
Unit: mm/mm
Time: 2
0,00051827 Max
0,00046069
0,00040311
0,00034552
0,00028794
0,00023036
0,00017277
0,00011519
5,7606e-5
2,2673e-8 Min
Max
ANSYS
R14.5

Fig. 3.3.40 Equivalent elastic strain distribution of the S rail

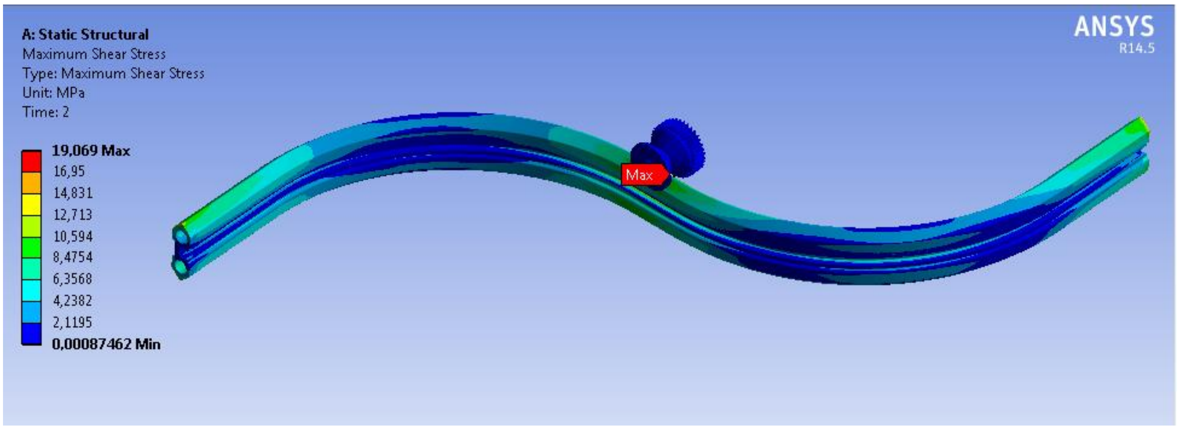
A: Static Structural
Maximum Shear Stress
Type: Maximum Shear Stress
Unit: MPa
Time: 2
19,069 Max
16,95
14,831
12,713
10,594
8,4754
6,3568
4,2382
2,1195
0,00087462 Min
Max
ANSYS
R14.5

Fig. 3.3.41 Maximum Shear Stress distribution of the S rail

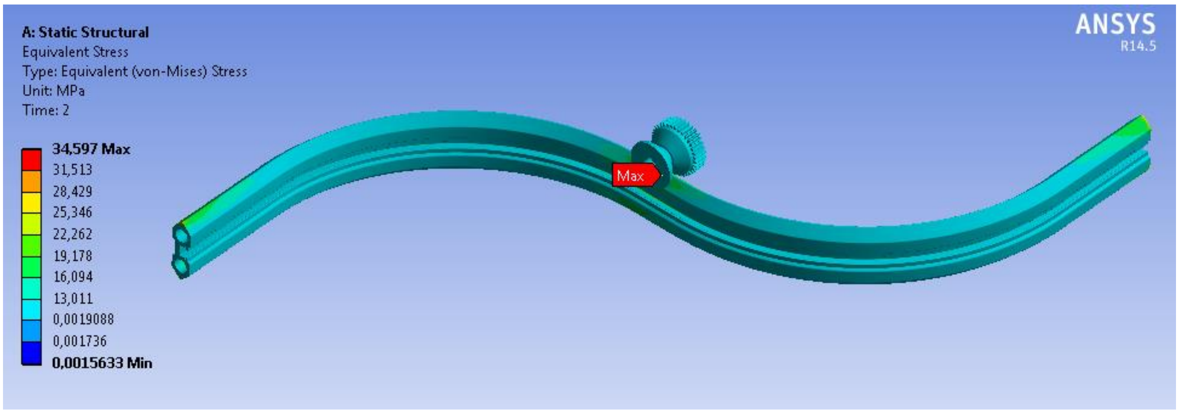
A: Static Structural
Equivalent Stress
Type: Equivalent (von-Mises) Stress
Unit: MPa
Time: 2
34,597 Max
31,513
28,429
25,346
22,262
19,178
16,094
13,011
0,0019088
0,001736
0,0015633 Min
Max
ANSYS
R14.5

Fig. 3.3.42 Von Mises Stress distribution of the S rail

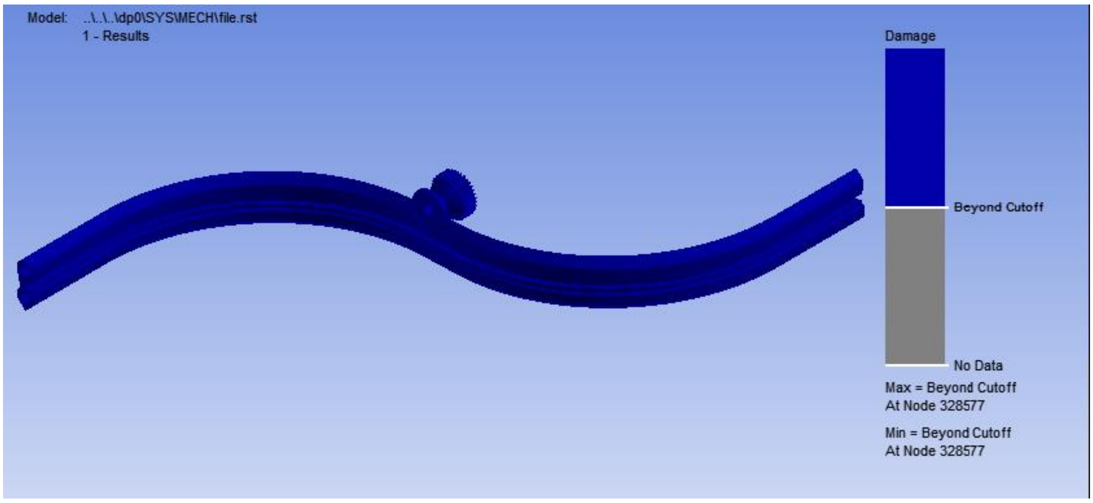
Model: ..\..\dp0\SYS\MECH\file.rst
1 - Results
Damage
Beyond Cutoff
No Data
Max = Beyond Cutoff
At Node 328577
Min = Beyond Cutoff
At Node 328577

Fig. 3.3.43 Damage distribution of the S rail

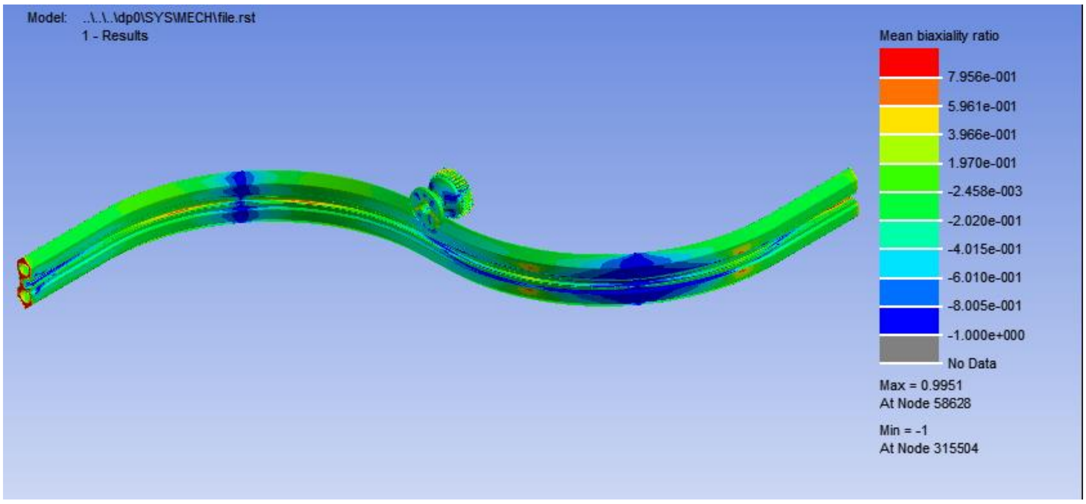
Model: ..\..\dp0\SYS\MECH\file.rst
1 - Results
Mean biaxiality ratio
7.956e-001
5.961e-001
3.966e-001
1.970e-001
-2.458e-003
-2.020e-001
-4.015e-001
-6.010e-001
-8.005e-001
-1.000e+000
No Data
Max = 0.9951
At Node 58628
Min = -1
At Node 315504

Fig. 3.3.44 Mean biaxiliaty ratio distribution of the S rail

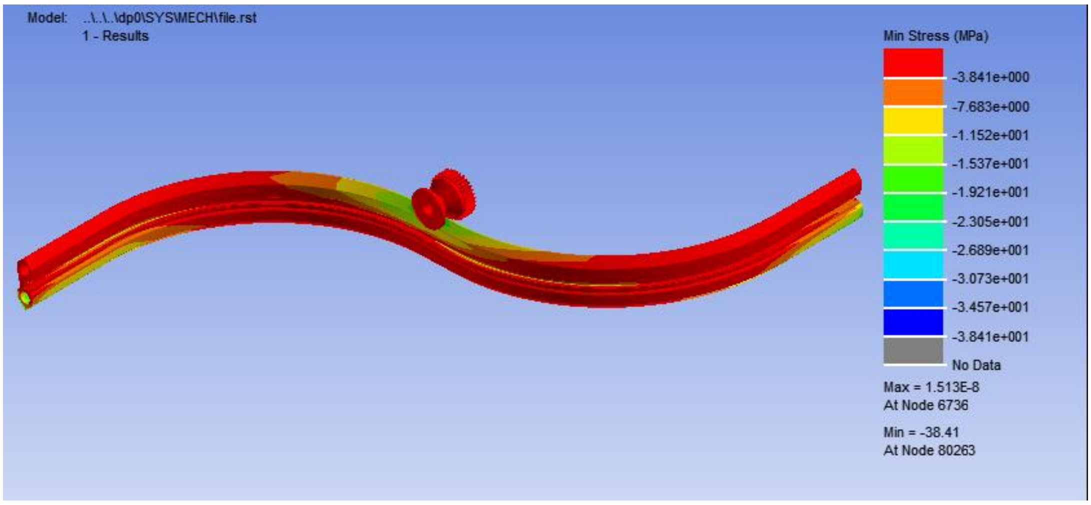
Model: ..\..\dp0\SYS\MECH\file.rst
1 - Results
Min Stress (MPa)
-3.841e+000
-7.683e+000
-1.152e+001
-1.537e+001
-1.921e+001
-2.305e+001
-2.689e+001
-3.073e+001
-3.457e+001
-3.841e+001
No Data
Max = 1.513E-8
At Node 6736
Min = -38.41
At Node 80263

Fig. 3.3.45 Min. stress distribution of the S rail

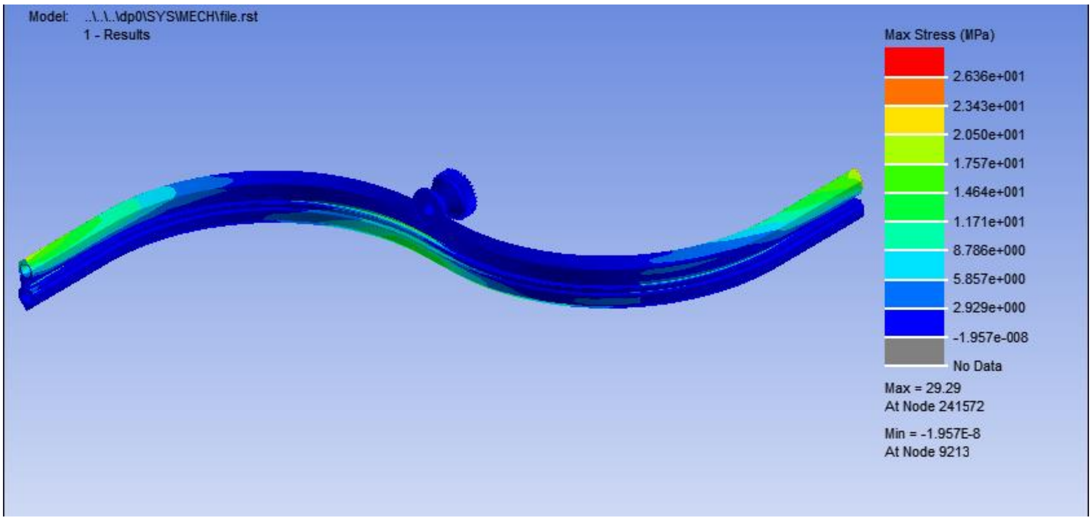
Model: ..\..\..\dp0\SYS\MECH\file.rst
1 - Results
Max Stress (MPa)
2.636e+001
2.343e+001
2.050e+001
1.757e+001
1.464e+001
1.171e+001
8.786e+000
5.857e+000
2.929e+000
-1.957e-008
No Data
Max = 29.29
At Node 241572
Min = -1.957E-8
At Node 9213

Fig. 3.3.46 Max. stress distribution of the S rail

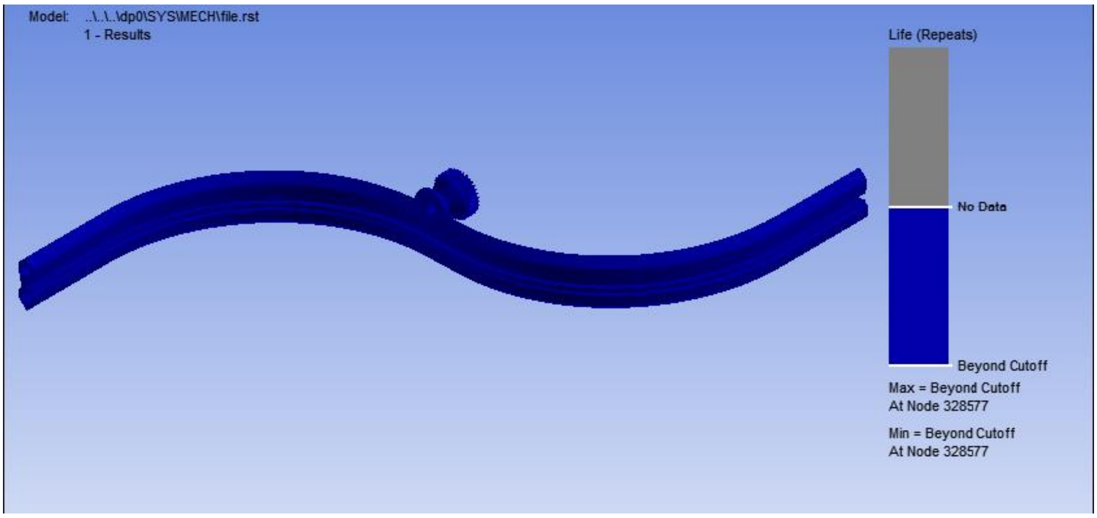
Model: ..\..\..\dp0\SYS\MECH\file.rst
1 - Results
Life (Repeats)
No Data
Beyond Cutoff
Max = Beyond Cutoff
At Node 328577
Min = Beyond Cutoff
At Node 328577

Fig. 3.3.47 Life of the S rail

3.3.3.2 Bended Rail With 90° Curvature

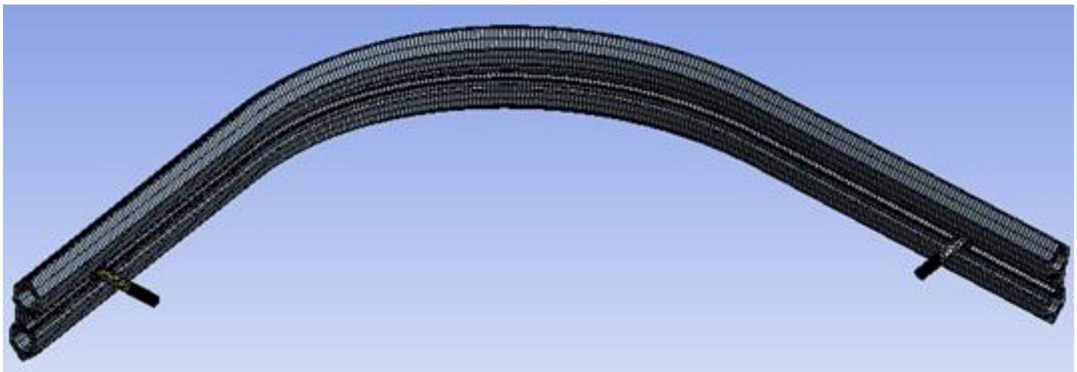

Fig. 3.3.48 Mesh view of the 90° curvature rail

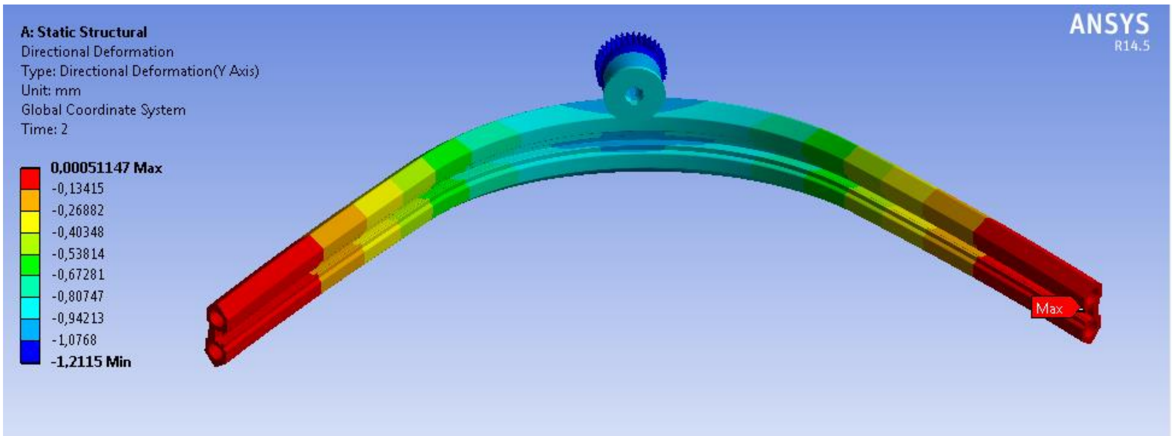
A: Static Structural
Directional Deformation
Type: Directional Deformation(Y Axis)
Unit: mm
Global Coordinate System
Time: 2
0,00051147 Max
-0,13415
-0,26882
-0,40348
-0,53814
-0,67281
-0,80747
-0,94213
-1,0768
-1,2115 Min
ANSYS
R14.5
Max

Fig. 3.3.49 Directional deformation distribution of the 90° curvature rail

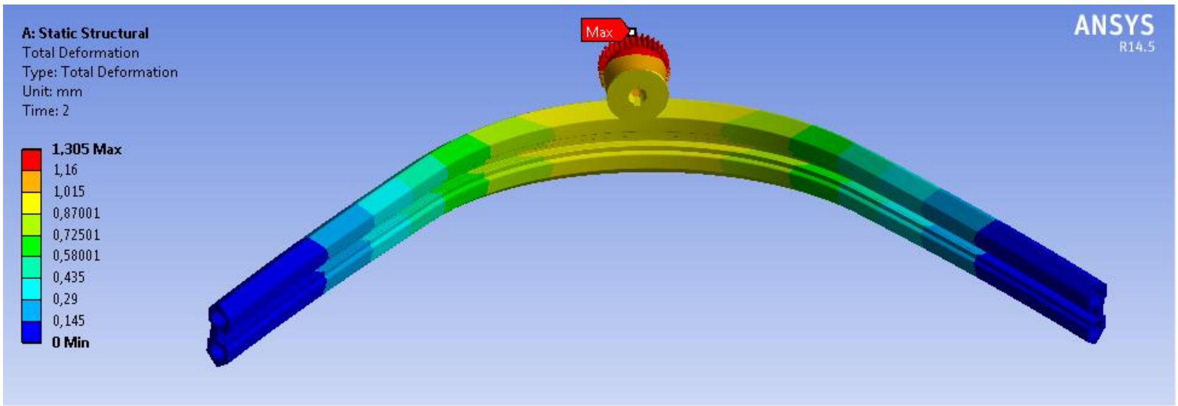
A: Static Structural
Total Deformation
Type: Total Deformation
Unit: mm
Time: 2
1,305 Max
1,16
1,015
0,87001
0,72501
0,58001
0,435
0,29
0,145
0 Min
ANSYS
R14.5
Max

Fig. 3.3.50 Total deformation distribution of the 90° curvature rail

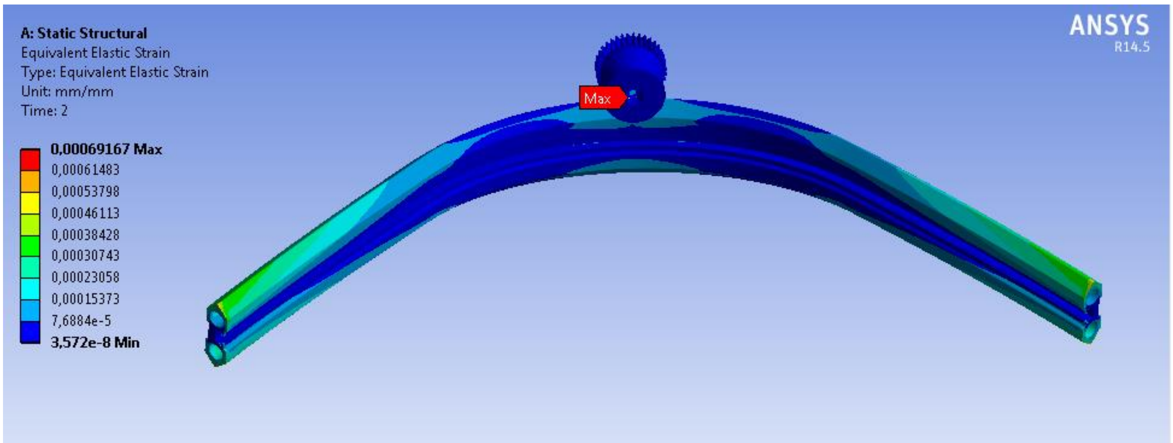
A: Static Structural
Equivalent Elastic Strain
Type: Equivalent Elastic Strain
Unit: mm/mm
Time: 2
0,00069167 Max
0,00061483
0,00053798
0,00046113
0,00038428
0,00030743
0,00023058
0,00015373
7,6884e-5
3,572e-8 Min
ANSYS
R14.5
Max

Fig. 3.3.51 Equivalent elastic strain distribution of the 90° curvature rail

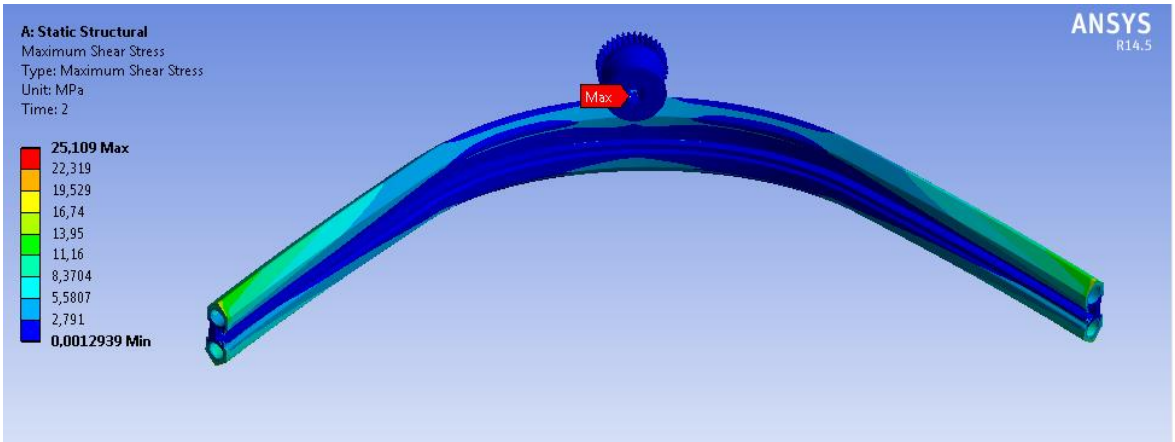
A: Static Structural
Maximum Shear Stress
Type: Maximum Shear Stress
Unit: MPa
Time: 2
25,109 Max
22,319
19,529
16,74
13,95
11,16
8,3704
5,5807
2,791
0,0012939 Min
Max
ANSYS
R14.5

Fig. 3.3.52 Maximum Shear Stress distribution of the 90° curvature rail

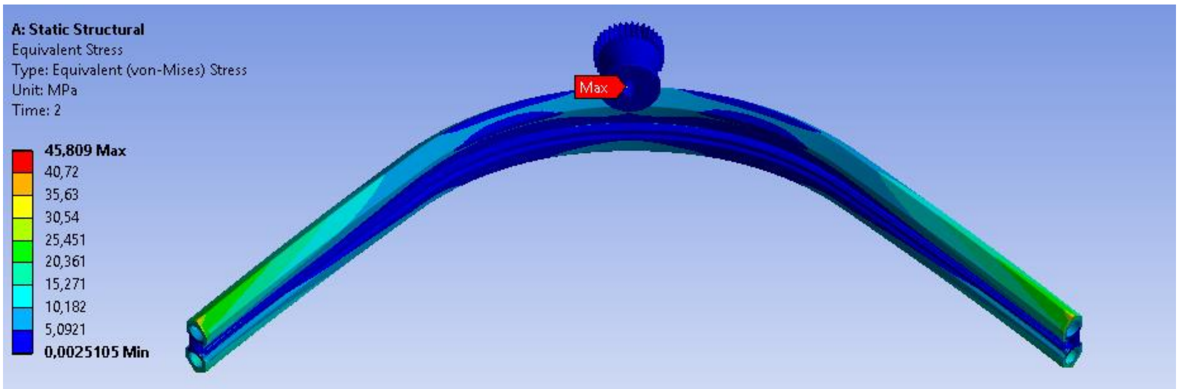
A: Static Structural
Equivalent Stress
Type: Equivalent (von-Mises) Stress
Unit: MPa
Time: 2
45,809 Max
40,72
35,63
30,54
25,451
20,361
15,271
10,182
5,0921
0,0025105 Min
Max

Fig. 3.3.53 Von Mises Stress distribution of the 90° curvature rail

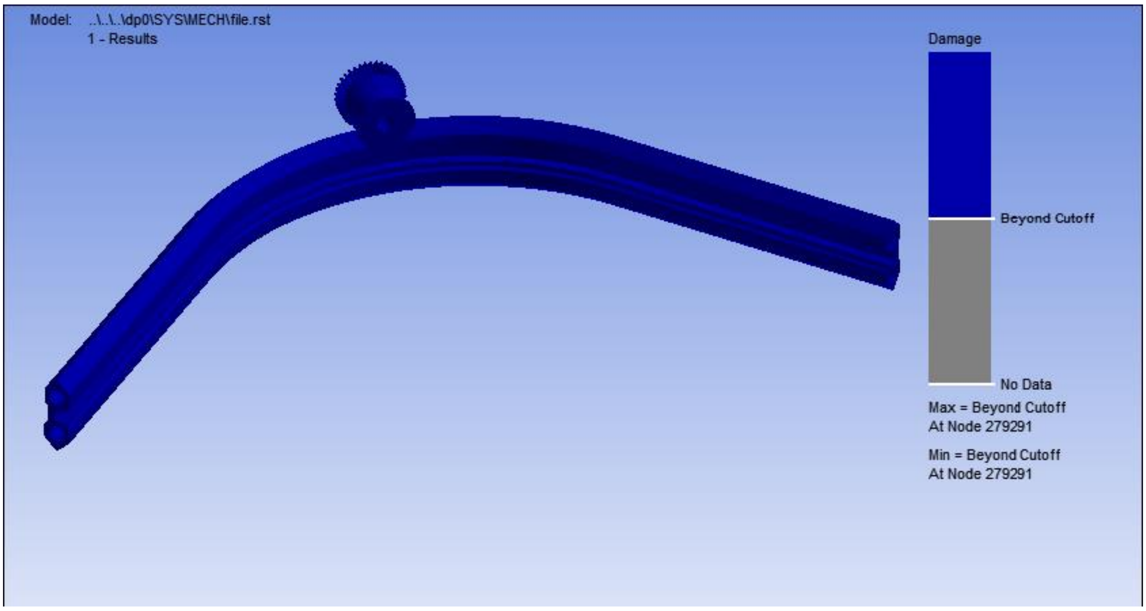
Model: ..\..\..\dp0\SYS\MECH\file.rst
1 - Results
Damage
Beyond Cutoff
No Data
Max = Beyond Cutoff
At Node 279291
Min = Beyond Cutoff
At Node 279291

Fig. 3.3.54 Damage distribution of the 90° curvature rail

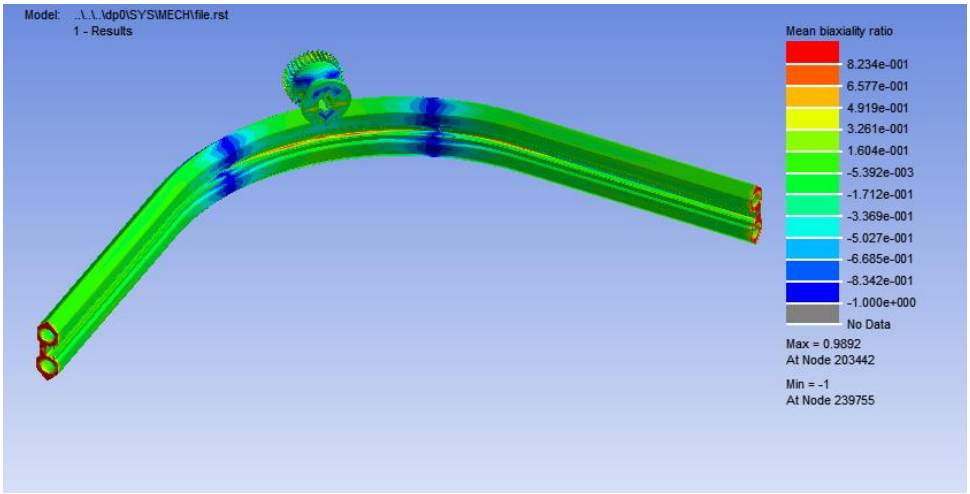
Model: ..\..\..\dp0\SYS\MECH\file.rst
1 - Results
Mean biaxiality ratio
8.234e-001
6.577e-001
4.919e-001
3.261e-001
1.604e-001
-5.392e-003
-1.712e-001
-3.369e-001
-5.027e-001
-6.685e-001
-8.342e-001
-1.000e+000
No Data
Max = 0.9892
At Node 203442
Min = -1
At Node 239755

Fig. 3.3.55 Mean biaxiliaty ratio distribution of the 90° curvature rail

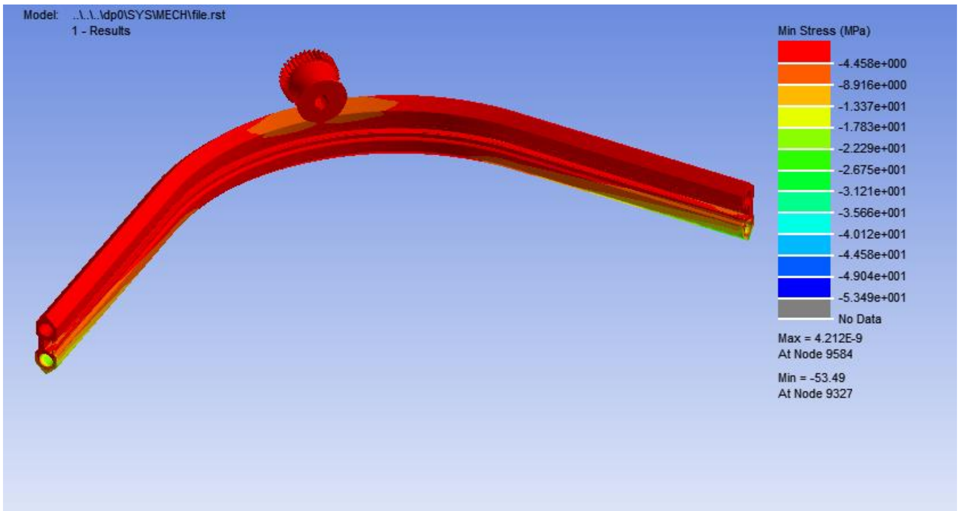
Model: ..\..\..\dp0\SYS\MECH\file.rst
1 - Results
Min Stress (MPa)
-4.458e+000
-8.916e+000
-1.337e+001
-1.783e+001
-2.229e+001
-2.675e+001
-3.121e+001
-3.566e+001
-4.012e+001
-4.458e+001
-4.904e+001
-5.349e+001
No Data
Max = 4.212E-9
At Node 9584
Min = -53.49
At Node 9327

Fig. 3.3.56 Min. stress distribution of the 90° curvature rail

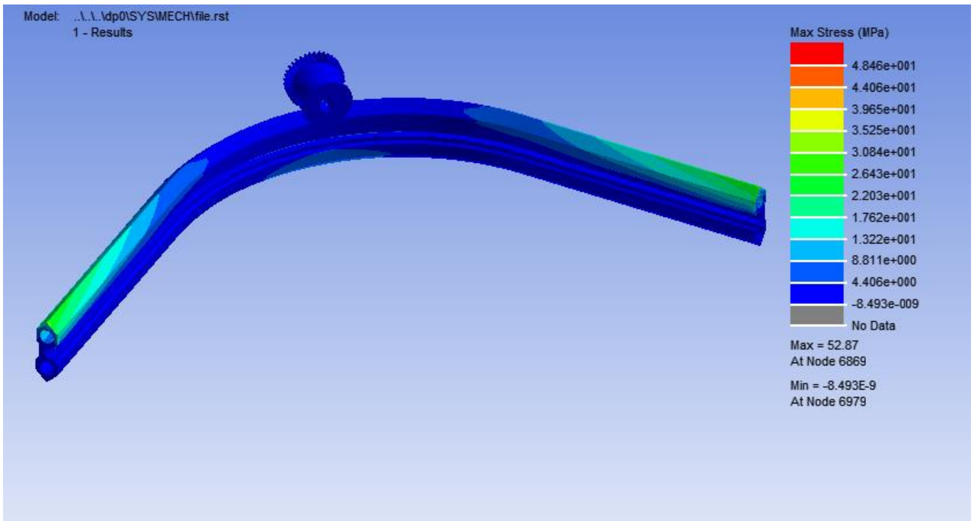
Model: ..\..\..\dp0\SYS\MECH\file.rst
1 - Results
Max Stress (MPa)
4.846e+001
4.406e+001
3.965e+001
3.525e+001
3.084e+001
2.643e+001
2.203e+001
1.762e+001
1.322e+001
8.811e+000
4.406e+000
-8.493e-009
No Data
Max = 52.87
At Node 6869
Min = -8.493E-9
At Node 6979

Fig. 3.3.57 Max. Stress of the 90° curvature rail

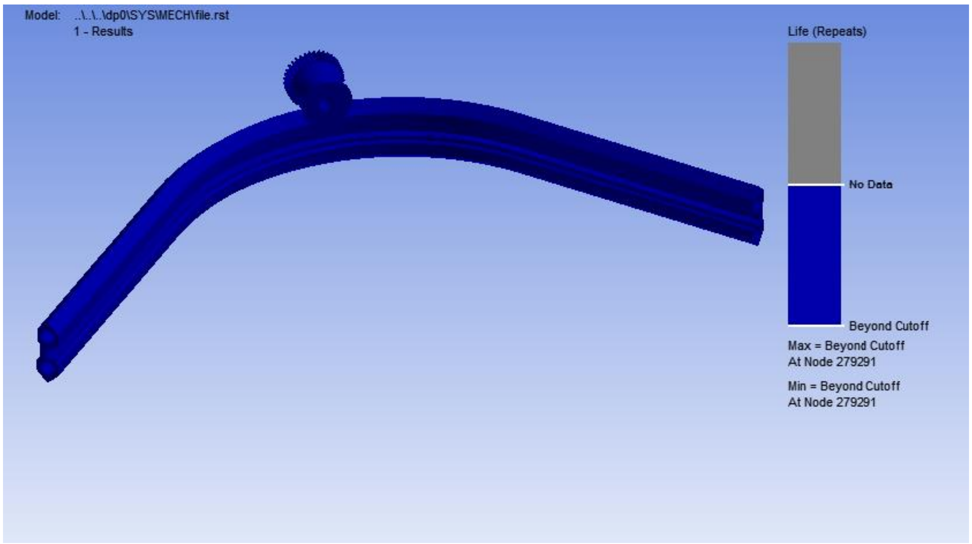
Model: ..\..\..\dp0\SYS\MECH\file.rst
1 - Results
Life (Repeats)
No Data
Beyond Cutoff
Max = Beyond Cutoff
At Node 279291
Min = Beyond Cutoff
At Node 279291

Fig. 3.3.58 Life of the 90° curvature rail

3.3.3.3 Bended Rail With 75° Curvature

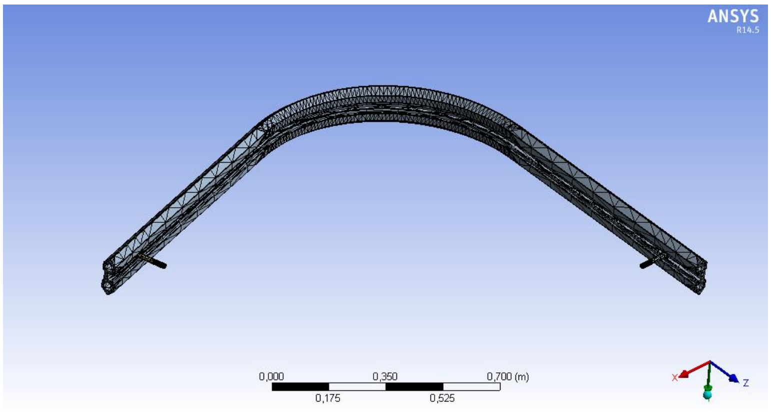
ANSYS
R14.5
0,000
0,350
0,700 (m)
0,175
0,525
X
Z

Fig.3.3.59 Mesh view of the 75° curvature rail

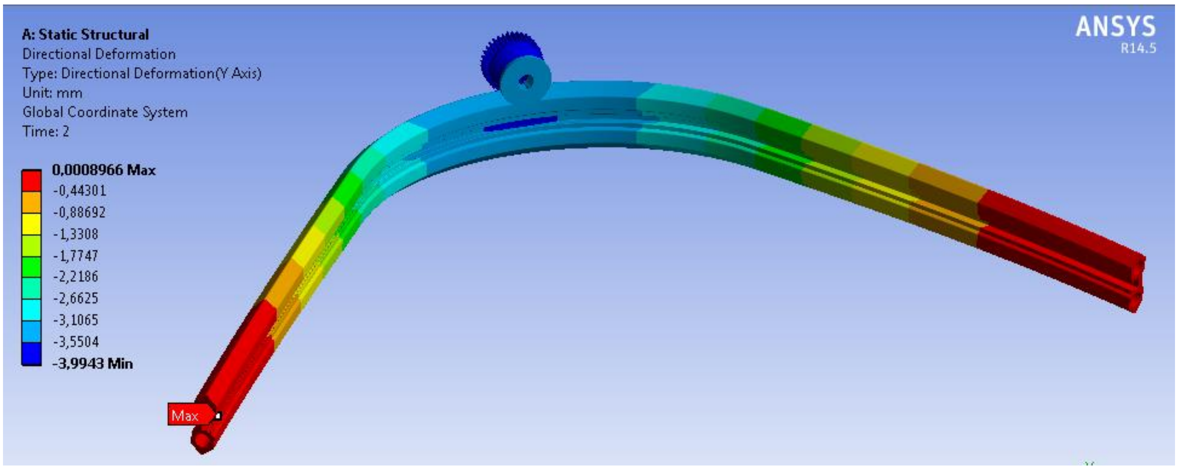
A: Static Structural
Directional Deformation
Type: Directional Deformation(Y Axis)
Unit: mm
Global Coordinate System
Time: 2
0,0008966 Max
-0,44301
-0,88692
-1,3308
-1,7747
-2,2186
-2,6625
-3,1065
-3,5504
-3,9943 Min
Max
ANSYS
R14.5

Fig. 3.3.60 Directional deformation distribution of the 75° curvature rail

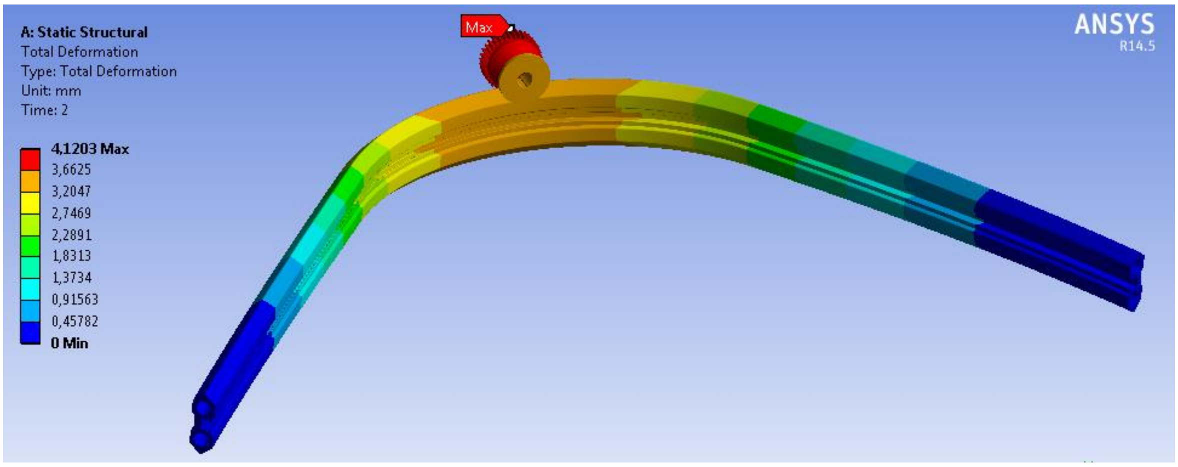
A: Static Structural
Total Deformation
Type: Total Deformation
Unit: mm
Time: 2
4,1203 Max
3,6625
3,2047
2,7469
2,2891
1,8313
1,3734
0,91563
0,45782
0 Min
Max
ANSYS
R14.5

Fig. 3.3.61 Total deformation distribution of the 75° curvature rail

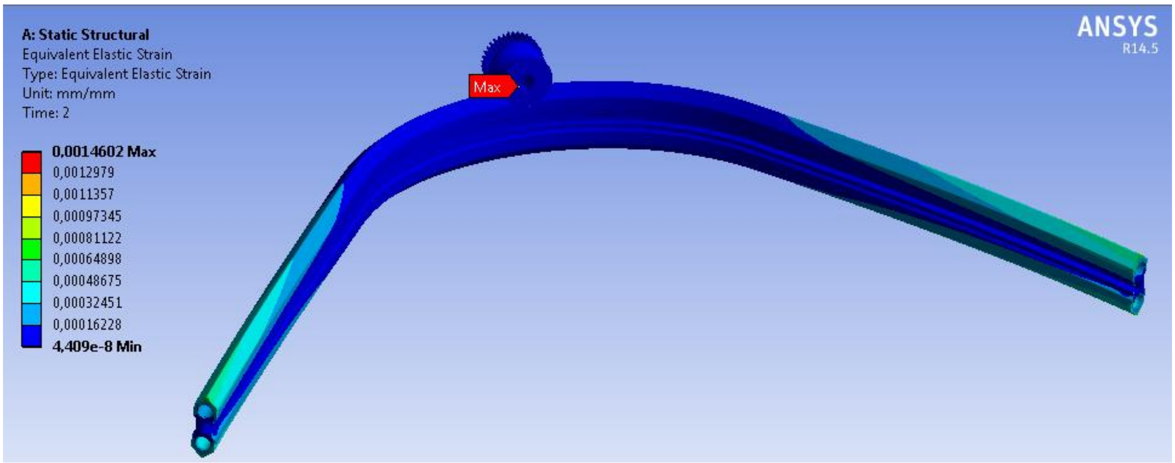
A: Static Structural
Equivalent Elastic Strain
Type: Equivalent Elastic Strain
Unit: mm/mm
Time: 2
0,0014602 Max
0,0012979
0,0011357
0,00097345
0,00081122
0,00064898
0,00048675
0,00032451
0,00016228
4,409e-8 Min
Max
ANSYS
R14.5

Fig. 3.3.62 Equivalent elastic strain distribution of the 75° curvature rail

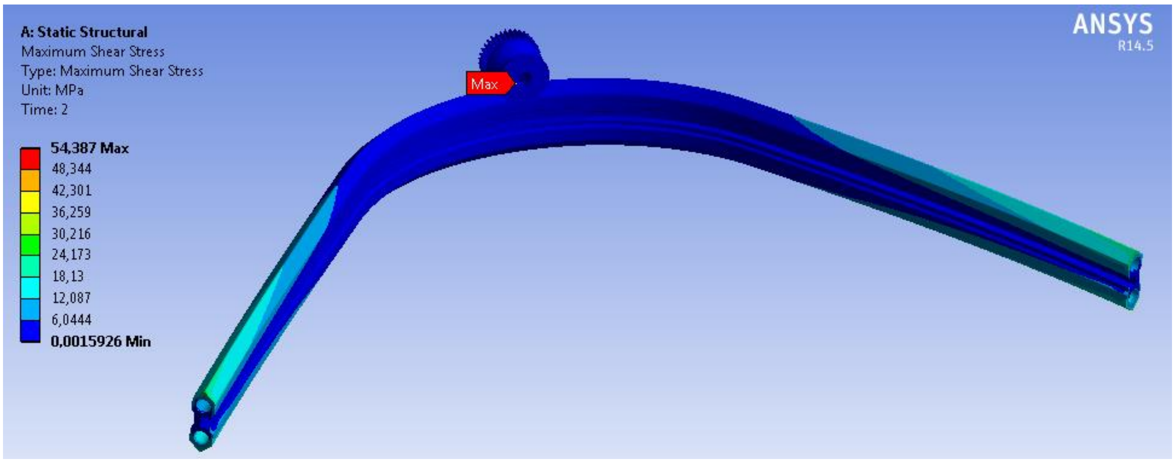
A: Static Structural
Maximum Shear Stress
Type: Maximum Shear Stress
Unit: MPa
Time: 2
54,387 Max
48,344
42,301
36,259
30,216
24,173
18,13
12,087
6,0444
0,0015926 Min
Max
ANSYS
R14.5

Fig. 3.3.63 Maximum Shear Stress distribution of the 75° curvature rail

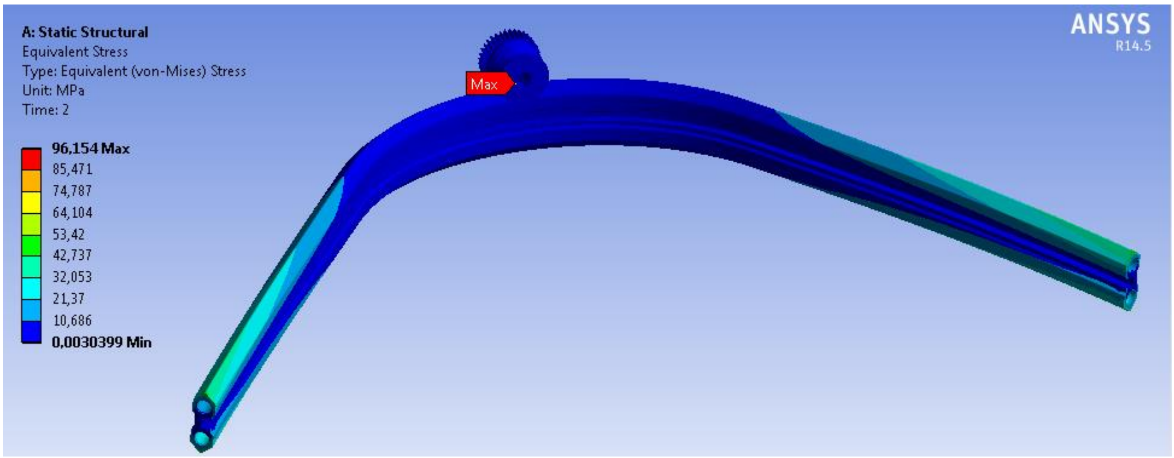
A: Static Structural
Equivalent Stress
Type: Equivalent (von-Mises) Stress
Unit: MPa
Time: 2
96,154 Max
85,471
74,787
64,104
53,42
42,737
32,053
21,37
10,686
0,0030399 Min
Max
ANSYS
R14.5

Fig. 3.3.64 Von Mises Stress distribution of the 75° curvature rail

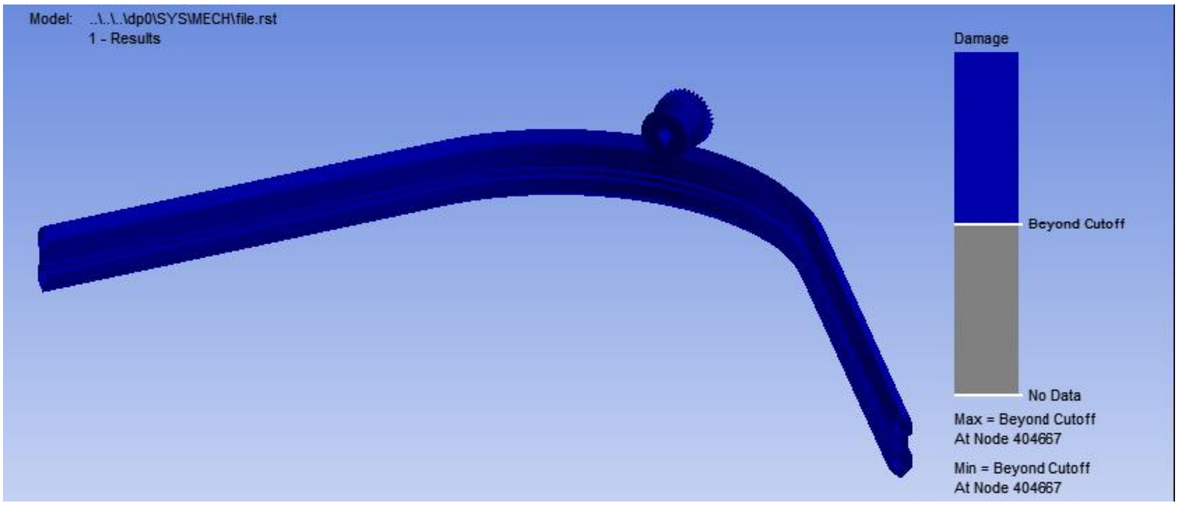
Model: ..\..\..\dp0\SYS\MECH\file.rst
1 - Results
Damage
Beyond Cutoff
No Data
Max = Beyond Cutoff
At Node 404667
Min = Beyond Cutoff
At Node 404667

Fig. 3.3.65 Damage distribution of the 75° curvature rail

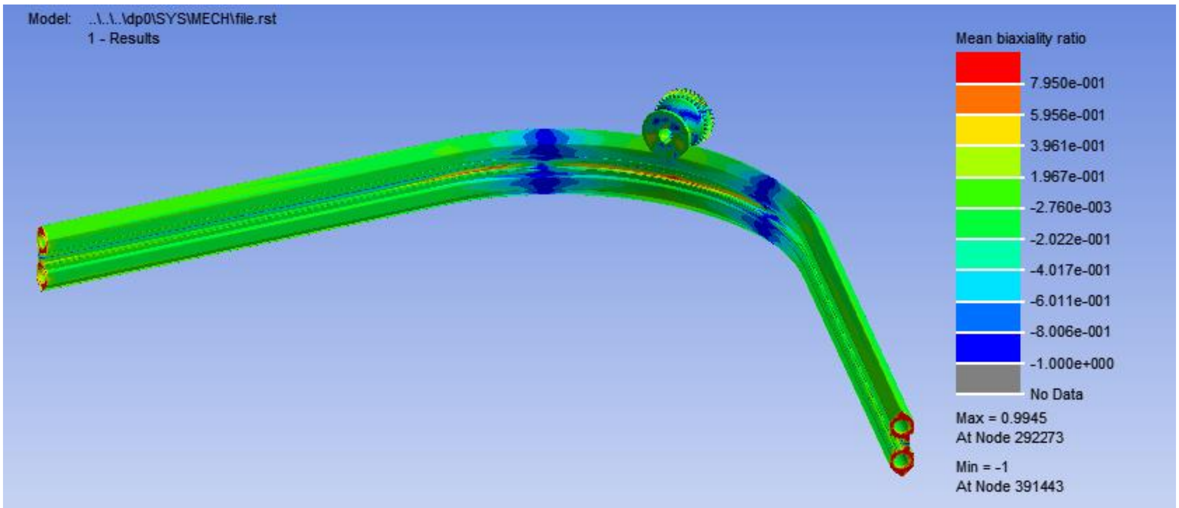
Model: ..\..\..\dp0\SYS\MECH\file.rst
1 - Results
Mean biaxiality ratio
7.950e-001
5.956e-001
3.961e-001
1.967e-001
-2.760e-003
-2.022e-001
-4.017e-001
-6.011e-001
-8.006e-001
-1.000e+000
No Data
Max = 0.9945
At Node 292273
Min = -1
At Node 391443

Fig. 3.3.66 Mean biaxiliaty ratio distribution of the 75° curvature rail

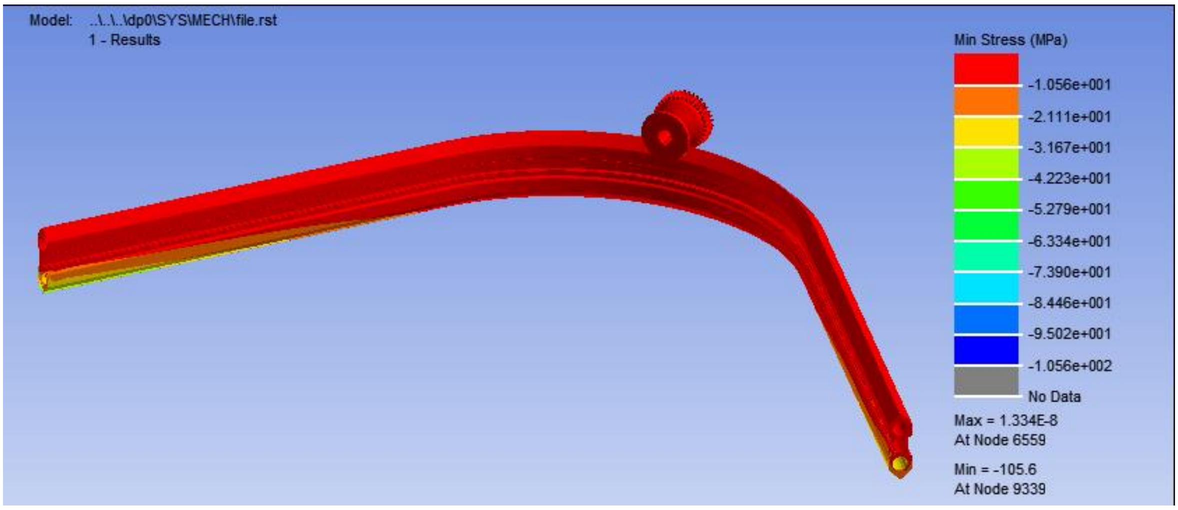
Model: ..\..\..\dp0\SYS\MECH\file.rst
1 - Results
Min Stress (MPa)
-1.056e+001
-2.111e+001
-3.167e+001
-4.223e+001
-5.279e+001
-6.334e+001
-7.390e+001
-8.446e+001
-9.502e+001
-1.056e+002
No Data
Max = 1.334E-8
At Node 6559
Min = -105.6
At Node 9339

Fig. 3.3.67 Min. stress of the 75° curvature rail

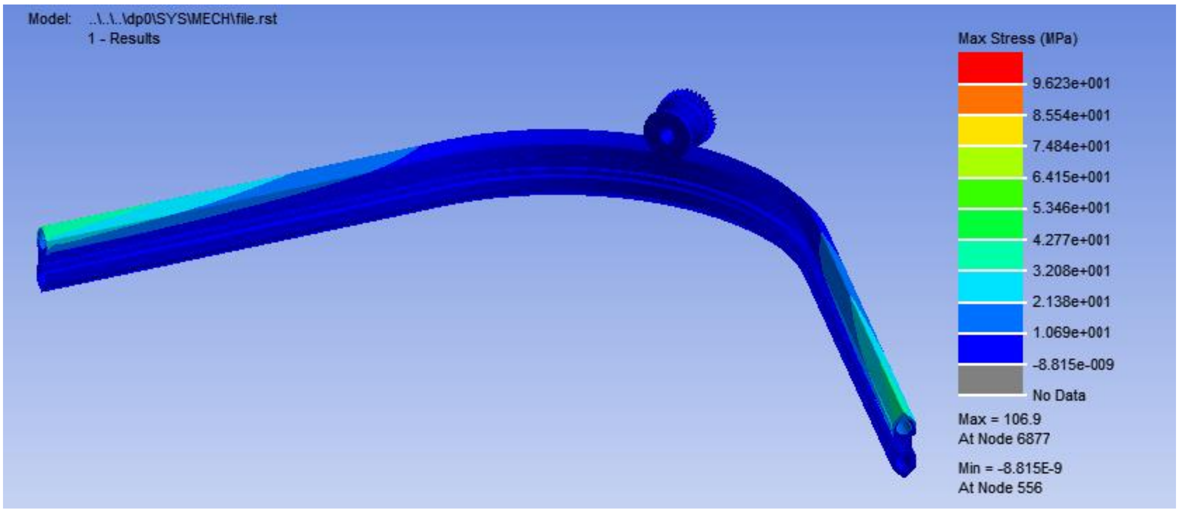
Model: ..\..\..\dp0\SYS\MECH\file.rst
1 - Results
Max Stress (MPa)
9.623e+001
8.554e+001
7.484e+001
6.415e+001
5.346e+001
4.277e+001
3.208e+001
2.138e+001
1.069e+001
-8.815e-009
No Data
Max = 106.9
At Node 6877
Min = -8.815E-9
At Node 556

Fig. 3.3.68 Max. stress of the 75° curvature rail

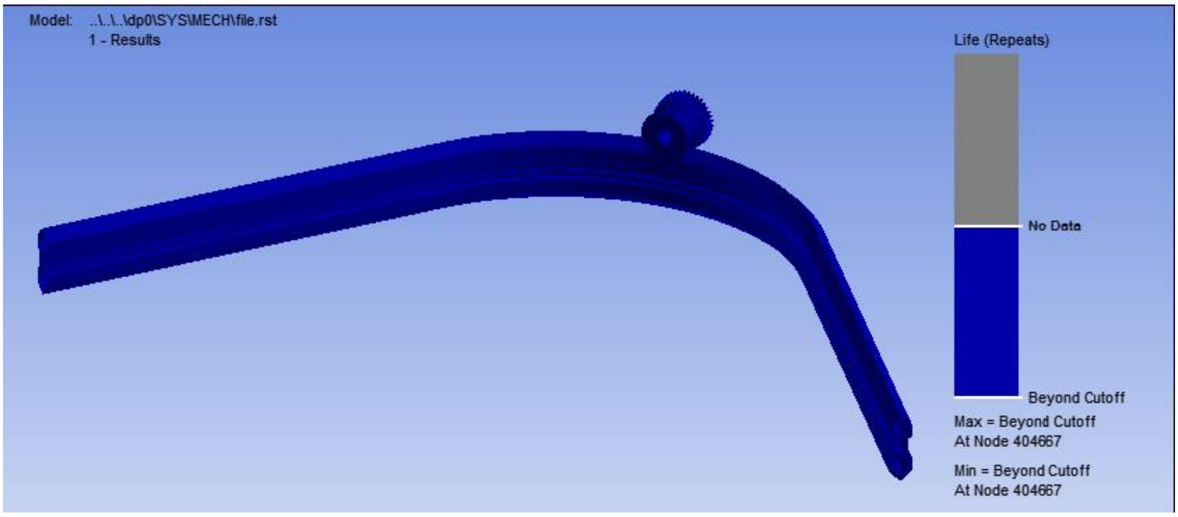
Model: ..\..\..\dp0\SYS\MECH\file.rst
1 - Results
Life (Repeats)
No Data
Beyond Cutoff
Max = Beyond Cutoff
At Node 404667
Min = Beyond Cutoff
At Node 404667

Fig. 3.3.69 Life of the 75° curvature rail

3.3.3.3 Bended Rail With 135° Curvature

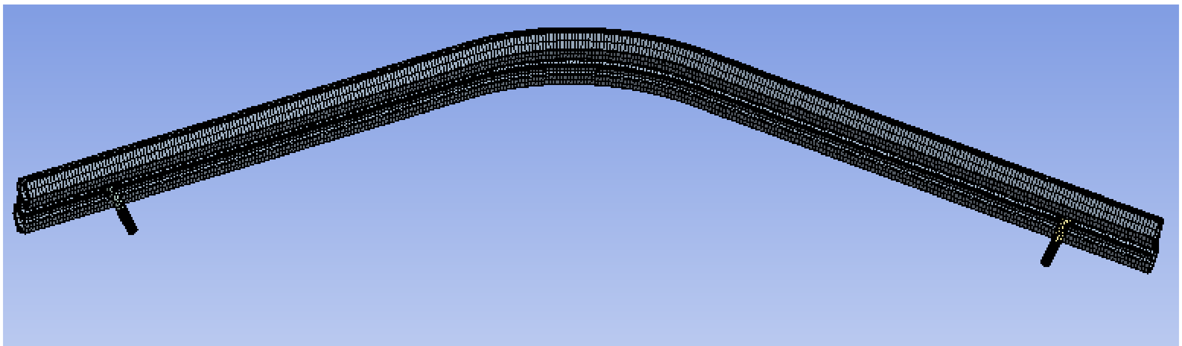

Fig. 3.3.70 Mesh view of the 135° curvature rail

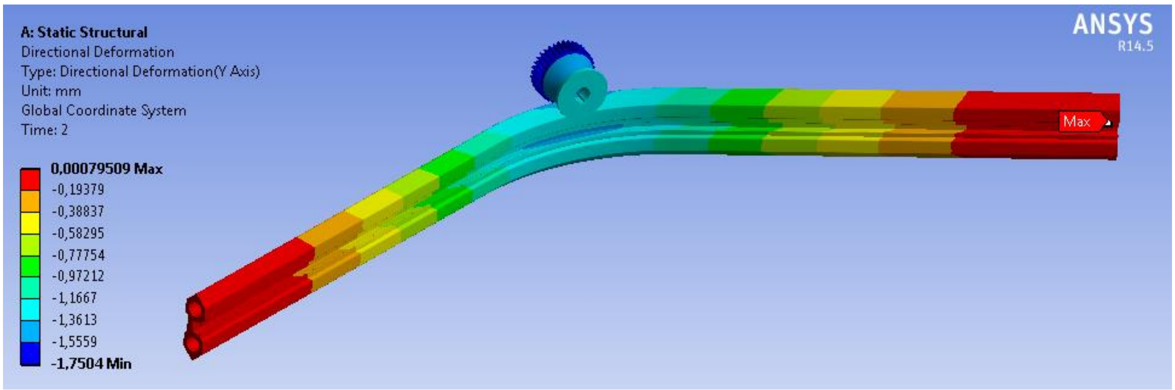
A: Static Structural
Directional Deformation
Type: Directional Deformation(Y Axis)
Unit: mm
Global Coordinate System
Time: 2
0,00079509 Max
-0,19379
-0,38837
-0,58295
-0,77754
-0,97212
-1,1667
-1,3613
-1,5559
-1,7504 Min
ANSYS
R14.5
Max

Fig. 3.3.71 Directional deformation distribution of the 135° curvature rail

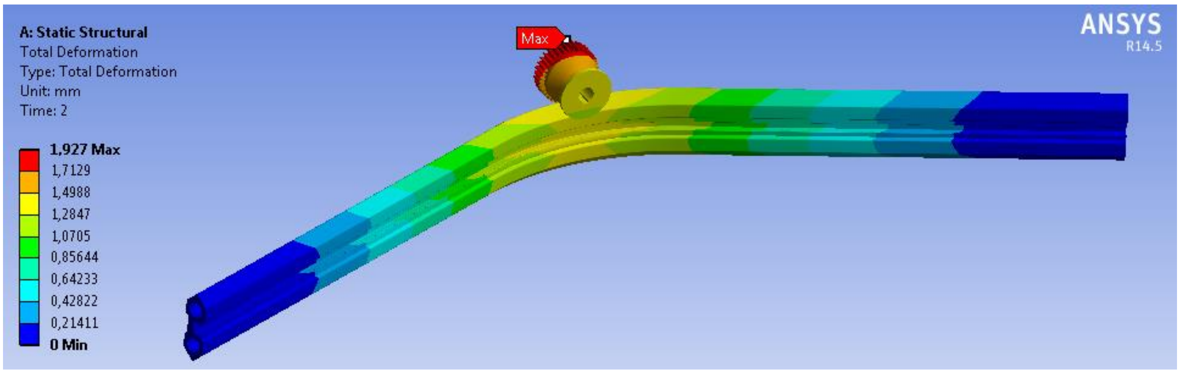
A: Static Structural
Total Deformation
Type: Total Deformation
Unit: mm
Time: 2
1,927 Max
1,7129
1,4988
1,2847
1,0705
0,85644
0,64233
0,42822
0,21411
0 Min
ANSYS
R14.5
Max

Fig. 3.3.72 Total deformation distribution of the 135° curvature rail

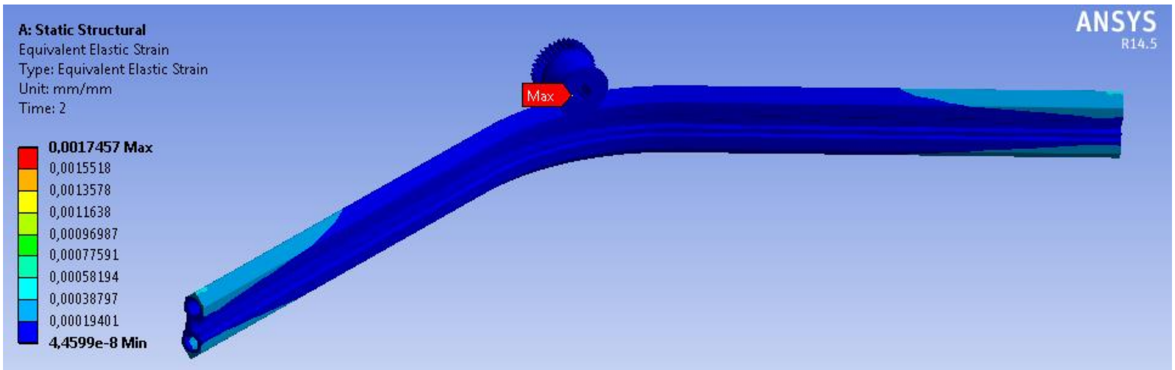
A: Static Structural
Equivalent Elastic Strain
Type: Equivalent Elastic Strain
Unit: mm/mm
Time: 2
0,0017457 Max
0,0015518
0,0013578
0,0011638
0,00096987
0,00077591
0,00058194
0,00038797
0,00019401
4,4599e-8 Min
Max
ANSYS
R14.5

Fig. 3.3.73 Equivalent elastic strain distribution of the 135° curvature rail

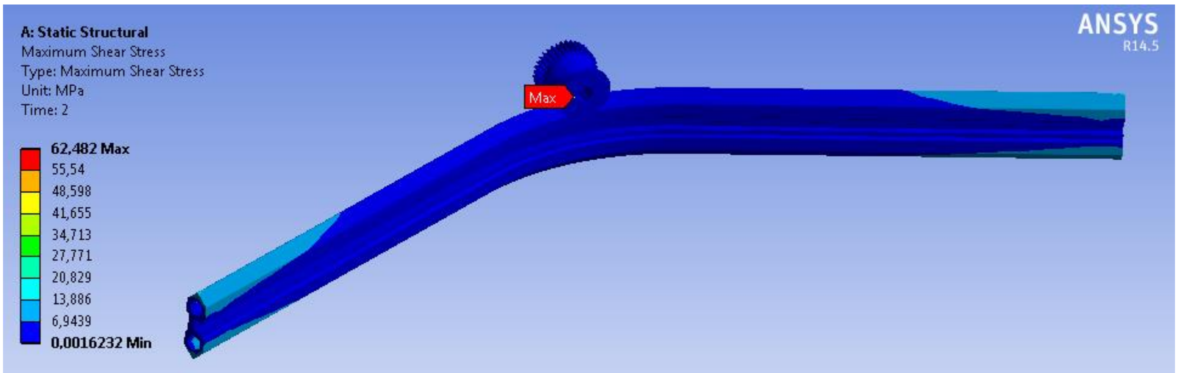
A: Static Structural
Maximum Shear Stress
Type: Maximum Shear Stress
Unit: MPa
Time: 2
62,482 Max
55,54
48,598
41,655
34,713
27,771
20,829
13,886
6,9439
0,0016232 Min
Max
ANSYS
R14.5

Fig. 3.3.74 Maximum Shear Stress distribution of the 135° curvature rail

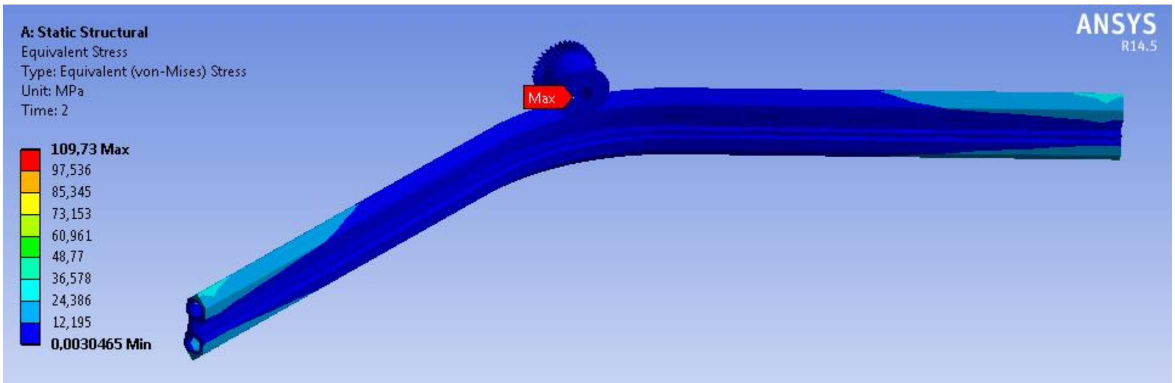
A: Static Structural
Equivalent Stress
Type: Equivalent (von-Mises) Stress
Unit: MPa
Time: 2
109,73 Max
97,536
85,345
73,153
60,961
48,77
36,578
24,386
12,195
0,0030465 Min
Max
ANSYS
R14.5

Fig. 3.3.75 Von Mises Stress distribution of the 135° curvature rail

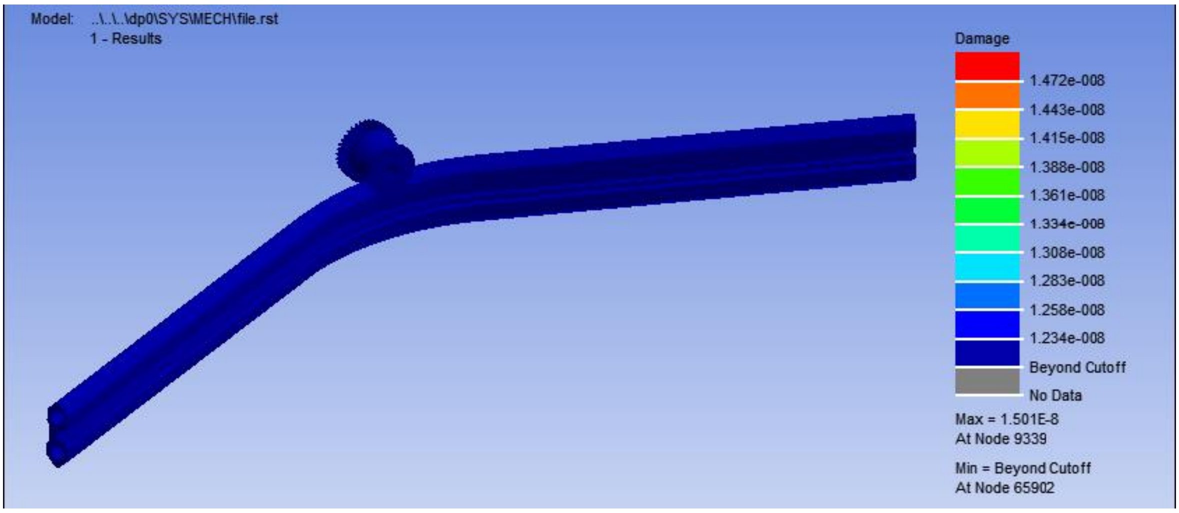
Model: ..\..\..\dp0\SYS\MECH\file.rst
1 - Results
Damage
1.472e-008
1.443e-008
1.415e-008
1.388e-008
1.361e-008
1.334e-008
1.308e-008
1.283e-008
1.258e-008
1.234e-008
Beyond Cutoff
No Data
Max = 1.501E-8
At Node 9339
Min = Beyond Cutoff
At Node 65902

Fig. 3.3.76 Damage distribution of the 135° curvature rail

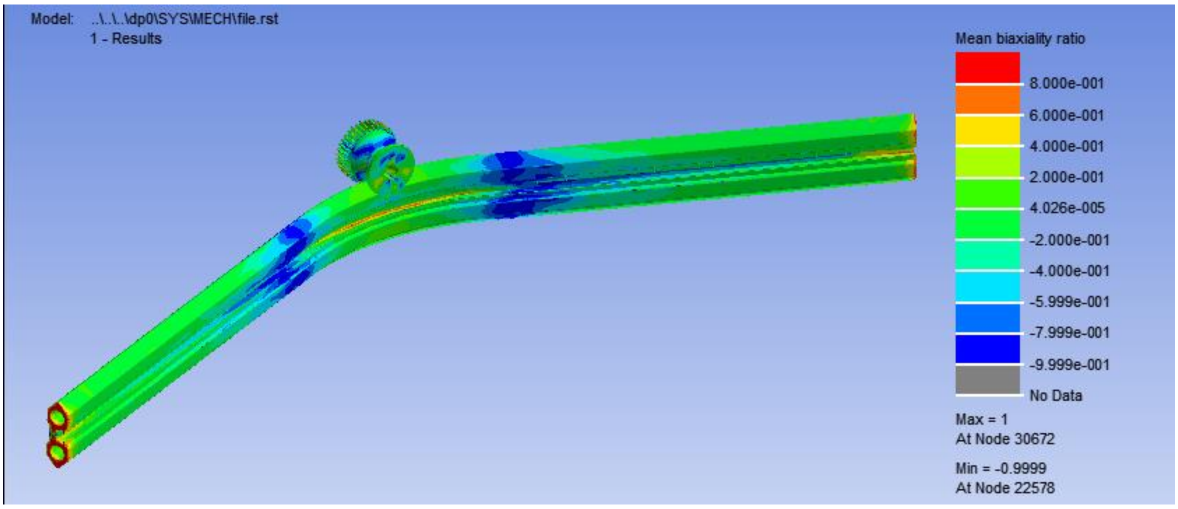
Model: ..\..\..\dp0\SYS\MECH\file.rst
1 - Results
Mean biaxiality ratio
8.000e-001
6.000e-001
4.000e-001
2.000e-001
4.026e-005
-2.000e-001
-4.000e-001
-5.999e-001
-7.999e-001
-9.999e-001
No Data
Max = 1
At Node 30672
Min = -0.9999
At Node 22578

Fig. 3.3.77 Mean biaxiliaty ratio distribution of the 135° curvature rail

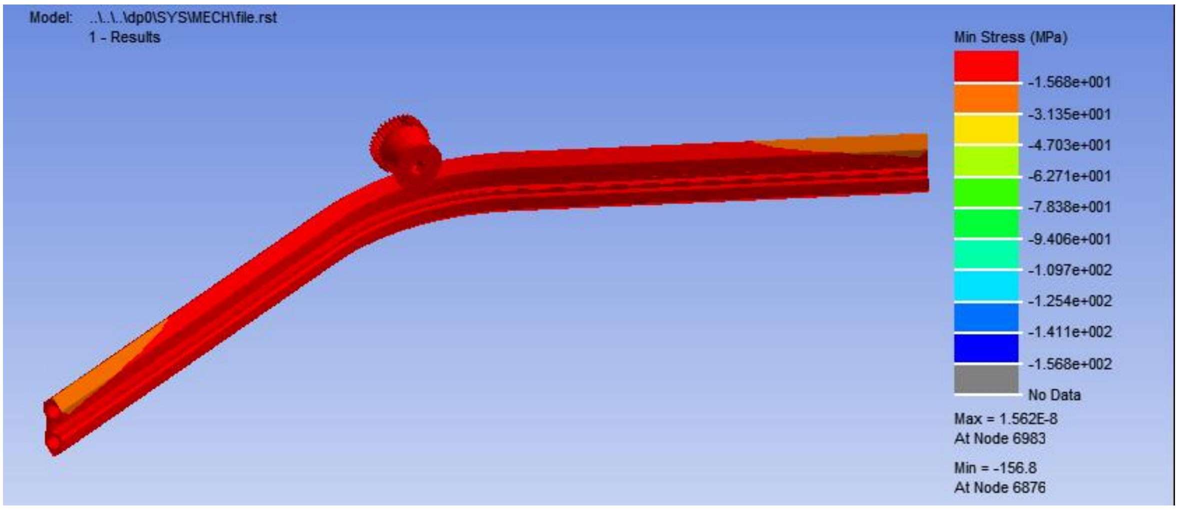
Model: ..\..\..\dp0\SYS\MECH\file.rst
1 - Results
Min Stress (MPa)
-1.568e+001
-3.135e+001
-4.703e+001
-6.271e+001
-7.838e+001
-9.406e+001
-1.097e+002
-1.254e+002
-1.411e+002
-1.568e+002
No Data
Max = 1.562E-8
At Node 6983
Min = -156.8
At Node 6876

Fig. 3.3.78 Min. Stress of the 135° curvature rail

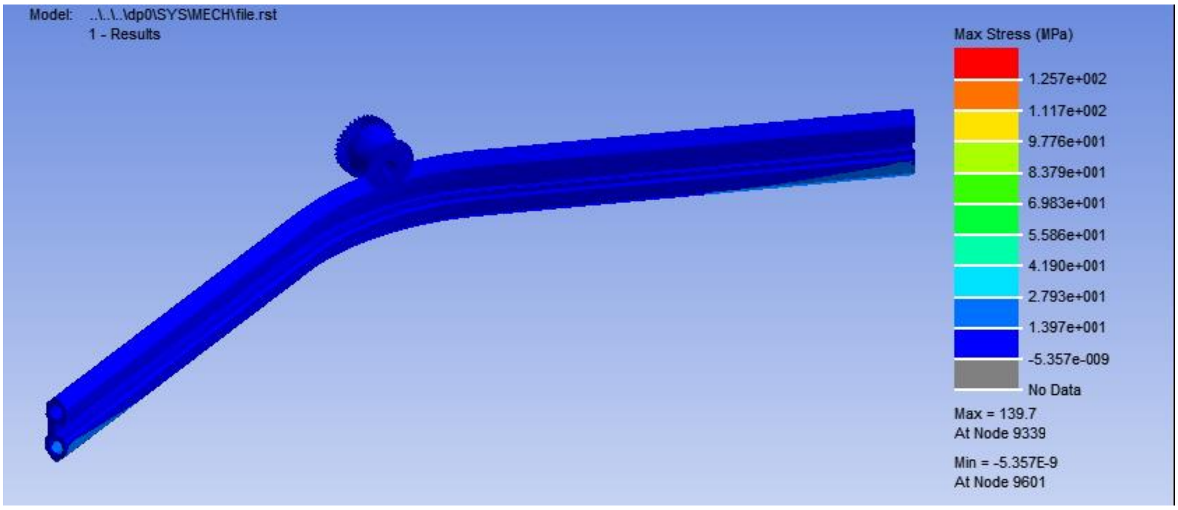
Model: ..\..\..\dp0\SYS\MECH\file.rst
1 - Results
Max Stress (MPa)
1.257e+002
1.117e+002
9.776e+001
8.379e+001
6.983e+001
5.586e+001
4.190e+001
2.793e+001
1.397e+001
-5.357e-009
No Data
Max = 139.7
At Node 9339
Min = -5.357E-9
At Node 9601

Fig. 3.3.79 Max. Stress of the 135° curvature rail

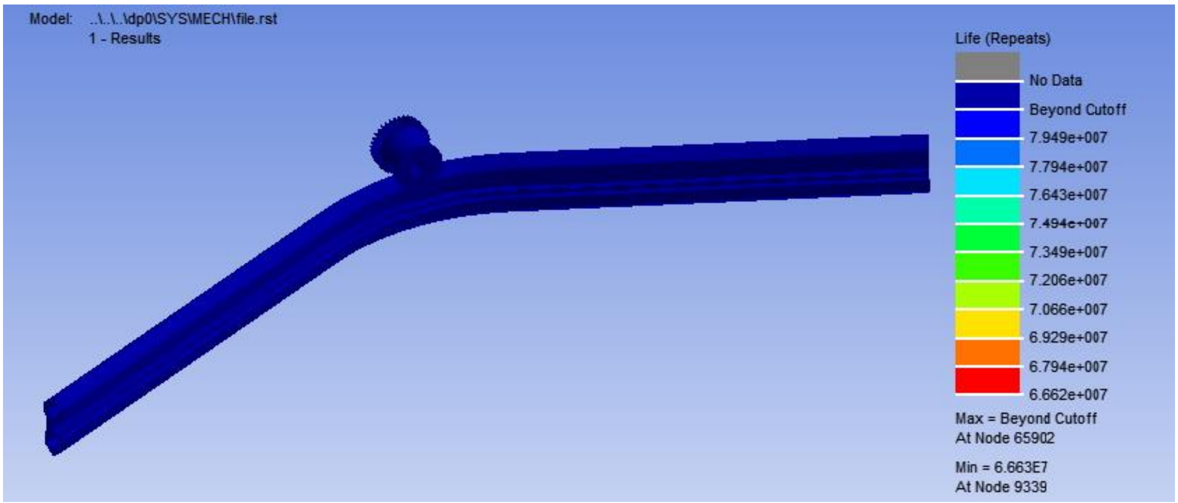
Model: ..\..\..\dp0\SYS\MECH\file.rst
1 - Results
Life (Repeats)
No Data
Beyond Cutoff
7.949e+007
7.794e+007
7.643e+007
7.494e+007
7.349e+007
7.206e+007
7.066e+007
6.929e+007
6.794e+007
6.662e+007
Max = Beyond Cutoff
At Node 65902
Min = 6.663E7
At Node 9339

Fig. 3.3.80 Life of the 135° curvature rail

3.4 Conclusion

In this study, a rail made of aluminum 6061-T6 has been examined. The optimum requirements of rail, such as section area and second moment of inertia has been optimized or designed in terms of the higher load that the monorail crane is able to remove and transform. To be able to predict the shape of contact region on the rail, the Hertz contact equations have been used and it is estimated that an eliptical area occurs on rail. Since the buildings in today have highly complicated or curvilinear shapes, this required that the rails should not only be as horizontal but also be bended in some common angles such as S - 75º - 90º and 135º.

Firstly horizontal rail have been examined and Von Mises stress have been found in the middle of the horizontal rail as 45 Mpa. Also a horizontal rail carrying two weights (425 kg's) have been considered and found the Von Mises Stresses as 28 Mpa. Those stress values are very small compared to yield stress of rail, Al6061. Total deformations of both type of rails can not be considered as a failure criteria. Max. And Min Stresses have been calculated for horizontal rail carrying 500 kg load as 76 Mpa, -74 Mpa and horizontal rail carrying two 425 kg loads as 52 Mpa -58 Mpa respectively and found life and damage values as infinite life.

Secondly vertical rail have been examined and Von Mises stress have been found in the middle of the vertical rail as 69 Mpa. Total deformationf of vertical rail can not be considered as a failure criteria. Max. And Min Stresses have been calculated, life and damage values found as infinite life.

Lastly, rails bended as S - 90º - 75º and 135º have been examined and Von Mises stresses found 35 MPa – 45 Mpa - 96 Mpa and 110 Mpa respectively and compared yield stress value of Al 6061, it can be said that bended rails satisfy the design requirements. Total deformations of all bended rails are very small and can not be considered as a failure criteria. Damage results and life results of the four curved rails show different results, because of having different lengths and loading conditions. But all of the damage values are high from 1 and life results values are high from 1e6. Max. stress distribution and Min. stress distribution results occuring by loads are also convenient in terms of yield stress Al6061.

4. GEARS

4.1 Introduction

In engineering applications, gears are used to transmit torque, power and angular velocity. In monorail crane machine, two types of gears, operating on parallel shafts of wheel and reductor, and a worm gear, transfering motion from electrical motor to shaft, have been used.

4.1.1 Gear Materials

Metals and alloys are limited in terms of gears transmitting significant powers. Table 4.1 shows some gear materials. The most common materials of gears are steels, cast irons, and malleable and nodular irons. In applications, high corrosion is needed bronzes are preferred as gear material. With the appliying surface or through hardening to gears, sufficient strength and wear resistance can be obtained on the tooths of gears.

Cast irons are also used for gears in some applications. Because, the there are outstanding advantages of gray cast irons compared to other type of cast irons such as low cost, ease of machining, high wear resistance, and internal damping (due to the graphite inclusions), which makes them acoustically quieter than steel gears. Also, they have low tensile strength, which requires larger teeth than steel gears to obtain sufficient bending strength. Nodular irons have higher tensile strength than gray CI and retain the other advantages of machinability, wear resistance, and internal damping, but they are more costly. The combination of a steel pinion and a cast iron gear is often used. Steels are also commonly used for gears because having superior tensile strength to cast iron and are cost competitive in their low-alloy forms. Many steels need heat treatment to get a surface hardness that will resist wear, but soft steel gears are sometimes used in low-load, low-speed applications or where long life may not be a prime concern. Small gears are typically through-hardened and larger gears flame are hardened by induction to minimize distortion.

Some surface methods such as carburizing or nitriding make lower-carbon steels case hardened. A case-hardened gear has the advantage of a tough core and a hard surface, but if the case hardening method is not deep enough, the teeth may fail in bending fatigue beneath the case in the soft, weaker core material. If high accuracy is needed, some manufacturing methods can be used such as grinding, lapping, and honing to remove the heat treatment distortion from hardened gears.

AGMA Elastic Coefficient C_p in Units of $[psi]^{0.5}$ ($[(MPA)]^{0.5}$)							
Pinion material	**E_p Psi (MPa)**						
		Steel	**Malleable Iron**	**Nodular Iron**	**Cast Iron**	**Aluminum Bronze**	**Tin Bronze**
Steel	30E6 (2E5)	2300 (191)	2180 (181)	2160 (179)	2100 (174)	1950 (162)	1900 (158)
Malleable Iron	25E6 (1.7E5)	2180 (181)	2090 (174)	2070 (172)	2020 (168)	1900 (154)	1850 (152)
Nodular Iron	24E6 (1.7E5)	2160 (179)	2070 (172)	2050 (170)	2000 (166)	1880 (156)	1830 (152)
Cast Iron	22E6 (1.5E5)	2100 (174)	2020 (168)	2000 (166)	1960 (163)	1850 (154)	1800 (149)
Aluminum Bronze	17.5E6 (1.2E5)	1950 (162)	1900 (158)	1880 (156)	1850 (154)	1750 (145)	1700 (141)
Tin Bronze	16E6 (1.1E5)	1900 (158)	1850 (154)	1830 (152)	1800 (149)	1700 (141)	1650 (137)

Table 4.1 Some metals and alloys for gears (Machine Design, Robert L. Norton*)*

4.2 SPUR GEAR DESİGN

4.2.1 Spur Gear Analytical And Fem Results

4.2.1.1 Spur Gear Analytical Study, Gear tooth and Gear Mesh Parameters

In this study, AGMA Stress and Strength Equations (Shigley’s Mechanical Enginnering Design, Richard G. Budynas – J. Keith Nisbett) have been used for the design of spur and worm gears. In spur gears, assuming center distance is increased 2%, the new pressure angle and the torques and transmitted loads on the gear teeth and the mean and alternating components of transmitted load on each gear have beebestimated. The pinion shaft passes 1850W at 52,5 rpm. The pinion has 17 teeth, a 20° pressure angle, and, the gear has 36 teeth.

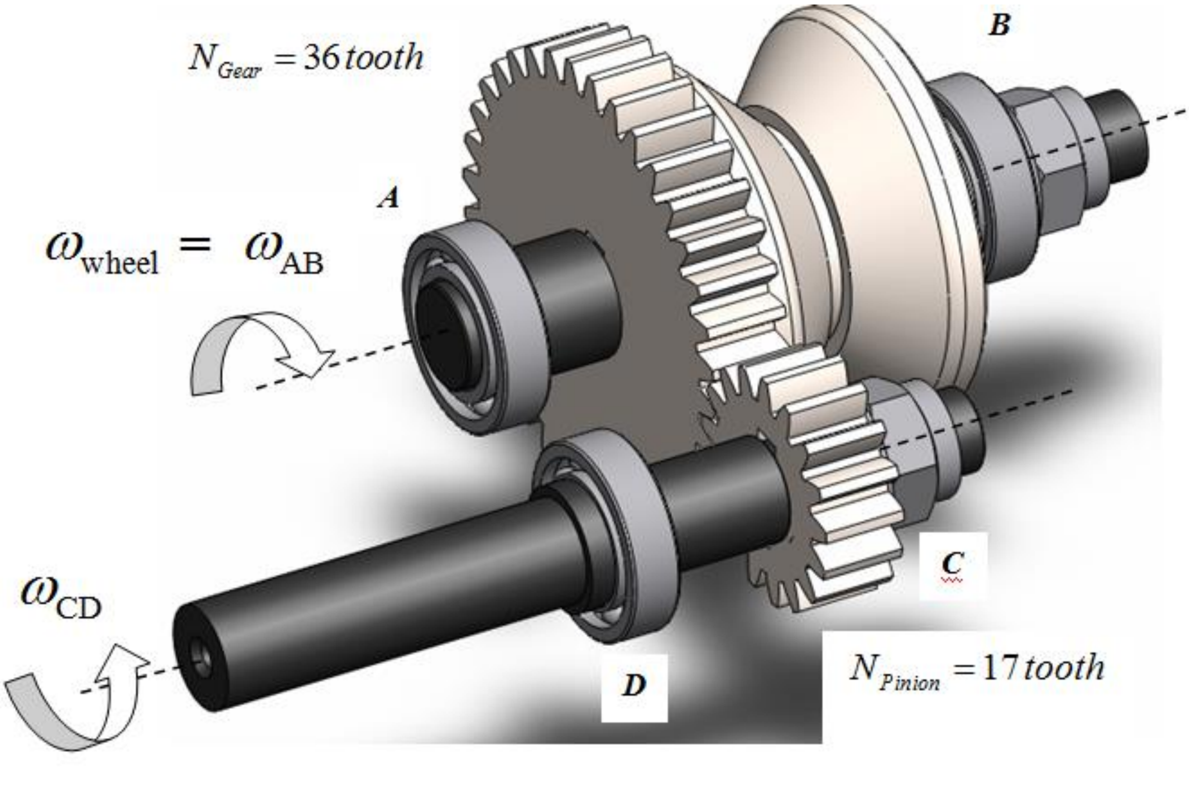

Fig. 4.1 Assembly view of the spur gears

The gear ratio is easily found from the given tooth numbers on pinion and gear;

$$m_G = \frac{N_G}{N_p} = \frac{36}{17} = 2{,}118$$

The torque on the pinion shaft; We have used a reductor that has worm gear mechanism having an efficiency 0,5 % in it.

$$P_{motor} = T_{motor}\, x W_{motor}$$

$$W_{motor} = \frac{2\pi\, x\, n}{60} = \frac{2\pi\, x 1740}{60} = 182,2\, rad / sn$$

Since motor outshaft is linked to the worm, we obtain the wormgear power by multiplying the motor power with the efficiency of the worm – gear.

$$P_{motor}\, x\, \eta_{worm-gear} = P_{\left(worm-gear\right)out}$$

$$P_{\left(worm-gear\right)out} = 3700\, x\, 0,5 = 1850W$$

$$P_{pinion} = T_{pinion}\, x W_{pinion}$$

$$1850W = T_{pinion}\, x 5,5$$

$$T_{pinion} = 336\, N.m$$

$$T_a = \frac{T_{\max} - T_{\min}}{2} = \frac{336-0}{2} = 168\, N.m \qquad T_m = \frac{T_{\max} + T_{\min}}{2} = \frac{336+0}{2} = 168\, N.m$$

$$N_{CD} = 52,5\, rpm = 0,875\, revolution\ per\ \sec$$

The transmitted load is the same on gears and can be found from the torque and radius of any one of the gears;

$$F_t = \frac{2\, x T}{d} = \frac{2\, x 336}{0,051} = 13177N$$

The radial component of load;

$$F_r = F_t\, x \tan\alpha = 13177\, x \tan 20^{\circ} = 4796\, N$$

The total load is,

$$F = \frac{F_t}{\cos\phi} = \frac{13177}{\cos 20^\circ} = 14023\,N$$

The repeated loads on any pinion or gear tooth are;

$$(F_t)_{alternating} = \frac{F_t}{2} = \frac{13177}{2} = 6588,5\,N$$

$$(F_t)_{mean} = \frac{F_t}{2} = \frac{13177}{2} = 6588,5\,N$$

A suitable face width;

$$b_{face} \cong 4\,x\,\pi\,x\,m = 4\,x\,\pi\,x\,3 \cong 40\,mm$$

The circular pitch is

$$p_c = \pi m = \pi x 3 = 9,42\,mm$$

$$p_d = \frac{\pi}{p_c} = \frac{\pi}{9,42} = 0,34\,mm$$

The base pitch measured on the base circle is

$$p_b = p_c \cos\phi = 9,42\,x \cos 20^\circ = 8,85\,mm$$

The pitch diameters and pitch radii of pinion and gear are,

$$(D_t)_P = m\,x\,N_p = 3\,x\,17 = 51\,mm$$

$$(D_t)_G = m\,x\,N_G = 3\,x\,36 = 108\,mm$$

The nominal center distance C is the sum o f the pitch radii:

$$C = \frac{(D_t)_p + (D_t)_G}{2} = \frac{51+108}{2} = 79{,}5\,mm$$

The addendum and dedendum are found,

$$a = m = 3\,mm \qquad b = 1{,}166\,xm = 3x1{,}166 = 3{,}49\,mm$$

The whole depth h, is the sum o f the addendum and dedendum.

$$h_t = a + b = 2{,}166\,m = 2{,}166x3 = 6{,}498\,mm$$

The clearance is the difference between dedendum and addendum.

$$c = b - a = 3{,}49 - 3 = 0{,}49\,mm$$

The outside diameter of each gear is the pitch diameter plus two addenda:

$$\begin{aligned}(D_o)_p &= (D_t)_p + 2m = (N_p + 2)m = (17+2)x3 = 57\,mm \\ (D_o)_G &= (D_t)_G + 2m = (N_G + 2)m = (36+2)x3 = 114\,mm\end{aligned}$$

The contact ratio is can be found,

$$\begin{aligned}Z &= \sqrt{(r_p + a_p)^2 - (r_p \cos\phi)^2} + \sqrt{(r_G + a_G)^2 - (r_G \cos\phi)^2} - C\sin\phi \\ &= \sqrt{(25{,}5+3)^2 - (25{,}5\cos 20)^2} + \sqrt{(54+3)^2 - (54\cos 20)^2} - 79{,}5\sin 20 = 14{,}2\,mm\end{aligned}$$

$$m_p = \frac{Z}{p_b} = \frac{14{,}2}{47{,}92} = 0{,}296$$

If the center distance is increased from the nominal value due to assembly errors or other factors, the effective pitch radii will change by the same percentage. The gears' base radii will remain the same. The new pressure angle can be found from the changed geometry. For a 2% increase in center distance (1.02x):

$$\phi_{new} = \cos^{-1}\left(\frac{r_{base,circle_p}}{1,02r_p}\right) = \cos^{-1}\left(\frac{r_p \cos\phi}{1,02r_p}\right) = \cos^{-1}\left(\frac{\cos 20^\circ}{1,02}\right) = 22,89^\circ$$

Even though the transmitted load is the same, the bending stress in the teeth of each size gear will be different because of its slightly different tooth geometry. The diametral pitch value is 51 mm, the face width 40 mm, and the quality standard is No.6. The gears are straddle-mounted with bearings immediately adjacent.

The pinion is a grade SAE 1050 steel (S_t = 538 Mpa, S_{ut}= 717Mpa, quenched and tempered) with a hardness of 650 Brinell tooth surface and through-hardened core.

The gear is SAE 1030 steel, through-hardened also, with a Brinell hardness of 495, tooth surface and core. Poisson's ratio is 0.30, J_P = 0.56, J_G = 0.47, and Young's modulus is 210Gpa. The loading is smooth because of motor and load. Assume a pinion life of 10^8 cycles and a reliability of 0.90, and use Y^N = $1.3558xN^{-0.0178}$, Z^N = $1.4488xN^{-0.023}$. The tooth profile is uncrowned. This is a commercial enclosed gear unit. Assuming uniform loading, K_o = 1. To evaluate K_v, with a quality number Q_v = 6,

$$\sigma_b = \left(F_t\, K_o\, K_v\, K_s\, \frac{P_d}{F}\, \frac{K_m\, K_b}{J}\right)$$

Wt, P_d, F, K_a, K_m, K_v, and K_s are common to all gears in the set and J, K_B and K_I are potentially different for each gear.

Based on the assumption of uniform load and source, the application factor K_o can be set to K_o = 1

The load distribution factor K_m is determined, from equation seen below, where five terms are needed. They are, where face width is 40 mm when needed:

$$C_{pf} = \frac{F}{10d} - 0,0375 + 0,0125F \quad 1 < F \leq 17\,in$$

$$C_{pf} = 0,5 - 0,0375 + \left(0,0125x0,04\right) = 0,463$$

Uncrowned: $C_{mc} = 1$,

Bearings immediately adjacent,: $C_{pm} = 1$

Commercial enclosed gear units: $C_{ma} = 0.15$

$C_e = 1$

Thus,

$$K_m = 1 + C_{mc}(C_{pf}C_{pm} + C_{ma}C_e) = 1 + \left(0,463x1 + 0,15x1\right) = 1,613$$

The velocity factor K_v can be calculated from equations seen below, based on the assumed gear-quality index Q_v and the pitch-line velocity V_t.

$$K_v = \frac{6.1+V}{6.1}(Cut\,or\,milled\ profile)$$

$$K_v = \frac{6.1+\pi xmxN}{6.1} = 1 + \frac{\pi xmx0,875}{6.1} = 1 + 0,45m$$

$$\sigma = \frac{K_v\,x\,F_t}{b\,x\,m\,x\,Y} = \frac{\sigma_y}{n}$$

$$\frac{538}{5} = \frac{\left(1+0,45m\right)x14023}{40x\pi xmxmx0,303}$$

$$m \cong 3mm$$

$$V = \pi xD_t xn = \pi x0,051x0,875 = 0,14\,m/s$$

$$K_v = \frac{6.1+0.14}{6.1} = 1.023$$

$$B = 0,25(12-6)^{2/3} = 0,8255$$

$$A = 50 + 56(1-0,8255) = 59,77$$

Then, the dynamic factor is

$$K_v = \left(\frac{59,77 + \sqrt{200x0.14}}{59,77} \right) = 1,089$$

To determine the size factor, K_S, the Lewis form factor is needed. From tables, with N_P = 17 teeth, Y_P = 0.303. Interpolation for the gear with N_G = 51 teeth yields Y_G = 0.4103.

$$\left(K_s\right)_P = 0,8433\left(m\,F\sqrt{Y}\right)^{0,0535} = 0,8433\left(3\,x\,40x\,\sqrt{0,303}\right)^{0,0535} = 1,055$$
$$\left(K_s\right)_G = 0,8433\left(m\,F\sqrt{Y}\right)^{0,0535} = 0,8433\left(3\,x\,40x\,\sqrt{0,4103}\right)^{0,0535} = 1,064$$

Assuming constant thickness gears, the rim-thickness factor K_B = 1. The speed ratio is $m_G = N_G / N_P = 36/17 = 2,12$. The load cycle factors given in the problem statement, with $N_{(pinion)}$ = 10^8 cycles and $N_{(gear)}$ = 10^8 / m_G = 10^8 / 2,12 cycles, are

$$(Y_N)_p = 1,3558\left(10^8\right)^{-0,0178} = 0,977$$
$$(Y_N)_G = 1,3558\left(10^8 / 2,12\right)^{-0,0178} = 0,989$$
$$\left(Y_j\right)_P = 0,46 \qquad \left(Y_j\right)_G = 0,37$$
$$Y_Z = 0,658 - 0,0759\ln(1-0,95) = 0,885$$

With a reliability of 0.9, K_R = 0.85. From Fig.s, the temperature and surface condition factors are KT = 1 and C_f = 1, with m_N = 3 for spur gears,

$$I = \left[\frac{\cos\phi_t \sin\phi_t}{2m_N}\,\frac{m_G}{m_G+1}\right] = \left[\frac{\cos 20^\circ x \sin 20^\circ}{2}\,x\,\frac{2,12}{2,12+1}\right] = 0,786$$

$$C_p = 191\sqrt{Mpa}$$

Next, we need the terms for the gear endurance strength values,

$$\left(S_t\right)_P = 0,533\,H_B + 88,3 = \left(0,533x650\right) + 88,3 = 434,75\,Mpa$$
$$\left(S_t\right)_G = 0,533\,H_B + 88,3 = \left(0,533x495\right) + 88,3 = 352Mpa$$

$$\left(S_c\right)_P = 2,22\,H_B + 200 = \left(2,22x650\right) + 200 = 1643Mpa$$
$$\left(S_c\right)_G = 2,22\,H_B + 200 = \left(2,22x495\right) + 200 = 1298Mpa$$

$$\left(Z_N\right)_P = 1,4488\left(10^8\right)^{-0,023} = 0,948$$
$$\left(Z_N\right)_G = 1,4488\left(10^8 / 2,12\right)^{-0,023} = 0,965$$

For the hardness ratio factor C$_H$, the hardness ratio is HBP / HBG = 650 / 495 = 1,3.

$$A^{'} = 8,97(10^{-3})x(H_{BP} / H_{BG}) - 8,29(10^{-3}) = 8,97(10^{-3})x(1,3) - 8,29(10^{-3}) = 3,3710^{-3}$$

Thus,

$$C_H = 1 + A^{'}(m_G - 1) = 1 + 0,00337x(2,12 - 1) = 1,00378$$

Pinion tooth bending,

$$\left(\sigma\right)_p = \left[F_t\,K_o\,K_v\,K_s\,\frac{1}{b\,m}\,\frac{K_m K_b}{J}\right] = \left[14023\,x1x1x1,089x1,055x\,\frac{1}{40x3}\,x\,\frac{1,613x1}{0,56}\right] = 335Mpa$$
$$\left(S_F\right)_P = \left(\frac{S_t Y_N / \left(K_T K_R\right)}{\left(\sigma\right)_P}\right) = \left(\frac{\left(434,75x0,977\right) / \left(1x0,85\right)}{335}\right) = 1,5$$

Gear tooth bending;

$$\left(\sigma\right)_p = \left[F_t\,K_o\,K_v\,K_s\,\frac{1}{b\,m}\,\frac{K_m K_b}{J}\right] = \left[14023\,x1x1x1,089x1,055x\,\frac{1}{40x3}\,x\,\frac{1,613x1}{0,48}\right] = 390Mpa$$
$$\left(S_F\right)_G = \left(\frac{S_t Y_N / \left(K_T K_R\right)}{\left(\sigma\right)_P}\right) = \left(\frac{\left(352x0,97\right) / \left(1x0,85\right)}{390}\right) = 1,2$$

Pinion tooth wear;

$$\left(\sigma_c\right)_p = C_p\left[F_t\,K_o\,K_v\,K_s\,\frac{K_m}{d_p F}\,\frac{C_f}{J}\right]_P^{1/2} = 191\sqrt{\left[14023\,x1x1x1,089x1,055x\,\frac{1,613}{51x40}\,x\,\frac{1}{0,786}\right]} = 769Mpa$$

$$\left(S_H\right)_P=\left(\frac{S_C Y_N/\left(K_T K_R\right)}{\sigma_C}\right)_P=\left(\frac{\left(1643x0,948\right)/\left(1x0,85\right)}{769}\right)=2,3$$

Gear tooth wear;

$$\left(\sigma_c\right)_G=\left[\frac{\left(K_S\right)_G}{\left(K_S\right)_P}\right]^{1/2}x\left(\sigma_c\right)_P=\left(\frac{1,055}{1,064}\right)^{1/2}x769=766\,Mpa$$

$$\left(S_H\right)_G=\left(\frac{S_C Z_N C_H/\left(K_T K_R\right)}{\sigma_c}\right)=\left(\frac{\left(1298x0,965x1,00378\right)/\left(1x0,85\right)}{766}\right)=1,9$$

It would be a good estimation by finding the bending of the gear using an infinite life in bending, the endurance limit is estimated as follows; (S_{ut} of the pinion is 717 Mpa)

$$S_e^{'}=0,5S_{ut}=0,5x717=358,5\,Mpa$$

To obtain the surface finish Marin factor k_a for machined surface, a = 4,51 and b = −0.265. Then the surface finish Marin factor k_a as

$$k_a=a\,S_{ut}^b=4,51x717^{-0,265}=0,79$$

The next step is to estimate the size factor k_b. The sum of the addendum and dedendum is

$$l=\frac{1}{P}+\frac{1,25}{P}=\frac{1}{3}+\frac{1,25}{3}=0,75$$

The tooth thickness t as $t=\left(4lx\right)^{1/2}$ when $x=3Y/2P$.Therefore, For 17 teeth, the Lewis Form Factor is 0,303 and $P=51/17=3mm$.

$$x=\frac{3Y}{2P}=\frac{3x0,303}{2x3}=0,1515$$

Then

$$t = (4lx)^{1/2} = (4x0,75x0,1515) = 0,4545$$

We have recognized the tooth as a cantilever beam of rectangular cross section, so the equivalent rotating-beam diameter is

$$d_e = 0,808\,(hb)^{1/2} = 0,808(Ft)^{1/2} = 0,808\,(1,5\,x\,0,4545)^{1/2} = 0,668$$

Then ;

$$k_b = \left(\frac{d_e}{0,3}\right)^{-0,107} = \left(\frac{0,668}{0,3}\right)^{-0,107} = 0,918$$

The load factor k_c is unity. $k_d = k_e = 1$. In general, a gear tooth is subjected only to one-way bending. Exceptions include idler gears and gears used in reversing mechanisms. I will account for one-way bending by establishing a miscellaneous-effects Marin factor k_f. For one-way bending the steady and alternating stress components are $\sigma_a = \sigma_m = \sigma/2$ where σ is the largest repeatedly applied bending stres. If a material exhibited a Goodman failure locus

$$\frac{S_a}{S_e^{'}} + \frac{S_m}{S_{ut}} = 1$$

Since S_a and S_m are equal for one-way bending, by substituting S_a for S_m and solving the preceding equation for S_a,

$$S_a = \frac{S_e^{'} S_{ut}}{S_e^{'} + S_{ut}}$$

By replacing S_a with σ/2, and in the denominator replace S_e’ with $0.5S_{ut}$ to obtain;

$$\sigma = \frac{2S_e^{'} S_{ut}}{0,5S_{ut} + S_{ut}} = \frac{2S_e^{'}}{0,5+1} = 1,33S_e^{'}$$

$$k_f = \sigma / S_e^{'} = 1,33S_e^{'} / S_e^{'} = 1,33$$

However, a Gerber fatigue locus gives mean values of;

$$\frac{S_a}{S_e^{'}} + \left(\frac{S_m}{S_{ut}}\right)^2 = 1$$

Setting $S_a = S_m$ and solving the quadratic in Sa gives,

$$S_a = \frac{S_{ut}^2}{2S_e^{'}}\left(-1+\sqrt{1+\frac{4S_e^{'2}}{S_{ut}^2}}\right)$$

Setting $S_a = \sigma/2$, $S_{ut} = S_e^{'}/ 0.5$ gives,

$$\sigma = \frac{S_e^{'}}{0,5^2}\left[-1+\sqrt{1+4\left(0,5\right)^2}\right] = 1,66S_e^{'}$$

and $k_f = \sigma/S_e' = 1.66$. Since a Gerber locus runs in and among fatigue data and Goodman does not, therefore $k_f = 1.66$. The second effect to be accounted for in using the miscellaneous-effects Marin factor k_f is stress concentration. For a 20° full-depth tooth the radius of the root fillet is denoted r_f, where

$$r_f = \frac{0,3}{P} = \frac{0,3}{3} = 0,1$$

$$\frac{r}{d} = \frac{r_f}{t} = \frac{0,1}{0,4545} = 0,22$$

Since D/d = ∞, the approximation value initially can be taken as D/d = 3, giving $K_t = 1.68$ and q = 0.62.

$$K_f = 1 + (0,62)(1,68 - 1) = 1,42$$

The miscellaneous-effects Marin factor for stress concentration can be expressed as

$$k_f = \frac{1}{K_f} = \frac{1}{1,42} = 0,704$$

The final value of k_f is the product of the two kf factors, that is, 1.66(0.704) = 1.17. The Marin equation for the fully corrected endurance strength is

$$S_e = k_a k_b k_c k_d k_e k_f S_e^{'} = 0,79x0,918x1x1x1x1,17x358,5 = 304,2Mpa$$

For a design factor of $n_d = 5$, applied to the load or strength, the maximum bending stress is

$$\sigma_{all} = \frac{S_e}{n_d} = \frac{304,2}{5} = 60,8\,Mpa$$

$$\sigma = \frac{F_t x K_v}{mxbxY} = \frac{14023x0,14}{0,003x0,04x0,303} = 54Mpa \le 60,8\,Mpa$$

$P = F_t xv = 14023x0,1 = 1402,3W$ is below the 1850 W ,

Lastly, the factor of safety of the drive based on the possibility of a surface fatigue failure can be estimates as follows; E_P = 207 Gpa, v_P = 0.292, E_G = 207 Gpa, v_G = 0.292.

$$C_p = \left[\frac{1}{\pi\left(\frac{1-\nu_p^2}{E_p} + \frac{1-\nu_G^2}{E_G} \right)} \right]^{1/2} = \left[\frac{1}{\pi\left(\frac{1-0,292^2}{207.10^9} + \frac{1-0,292^2}{207.10^9} \right)} \right]^{1/2} = 189660,8$$

$$r_1 = \frac{d_p \sin\phi}{2} = \frac{51x\sin 20°}{2} = 8,7\,mm \qquad r_2 = \frac{d_G \sin\phi}{2} = \frac{108x\sin 20°}{2} = 18,47\,mm$$

$$\sigma_c = -C_p\left[\frac{K_v W^t}{F\cos\phi}\left(\frac{1}{r_1}+\frac{1}{r_2}\right)\right]^{1/2} = -189660,8\left[\frac{13177x1,089}{0,04x\cos 20°}\left(\frac{1}{8,7}+\frac{1}{18,47}\right)\right]^{1/2} = -1523\,Mpa$$

The surface endurance strength of pinion for 10^8 cycles;

$$(S_c)_P = 2,41H_B + 200 = (2,41x514) + 237 = 1475,75\,Mpa$$.

In generally, contact stresses is not linear with transmitted load. If the factor of safety is defined as the loss-of-function load divided by the imposal load, then the ratio of loads is the ratio of stresses squared. In other words;

$$n = \frac{loss-of-function}{imposed\ load} = \frac{S_c^2}{\sigma_c^2} = \left(\frac{1643}{1523}\right)^2 = 1,2$$

4.2.1.2 Spur Gear Fem Results

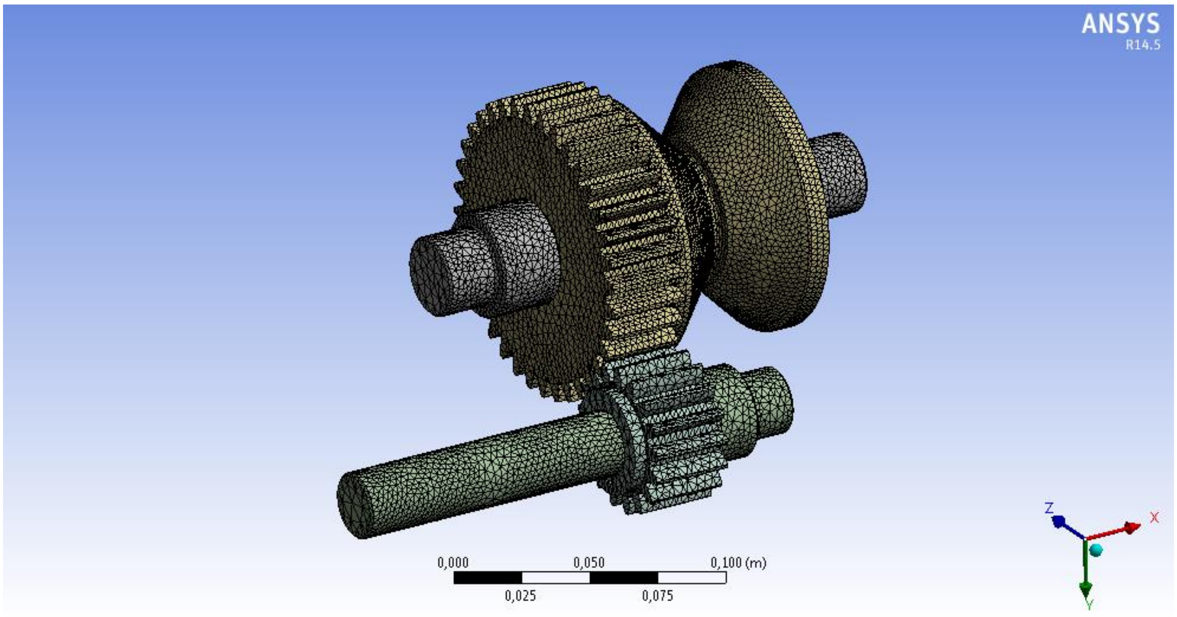
ANSYS
R14.5
0,000
0,050
0,100 (m)
0,025
0,075
Z
X
Y

Fig. 4.2 Mesh view of the gear – wheel and pinion

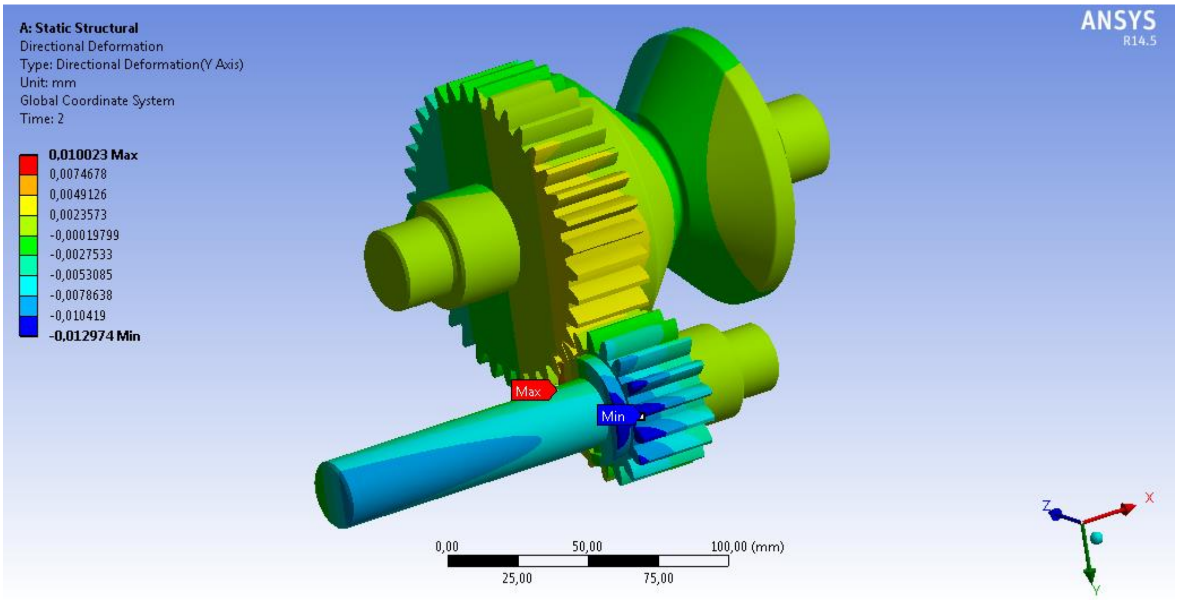
A: Static Structural
Directional Deformation
Type: Directional Deformation(Y Axis)
Unit: mm
Global Coordinate System
Time: 2

ANSYS
R14.5
0,010023 Max
0,0074678
0,0049126
0,0023573
-0,00019799
-0,0027533
-0,0053085
-0,0078638
-0,010419
-0,012974 Min
Max
Min
0,00
50,00
100,00 (mm)
25,00
75,00
Z
X
Y

Fig. 4.3 Directional deformations of the gear – wheel and pinion

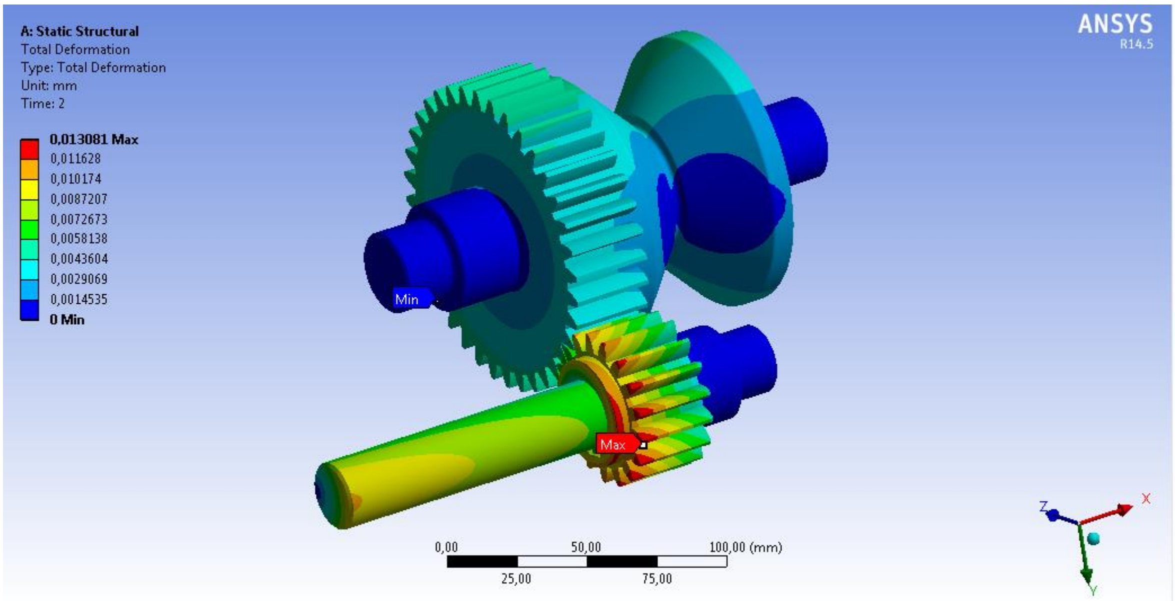
A: Static Structural
Total Deformation
Type: Total Deformation
Unit: mm
Time: 2
0,013081 Max
0,011628
0,010174
0,0087207
0,0072673
0,0058138
0,0043604
0,0029069
0,0014535
0 Min
ANSYS
R14.5
Min
Max
0,00
50,00
100,00 (mm)
25,00
75,00
Z
X
Y

Fig. 4.4 Total deformations of the gear – wheel and pinion

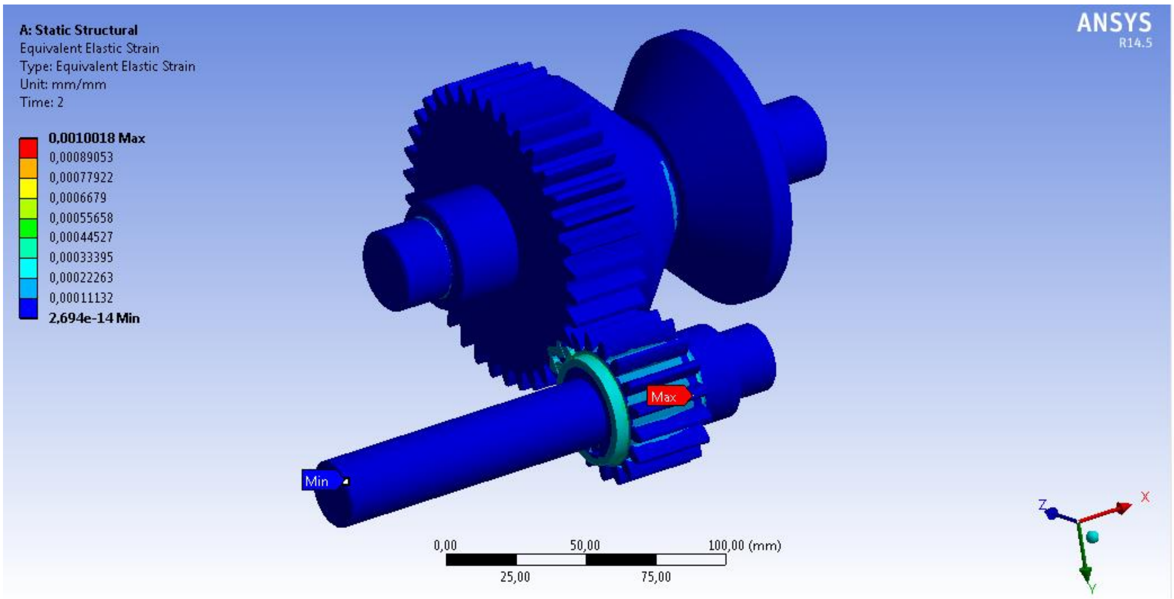
A: Static Structural
Equivalent Elastic Strain
Type: Equivalent Elastic Strain
Unit: mm/mm
Time: 2
0,0010018 Max
0,00089053
0,00077922
0,0006679
0,00055658
0,00044527
0,00033395
0,00022263
0,00011132
2,694e-14 Min
ANSYS
R14.5
Max
Min
0,00
50,00
100,00 (mm)
25,00
75,00
Z
X
Y

Fig. 4.5 Equivalent elastic strain distribution of the gear – wheel and pinion

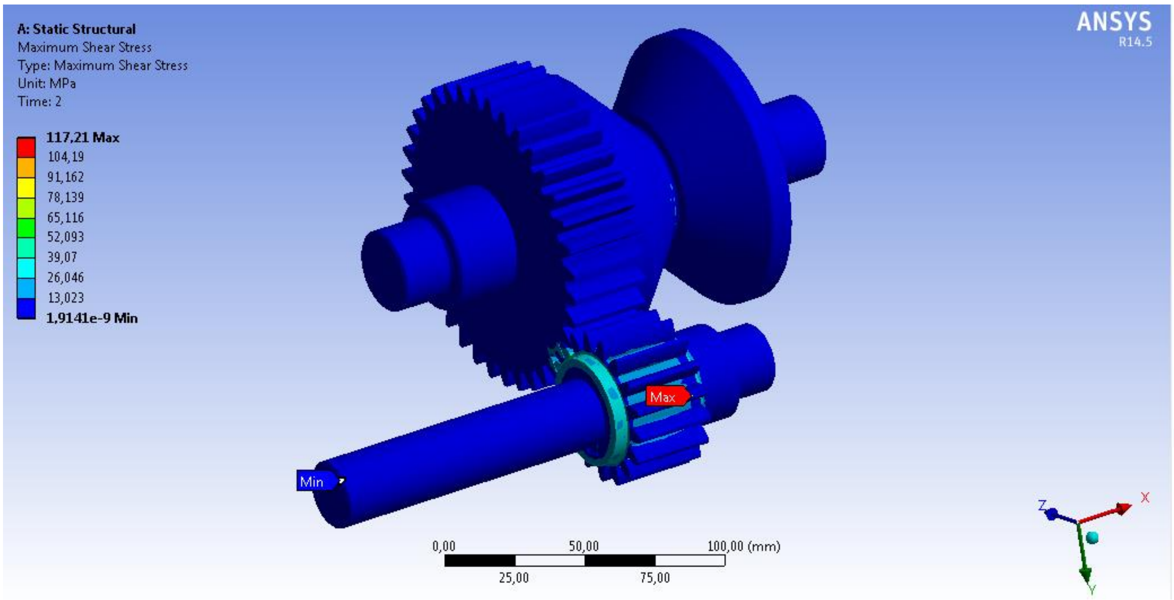
A: Static Structural
Maximum Shear Stress
Type: Maximum Shear Stress
Unit: MPa
Time: 2
117,21 Max
104,19
91,162
78,139
65,116
52,093
39,07
26,046
13,023
1,9141e-9 Min
ANSYS
R14.5
Max
Min
0,00
50,00
100,00 (mm)
25,00
75,00
Z
X
Y

Fig. 4.6 Maximum shear stresses of the gear – wheel and pinion

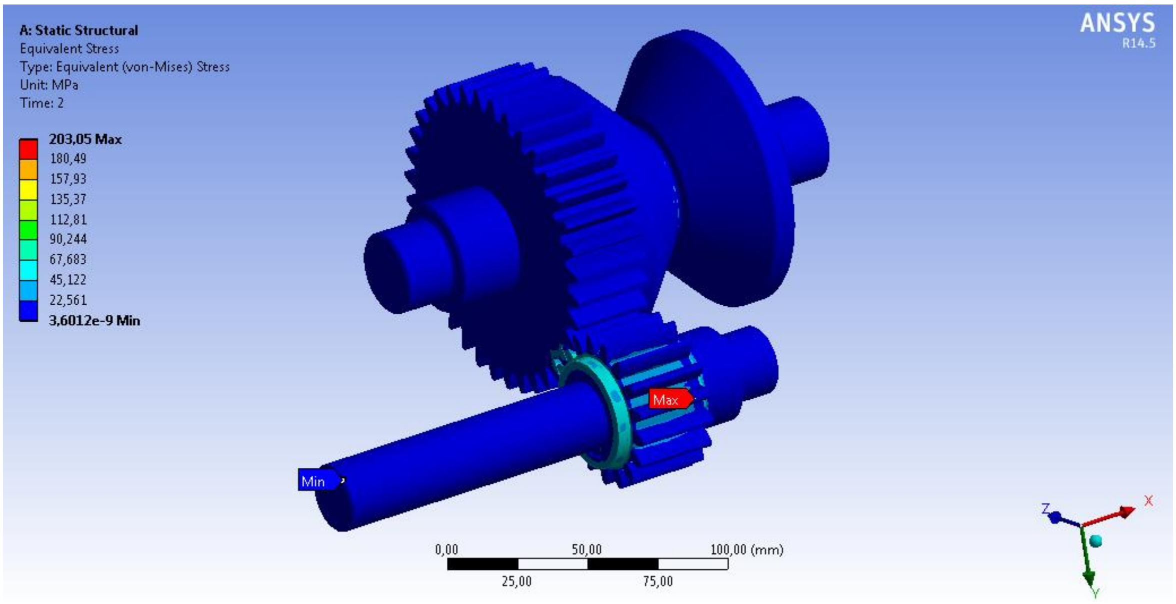
A: Static Structural
Equivalent Stress
Type: Equivalent (von-Mises) Stress
Unit: MPa
Time: 2
203,05 Max
180,49
157,93
135,37
112,81
90,244
67,683
45,122
22,561
3,6012e-9 Min
ANSYS
R14.5
Max
Min
0,00
50,00
100,00 (mm)
25,00
75,00
Z
X
Y

Fig. 4.7 Von Mises Stress distribution of the gear – wheel and pinion

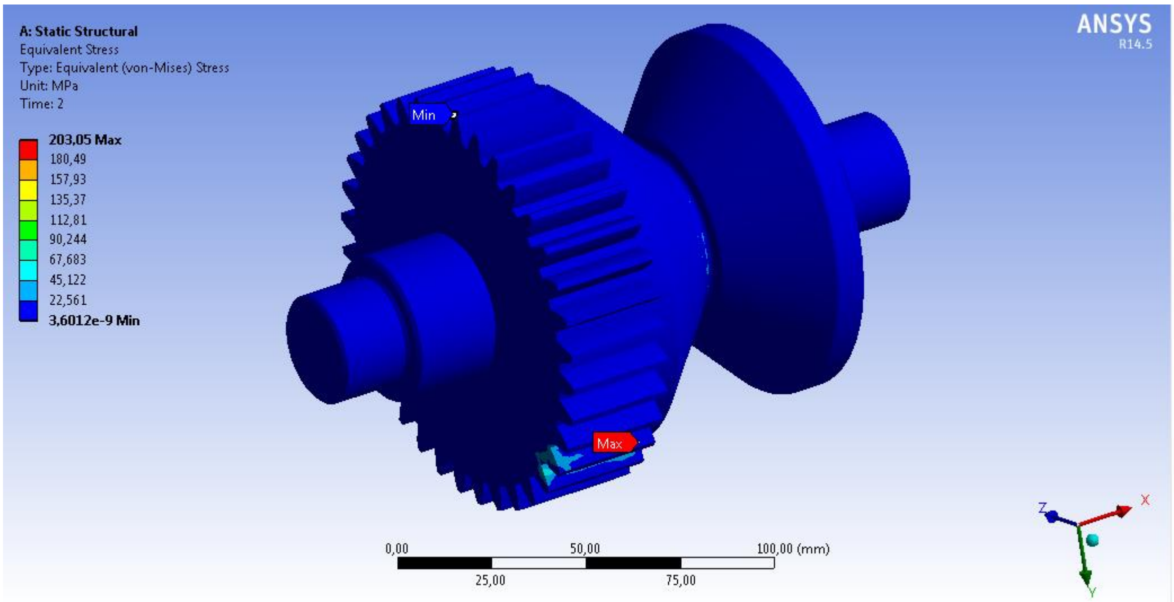
A: Static Structural
Equivalent Stress
Type: Equivalent (von-Mises) Stress
Unit: MPa
Time: 2
203,05 Max
180,49
157,93
135,37
112,81
90,244
67,683
45,122
22,561
3,6012e-9 Min
ANSYS
R14.5
Min
Max
0,00
50,00
100,00 (mm)
25,00
75,00
Z
X
Y

Fig. 4.8 Von Mises Stress distribution of the gear – wheel

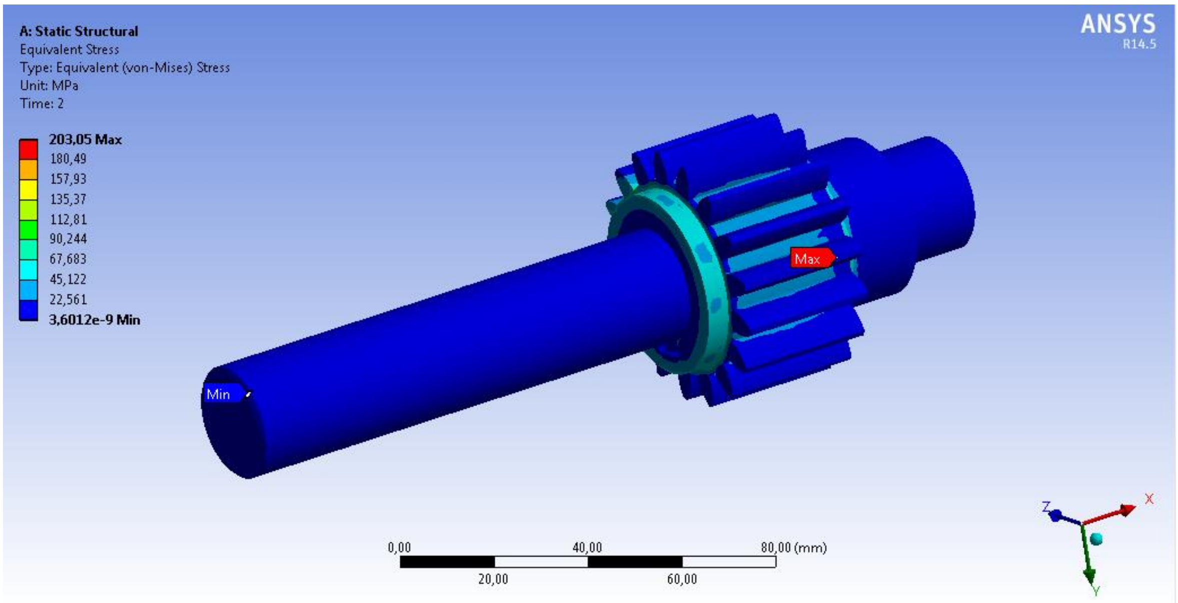
A: Static Structural
Equivalent Stress
Type: Equivalent (von-Mises) Stress
Unit: MPa
Time: 2
203,05 Max
180,49
157,93
135,37
112,81
90,244
67,683
45,122
22,561
3,6012e-9 Min
ANSYS
R14.5
Max
Min
0,00
40,00
80,00 (mm)
20,00
60,00
Z
X
Y

Fig. 4.9 Von Mises Stress distribution of the pinion

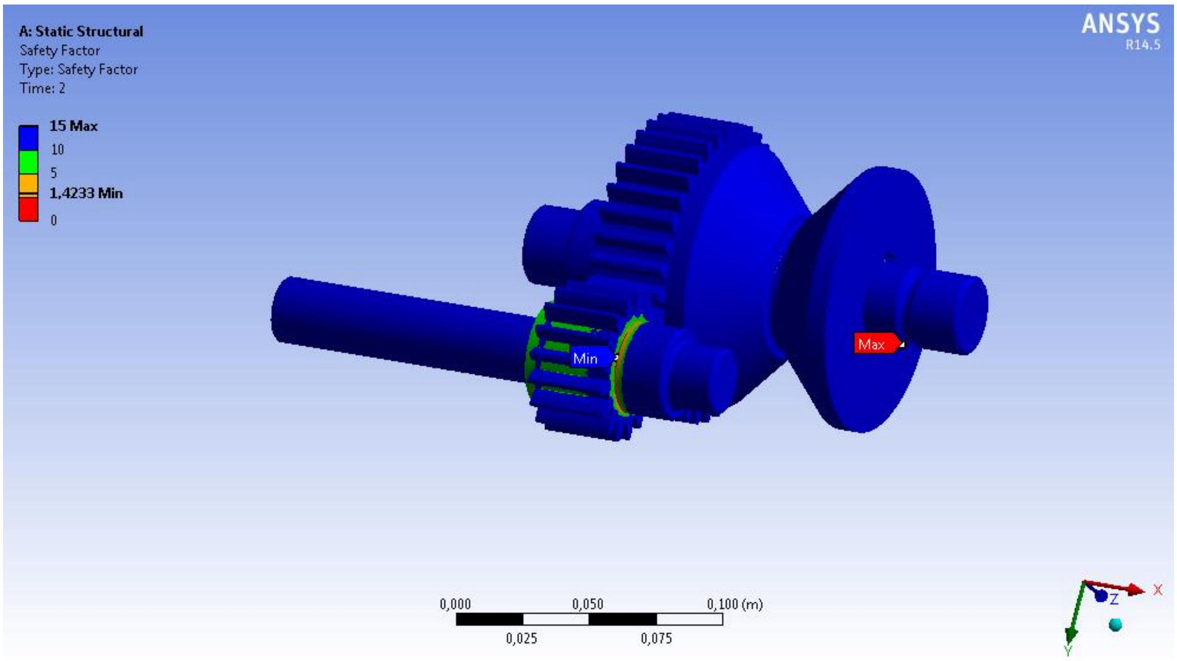
A: Static Structural
Safety Factor
Type: Safety Factor
Time: 2
15 Max
10
5
1,4233 Min
0
ANSYS
R14.5
Min
Max
0,000
0,050
0,100 (m)
0,025
0,075
X
Z
Y

Fig. 4.10 Safety factor of the gear – wheel and pinion

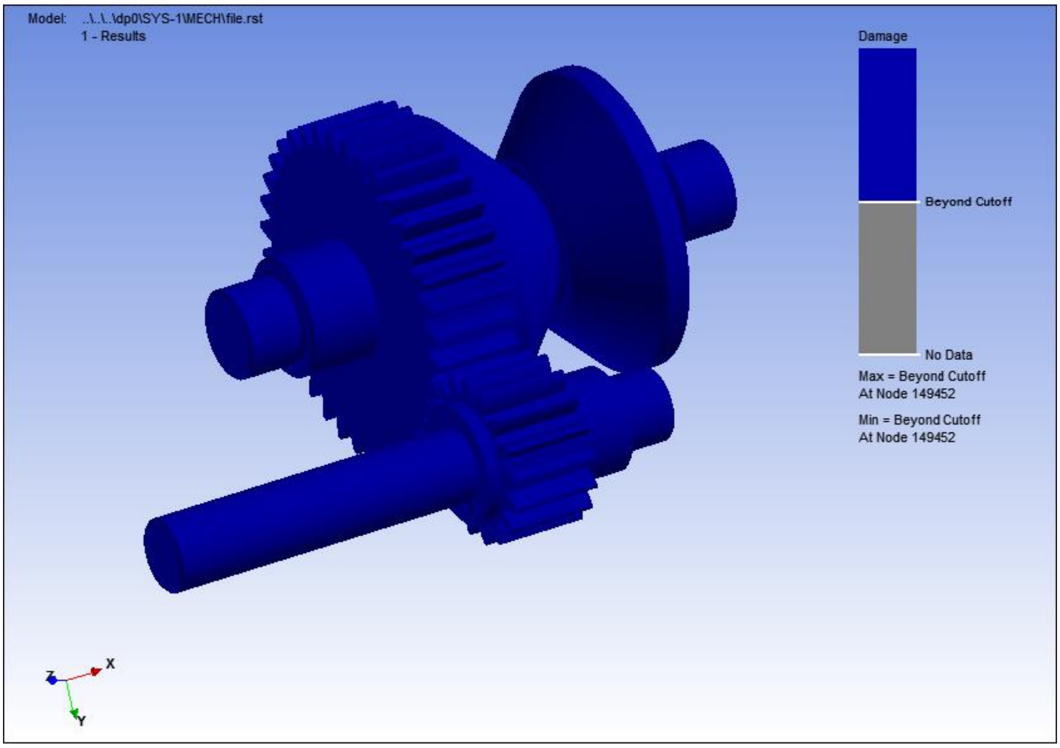
Model: ..\..\dp0\SYS-1\MECH\file.rst
1 - Results
Damage
Beyond Cutoff
No Data
Max = Beyond Cutoff
At Node 149452
Min = Beyond Cutoff
At Node 149452
X
Z
Y

Fig. 4.11 Damage distribution of the gear – wheel and pinion

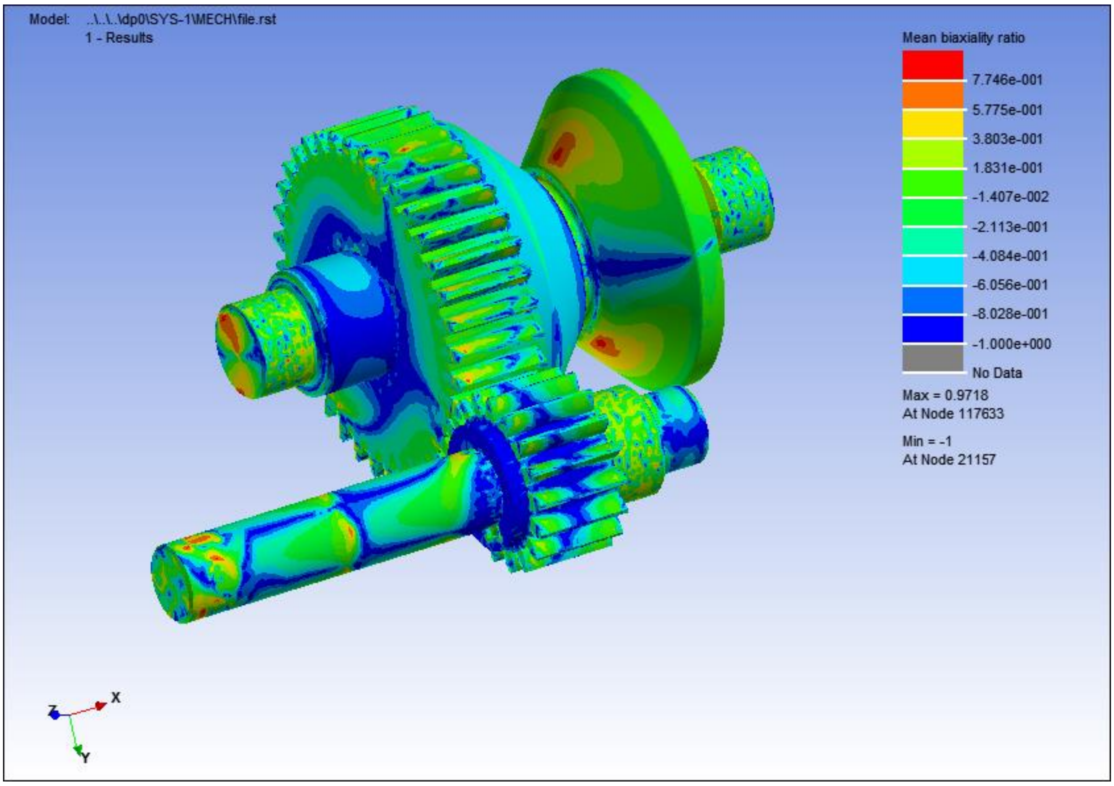
Model: ..\..\..\dp0\SYS-1\MECH\file.rst
1 - Results
Mean biaxiality ratio
7.746e-001
5.775e-001
3.803e-001
1.831e-001
-1.407e-002
-2.113e-001
-4.084e-001
-6.056e-001
-8.028e-001
-1.000e+000
No Data
Max = 0.9718
At Node 117633
Min = -1
At Node 21157
Z
X
Y

Fig. 4.12 Mean biaxiliaty ratio distribution of the gear – wheel and pinion

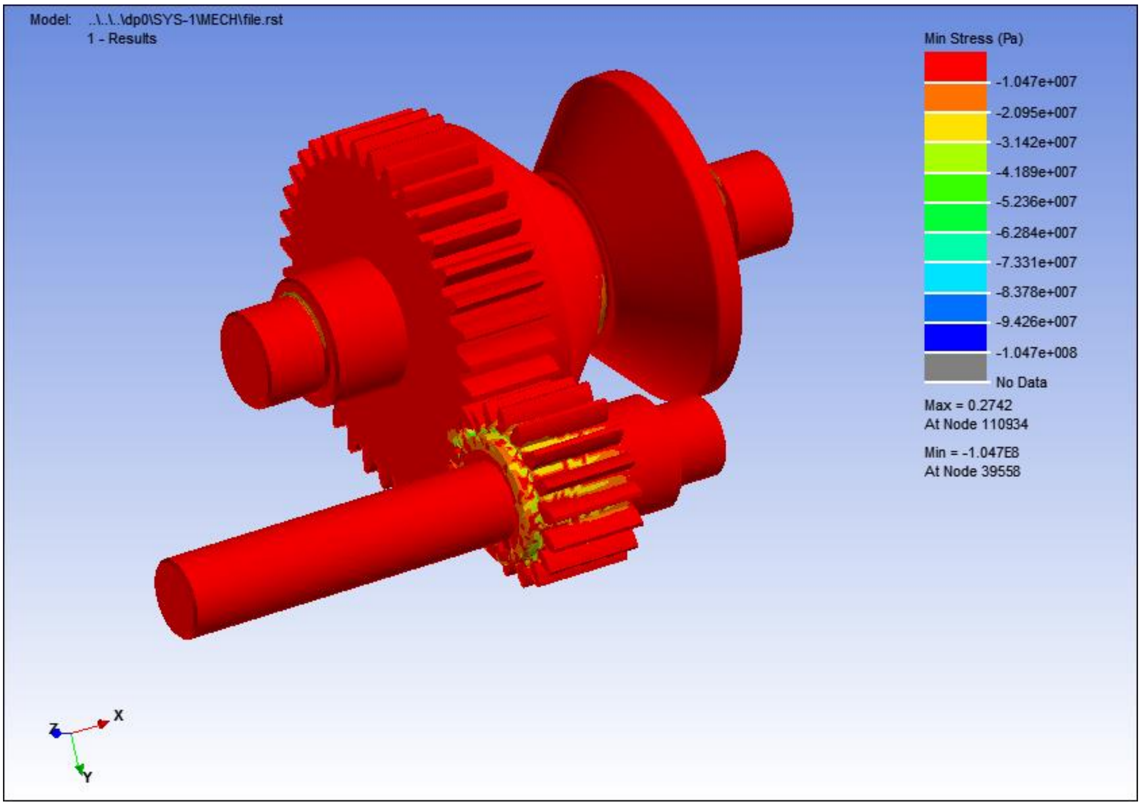
Model: ..\..\..\dp0\SYS-1\MECH\file.rst
1 - Results
Min Stress (Pa)
-1.047e+007
-2.095e+007
-3.142e+007
-4.189e+007
-5.236e+007
-6.284e+007
-7.331e+007
-8.378e+007
-9.426e+007
-1.047e+008
No Data
Max = 0.2742
At Node 110934
Min = -1.047E8
At Node 39558
Z
X
Y

Fig. 4.13 Min stresses of the gear – wheel and pinion

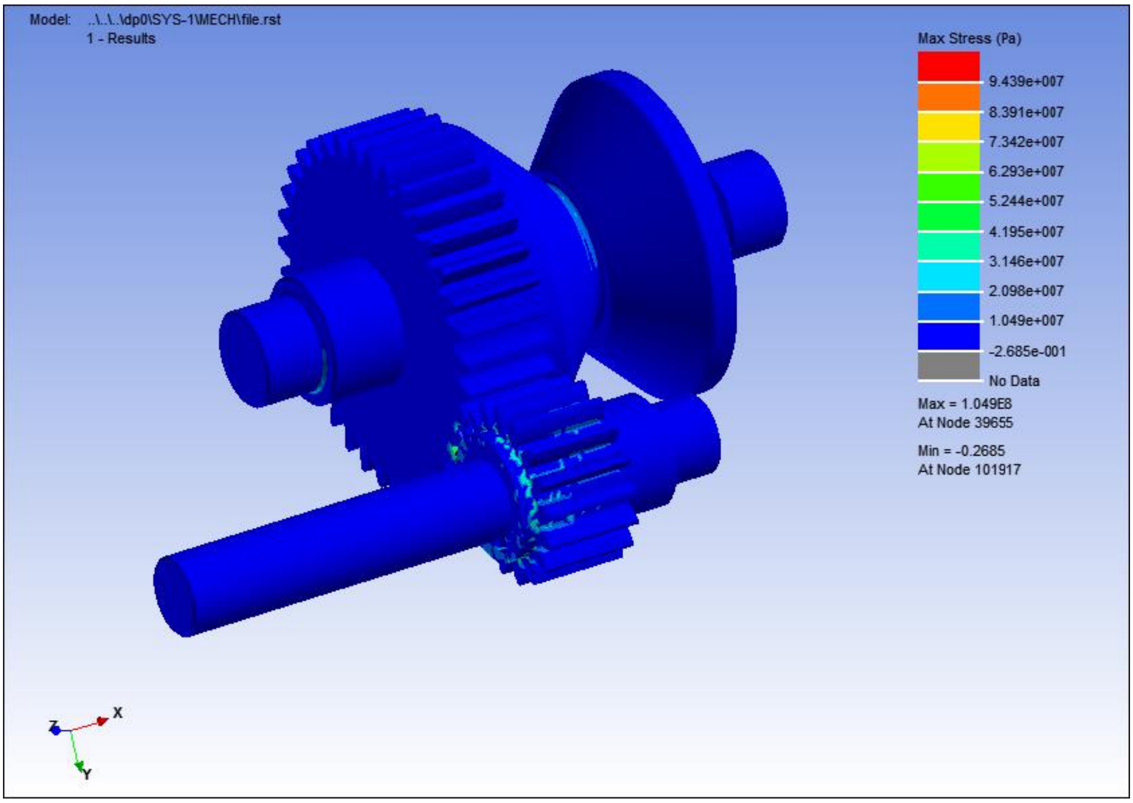
Model: ..\..\..\dp0\SYS-1\MECH\file.rst
1 - Results
Max Stress (Pa)
9.439e+007
8.391e+007
7.342e+007
6.293e+007
5.244e+007
4.195e+007
3.146e+007
2.098e+007
1.049e+007
-2.685e-001
No Data
Max = 1.049E8
At Node 39655
Min = -0.2685
At Node 101917
Z
X
Y

Fig. 4.14 Max stresses of the gear – wheel and pinion

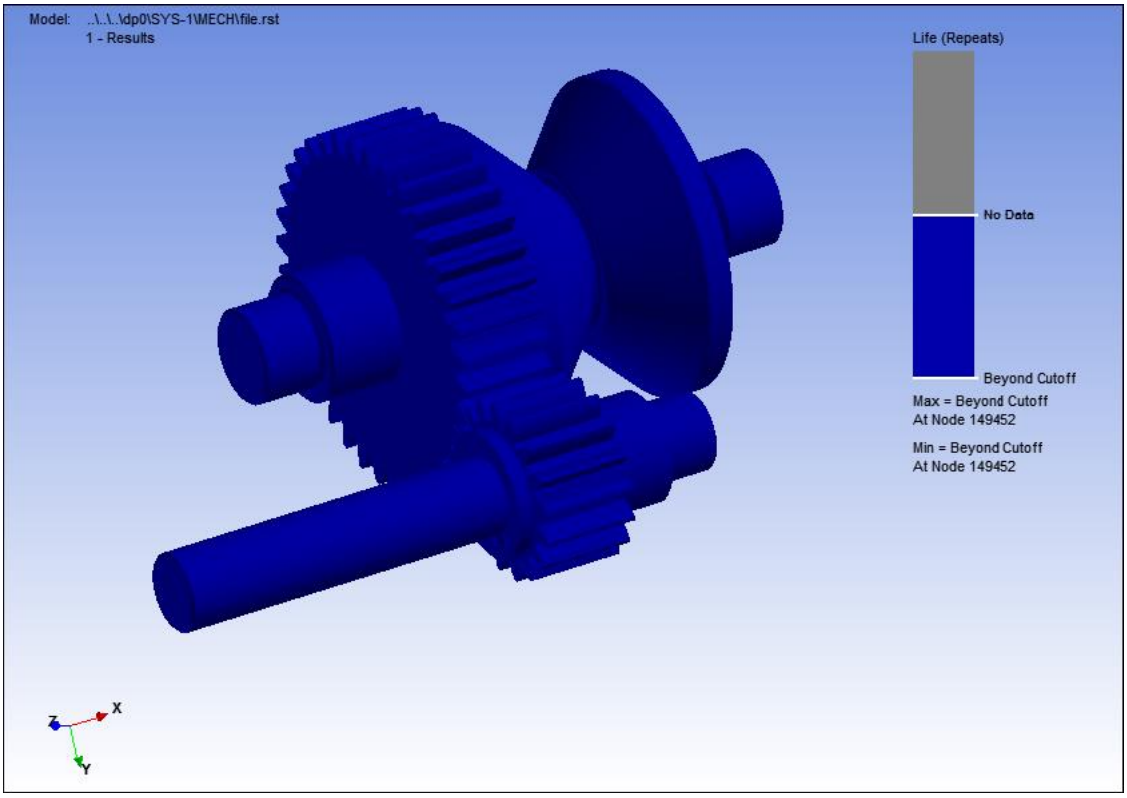
Model: ..\..\..\dp0\SYS-1\MECH\file.rst
1 - Results
Life (Repeats)
No Data
Beyond Cutoff
Max = Beyond Cutoff
At Node 149452
Min = Beyond Cutoff
At Node 149452
Z
X
Y

Fig. 4.15 Life of the gear – wheel and pinion

4.2.2 Conclusion

In this study, spur gears have been examined in terms of stress, deflection and fatigue by considering both the AGMA Stress and Strength Equations (Spur Gear Design, Shigley’s Mechanical Enginnering Design, Richard G. Budynas – J. Keith Nisbett) and finite element modeling.

In the study of analytical design, firstly the radial and tangential loads have been calculated by using the previous power and torque results and secondly bending, and wear of spur gears have been taken into consideration.

In the study of fem design, materials chosen for spur gears by the results of analytical equations have been used and the tangential and radial forces, found in analytical design eq.s, have been applied on the tooths of spur gear assembly.

Deflections of gears can not be considered as dangerous values for both type of spur gears because of very small.

Von Mises stresses of the both type of spur gears are convenient compared to material yield strengths.

And finally, fatigue results of both spur gears in terms of damage and life distributions are beyond cut off which means that both have infinite life.

4.3 WORM GEAR

In worm-gear mechanicsm, worm and worm gear of a set have the same hand of helix as for crossed helical gears, but the helix angles are usually quite different in this gear ype.. The nomenclature of a worm gearset is shown in Fig. 4.16. The helix angle on the worm is generally quite large, while on the gear very small. Because of this, it is usual to specify the lead angle λ on the worm and helix angle ψ_G on the gear; the two angles are equal for a 90° shaft angle. The worm lead angle is the complement of the worm helix angle. In specifying the pitch of worm gearsets, the axial pitch p_x of the worm and the transverse circular pitch p, is called the circular pitch, of the mating gear. These are equal if the shaft angle is 90°. The pitch diameter of the gear is the diameter measured on a plane containing the worm axis; it is the same as for spur gears and is

$$d_G = \frac{N_G p_t}{\pi} \tag{4.3.1}$$

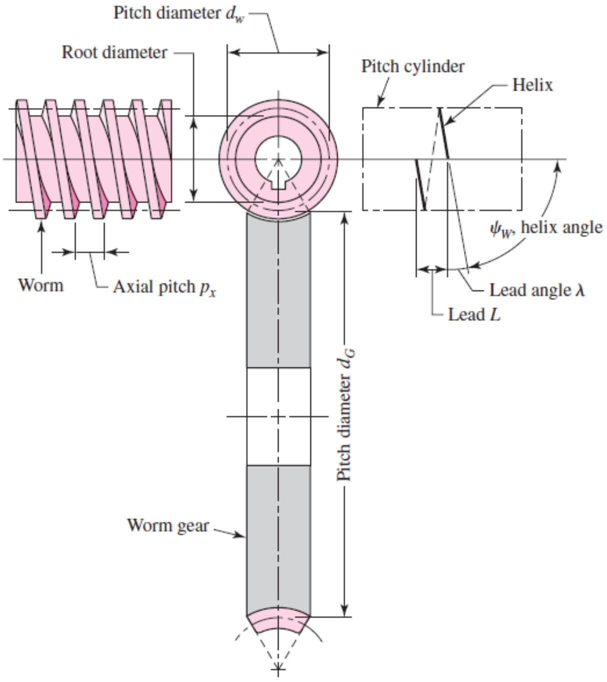
Pitch diameter d_W
Root diameter
Pitch cylinder
Helix
ψ_W, helix angle
Lead angle λ
Lead L
Worm
Axial pitch p_x
Pitch diameter d_G
Worm gear

Fig. 4.16 Nomenclature of a single enveloping worm gearset.
(Shigley’s Mechanical Enginnering Design, Richard G. Budynas – J. Keith Nisbett)

4.3.1 Design of a Worm-Gear Mesh

A usable decision set for a worm-gear mesh includes the following steps; (Shigley's Mechanical Enginnering Design, Richard G. Budynas – J. Keith Nisbett)

- Function: power, speed, m_G, K_a
- Design factor: n_d
- Tooth system
- Materials and processes
- Number of threads on the worm: N_W
- Axial pitch of worm: p_x
- Pitch diameter of the worm: d_W
- Face width of gear: F_G
- Lateral area of case: A

4.3.2 WORM GEAR ANALYTICAL AND FEM RESULTS

4.3.2.1 Worm gear analytical results

In this worm-gear set, a 2-tooth right-hand worm transmits 0,37kW at 1200 rev/min to a 66-tooth worm gear have been used. The normal pressure angle of gear have been chosen as 14,5°, and assumed the ambient temperature as 35°C, the application factor as 1.25 and the design factor as 1; Then we can calculate the design requirements of worm-gear the axial pitch, the center distance, the lead, and the lead angle, the gear geometry, and the transmitted gear forces and the mesh efficiency, the lubricant sump temperature.

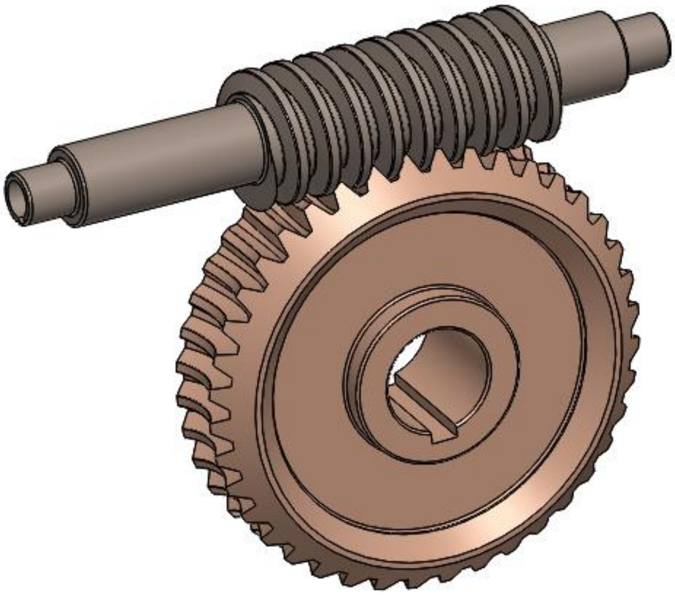

Fig. 4.17 Worm - Gear assembly view

A double-start worm will require a 66-tooth worm gear for the desired 33:1 ratio. This number of worm-gear teeth is well above the minimum recommended values in tables (Shigley's Mechanical Enginnering Design, Richard G. Budynas – J. Keith Nisbett). Assuming a center distance of 100 mm for a trial calculation, we can find a suitable worm diameter based on assumptions.

$$d_w \cong \frac{C^{0,875}}{2,2}$$

$$d_w \cong \frac{100^{0,875}}{2,2} \cong 30\,mm$$

Worm-gear diameter and transverse circular pitch;

$$d_g = 2C - d_w = 2x100 - 30 = 170\,mm$$

$$\begin{aligned} & d_G = mxZ_G \\ & mx33 = 170\,mm \\ & m \cong 5 \end{aligned}$$

$$P_t = \frac{N_g}{D_g} = \frac{33}{170} = 0,195$$

$$p_x = \frac{\pi}{p_t} = \frac{\pi}{0,195} = 16,12\,mm$$

$$a = \frac{p_x}{\pi} = \frac{16,12}{\pi} = 5,12\,mm$$
$$b = 0,3686\,p_x = 0,3683\,x16,12 = 5,94\,mm$$
$$h_t = 0,6866\,p_x = 0,6866x16,12 = 11,06\,mm$$
$$d_o = d + 2a = 30 + 2x5,12 = 40,24\,mm$$
$$d_r = d - 2b = 30 - 2x5,94 = 18,12\,mm$$
$$D_t = D_G + 2a = 170 + 2x5,12 = 180,24\,mm$$
$$D_r = D_G - 2b = 170 - 2x5,94 = 158,12\,mm$$
$$c = b - a = 5,94 - 5,12 = 0,82\,mm$$
$$\left(F_W\right)_{\max} = 2\sqrt{2Da} = 2\sqrt{2x30x5,12} = 35\,mm$$

The tangential speeds of the worm (V_W) and gear (V_G) are respectively

$$V_W = \omega_w x \frac{D_w}{2} = 5,5x\frac{0,03}{2} = 0,0825\,m/sn$$
$$V_G = \omega_G x \frac{D_G}{2} = 5,5x\frac{0,17}{2} = 0,4675\,m/sn$$

The lead of the worm,

$$L = p_x N_w = 16,12x1 = 16,12\,mm$$

The lead angle,

$$\lambda = \tan^{-1}\frac{L}{\pi\,d} = \tan^{-1}\frac{16,12}{\pi\,x30} = 9,7^\circ$$

The normal diametral pitch for a worm gear with ψ = λ is

$$P_n = \frac{p_t}{\cos\lambda} = \frac{0{,}195}{\cos 9{,}7} = 0{,}198\,mm$$

$$p_n = \frac{\pi}{P_n} = \frac{\pi}{0{,}198} = 15{,}866\,mm$$

The sliding velocity,

$$V_s = \frac{\pi\, d\, n_W}{12\cos\lambda} = \frac{\pi\, x 30\, x\, 52{,}5}{12\, x \cos 9{,}7} = 0{,}4183\, m / \min$$

The coefficient of friction,

$$f = 0{,}124 e^{-0{,}11 V_s^{0{,}645}} = 0{,}124 e^{-0{,}11 x 0{,}4184^{0{,}645}} = 0{,}116$$

The efficiency e,

$$e = \frac{\cos\phi_n - f\tan\lambda}{\cos\phi_n + f\cot\lambda} = \frac{\cos 14{,}5^\circ - 0{,}116 x \tan 9{,}7^\circ}{\cos 14{,}5^\circ + 0{,}116 x \cot 9{,}7^\circ} = 0{,}515$$

The design factor used $n_d = 1$, $K_a = 1{,}25$ and an output power is 3700 W. The gear tangential force component and the torque value is

$$P_{out} = P_{in}\, x\, e = 3700 x 0{,}5 = 1850\, W$$
$$n_{out} = \frac{n_{in}}{i_2} = \frac{1740}{33} \cong 52{,}5\, rpm$$
$$P_{new} = T_{CD} x W_{CD}$$
$$1850 = T_{CD} x 5{,}5$$
$$T_{CD} = 336{,}36\, N.m$$

$$W_G^t = \frac{2 x T_{CD} x n_d x K_a}{D_g} = \frac{2 x 336{,}36 x 1 x 1{,}25}{0{,}17} = 4946{,}47\, N$$

The tangential force on the worm,

$$W_W^t = W_G^t \frac{\cos\phi_n \sin\lambda + f\cos\lambda}{\cos\phi_n \cos\lambda - f\cos\lambda} = 4946,47 \frac{\cos 14,5^\circ \sin 9,7^\circ + 0,116\cos 9,7^\circ}{\cos 14,5^\circ \cos 9,7^\circ - 0,116\cos 9,7^\circ} = 1637\,N$$

The materials factor Cs and the ratio-correction factor $C_{m;}$

$$C_s = 1000$$
$$C_m = 0,0107\sqrt{-m_G^2 + 56m_G + 5145} = 0,0107\sqrt{-33^2 + (56x33) + 5145} = 0,822$$
$$C_v = 0,659e^{-0,0011V_S} = 0,659e^{(-0,0011x0,4183)} = 0,658$$

$$\left(W^t\right)_{all} = C_s D_m^{0,8} F_e C_m C_v = 1000x0,17^{0,8}x0,035x0,822x0,658 = 1152192N$$

Since $(W_t)_G$ < $(W_t\ )$all , the mesh will survive at least 25 000 h. The friction force W_f is

$$W_f = \frac{fW_G^t}{f\sin\lambda - \cos\phi_n \cos\lambda} = \frac{0,116x4946,47}{0,116x\sin 9,7^\circ - \cos 14,5^\circ \cos 9,7^\circ} = 613,68N$$

The power dissipiated in frictional work H_f is;

$$H_f = \left|W_f\right| xV_s = 613,68x0,4183 = 256,7W$$

The worm and gear powers, H_W and H_G, are given by

$$H_W = W_w^t xV_w = 1637x0,0825 = 960,05W$$
$$H_G = W_G^t xV_G = 4946,47x0,4675 = 2312,48W$$

Gear power is satisfactory. Now,

$$P_n = \frac{p_t}{\cos\lambda} = \frac{0,195}{\cos 9,7} = 0,198\,mm$$
$$p_n = \frac{\pi}{P_n} = \frac{\pi}{0,198} = 15,866\,mm$$

The bending stress in a gear tooth is given by Buckingham’s adaptation of the Lewis equation,

$$\left(\sigma\right)_G = \frac{W_G^t}{P_n F_G y} = \frac{4946,47}{15,866x35x0,1} = 90\,Mpa$$

Stress in gear satisfactory.

$$A_{\min} = 43,2C^{1,7} = 43,2x100^{1,7} = 108513,5\,mm^2$$

$$H_{loss} = (1-e)H_{in} = \left(1-0,5\right) = 960,05x0,5 = 480,025W$$

$$h_{cr} = \frac{n_w}{3939} + 0,13 = \frac{1740}{3939} + 0,13 = 0,571mm\,N/(\min m^2\,C)$$

$$t_s = t_a + \frac{H_{loss}}{h_{CR}A} = 35 + \frac{480,025}{0,571x108513,5} = 36\,^{\circ}C$$

The rated output torque

$$T_G = W_G^t x \frac{d_G}{2} = 4946,47x\frac{0,17}{2} = 420,45\,N.m$$

The allowable gear wear load $(W_G^t)_{all}$ using Buckingham’s wear equation;

$$\left(W_G^t\right)_{all} = K_W d_G F_e = 125x170x35 = 476\,000\,N$$

which is smaller than the 1152192 N of the AGMA method.

4.3.2.2 Worm gear fem results

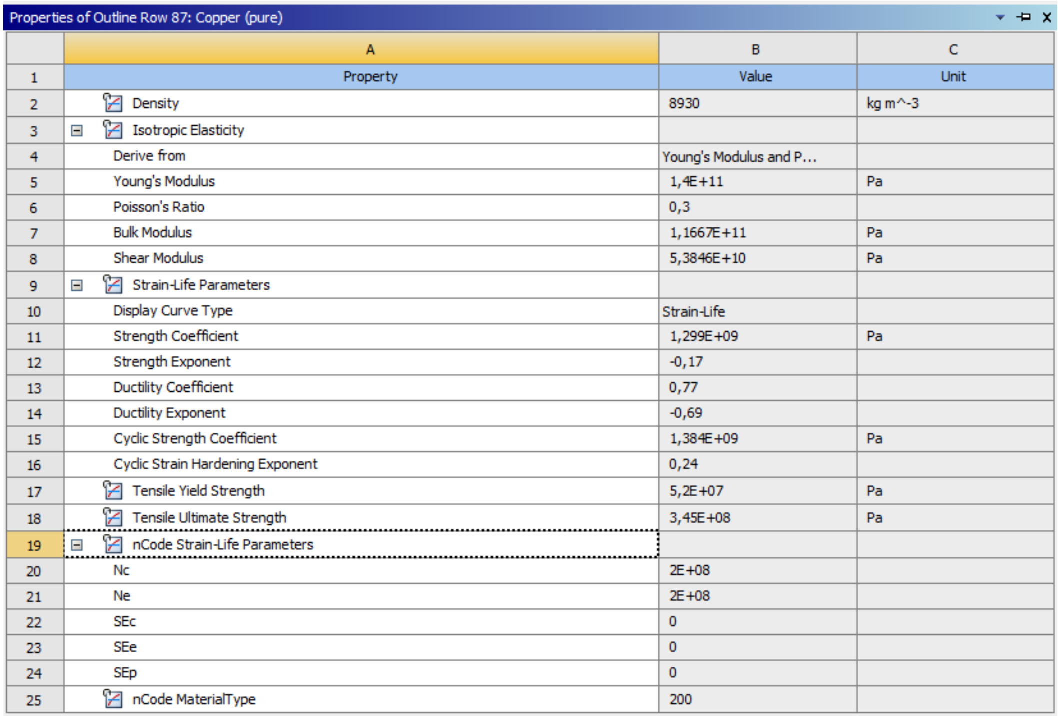

Properties of Outline Row 87: Copper (pure)

	A	B	C
1	Property	Value	Unit
2	Density	8930	kg m^-3
3	⊟ Isotropic Elasticity		
4	Derive from	Young's Modulus and P...	
5	Young's Modulus	1,4E+11	Pa
6	Poisson's Ratio	0,3	
7	Bulk Modulus	1,1667E+11	Pa
8	Shear Modulus	5,3846E+10	Pa
9	⊟ Strain-Life Parameters		
10	Display Curve Type	Strain-Life	
11	Strength Coefficient	1,299E+09	Pa
12	Strength Exponent	-0,17	
13	Ductility Coefficient	0,77	
14	Ductility Exponent	-0,69	
15	Cyclic Strength Coefficient	1,384E+09	Pa
16	Cyclic Strain Hardening Exponent	0,24	
17	Tensile Yield Strength	5,2E+07	Pa
18	Tensile Ultimate Strength	3,45E+08	Pa
19	⊟ nCode Strain-Life Parameters		
20	Nc	2E+08	
21	Ne	2E+08	
22	SEc	0	
23	SEe	0	
24	SEp	0	
25	nCode MaterialType	200	

Table 4.2 Material properties of the gear (Ansys ncode material prop.)

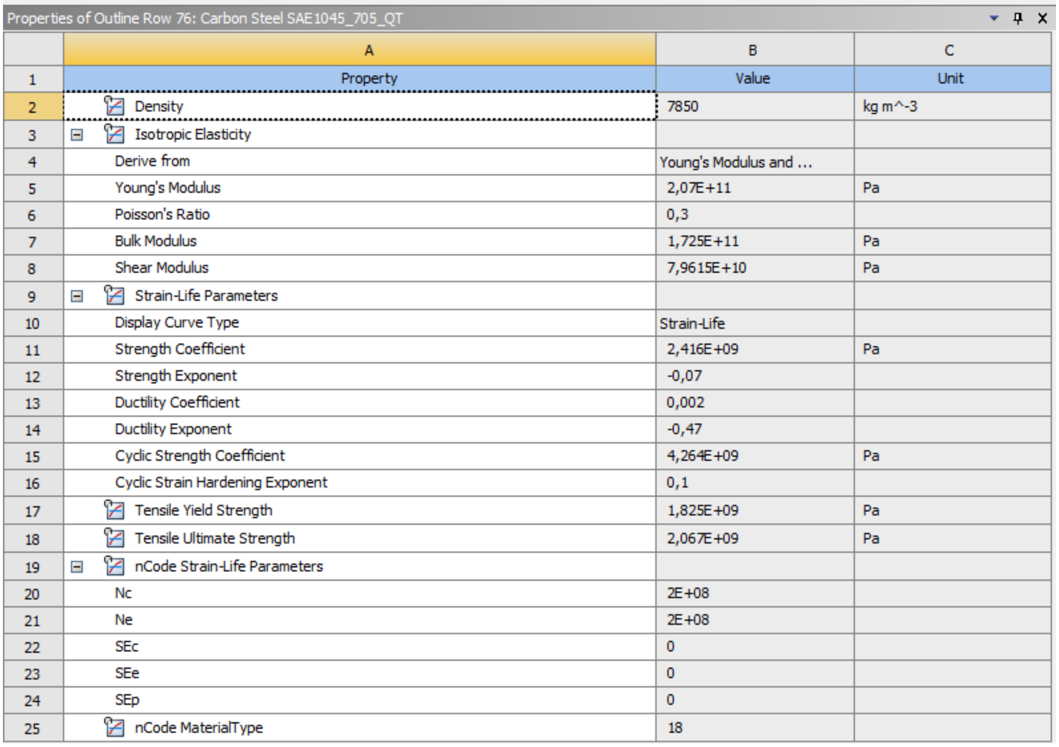

Properties of Outline Row 76: Carbon Steel SAE1045_705_QT

	A	B	C
1	Property	Value	Unit
2	Density	7850	kg m^-3
3	⊟ Isotropic Elasticity		
4	Derive from	Young's Modulus and ...	
5	Young's Modulus	2,07E+11	Pa
6	Poisson's Ratio	0,3	
7	Bulk Modulus	1,725E+11	Pa
8	Shear Modulus	7,9615E+10	Pa
9	⊟ Strain-Life Parameters		
10	Display Curve Type	Strain-Life	
11	Strength Coefficient	2,416E+09	Pa
12	Strength Exponent	-0,07	
13	Ductility Coefficient	0,002	
14	Ductility Exponent	-0,47	
15	Cyclic Strength Coefficient	4,264E+09	Pa
16	Cyclic Strain Hardening Exponent	0,1	
17	Tensile Yield Strength	1,825E+09	Pa
18	Tensile Ultimate Strength	2,067E+09	Pa
19	⊟ nCode Strain-Life Parameters		
20	Nc	2E+08	
21	Ne	2E+08	
22	SEc	0	
23	SEe	0	
24	SEp	0	
25	nCode MaterialType	18	

Table 4.3 Material properties of the worm (Ansys ncode material prop.)

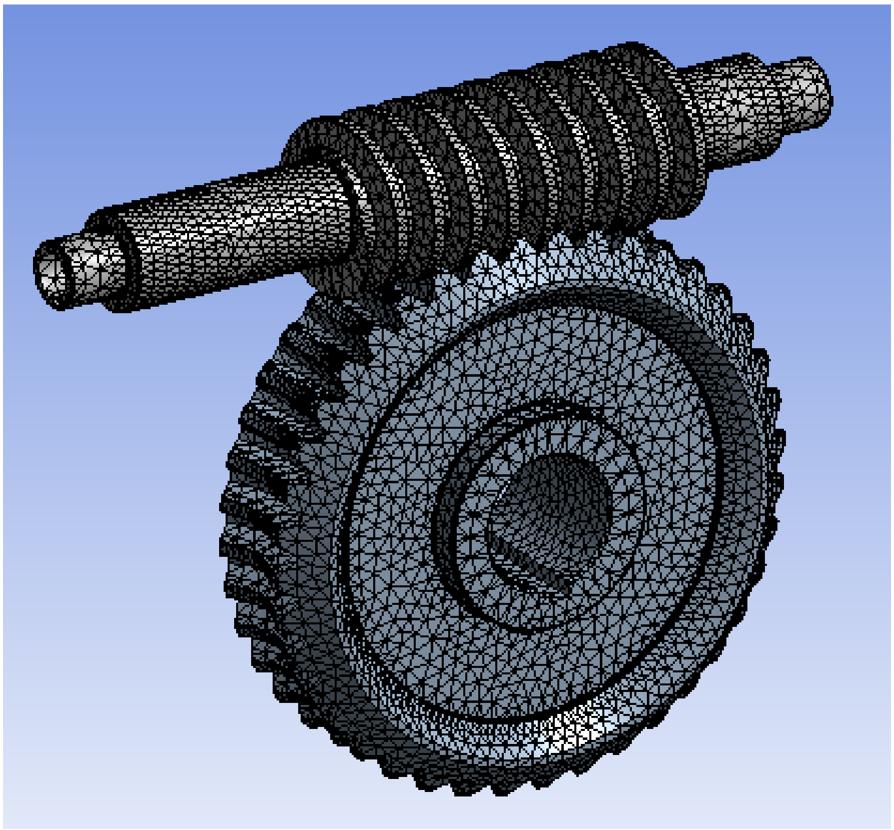

Fig. 4.18 Worm - Gear mesh assembly view

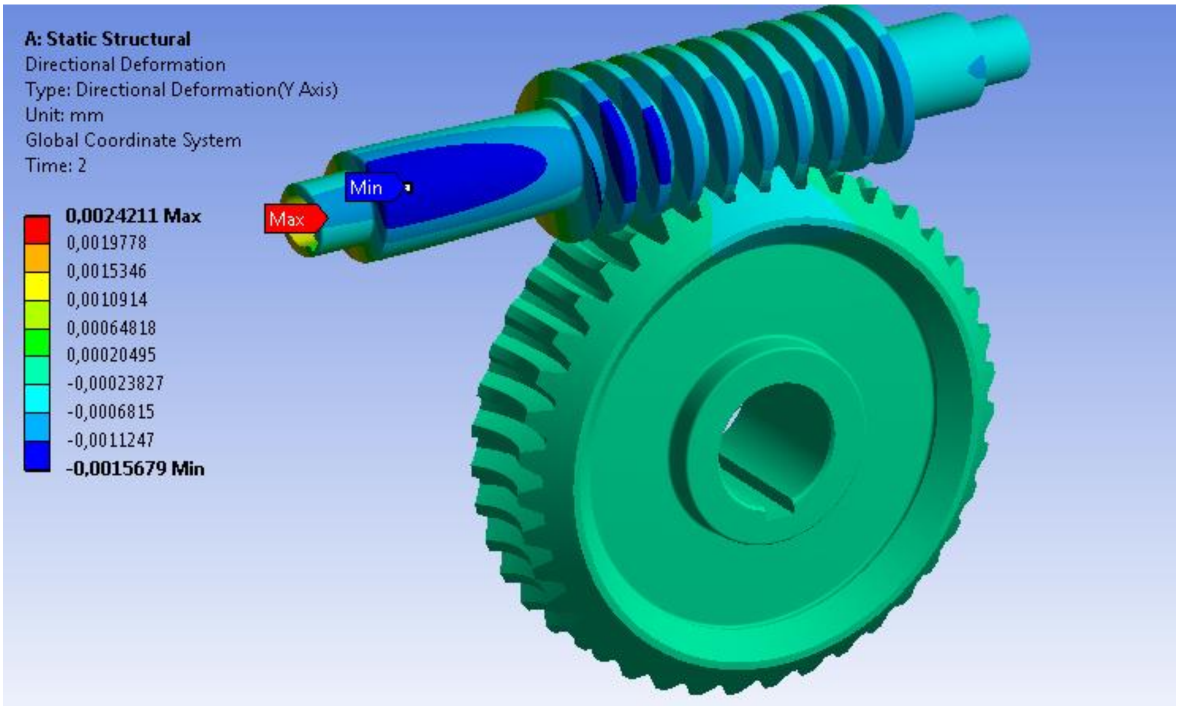
A: Static Structural
Directional Deformation
Type: Directional Deformation(Y Axis)
Unit: mm
Global Coordinate System
Time: 2
0,0024211 Max
0,0019778
0,0015346
0,0010914
0,00064818
0,00020495
-0,00023827
-0,0006815
-0,0011247
-0,0015679 Min
Min
Max

Fig. 4.19 Directional deformation distribution of the worm – gear

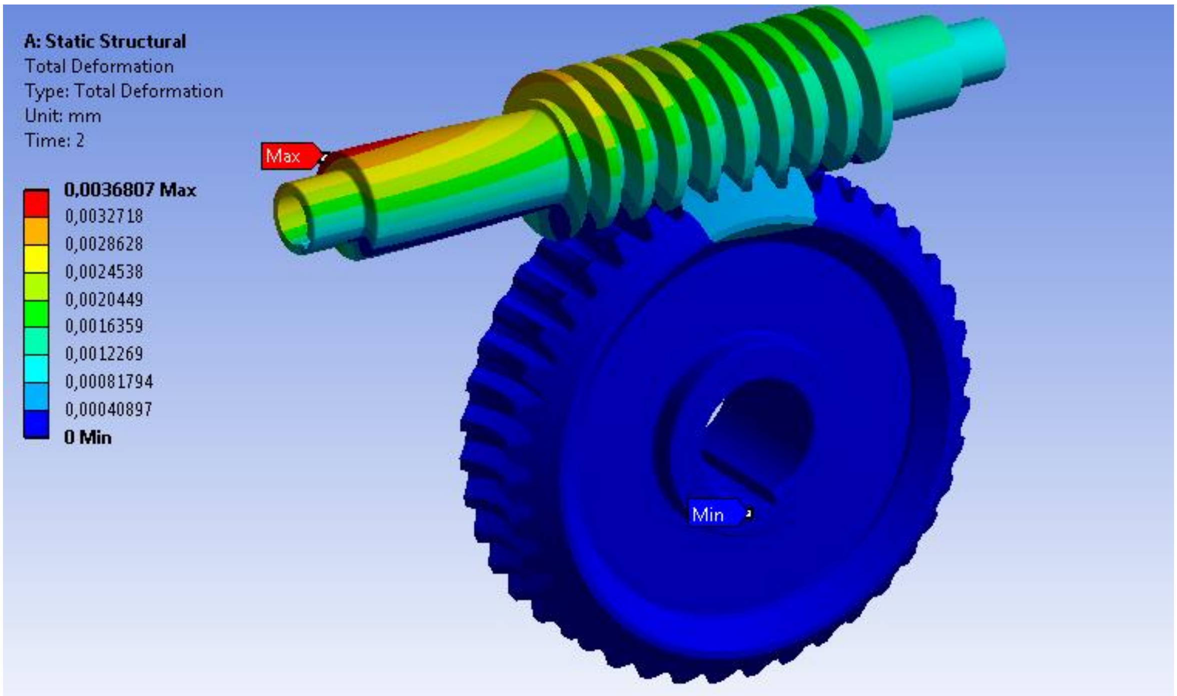
A: Static Structural
Total Deformation
Type: Total Deformation
Unit: mm
Time: 2
0,0036807 Max
0,0032718
0,0028628
0,0024538
0,0020449
0,0016359
0,0012269
0,00081794
0,00040897
0 Min
Max
Min

Fig. 4.20 Total deformation distribution of the worm – gear

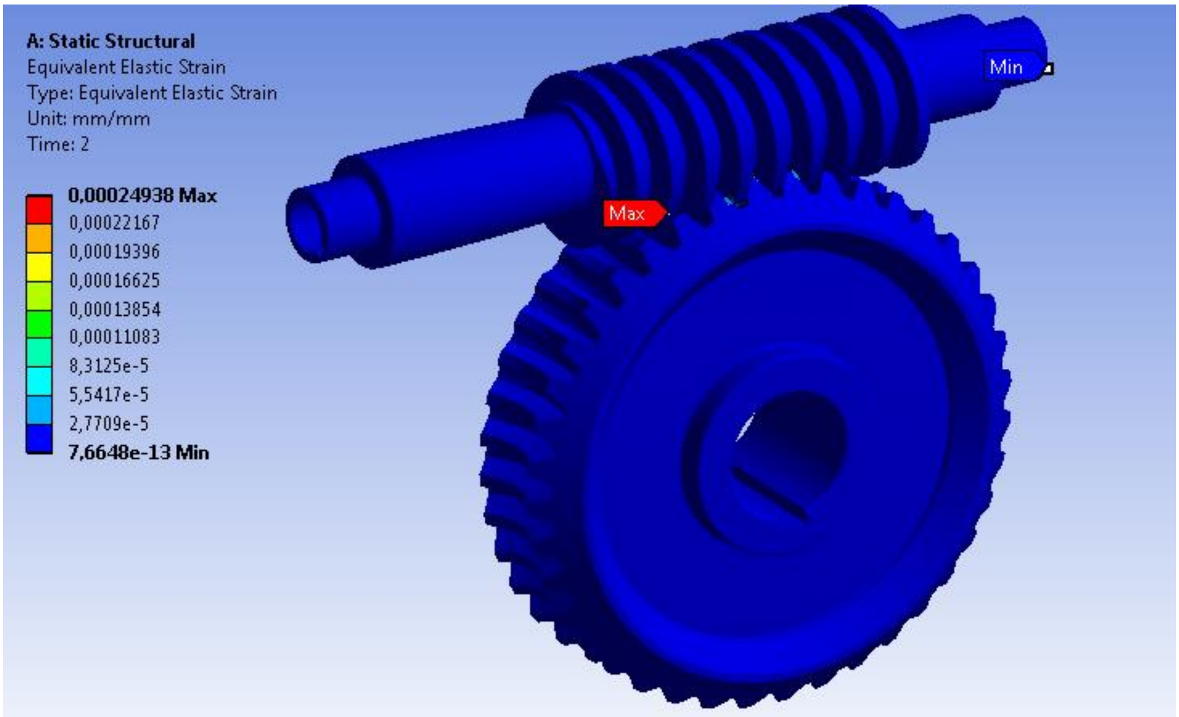
A: Static Structural
Equivalent Elastic Strain
Type: Equivalent Elastic Strain
Unit: mm/mm
Time: 2
0,00024938 Max
0,00022167
0,00019396
0,00016625
0,00013854
0,00011083
8,3125e-5
5,5417e-5
2,7709e-5
7,6648e-13 Min
Max
Min

Fig. 4.21 Equivalent elastic strain distribution of the worm – gear

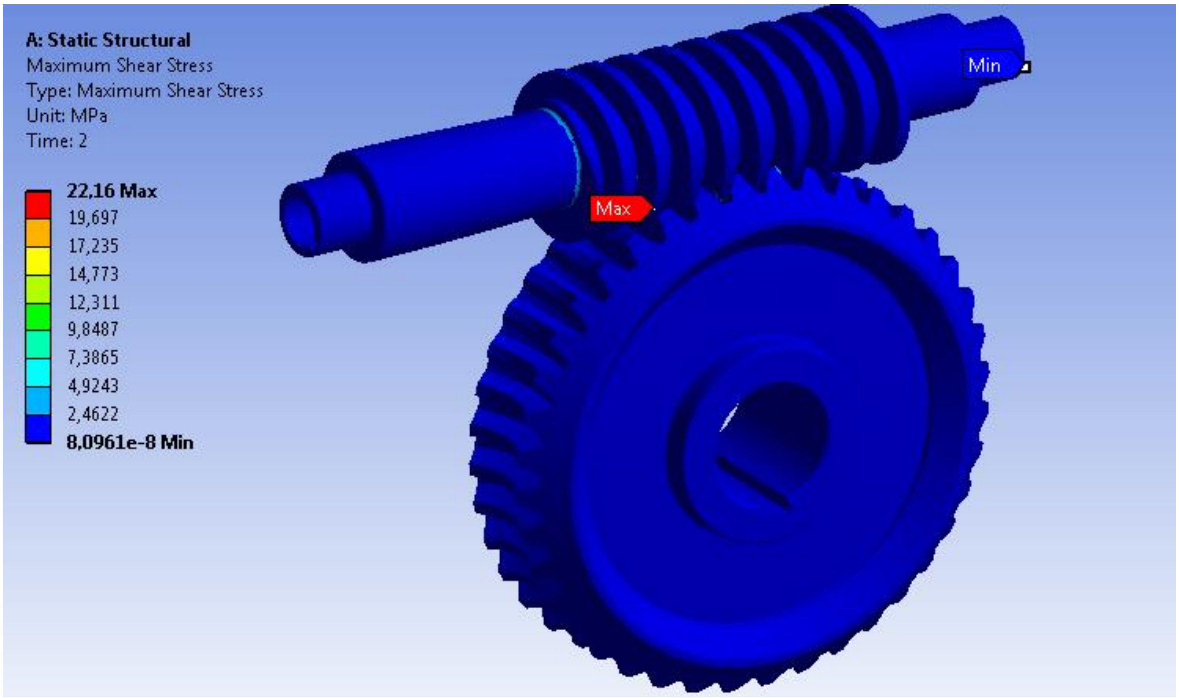
A: Static Structural
Maximum Shear Stress
Type: Maximum Shear Stress
Unit: MPa
Time: 2
22,16 Max
19,697
17,235
14,773
12,311
9,8487
7,3865
4,9243
2,4622
8,0961e-8 Min
Max
Min

Fig. 4.22 Maximum Shear Stress distribution of the worm – gear

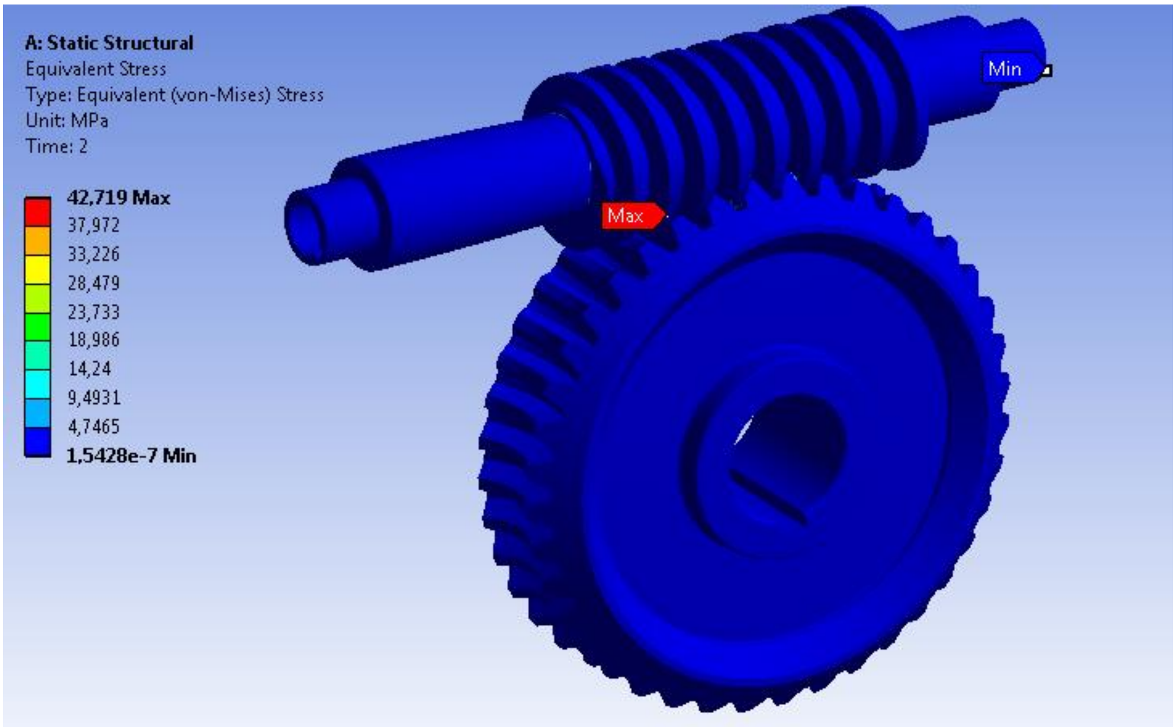
A: Static Structural
Equivalent Stress
Type: Equivalent (von-Mises) Stress
Unit: MPa
Time: 2
42,719 Max
37,972
33,226
28,479
23,733
18,986
14,24
9,4931
4,7465
1,5428e-7 Min
Max
Min

Fig. 4.23 Von Mises Stress distribution of the worm – gear

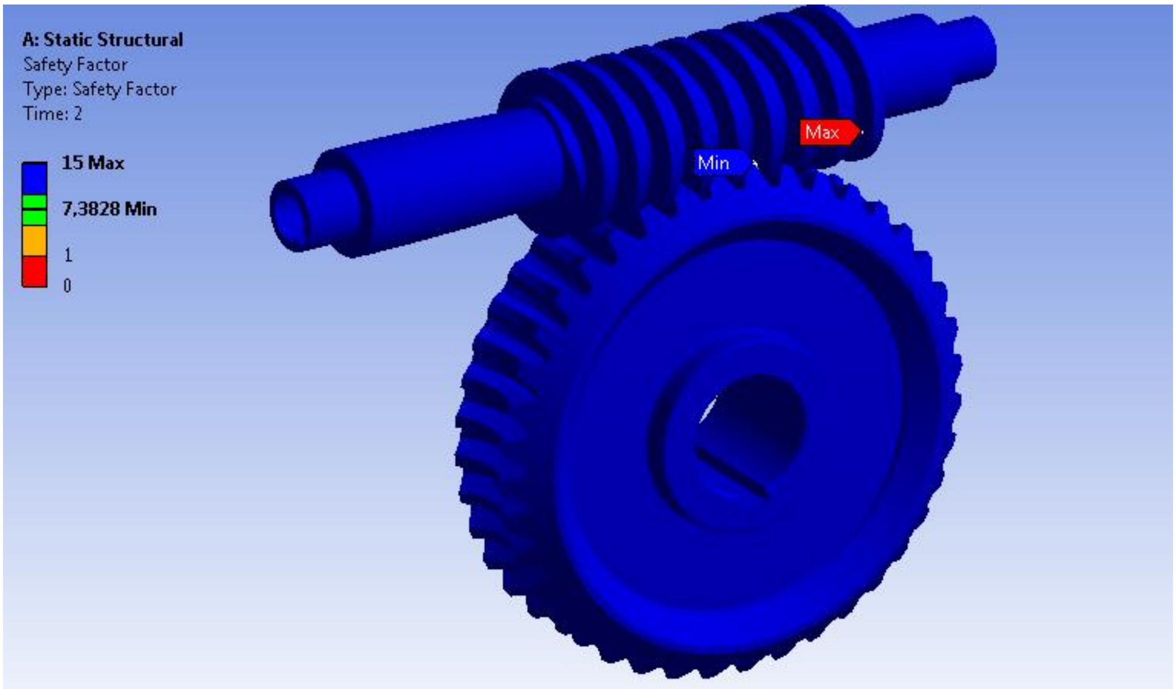
A: Static Structural
Safety Factor
Type: Safety Factor
Time: 2
15 Max
7,3828 Min
1
0
Max
Min

Fig. 4.24 Safety factor of the worm – gear

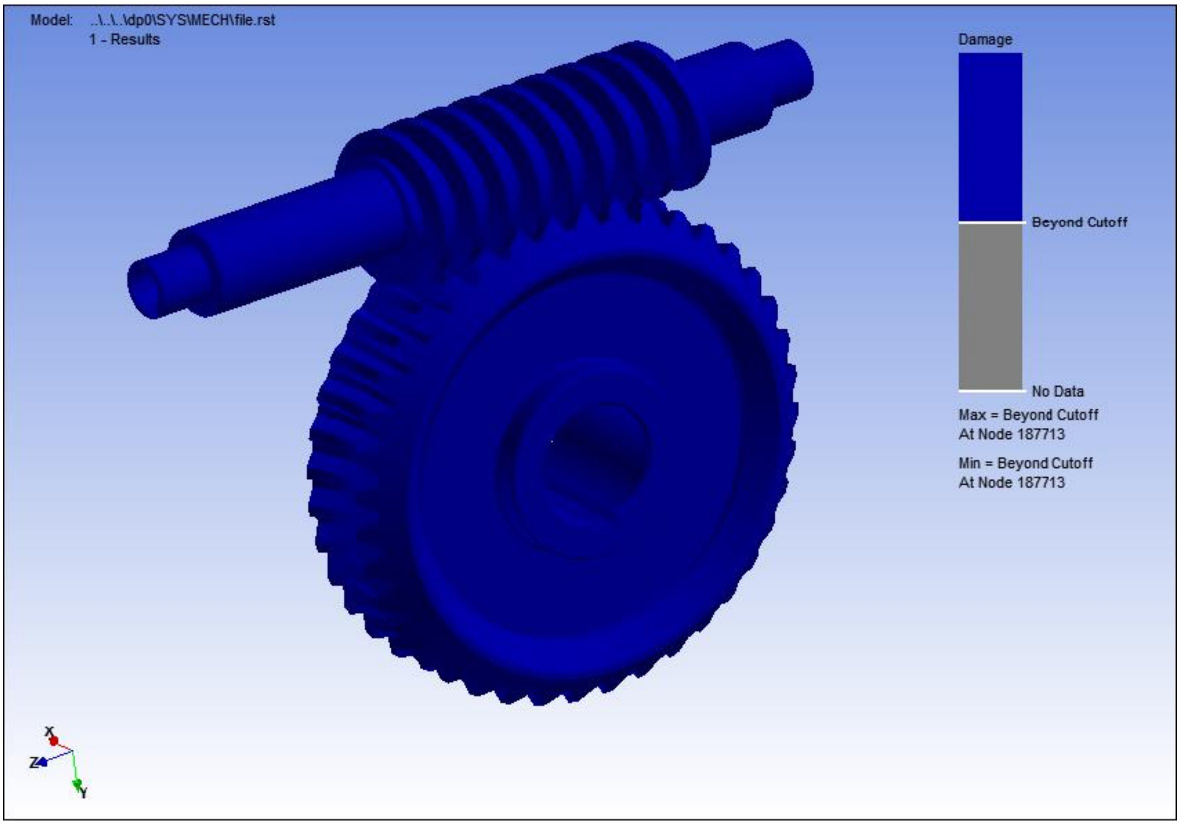
Model: ..\..\..\dp0\SYS\MECH\file.rst
1 - Results
Damage
Beyond Cutoff
No Data
Max = Beyond Cutoff
At Node 187713
Min = Beyond Cutoff
At Node 187713
X
Z
Y

Fig. 4.25 Damage distribution of the worm – gear

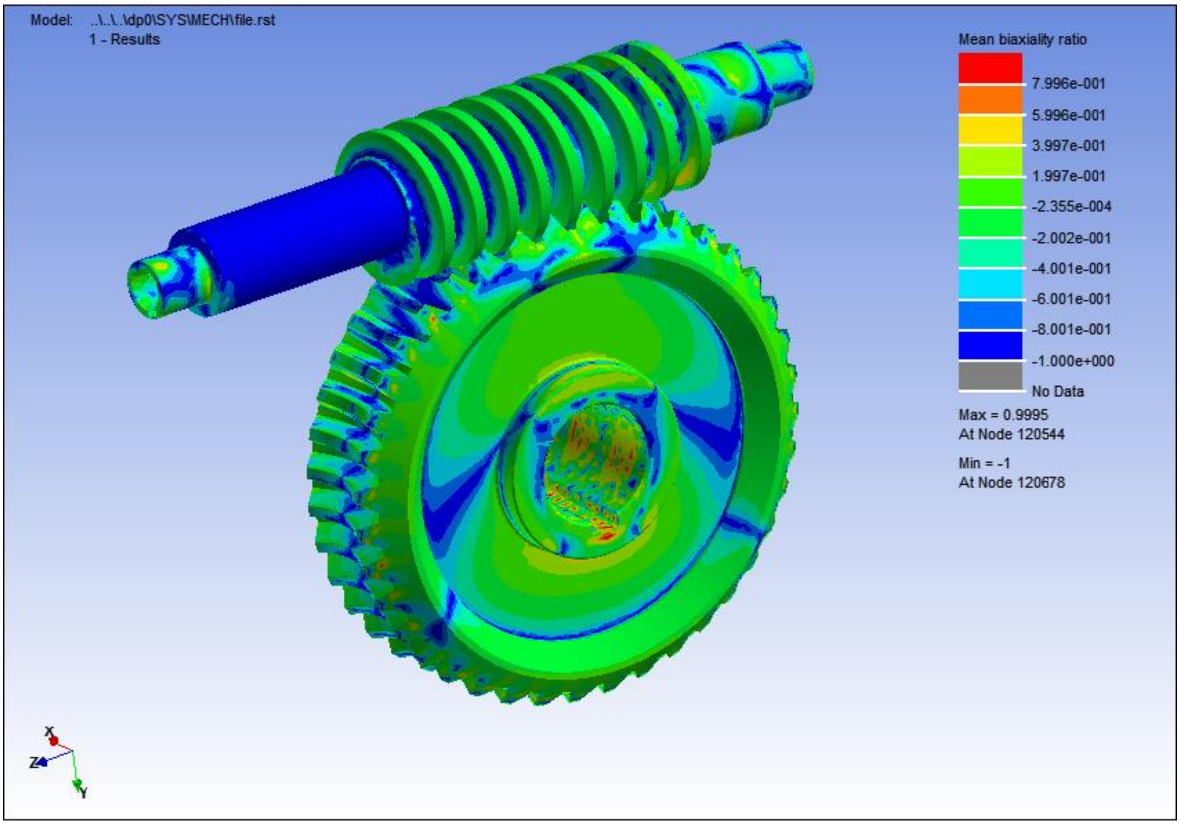
Model: ..\..\..\dp0\SYS\MECH\file.rst
1 - Results
Mean biaxiality ratio
7.996e-001
5.996e-001
3.997e-001
1.997e-001
-2.355e-004
-2.002e-001
-4.001e-001
-6.001e-001
-8.001e-001
-1.000e+000
No Data
Max = 0.9995
At Node 120544
Min = -1
At Node 120678
X
Z
Y

Fig. 4.26 Mean biaxiliaty ratio distribution of the worm – gear

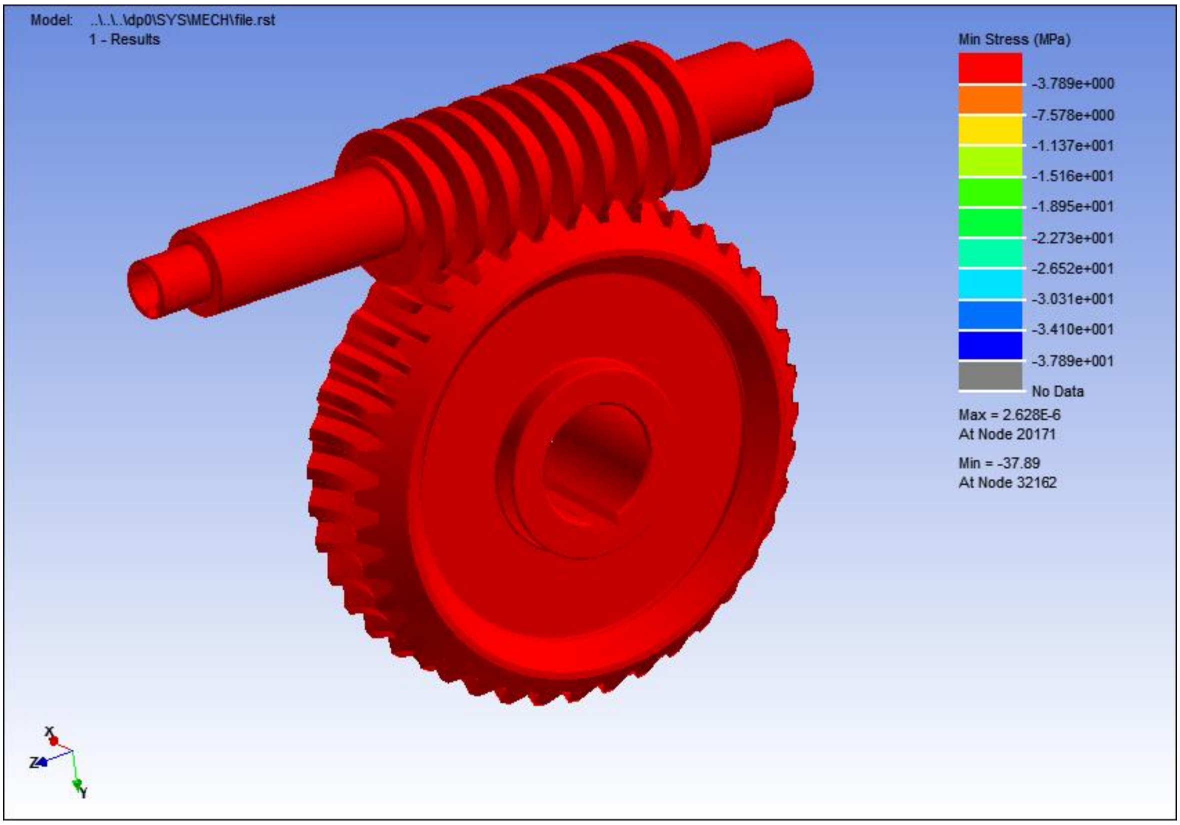
Model: ..\..\..\dp0\SYS\MECH\file.rst
1 - Results
Min Stress (MPa)
-3.789e+000
-7.578e+000
-1.137e+001
-1.516e+001
-1.895e+001
-2.273e+001
-2.652e+001
-3.031e+001
-3.410e+001
-3.789e+001
No Data
Max = 2.628E-6
At Node 20171
Min = -37.89
At Node 32162
X
Z
Y

Fig. 4.27 Min. stress distribution of the worm – gear assembly view

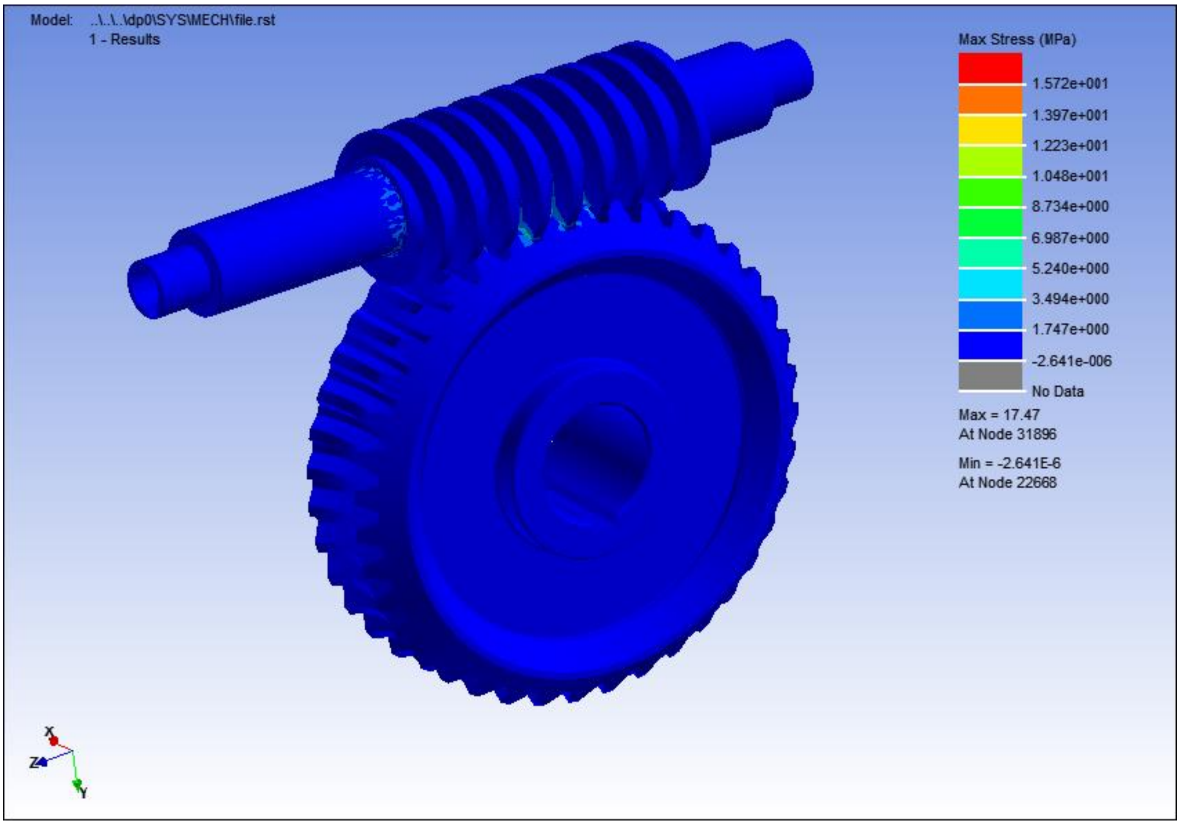
Model: ..\..\..\dp0\SYS\MECH\file.rst
1 - Results
Max Stress (MPa)
1.572e+001
1.397e+001
1.223e+001
1.048e+001
8.734e+000
6.987e+000
5.240e+000
3.494e+000
1.747e+000
-2.641e-006
No Data
Max = 17.47
At Node 31896
Min = -2.641E-6
At Node 22668
X
Z
Y

Fig. 4.28 Max. stress distribution of the worm – gear assembly view

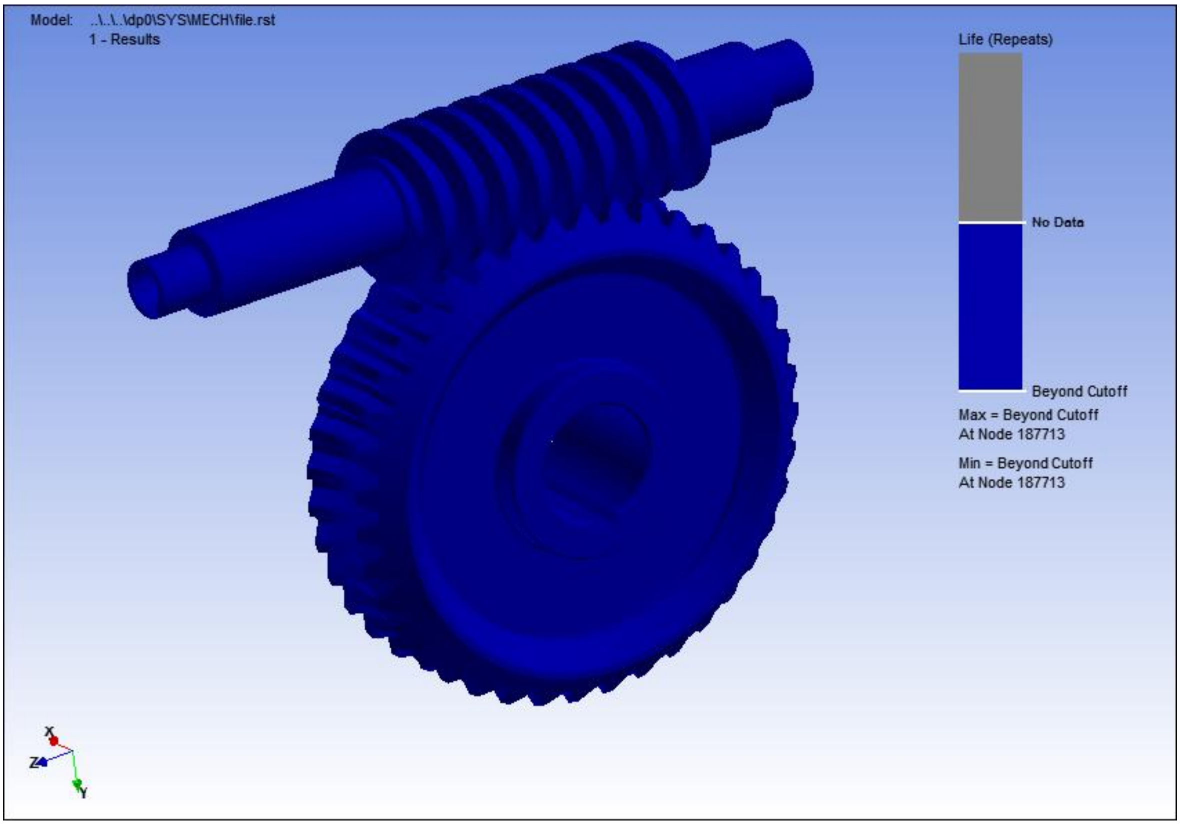
Model: ..\..\..\dp0\SYS\MECH\file.rst
1 - Results
Life (Repeats)
No Data
Beyond Cutoff
Max = Beyond Cutoff
At Node 187713
Min = Beyond Cutoff
At Node 187713
X
Z
Y

Fig. 4.29 Life of the worm – gear

4.3.3 Conclusion

In this study, worm-gear mechanism used in reductor of monorail crane have been examined in terms of stress, deflection and fatigue by considering both the AGMA Stress and Strength Equations (Spur Gear Design, Shigley’s Mechanical Enginnering Design, Richard G. Budynas – J. Keith Nisbett) and finite element modeling.

In the study of analytical design, firstly the axial, radial and tangential loads have been calculated by using the previous power and torque results and secondly bending, and wear of worm-gear mechanism have been taken into consideration.

Deflections of gears can not be considered as dangerous values for worm-gear mechanism because of very small.

Von Mises stresses of the worm-gear mechanism are convenient compared to material (bronze-ateel)) yield strengths.

And finally, fatigue results of worm-gear mechanism are in terms of damage and life distributions are beyond cut off which means that both have infinite life.

5. SHAFTS

In many enginnering applications, transmission shafts are used in every piece of rotating machinery to transmit rotary motion and torque from one location to another. In the design of monorail crane two shafts have been used, one shaft transfers power or torque from reductor to wheel, the other shaft balances wheel and takes an important role during the carry of loads.

Sometimes shafts carry gears, as in monorail crane, transmitting the rotary motion via gears, belts, or chains from shaft to shaft. The shaft may be an integral part of the driver, such as a motor shaft or engine crankshaft, or it may be a freestanding shaft connected to its neighbor by a coupling of some design. Shafts are carried in bearings, in a simply supported configuration, cantilevered or overhung, depending on the machine configuration.

5.1 Introduction to Shaft Design

In shaft design, both stresses and deflections should be considered. Often, deflection can be the critical factor, because it may cause rapid wear on the surface of bearings. Due to misalignment of shafts gears, belts, or chains driven from the shaft can also de damaged by shaft deflections. The stresses in a shaft can be calculated locally for various points along the shaft based on known loads and assumed cross sections and the deflection calculations require that the entire shaft geometry be defined. Therefore, a shaft is typically first designed using stress considerations and then the deflections. In the following study, both the analytical and finite element method results of two shafts used in monorail crane have examined.

5.2 Shaft analytical and fem results

5.2.1 Wheel Shaft Force and Stress Analysis

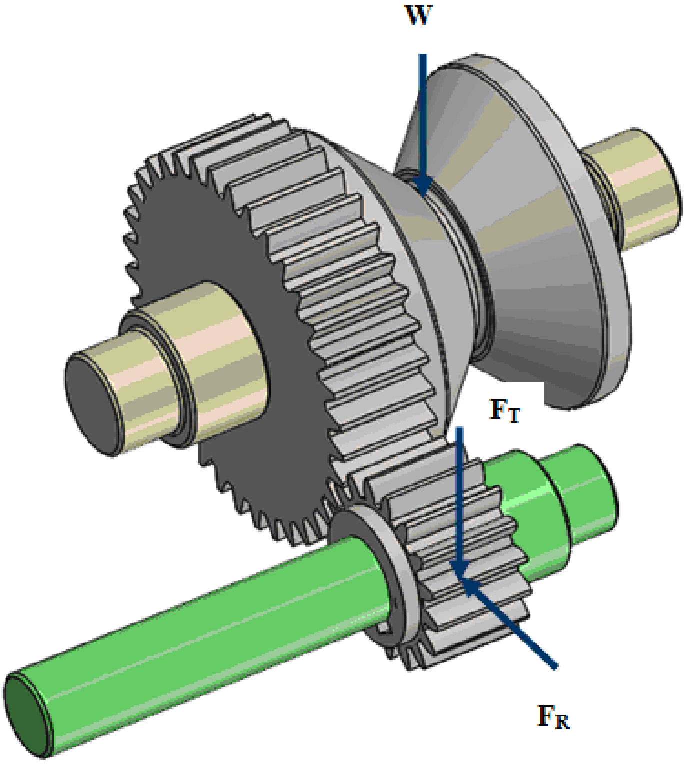

Fig. 5.1 Gear forces

Since the gear diameters are known from sect.4 and the axial locations of the components are set, the free-body diagrams and shear force and bending moment diagrams for the shafts can be produced. From spur gear calculations section 4, F_t = 13166 N, F_R = 4696 N and T = 336 N.m. From summation of forces and moments on each shaft, reaction forces at the bearings can be determined. For shafts with gears and pulleys, the forces and moments will usually have components in two planes along the shaft. For rotating shafts, usually only the resultant magnitude is needed, so force components at bearings are summed as vectors. Shear force and bending moment diagrams are usually obtained in two planes, then summed as vectors at any point of interest. A torque diagram should also be generated to clearly visualize the transfer of torque from an input component, through the shaft, and to an output component.

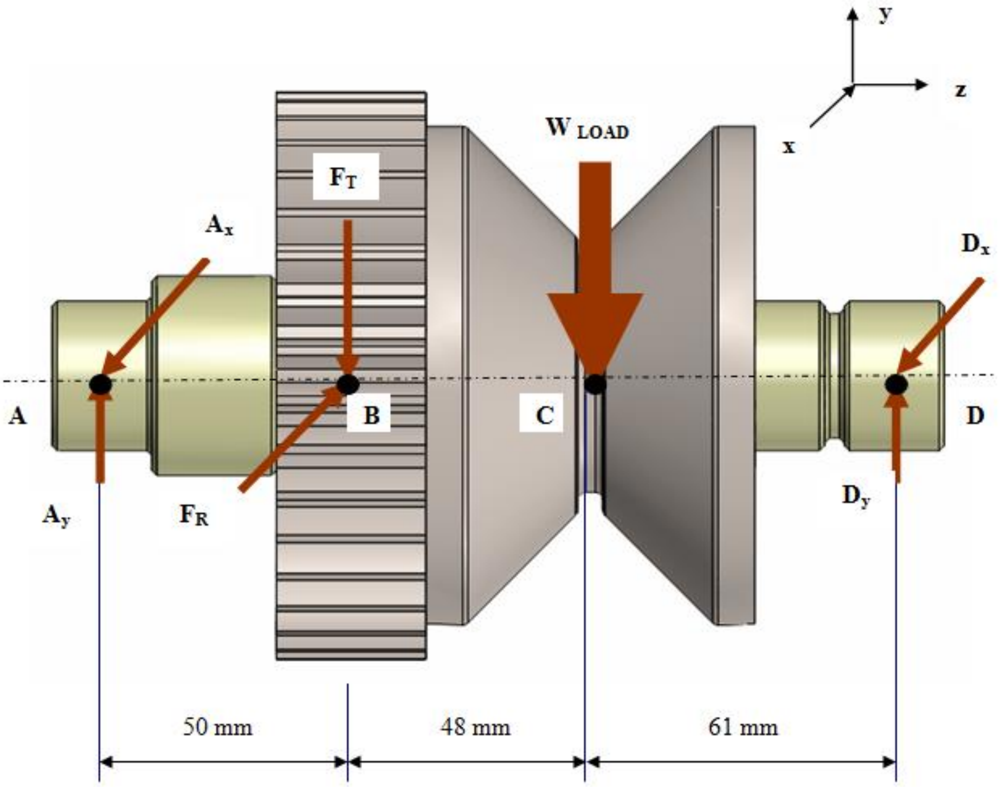
y
z
x
W LOAD
F_T
A_x
D_x
A
B
C
D
A_y
F_R
D_y
50 mm
48 mm
61 mm

Fig. 5.2 Resultant forces on gear – wheel and shaft

$$M_{xy} = F_t x \frac{D_t}{2} = 13177\,x\,\frac{3x36}{2} = 711{,}5\,N.m$$

y-z plane;

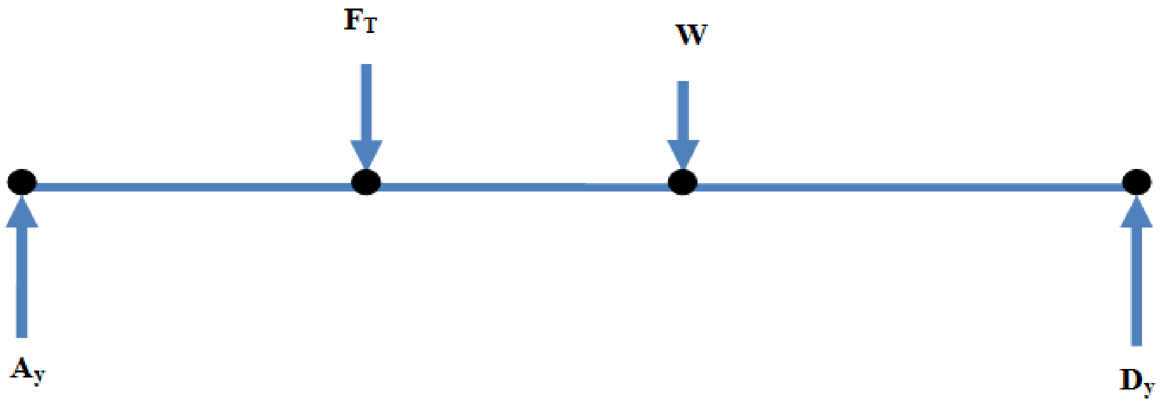

Fig. 5.3 a Force diagram

Taking moment at point A; We find D_y

$$D_y x159 = (500x9.81x98) + (13177x50) + 711,5$$

$$D_y = 11641,76\,N$$

$$\sum F_y = 0;\ A_y + D_y - F_T - W = 0$$

$$A_y + 11641,76 - 13177 - (500x9,81) = 0$$

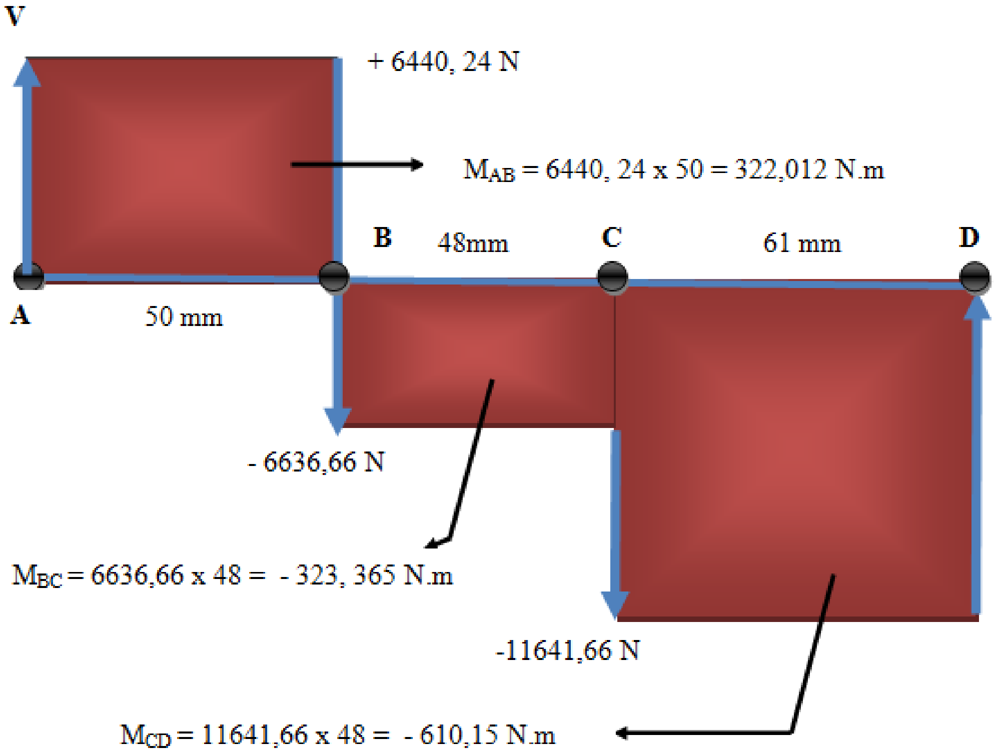
V
+ 6440, 24 N
MAB = 6440, 24 x 50 = 322,012 N.m
B
48mm
C
61 mm
D
A
50 mm
- 6636,66 N
MBC = 6636,66 x 48 = - 323, 365 N.m
-11641,66 N
MCD = 11641,66 x 48 = - 610,15 N.m

Fig. 5.3 b Shear diagram

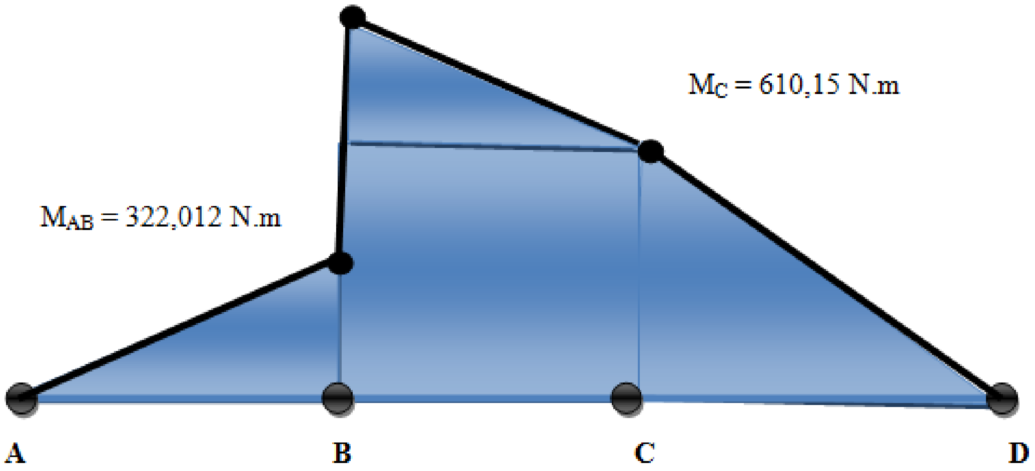
Mc = 610,15 N.m
MAB = 322,012 N.m
A
B
C
D

Fig. 5.3 c Moment diagram

x-z plane;

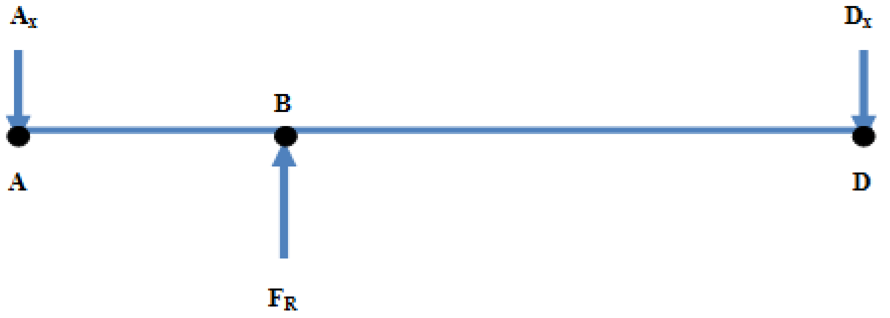

Fig. 5.4 a Force diagram

$$\sum M_A = 0;\quad F_R\, x\,|AB| = D_x\, x\,|AD|$$

$$4796\,x\,50 = D_x\,x159 \rightarrow D_x = 1509\,N$$

$$\sum F_y = 0;\quad F_R - A_x - D_x = 0$$

$$4796 - A_x - 1509 = 0 \rightarrow A_x = 3287\,N$$

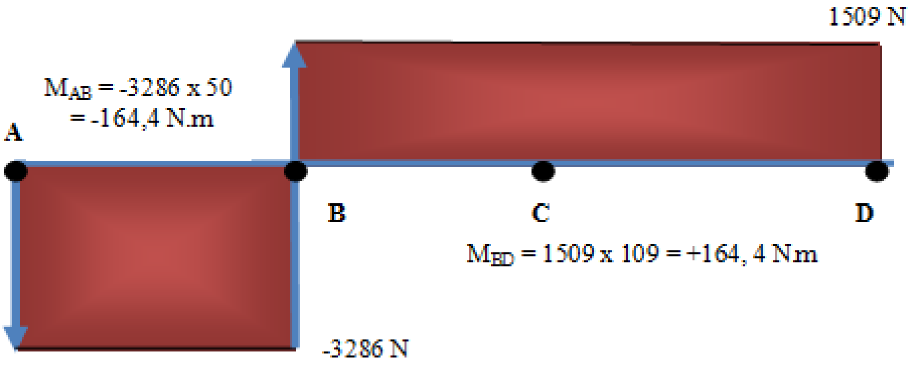
1509 N
M_{AB} = -3286 x 50
= -164,4 N.m
A
B
C
D
M_{BD} = 1509 x 109 = +164, 4 N.m
-3286 N

Fig. 5.4 b Shear diagram

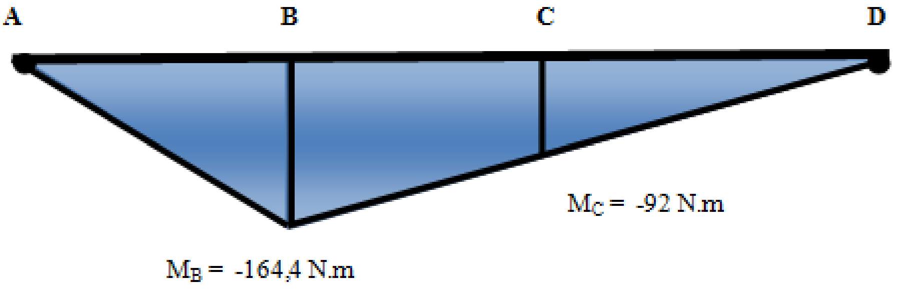
A
B
C
D
M_C = -92 N.m
M_B = -164,4 N.m

Fig. 5.4 c Moment diagram

$$M_B = \sqrt{(M_B)_{xz}^2 + (M_B)_{yz}^2} = \sqrt{(1033,512)^2 + (164,4)^2} = 1046,5\, N.m$$

$$M_C = \sqrt{(M_C)_{xz}^2 + (M_C)_{yz}^2} = \sqrt{(710,15)^2 + (-92)^2} = 716\, N.m$$

The bending moment is largest at the point b, where the gear is replaced. A trial material for the shaft can be selected at any point before the stress design of the shaft, and can be modified as necessary during the stress design process. For the case study, an inexpensive steel, 1020 CD, is initially selected.

The critical shaft diameters are to be determined by stress analysis at critical locations. Since the bending moment is highest at point b, potentially critical stress points are at its shoulder, keyway, and retaining ring groove. It turns out that the keyway is the critical location.

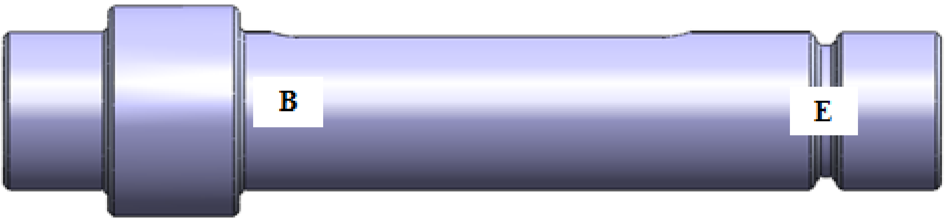

Fig. 5.5 Wheel shaft

$$(M_B)_{alt} = 1046,5\, N.m, \quad T_m = 336\, N.m, \quad (M_B)_{mean} = 0 = T_{alt.}$$

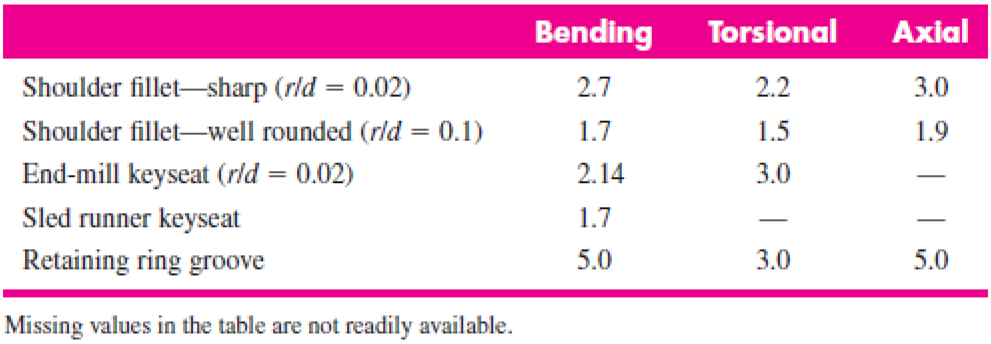

	Bending	Torsional	Axial
Shoulder fillet—sharp (r/d = 0.02)	2.7	2.2	3.0
Shoulder fillet—well rounded (r/d = 0.1)	1.7	1.5	1.9
End-mill keyseat (r/d = 0.02)	2.14	3.0	—
Sled runner keyseat	1.7	—	—
Retaining ring groove	5.0	3.0	5.0

Missing values in the table are not readily available.

Table 5.1 First Iteration Estimates for Stress-Concentration Factors K_t and K_{ts}. (Shigley's Mechanical Enginnering Design, Richard G. Budynas – J. Keith Nisbett)

Assuming generous fillet radius for gear at B. From Table 5.1, we can take K_t and K_{ts} as 1.6, 1.5 respectively. For quick, conservative first pass, if we assume $K_f = K_t$, $K_{fs} = K_{ts}$. and choose inexpensive steel, 1020 CD, with S_{ut} = 469 Mpa. For S_e,

$$k_a = a\,S_{ut}^{b} = 4,51x\,469^{-0,265} = 0,883$$

Guessing k_b = 0.9, on condition we can check this value when d is known.

$$k_c = k_d = k_e = 1$$

$$S_e = 0,883x\,0,9x\,0,5x\,469 = 186\,Mpa$$

For first estimate of the small diameter at the shoulder at point B, lets use the DE-Goodman criterion. (Shaft Design, Shigley's Mechanical Enginnering Design, Richard G. Budynas – J. Keith Nisbett). This criterion is good for the initial design, since it is simple and conservative. With $M_m = T_a = 0$,

$$d = \left\{ \frac{16n}{\pi} \left(\frac{2(K_f\,M_a)}{S_e} + \frac{\left[3(K_{fs}\,T_m)^2\right]^{1/2}}{S_{ut}} \right) \right\}^{1/3}$$

(Shaft Design in Shigley's Mechanical Enginnering Design, Richard G. Budynas – J. Keith Nisbett)

$$d = \left\{ \frac{16x1,5}{\pi} \left(\frac{2(2,2x1046,5)}{186x10^6} + \frac{\left[3(3x336)^2\right]^{1/2}}{469x10^6} \right) \right\}^{1/3} = 0,0562\,m = 56,2\,mm$$

All estimates have probably been conservative, so by selecting the next standard size below 56,2 mm. and check, d = 50 mm. A typical D/d ratio for support at a shoulder is D/d =1.2, thus, D = 1.2 x 50 = 60 mm. A nominal 60 mm cold-drawn shaft diameter can be used. Assuming fillet radius $r = d/10$ =5 mm. r/d = 0,1.

$$K_t = 1,6 \quad , \quad q = 0,82$$

$$K_f = 1 + 0,82(1,6-1) = 1,49$$

$$K_{ts}=1,35 \quad , \qquad q_s=0,95$$

$$K_{fs}=1+0,95(1,35-1)=1,33$$

$$k_a=0,883$$

$$k_b=\left(\frac{50}{7,62}\right)^{-0,107}=0,818$$

$$S_e=0,883x0,818x0,5x469=169,38Mpa$$

$$\sigma_a^{'}=\frac{32K_f\,M_a}{\pi\,d^3}=\frac{32x1,49x1046,5}{\pi\,x0,05^3}=127Mpa$$

$$\sigma_m^{'}=\left[3\left(\frac{16K_{fs}\,T_m}{\pi\,d^3}\right)\right]^{1/2}=\left(\frac{\sqrt{3}x16x1,33x336}{\pi\,x0,05^3}\right)=31,5Mpa$$

If we use goodman criterion;

$$\frac{1}{n_f}=\frac{\sigma_a^{'}}{S_e}+\frac{\sigma_m^{'}}{S_{ut}}$$

$$\frac{1}{n_f}=\frac{127}{169,38}+\frac{31,5}{469}$$

$$n_f=1,2$$

If we check yielding;

$$n_y=\frac{S_y}{\sigma_{\max}^{'}}>\frac{S_y}{\sigma_a^{'}+\sigma_m^{'}}=\frac{393}{127+31,5}=2,4$$

Also if we check this diameter at the end of the keyway, just to the right of point *B,* and at the groove near at point B, by assuming the radius at the bottom of the keyway will be the standard; r / d =0,02.

$$r = 0,02\,x\,d = 0,02\,x\,50 = 1mm$$

$$K_t = 1,9 \quad , \quad q = 0,2$$

$$K_f = 1 + 0,2(1,9 - 1) = 1,2$$

$$K_{ts} = 1,4 \quad , \qquad q_s = 0,75$$

$$K_{fs} = 1 + 0,75(1,4 - 1) = 1,3$$

$$\sigma_a^{'} = \frac{32\,K_f\,M_a}{\pi\,d^3} = \frac{32\,x1,2\,x1046,5}{\pi\,x\,0,05^3} = 102\,Mpa$$

$$\sigma_m^{'} = \left[3\left(\frac{16\,K_{fs}\,T_m}{\pi\,d^3} \right) \right]^{1/2} = \left(\frac{\sqrt{3}x16\,x1,3\,x\,336}{\pi\,x\,0,05^3} \right) = 30,8\,Mpa$$

$$\frac{1}{n_f} = \frac{\sigma_a^{'}}{S_e} + \frac{\sigma_m^{'}}{S_{ut}} = \frac{102}{169,38} + \frac{30,8}{469} = 1,4$$

From the above results, the keyway turns out to be more critical than the shoulder. Then to be able to obtain more bigger safety factor, we can either increase the diameter or use a higher strength material. Unless the deflection analysis shows a need for larger diameters, let us choose to increase the strength. We started with a very low strength and can afford to increase it some to avoid larger sizes. We can try 1045 HR with S_{ut} = 690 Mpa and recalculating factors affected by S_{ut} ;

$$k_a = 4,51\,x\,690^{-0,265} = 0,8$$

$$S_e = 0,8\,x\,0,818\,x\,0,5\,x\,690 = 225,8\,Mpa$$

$$\frac{1}{n_f} = \frac{\sigma_a^{'}}{S_e} + \frac{\sigma_m^{'}}{S_{ut}} = \frac{102}{225,8} + \frac{30,8}{690}$$

$$n_f = 2$$

Let's check at the groove at *E*, since K_t for flat-bottomed grooves are often very high.

$$\left(M_E\right)_{xz} = -11641\,x\,25 = -292\,N.m$$

$$\left(M_E\right)_{yz} = -1509\,x\,25 = -38\,N.m$$

$$M_E = \sqrt{\left(M_E\right)_{xz}^2 + \left(M_E\right)_{yz}^2} = \sqrt{\left(292\right)^2 + (38)^2} = 294,5\,N.m$$

To quickly check if this location is potentially critical, just use $K_f = K_t = 5.0$ as an estimate, from Table 5.1.

$$\sigma_a^{'} = \frac{32\,K_f\,M_a}{\pi\,d^3} = \frac{32\,x\,5\,x\,294,5}{\pi\,x\,0,05^3} = 120\,Mpa$$

$$\sigma_m^{'} = \left[3\left(\frac{16\,K_{fs}\,T_m}{\pi\,d^3}\right)\right]^{1/2} = \left(\frac{\sqrt{3}x16\,x\,5\,x\,336}{\pi\,x\,0,05^3}\right) = 119\,Mpa$$

$$\frac{1}{n_f} = \frac{\sigma_a^{'}}{S_e} + \frac{\sigma_m^{'}}{S_{ut}} = \frac{120}{225,8} + \frac{119}{690}$$

$$n_f = 1,42$$

We can look up data for a specific retaining ring to obtain K_f more accurately. Appropriate groove specifications for a retaining ring for a shaft diameter of 50 mm are obtained from tables (Shaft Design, Shigley's Mechanical

Enginnering Design, Richard G. Budynas – J. Keith Nisbett) as follows: width, *a* = 2 mm; depth, *t* = 1,5; and corner radius at bottom of groove, *r* = 0.5 mm. With *r / t* = 0.5 / *1,5* = 0.33, and *a / t* = 2 / 1.5 = 1.33.

$$K_t = 6{,}5 \quad , \quad q = 0{,}8$$

$$K_f = 1 + 0{,}8(6{,}5 - 1) = 5{,}4$$

$$K_{ts} = 4{,}75 \quad , \quad q_s = 0{,}75$$

$$K_{fs} = 1 + 0{,}75(4{,}75 - 1) = 3{,}9$$

$$\sigma_a^{'} = \frac{32 K_f M_a}{\pi d^3} = \frac{32\,x\,5{,}4\,x\,294{,}5}{\pi\,x\,0{,}05^3} = 129{,}5\,Mpa$$

$$\sigma_m^{'} = \left[3\left(\frac{16 K_{fs} T_m}{\pi d^3}\right)\right]^{1/2} = \left(\frac{\sqrt{3}x16\,x\,3{,}9\,x\,336}{\pi\,x\,0{,}05^3}\right) = 92{,}5\,Mpa$$

$$\frac{1}{n_f} = \frac{\sigma_a^{'}}{S_e} + \frac{\sigma_m^{'}}{S_{ut}} = \frac{129{,}5}{225{,}8} + \frac{92{,}5}{690} \Rightarrow n_f = 1{,}4$$

5.2.2 Wheel Shaft Fem Results

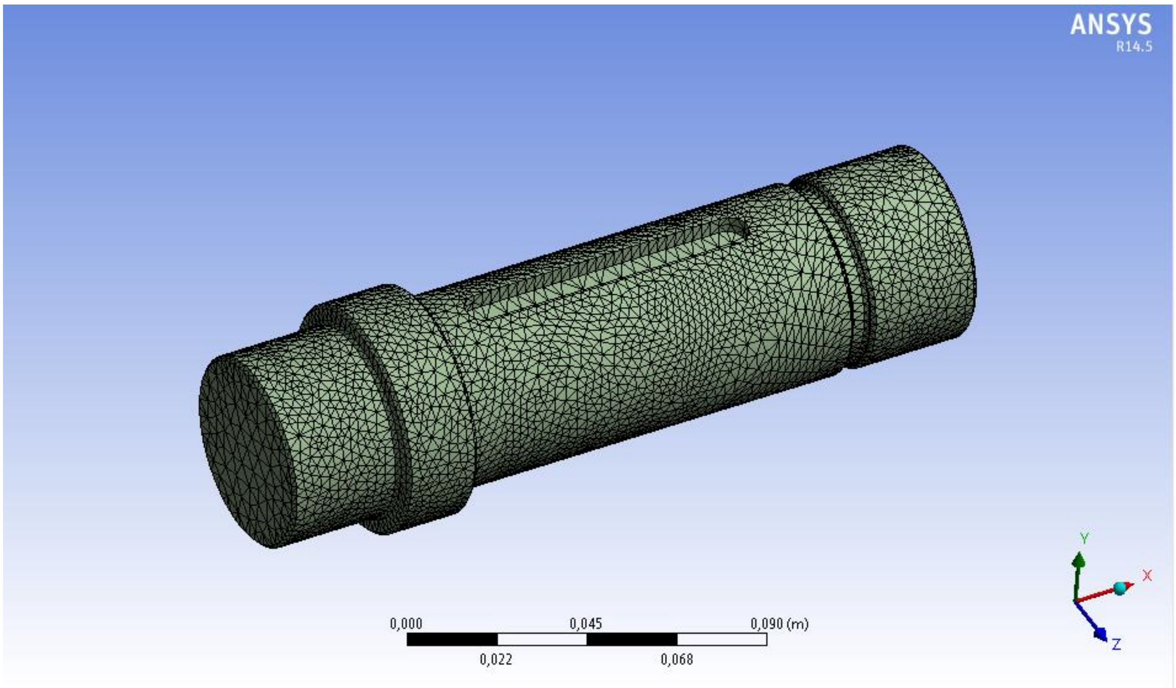
ANSYS
R14.5
0,000
0,045
0,090 (m)
0,022
0,068
Y
X
Z

Fig. 5.6 Mesh view of the wheel shaft

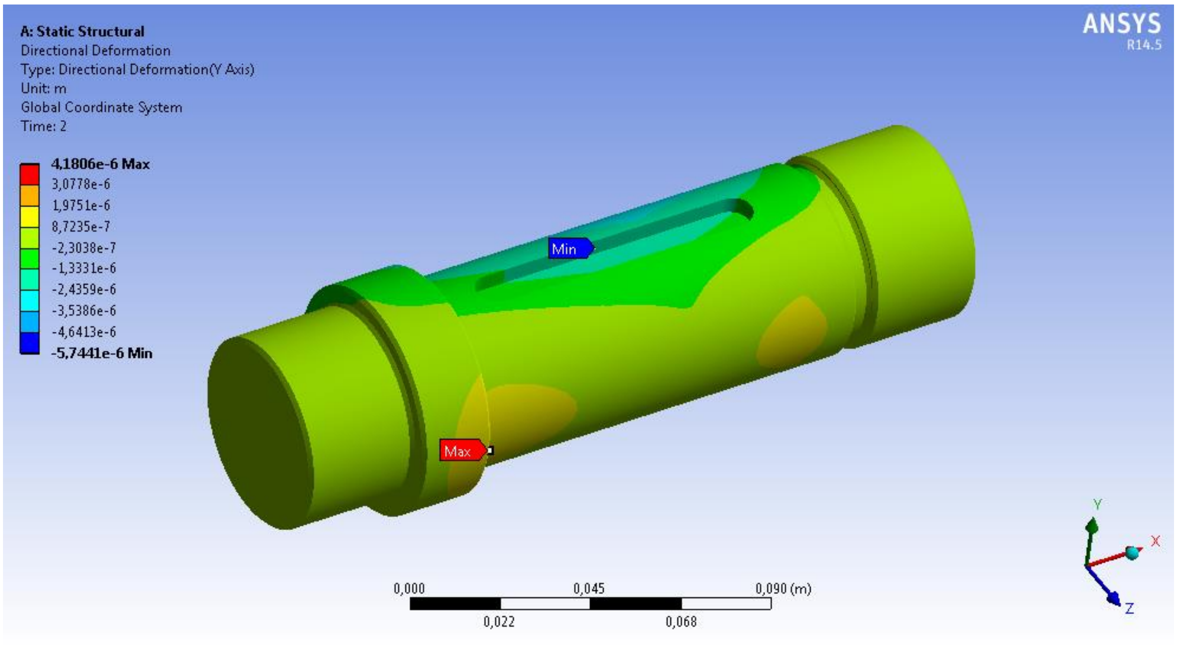
A: Static Structural
Directional Deformation
Type: Directional Deformation(Y Axis)
Unit: m
Global Coordinate System
Time: 2
4,1806e-6 Max
3,0778e-6
1,9751e-6
8,7235e-7
-2,3038e-7
-1,3331e-6
-2,4359e-6
-3,5386e-6
-4,6413e-6
-5,7441e-6 Min
ANSYS
R14.5
Min
Max
0,000
0,045
0,090 (m)
0,022
0,068
Y
X
Z

Fig. 5.7 Directional deformation distribution of the wheel shaft

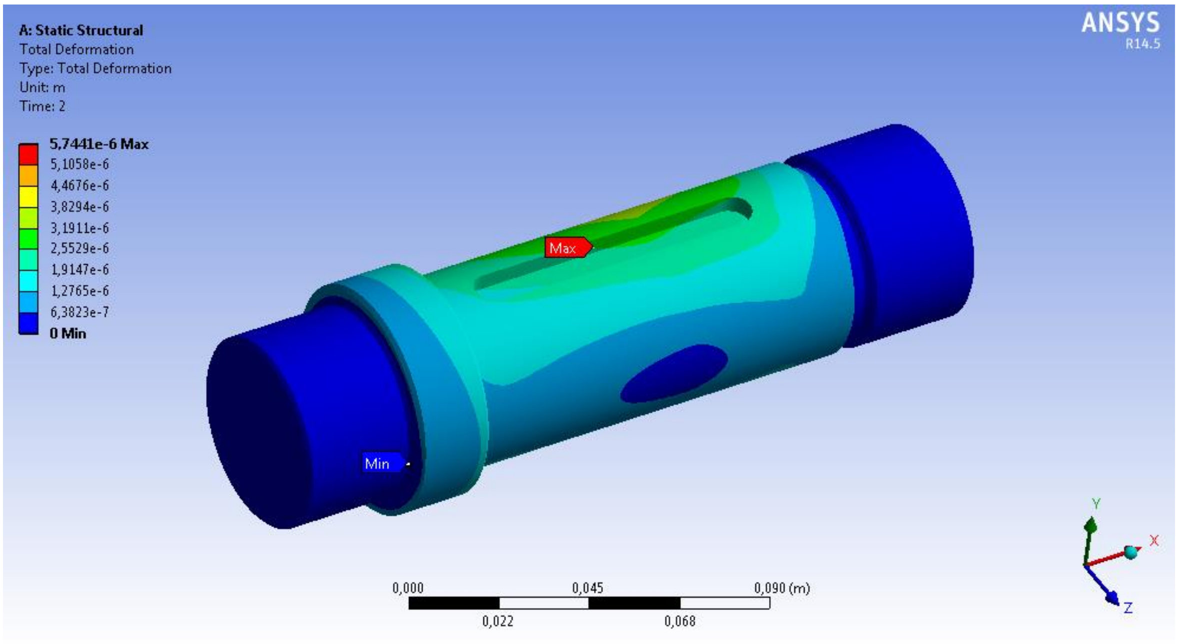
A: Static Structural
Total Deformation
Type: Total Deformation
Unit: m
Time: 2
5,7441e-6 Max
5,1058e-6
4,4676e-6
3,8294e-6
3,1911e-6
2,5529e-6
1,9147e-6
1,2765e-6
6,3823e-7
0 Min
ANSYS
R14.5
Max
Min
0,000
0,045
0,090 (m)
0,022
0,068
Y
X
Z

Fig. 5.8 Total deformation distribution of the wheel shaft

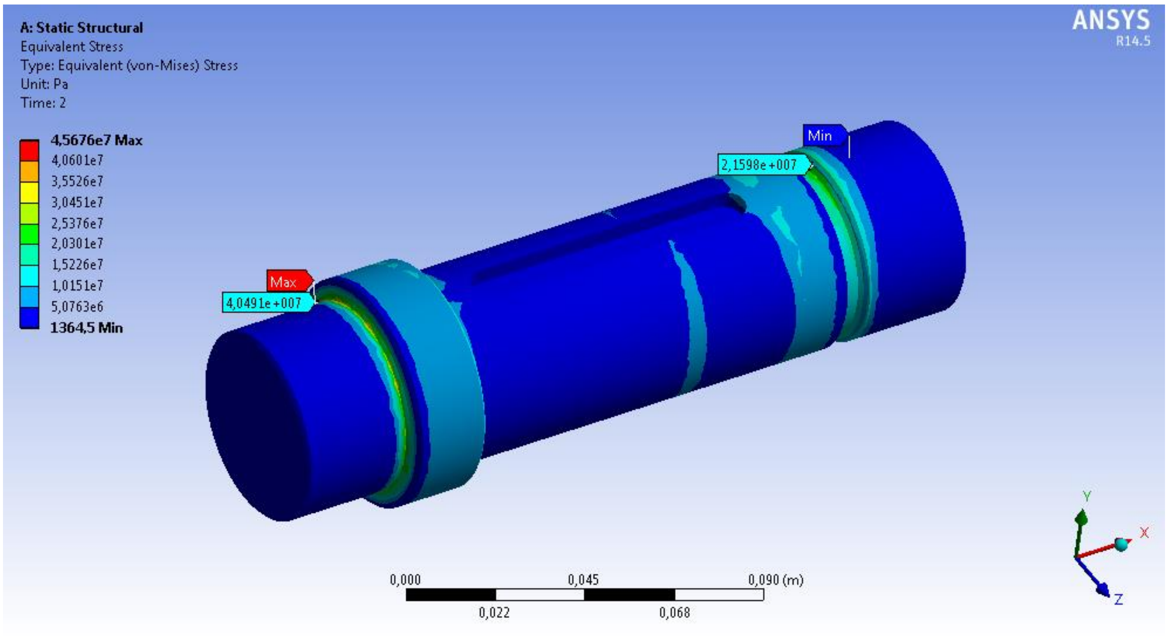
A: Static Structural
Equivalent Stress
Type: Equivalent (von-Mises) Stress
Unit: Pa
Time: 2
4,5676e7 Max
4,0601e7
3,5526e7
3,0451e7
2,5376e7
2,0301e7
1,5226e7
1,0151e7
5,0763e6
1364,5 Min
ANSYS
R14.5
Min
2,1598e+007
Max
4,0491e+007
0,000
0,045
0,090 (m)
0,022
0,068
Y
X
Z

Fig. 5.9 Von Mises Stress distribution of the wheel shaft

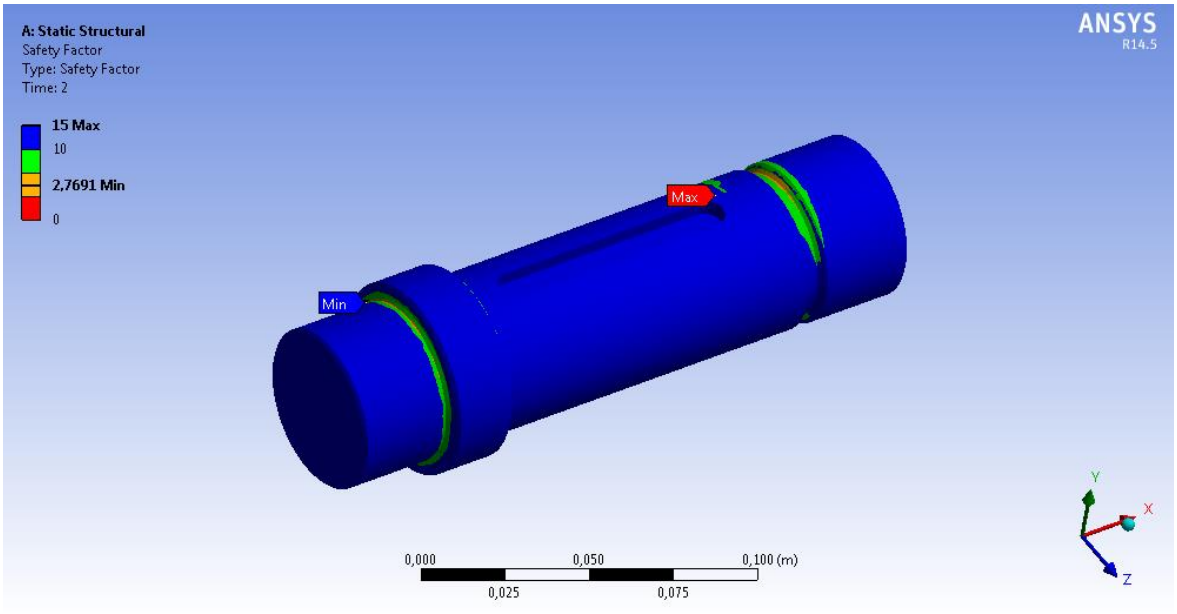
A: Static Structural
Safety Factor
Type: Safety Factor
Time: 2
15 Max
10
2,7691 Min
0
ANSYS
R14.5
Max
Min
0,000
0,050
0,100 (m)
0,025
0,075
Y
X
Z

Fig. 5.10 Safety factor of the wheel shaft

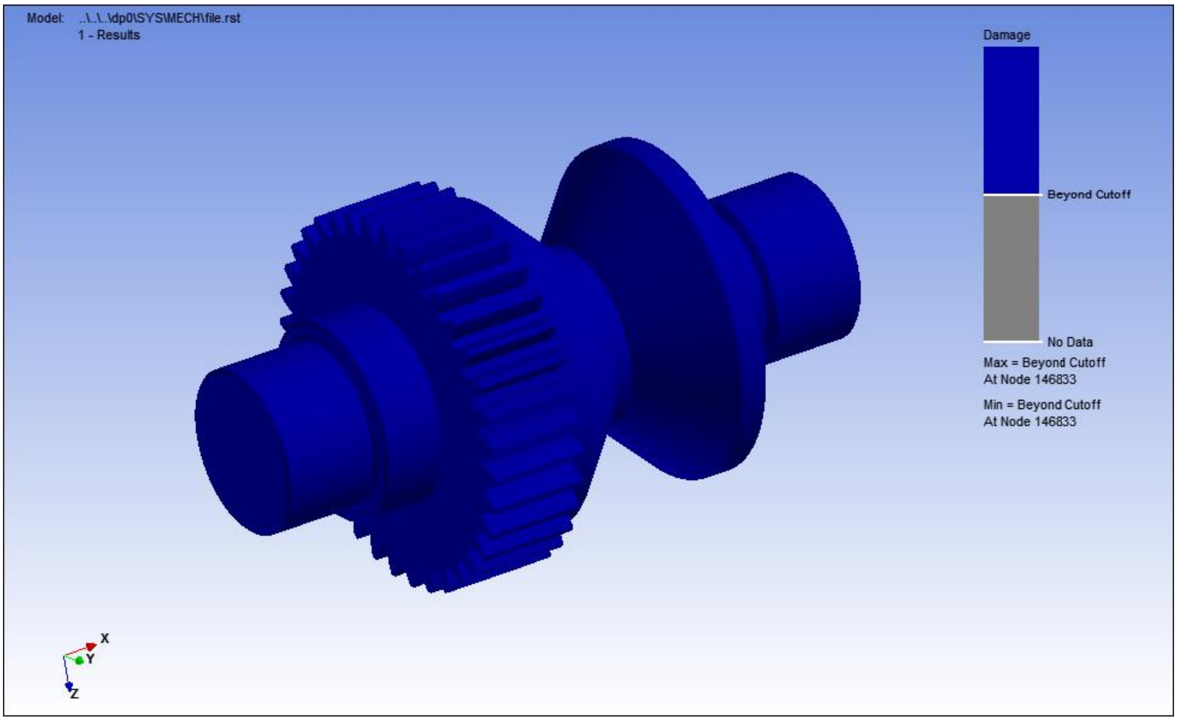
Model: ..\..\dp0\SYS\MECH\file.rst
1 - Results
Damage
Beyond Cutoff
No Data
Max = Beyond Cutoff
At Node 146833
Min = Beyond Cutoff
At Node 146833
X
Y
Z

Fig. 5.11 Damage distribution of the wheel shaft

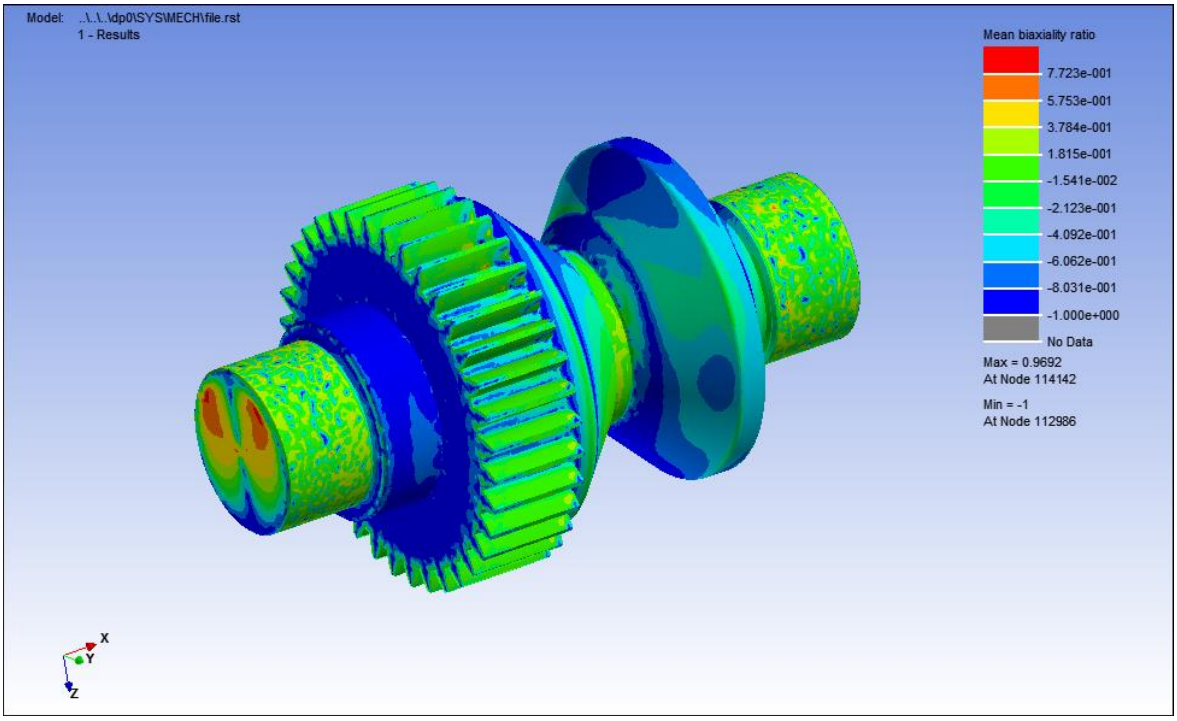
Model: ..\..\..\dp0\SYS\MECH\file.rst
1 - Results
Mean biaxiality ratio
7.723e-001
5.753e-001
3.784e-001
1.815e-001
-1.541e-002
-2.123e-001
-4.092e-001
-6.062e-001
-8.031e-001
-1.000e+000
No Data
Max = 0.9692
At Node 114142
Min = -1
At Node 112986
X
Y
Z

Fig. 5.12 Mean biaxiliaty ratio distribution of the wheel shaft

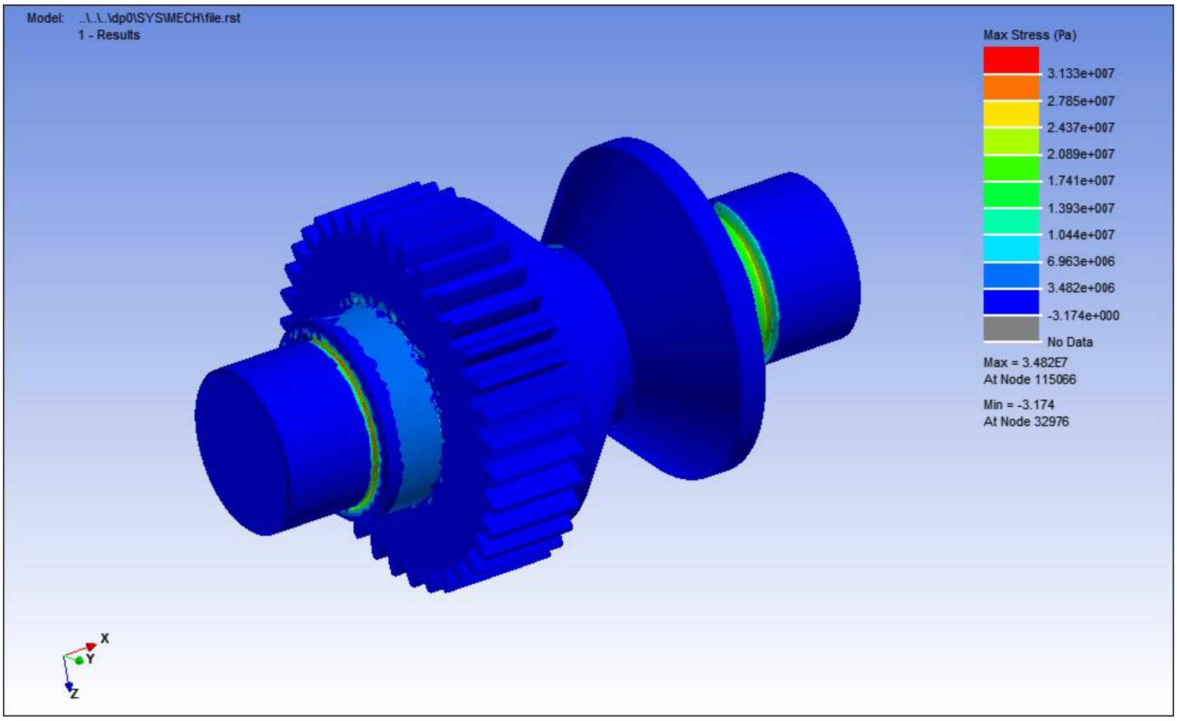
Model: ..\..\..\dp0\SYS\MECH\file.rst
1 - Results
Max Stress (Pa)
3.133e+007
2.785e+007
2.437e+007
2.089e+007
1.741e+007
1.393e+007
1.044e+007
6.963e+006
3.482e+006
-3.174e+000
No Data
Max = 3.482E7
At Node 115066
Min = -3.174
At Node 32976
X
Y
Z

Fig. 5.13 Max. stress distribution of the wheel shaft

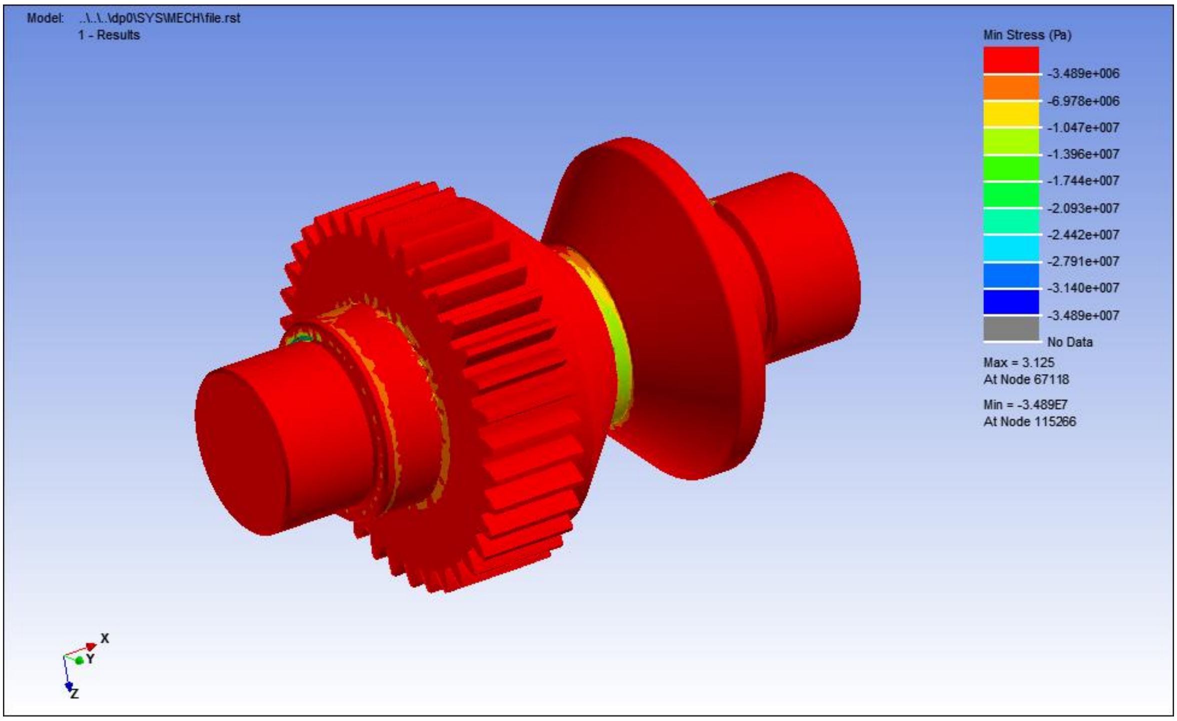
Model: ..\..\..\dp0\SYS\MECH\file.rst
1 - Results
Min Stress (Pa)
-3.489e+006
-6.978e+006
-1.047e+007
-1.396e+007
-1.744e+007
-2.093e+007
-2.442e+007
-2.791e+007
-3.140e+007
-3.489e+007
No Data
Max = 3.125
At Node 67118
Min = -3.489E7
At Node 115266
X
Y
Z

Fig. 5.14 Min. stress distribution of the wheel shaft

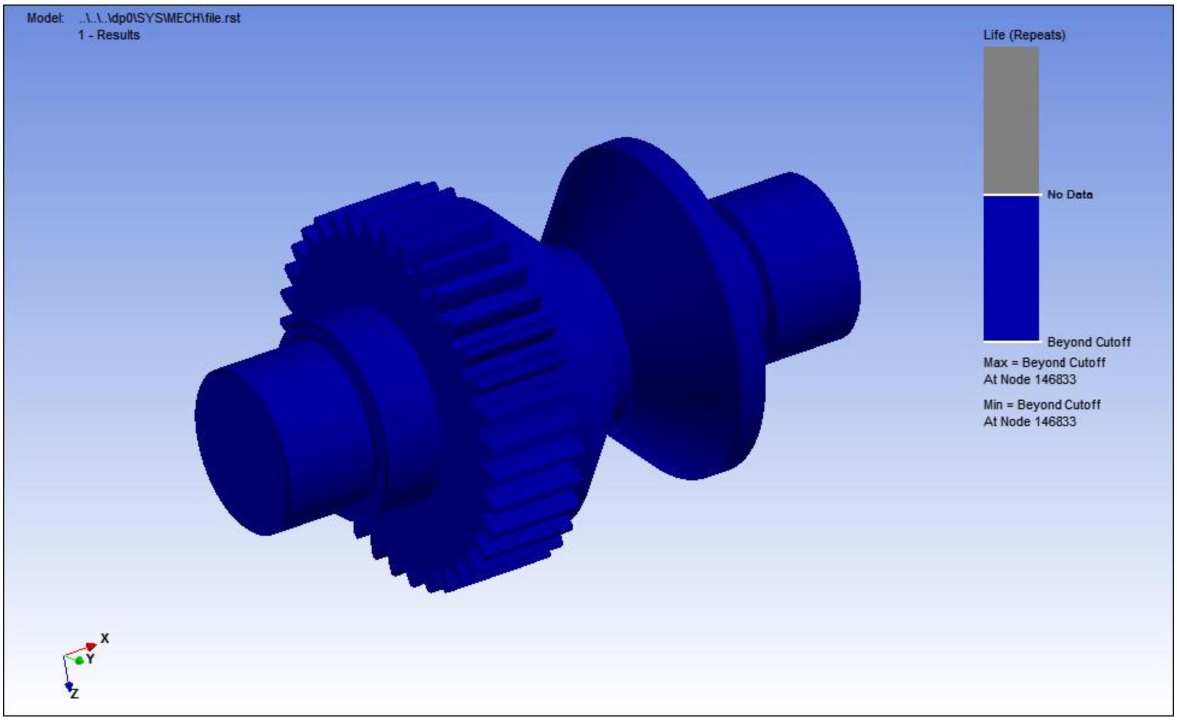
Model: ..\..\..\dp0\SYS\MECH\file.rst
1 - Results
Life (Repeats)
No Data
Beyond Cutoff
Max = Beyond Cutoff
At Node 146833
Min = Beyond Cutoff
At Node 146833
X
Y
Z

Fig. 5.15 Life of the wheel shaft

5.2.3 Pinion Shaft Analytical Results

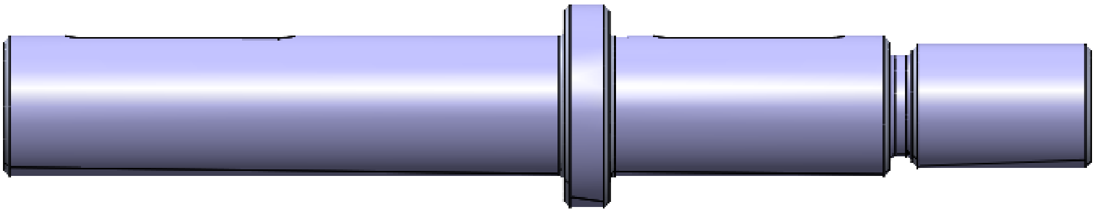

Fig. 5.16 Pinion shaft

With the weights of electric motor and reductors, the dead weight has taken as 75 kg. Since the length of the shaft from the reductor to the frame link is 100 mm, then M_a = 65 x 9,81 x 0,1 = 63,6 N.m and torque value is 336 N.m

Again if we apply the same assumptions that we made with wheel shaft, 1020 CD material, with S_{ut} = 469 Mpa. For S_e,

$$k_a = a\,S_{ut}^b = 4,51x\,469^{-0,265} = 0,883$$

k_b = 0,9. $k_c = k_d = k_e = 1$

$$S_e = 0,883x\,0,9\,x\,0,5\,x\,469 = 186\,Mpa$$

Lets use the DE-Goodman criterion. With $M_m = T_a = 0$,

$$d = \left\{ \frac{16n}{\pi} \left(\frac{2\,(K_f\,M_a)}{S_e} + \frac{\left[3(K_{fs}\,T_m)^2\right]^{1/2}}{S_{ut}} \right) \right\}^{1/3}$$

(Shaft Design in Shigley’s Mechanical Enginnering Design, Richard G. Budynas – J. Keith Nisbett)

$$d = \left\{ \frac{16\,x1,5}{\pi} \left(\frac{2\,(1,7\,x\,73,6)}{186\,x10^6} + \frac{\left[3(1,5\,x\,336)^2\right]^{1/2}}{469\,x10^6} \right) \right\}^{1/3} = 0,029 = 30\,mm$$

Since the goodman criterion is the best conservative, all estimates have probably been true, so select the next standard size above 0,029 mm. and check, *d* = 30 mm. A typical *D/d* ratio for support at a shoulder is *D/d* =1,2, thus, *D* = 1,2 x 30 = 36mm. A nominal 36 mm cold-drawn bigger shaft diameter can be used. Assuming fillet radius r = d / 10 = 3,6 mm. r / d = 0,1.

$$K_t = 2 \ , \quad q = 0,95$$

$$K_f = 1 + 0,95(2-1) = 1,95$$

$$K_{ts} = 1,5 \quad , \qquad q_s = 0,95$$

$$K_{fs} = 1 + 0,95(1,5-1) = 1,5$$

$$k_a = 0,883$$

$$k_b = \left(\frac{36}{7,62}\right)^{-0,107} = 0,85$$

$$S_e = 0,883 x 0,85 x 0,5 x 469 = 176 Mpa$$

$$\sigma_a^{'} = \frac{32 K_f \, M_a}{\pi \, d^3} = \frac{32 x 1,95 x 73,6}{\pi \, x 0,036^3} = 32 Mpa$$

$$\sigma_m^{'} = \left[3\left(\frac{16 K_{fs} \, T_m}{\pi \, d^3}\right)\right]^{1/2} = \left(\frac{\sqrt{3} x 16 x 1,5 x 336}{\pi \, x 0,036^3}\right) = 96 Mpa$$

If we use goodman criterion;

$$\frac{1}{n_f} = \frac{\sigma_a^{'}}{S_e} + \frac{\sigma_m^{'}}{S_{ut}}$$

$$\frac{1}{n_f}=\frac{32}{176}+\frac{96}{469}$$

$$n_f=2,5$$

If we check yielding;

$$n_y=\frac{S_y}{\sigma'_{\max}}>\frac{S_y}{\sigma'_a+\sigma'_m}=\frac{393}{32+96}$$

$$n_y=3$$

There are two keyway between the pinion and shaft, also reducot and shaft. Assumeing the radius at the bottom of the keyway will be the standard; r/d =0,02.

$$r=0,02\,x\,d=0,02\,x\,36=0,72\,mm$$

$$K_t=2,2\quad,\quad q=0,65$$

$$K_f=1+0,65(2,2-1)=1,78$$

$$K_{ts}=3\quad,\quad q_s=0,75$$

$$K_{fs}=1+0,75(3-1)=2,5$$

$$\sigma'_a=\frac{32K_f\,M_a}{\pi\,d^3}=\frac{32\,x\,1,78\,x\,73,6}{\pi\,x\,0,036^3}=33\,Mpa$$

$$\sigma'_m=\left[3\left(\frac{16K_{fs}\,T_m}{\pi\,d^3}\right)^2\right]^{1/2}=\left(\frac{\sqrt{3}x16\,x\,2,5\,x\,336}{\pi\,x\,0,036^3}\right)=158,8Mpa$$

$$\frac{1}{n_f}=\frac{\sigma'_a}{S_e}+\frac{\sigma'_m}{S_{ut}}=\frac{33}{169,38}+\frac{158,8}{469}\Rightarrow n_f=1,8$$

5.2.4 Pinion shaft fem results

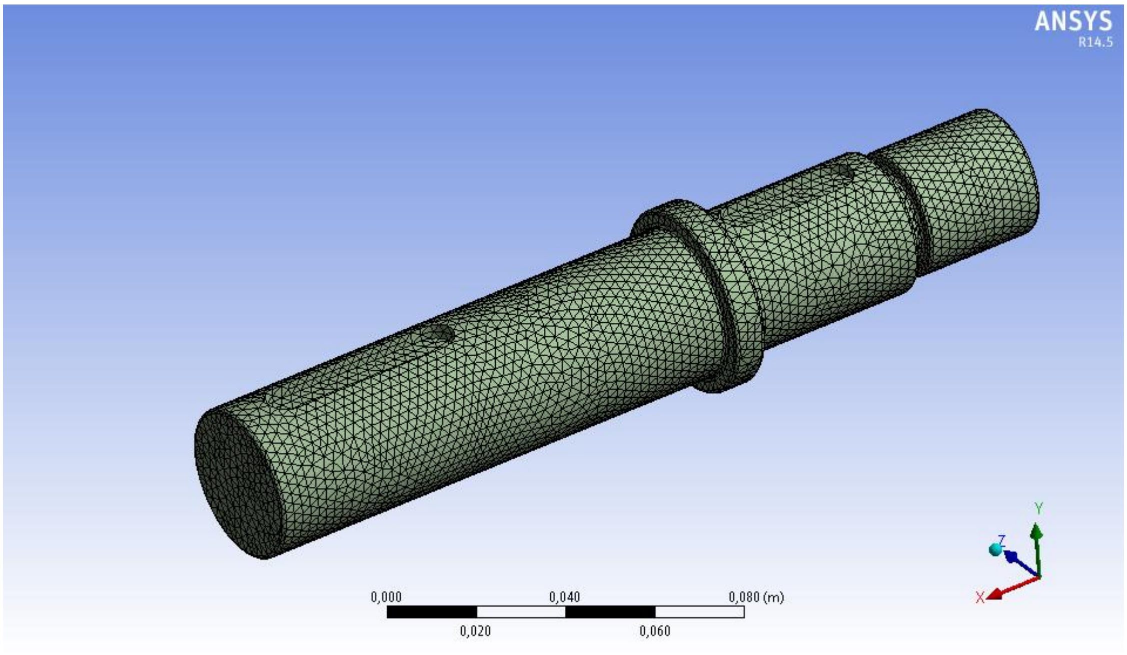
ANSYS
R14.5
0,000
0,040
0,080 (m)
0,020
0,060
Y
Z
X

Fig. 5.17 Mesh view of the pinion shaft

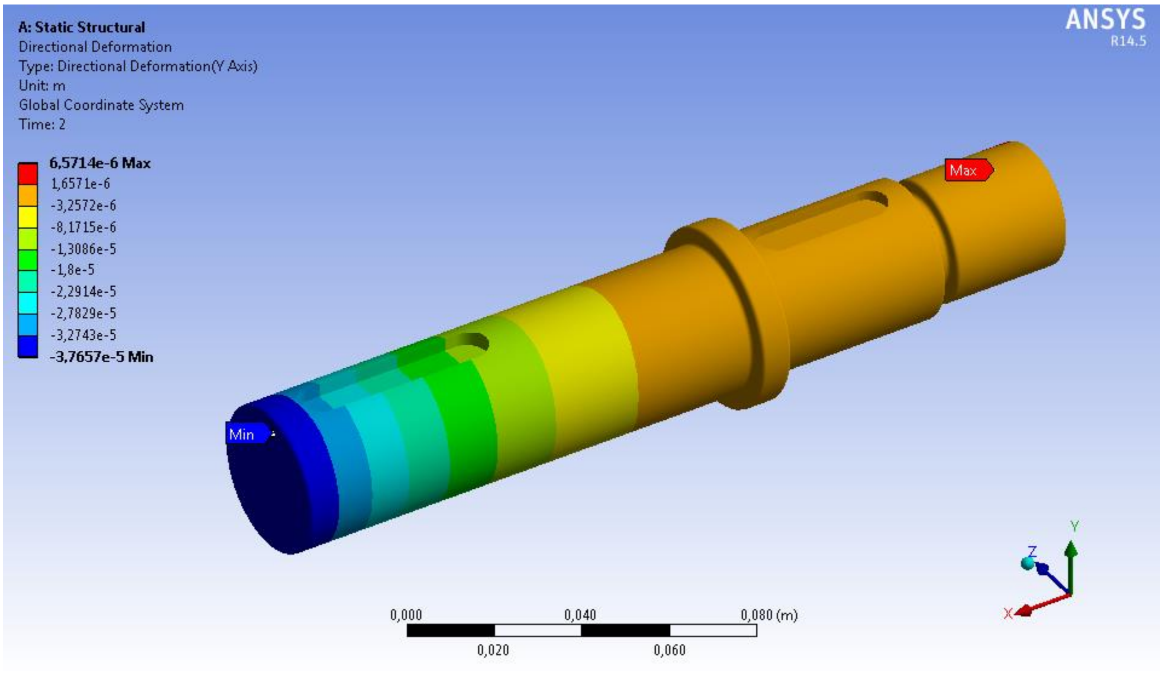
A: Static Structural
Directional Deformation
Type: Directional Deformation(Y Axis)
Unit: m
Global Coordinate System
Time: 2

ANSYS
R14.5
6,5714e-6 Max
1,6571e-6
-3,2572e-6
-8,1715e-6
-1,3086e-5
-1,8e-5
-2,2914e-5
-2,7829e-5
-3,2743e-5
-3,7657e-5 Min
Max
Min
0,000
0,040
0,080 (m)
0,020
0,060
Y
Z
X

Fig. 5.18 Directional deformation distribution of the pinion shaft

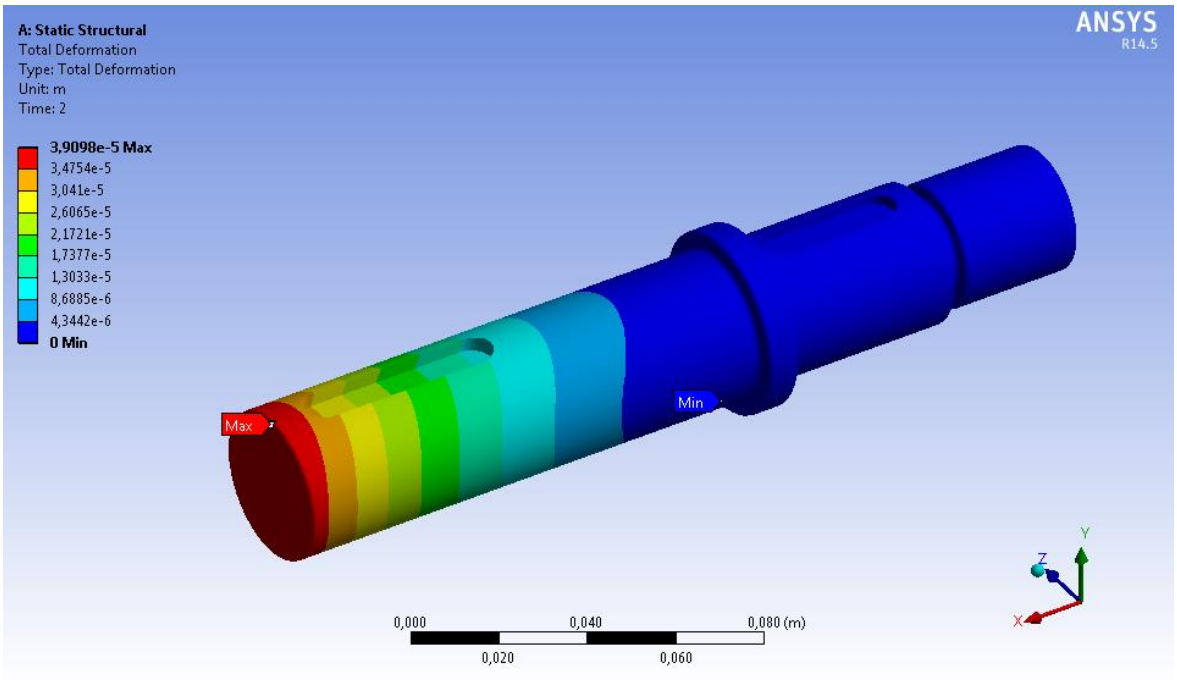
A: Static Structural
Total Deformation
Type: Total Deformation
Unit: m
Time: 2
3,9098e-5 Max
3,4754e-5
3,041e-5
2,6065e-5
2,1721e-5
1,7377e-5
1,3033e-5
8,6885e-6
4,3442e-6
0 Min
ANSYS
R14.5
Max
Min
0,000
0,040
0,080 (m)
0,020
0,060
Y
Z
X

Fig. 5.19 Total deformation distribution of the pinion shaft

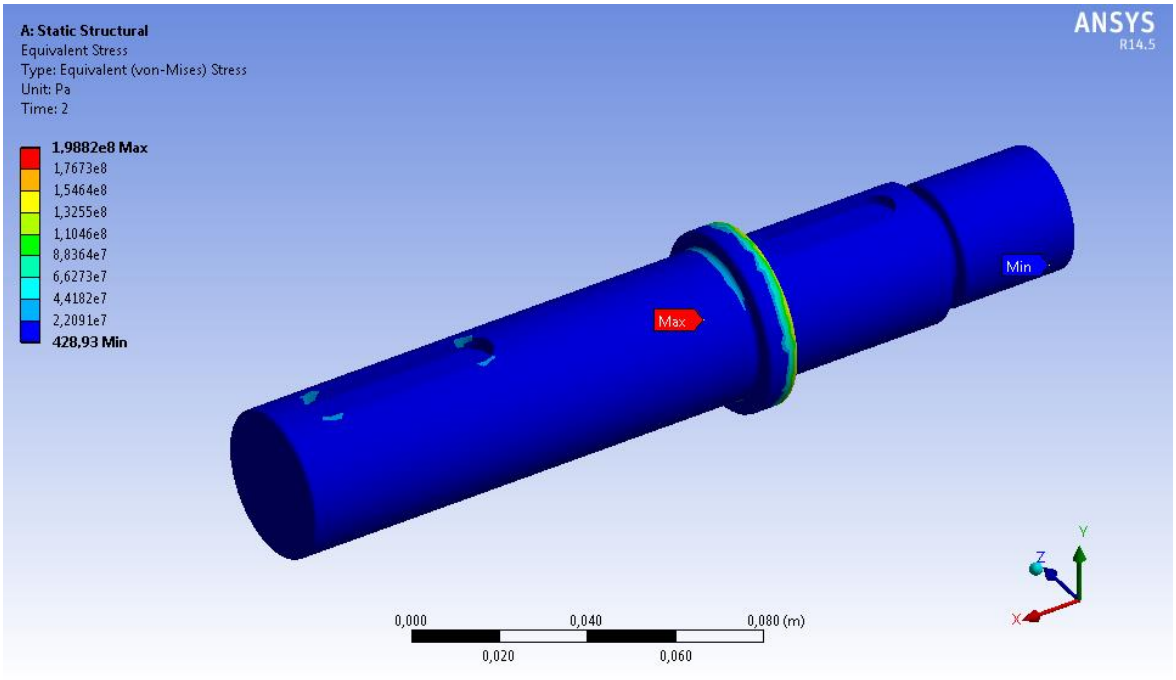
A: Static Structural
Equivalent Stress
Type: Equivalent (von-Mises) Stress
Unit: Pa
Time: 2
1,9882e8 Max
1,7673e8
1,5464e8
1,3255e8
1,1046e8
8,8364e7
6,6273e7
4,4182e7
2,2091e7
428,93 Min
ANSYS
R14.5
Max
Min
0,000
0,040
0,080 (m)
0,020
0,060
Y
Z
X

Fig. 5.20 Von Mises Stress distribution of the pinion shaft

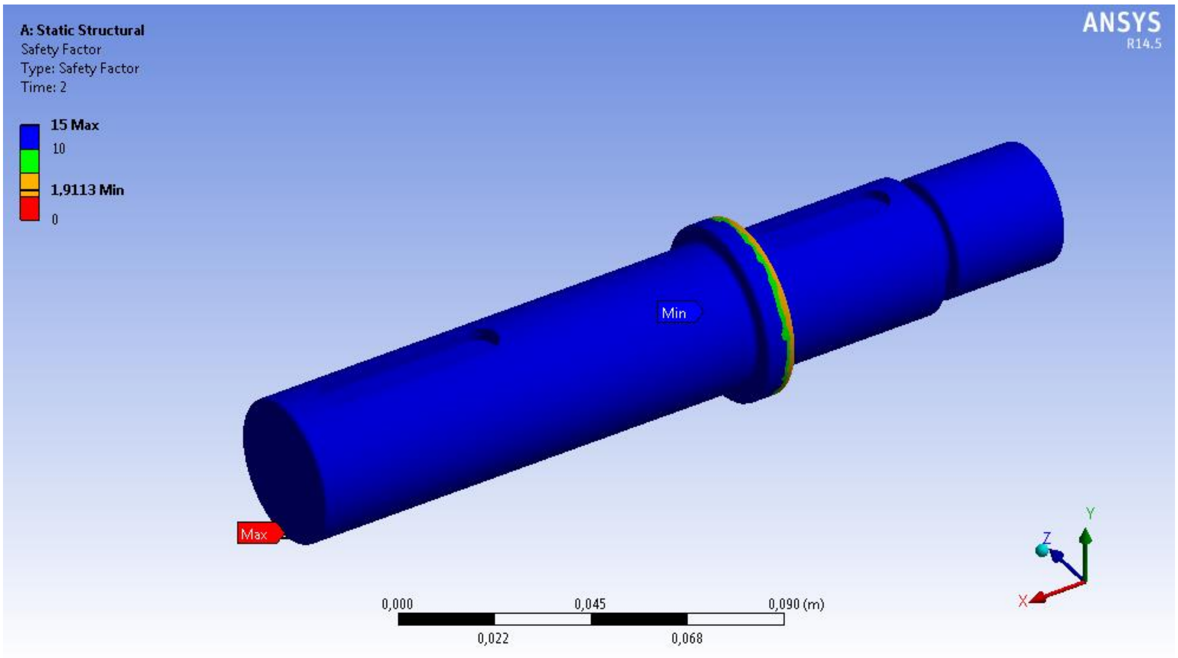
A: Static Structural
Safety Factor
Type: Safety Factor
Time: 2
15 Max
10
1,9113 Min
0
ANSYS
R14.5
Min
Max
0,000
0,045
0,090 (m)
0,022
0,068
Y
Z
X

Fig. 5.21 Safety factor of the pinion shaft

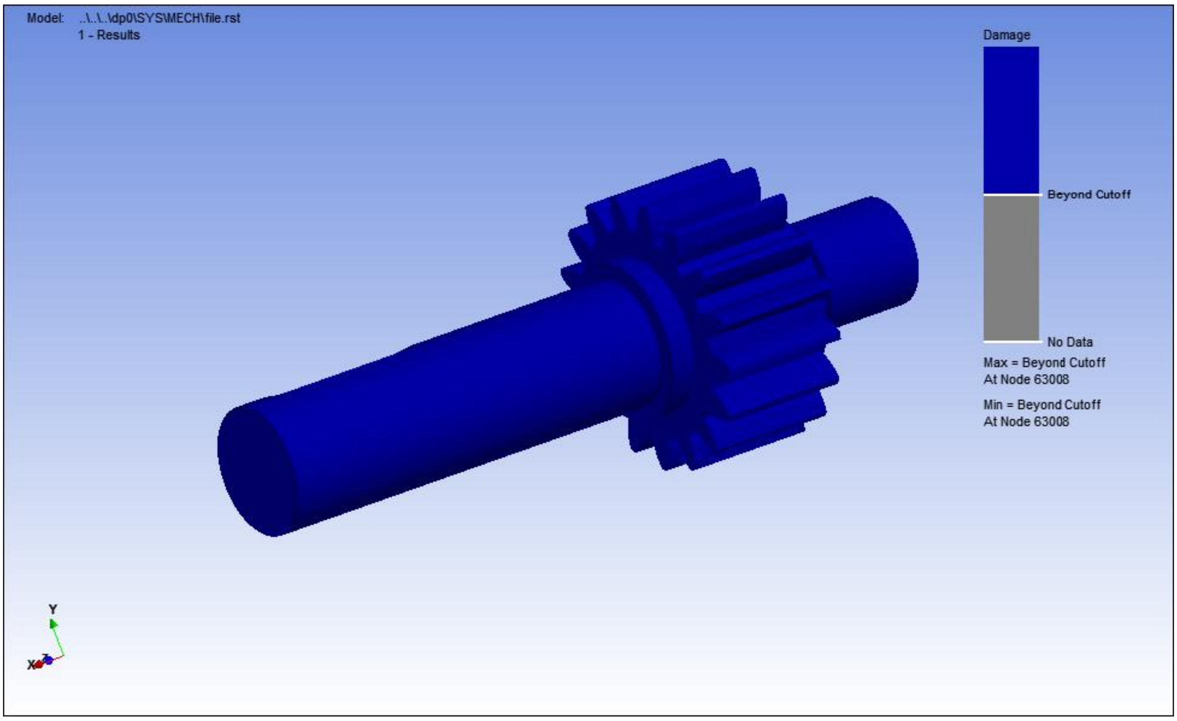
Model: ..\..\..\dp0\SYS\MECH\file.rst
1 - Results
Damage
Beyond Cutoff
No Data
Max = Beyond Cutoff
At Node 63008
Min = Beyond Cutoff
At Node 63008
Y
X
Z

Fig. 5.22 Damage distribution of the pinion shaft

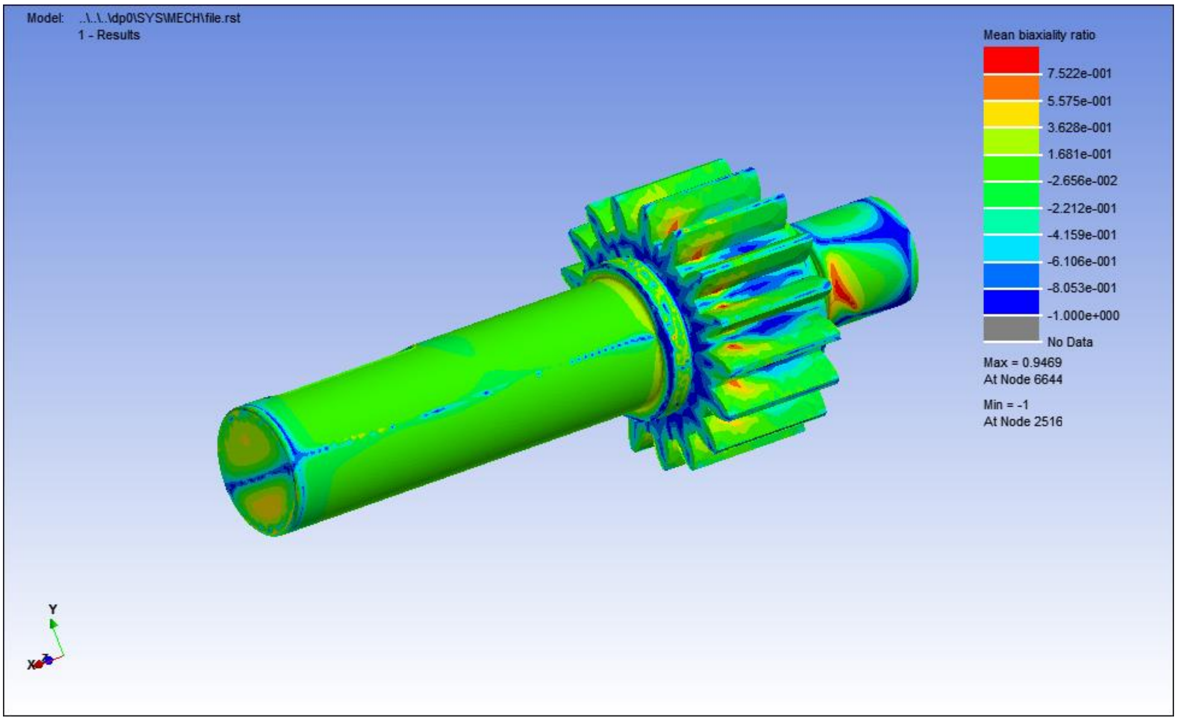
Model: ..\..\..\dp0\SYS\MECH\file.rst
1 - Results
Mean biaxiality ratio
7.522e-001
5.575e-001
3.628e-001
1.681e-001
-2.656e-002
-2.212e-001
-4.159e-001
-6.106e-001
-8.053e-001
-1.000e+000
No Data
Max = 0.9469
At Node 6644
Min = -1
At Node 2516
Y
X
Z

Fig. 5.23 Mean biaxiliaty ratio distribution of the pinion shaft

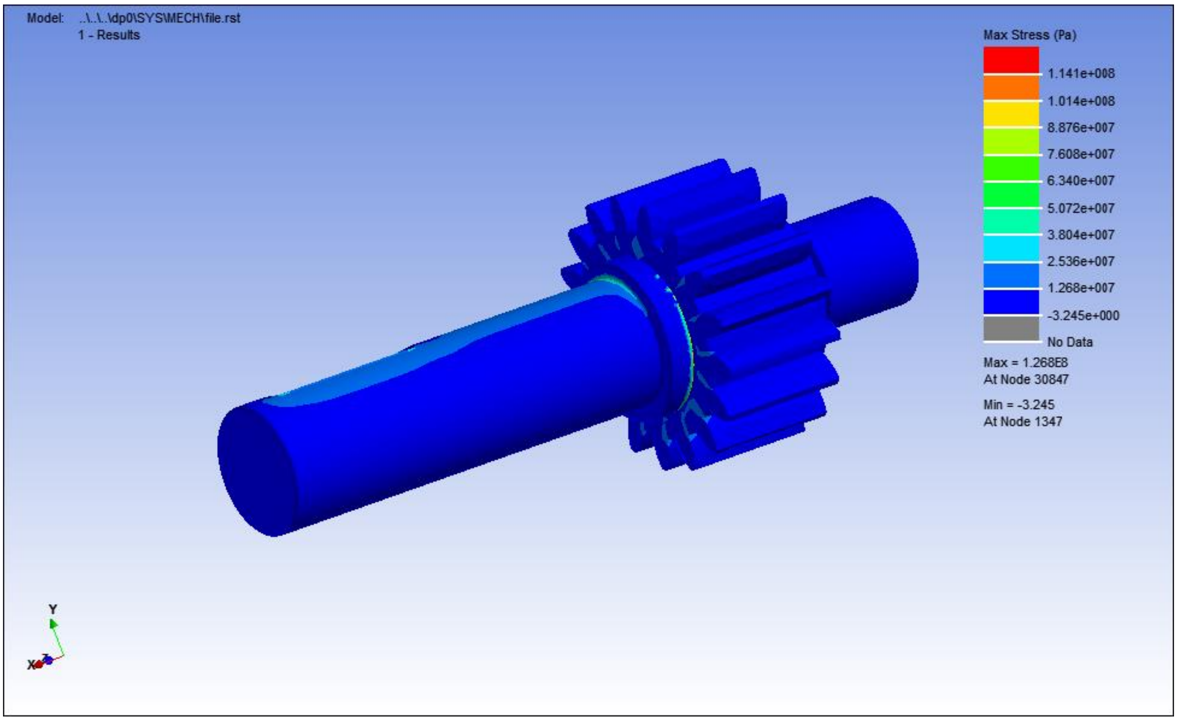
Model: ..\..\..\dp0\SYS\MECH\file.rst
1 - Results
Max Stress (Pa)
1.141e+008
1.014e+008
8.876e+007
7.608e+007
6.340e+007
5.072e+007
3.804e+007
2.536e+007
1.268e+007
-3.245e+000
No Data
Max = 1.268E8
At Node 30847
Min = -3.245
At Node 1347
Y
X
Z

Fig. 5.24 Max. stress distribution of the pinion shaft

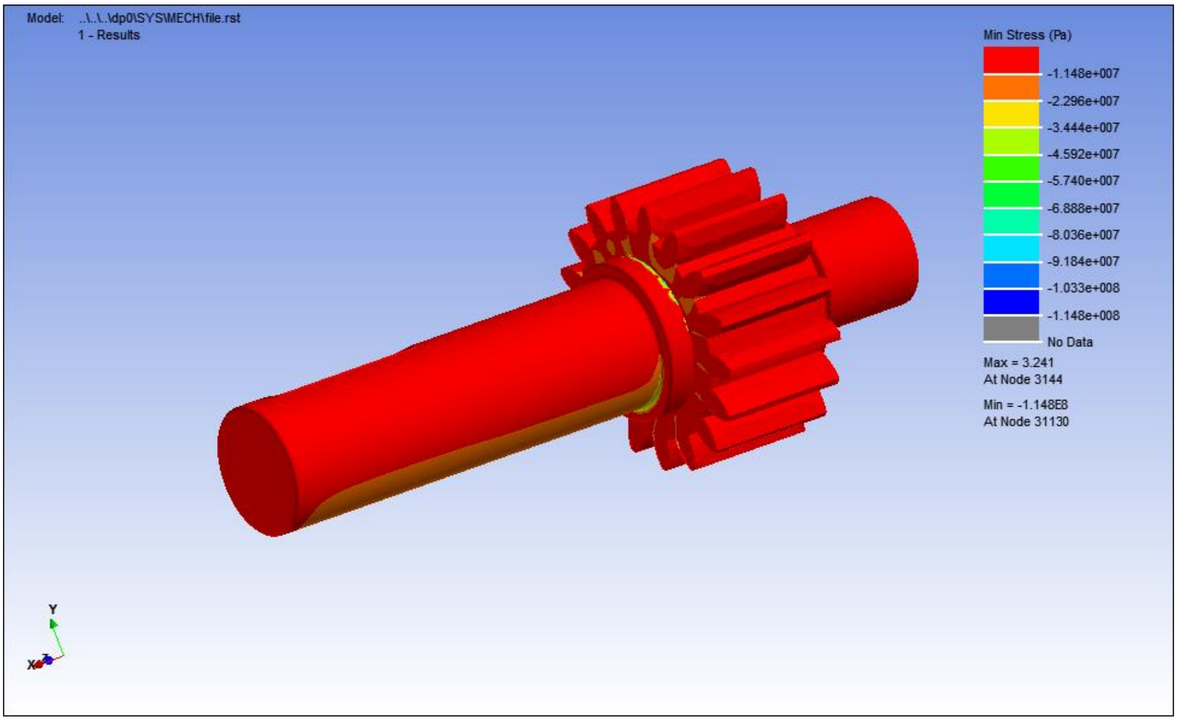
Model: ..\..\..\dp0\SYS\MECH\file.rst
1 - Results
Min Stress (Pa)
-1.148e+007
-2.296e+007
-3.444e+007
-4.592e+007
-5.740e+007
-6.888e+007
-8.036e+007
-9.184e+007
-1.033e+008
-1.148e+008
No Data
Max = 3.241
At Node 3144
Min = -1.148E8
At Node 31130
Y
X
Z

Fig. 5.25 Min. stress distribution of the pinion shaft

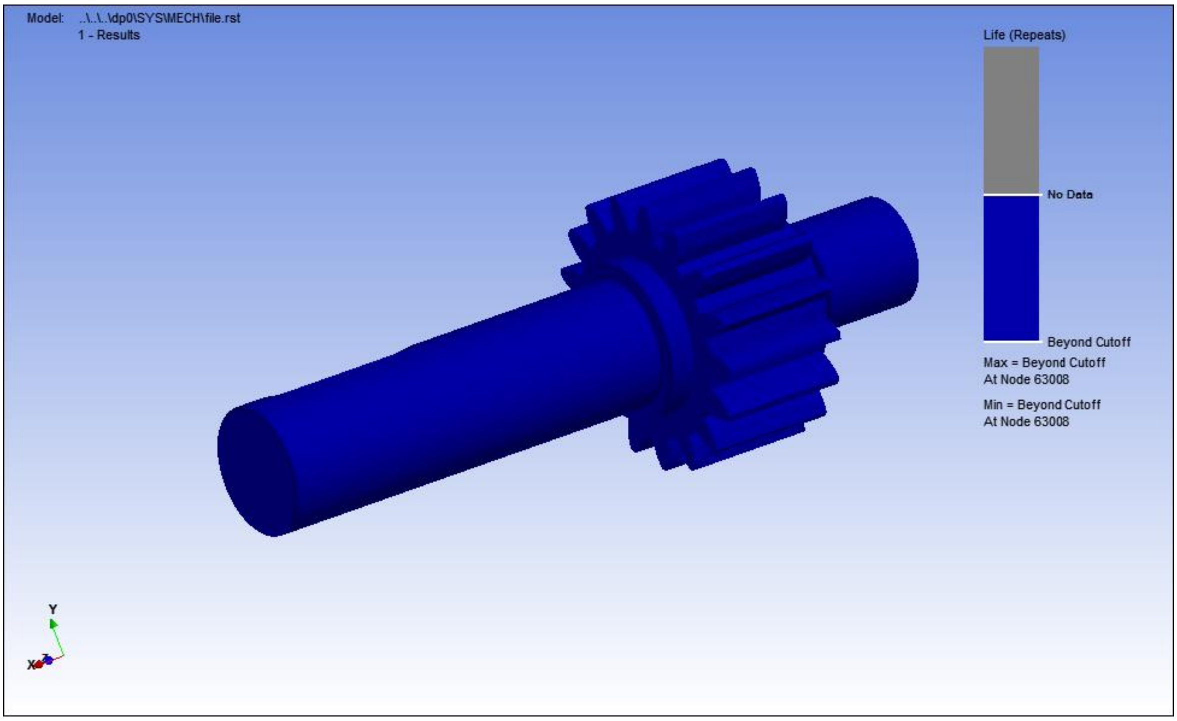
Model: ..\..\..\dp0\SYS\MECH\file.rst
1 - Results
Life (Repeats)
No Data
Beyond Cutoff
Max = Beyond Cutoff
At Node 63008
Min = Beyond Cutoff
At Node 63008
Y
X
Z

Fig. 5.26 Life of the pinion shaft

5.3 Conclusion

In this study, two shafts have been examined in terms of stress, deflection and fatigue by considering both the analytical shaft equations (Shaft Design, Shigley's Mechanical Enginnering Design, Richard G. Budynas – J. Keith Nisbett). and finite element modeling.

In the study of analytical design, firstly stress concentration factors at the critical regions of shafts have been found or calculated from tables, and secondly taking into consideration maximum torques and moments, the diameters of shafts have been estimated by using the DE-Goodman equation. The materials of shafts used in monorail crane design have been also chosen from the analytical equations.

In the study of fem design, the materials chosen by the results of analytical equations have been used and obtained the following results;

Deflections of both shafts satisfy the shaft design requirements suggested by in the book, Shigley's Mechanical Enginnering Design Richard G. Budynas – J. Keith Nisbett.

Von Mises stresses of the both type of shafts are convenient compared to shafts material yield strengths and the safety factors are good at the keyway and ring regions.

And finally, fatigue results of both shafts in terms of damage and life distributions are beyond cut off which means that both have infinite life.

Appendix (1) Contact results of wheel and rail in terms of different angles

For $Ø_0 = 30^{\circ}$ rail type section results

Vertical Diplacement

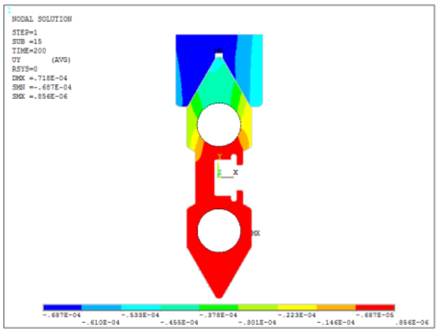

Total Displacement Sum

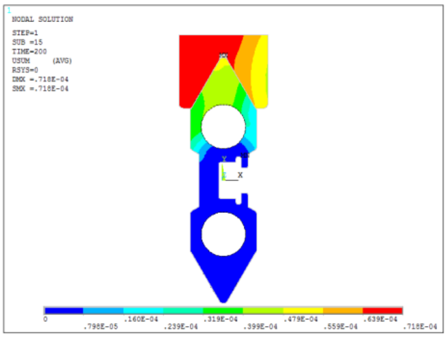

Von Mises Stress

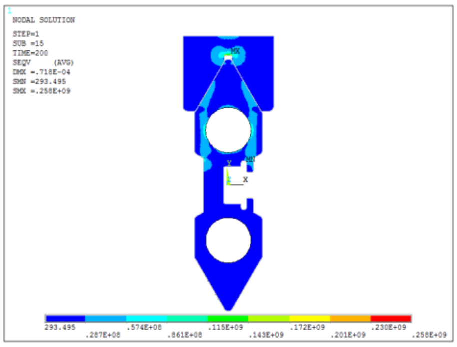

Contact Pressure

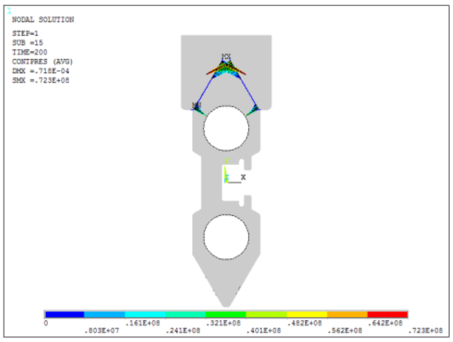

Contact Frictional Stress

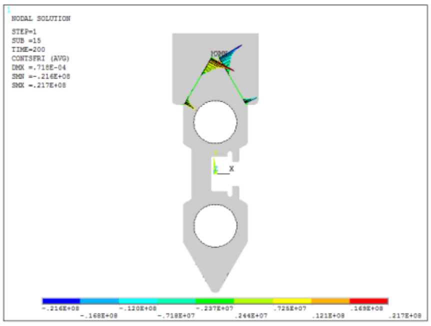

Contact Total Stress

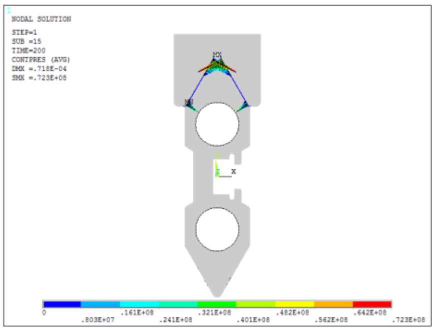

Contact Status

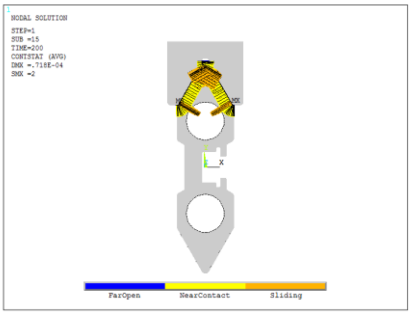

Contact Penetration

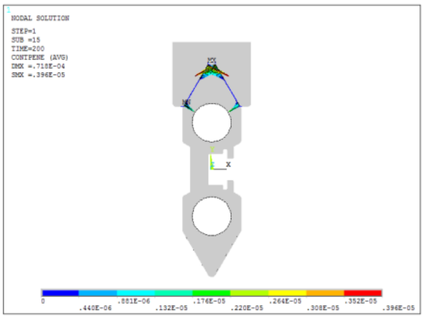

For $Ø_0 = 32{,}5^{\circ}$ rail type section results

Vertical Diplacement

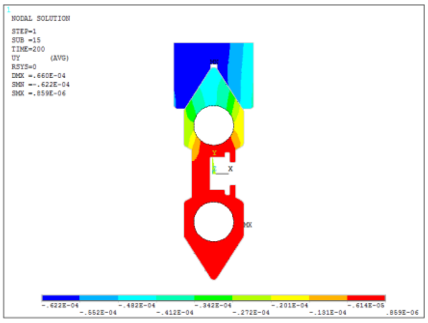

Total Displacement Sum

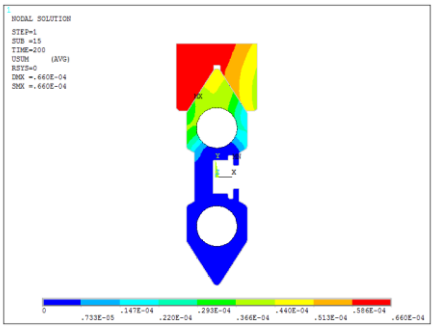

Von Mises Stress

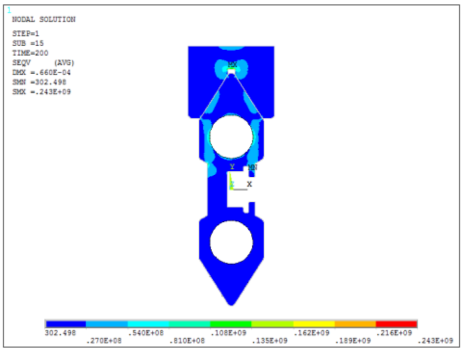

Contact Pressure

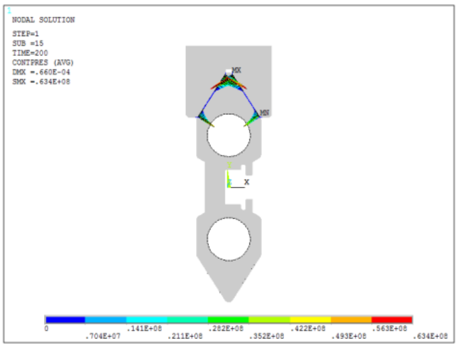

Contact Frictional Stress

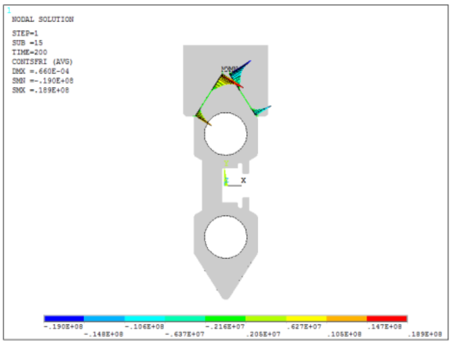

Contact Total Stress

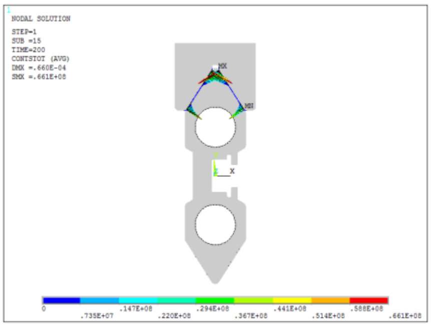

Contact Status

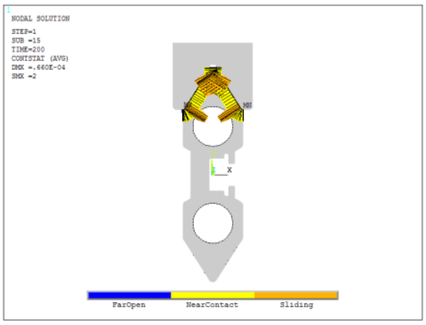

Contact Penetration

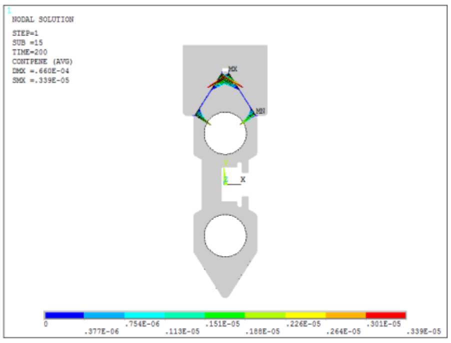

For $Ø_0 = 35^{\circ}$ rail type section results

Vertical Diplacement

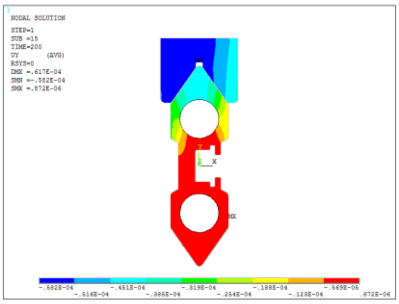

Total Displacement Sum

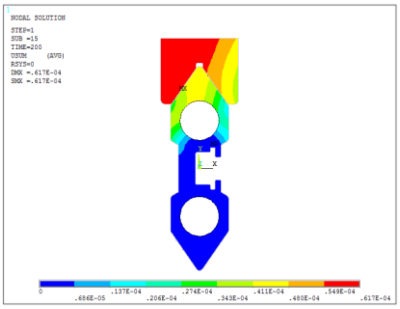

Von Mises Stress

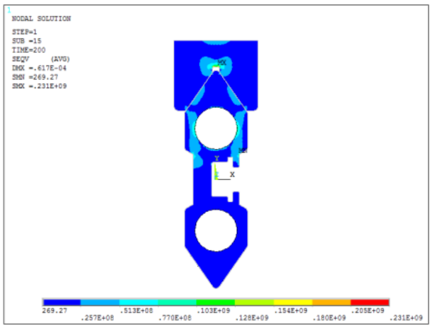

Contact Pressure

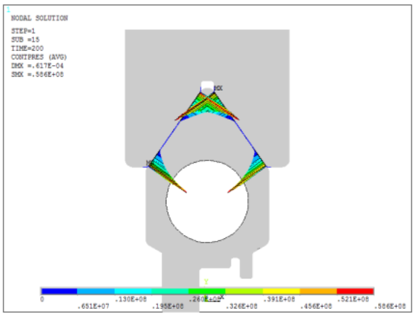

Contact Frictional Stress

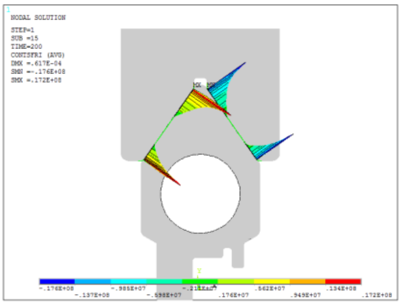

Contact Total Stress

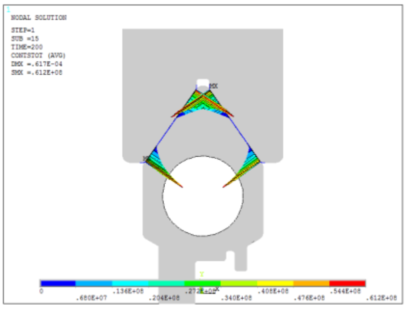

Contact Status

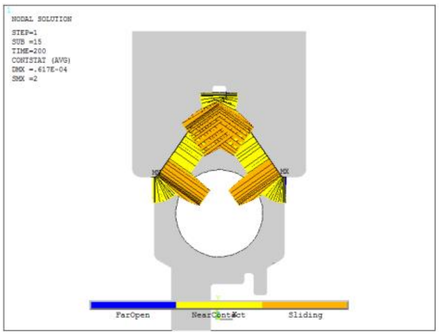

Contact Penetration

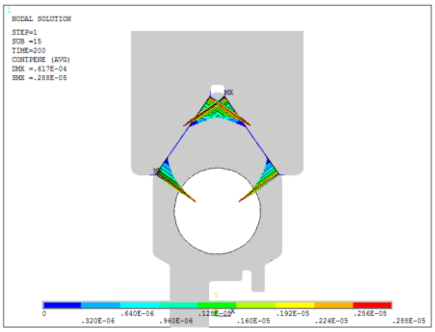

For $Ø_0$ = 37,5° rail type section results

Vertical Diplacement

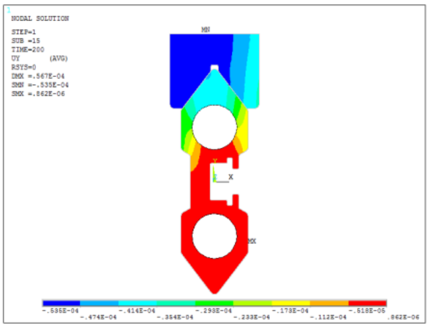

Total Displacement Sum

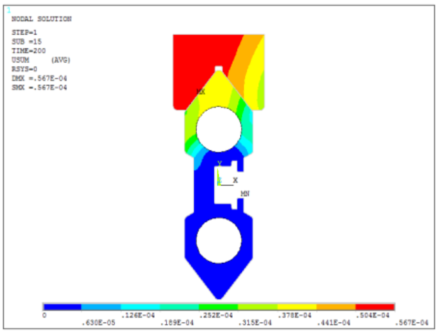

Von Mises Stress

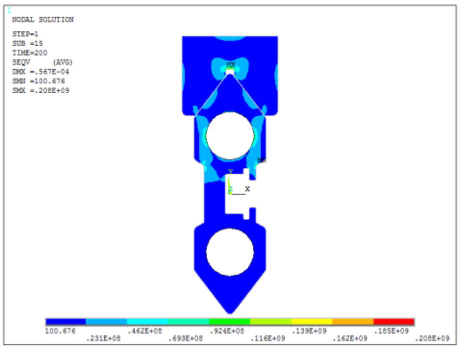

Contact Pressure

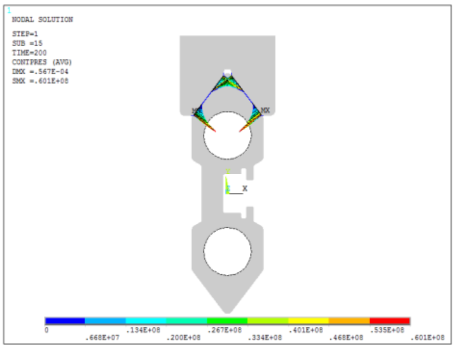

Contact Frictional Stress

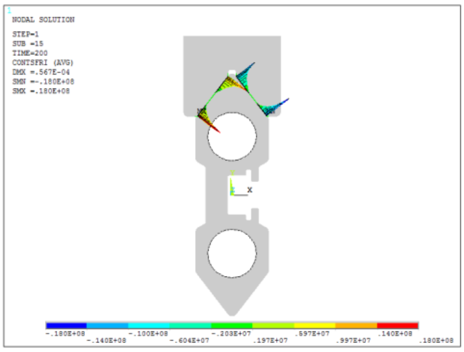

Contact Total Stress

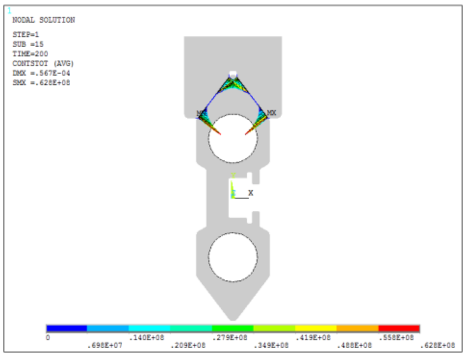

Contact Status

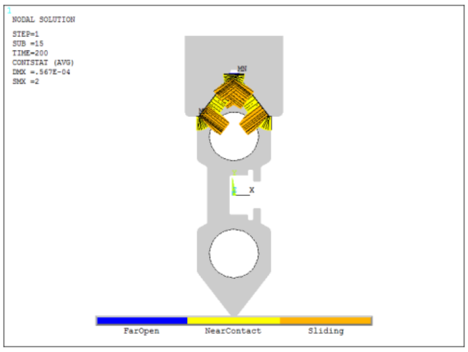

Contact Penetration

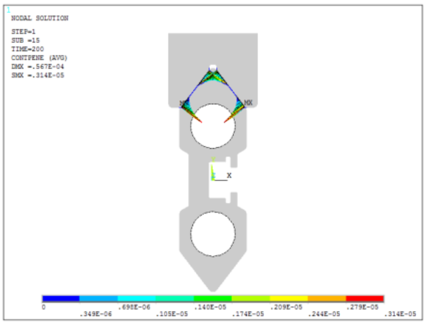

For $\O_0 = 40^{\circ}$ rail type section results

Vertical Diplacement

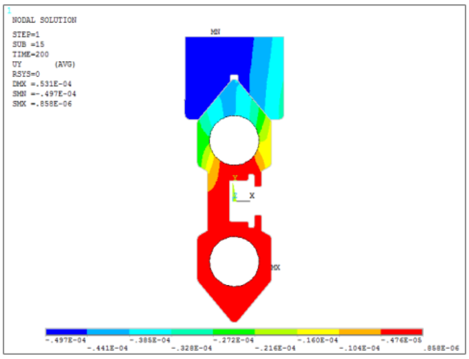

Total Displacement Sum

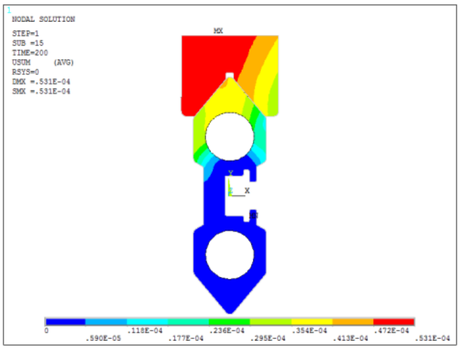

Von Mises Stress

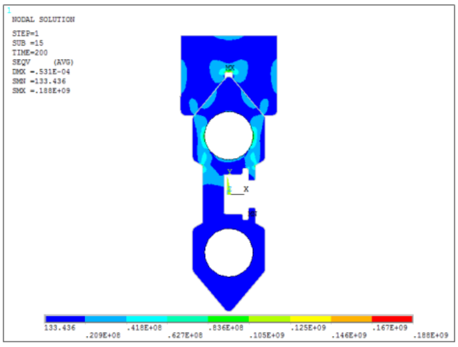

Contact Pressure

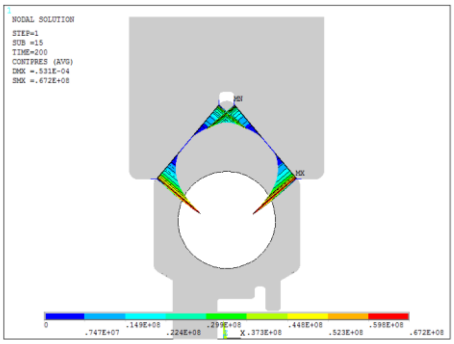

Contact Frictional Stress

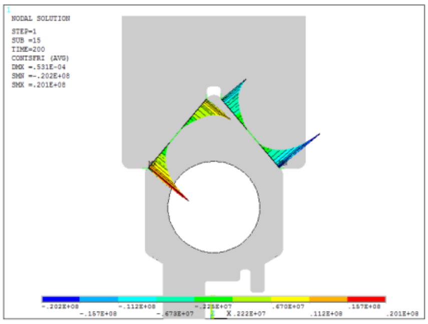

Contact Total Stress

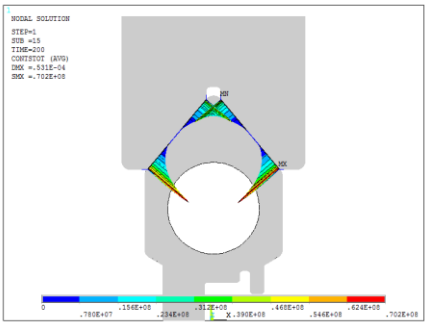

Contact Status

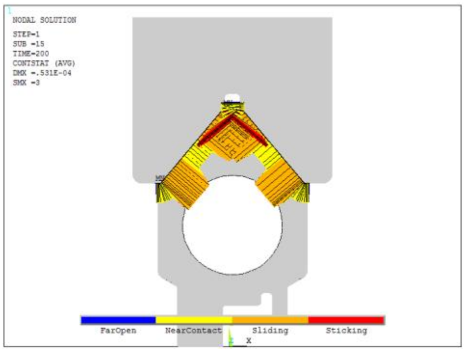

Contact Penetration

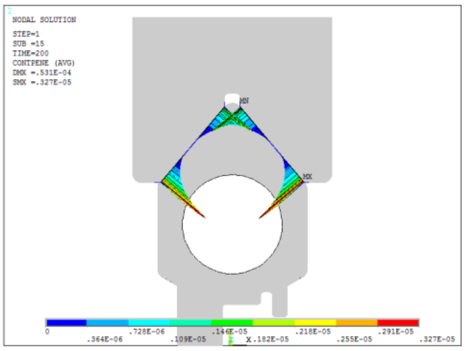

For $Ø_0 = 42,5^\circ$ rail type section results

Vertical Diplacement

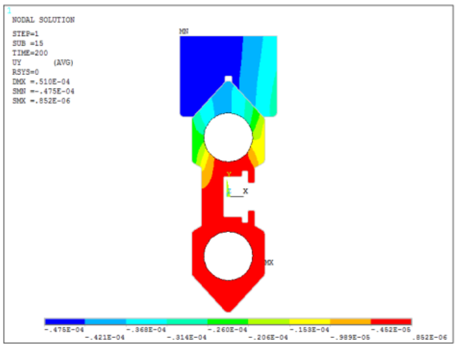

Total Displacement Sum

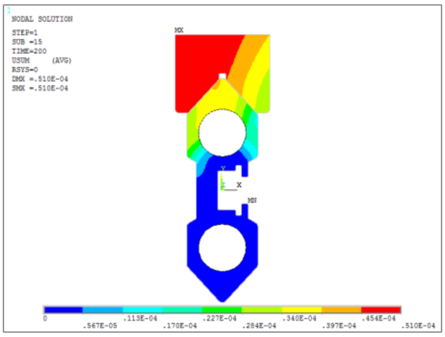

Von Mises Stress

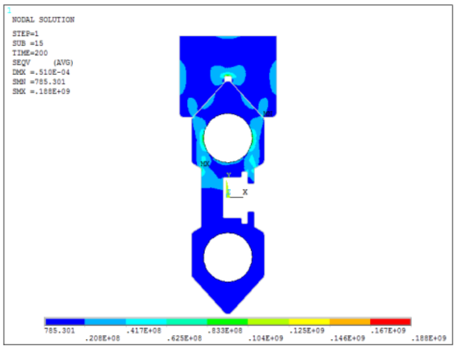

Contact Pressure

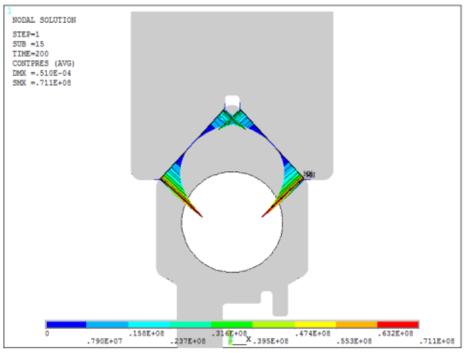

Contact Frictional Stress

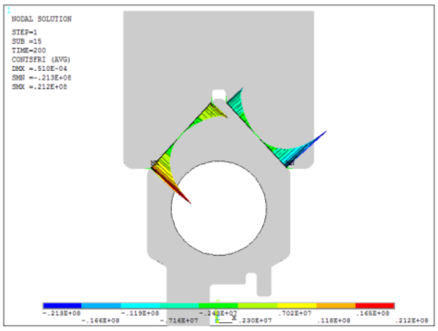

Contact Total Stress

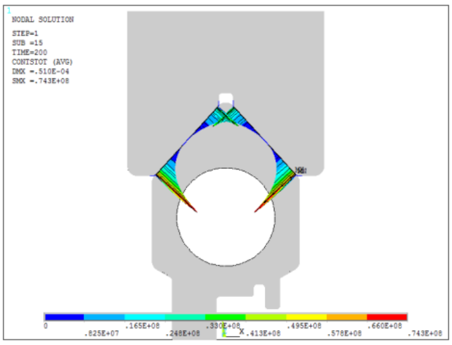

Contact Status

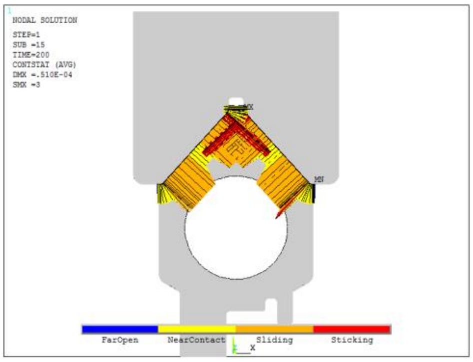

Contact Penetration

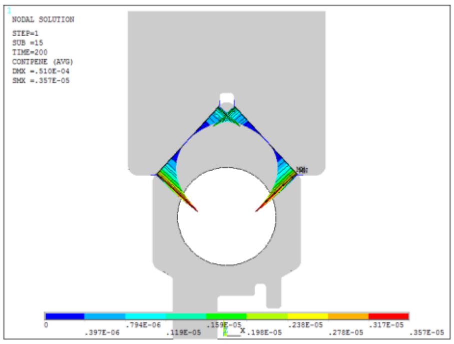

For $\O_0 = 45^{\circ}$ rail type section results

Vertical Diplacement

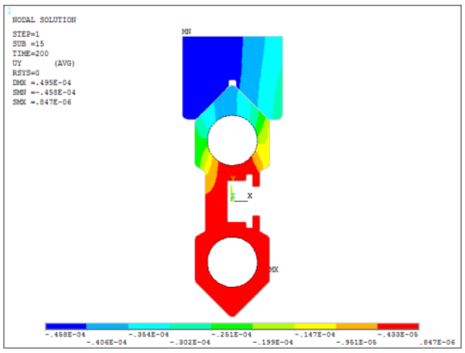
NODAL SOLUTION
STEP=1
SUB =15
TIME=200
UY (AVG)
RSYS=0
DMX =.495E-04
SMN =-.458E-04
SMX =.847E-06
MN
MX
-.458E-04
-.406E-04
-.354E-04
-.302E-04
-.251E-04
-.199E-04
-.147E-04
-.951E-05
-.433E-05
.847E-06

Total Displacement Sum

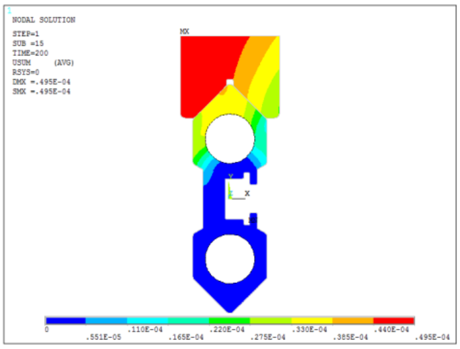
NODAL SOLUTION
STEP=1
SUB =15
TIME=200
USUM (AVG)
RSYS=0
DMX =.495E-04
SMX =.495E-04
MX
0
.551E-05
.110E-04
.165E-04
.220E-04
.275E-04
.330E-04
.385E-04
.440E-04
.495E-04

Von Mises Stress

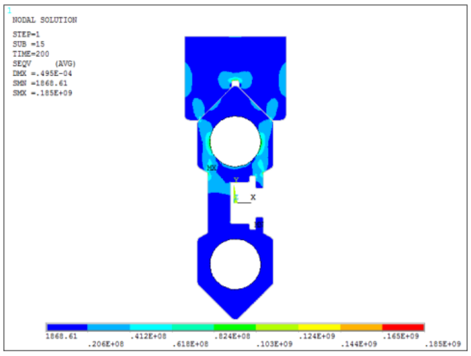
NODAL SOLUTION
STEP=1
SUB =15
TIME=200
SEQV (AVG)
DMX =.495E-04
SMN =1868.61
SMX =.185E+09
1868.61
.206E+08
.412E+08
.618E+08
.824E+08
.103E+09
.124E+09
.144E+09
.165E+09
.185E+09

Contact Pressure

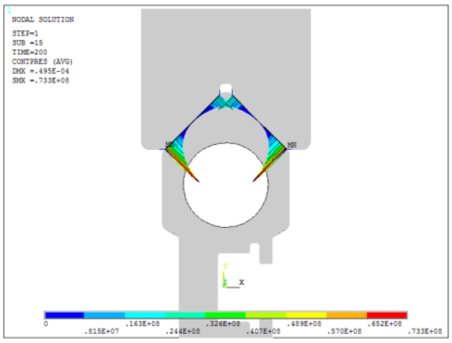
NODAL SOLUTION
STEP=1
SUB =15
TIME=200
CONTPRES (AVG)
DMX =.495E-04
SMX =.733E+08
MN
0
.815E+07
.163E+08
.244E+08
.326E+08
.407E+08
.489E+08
.570E+08
.652E+08
.733E+08

Contact Frictional Stress

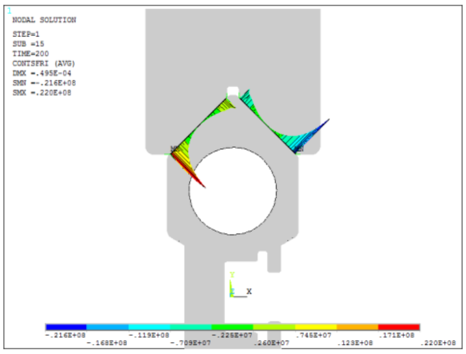
NODAL SOLUTION
STEP=1
SUB =15
TIME=200
CONTSFRI (AVG)
DMX =.495E-04
SMN =-.216E+08
SMX =.220E+08
-.216E+08
-.168E+08
-.119E+08
-.709E+07
-.225E+07
.240E+07
.745E+07
.123E+08
.171E+08
.220E+08

Contact Total Stress

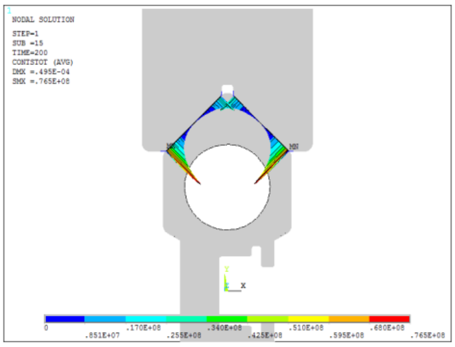
NODAL SOLUTION
STEP=1
SUB =15
TIME=200
CONTSTOT (AVG)
DMX =.495E-04
SMX =.765E+08
MN
0
.851E+07
.170E+08
.255E+08
.340E+08
.425E+08
.510E+08
.595E+08
.680E+08
.765E+08

Contact Status

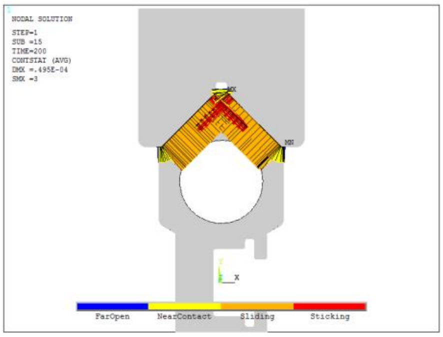
NODAL SOLUTION
STEP=1
SUB =15
TIME=200
CONTSTAT (AVG)
DMX =.495E-04
SMX =3
MX
MN
FarOpen
NearContact
Sliding
Sticking

Contact Penetration

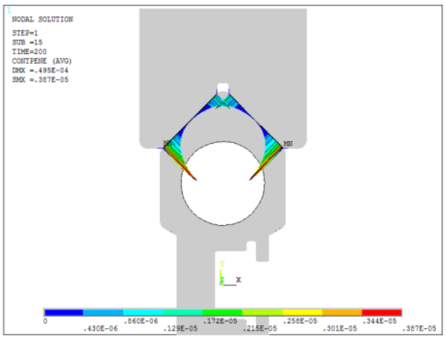
NODAL SOLUTION
STEP=1
SUB =15
TIME=200
CONTPENE (AVG)
DMX =.495E-04
SMX =.387E-05
MN
0
.430E-06
.860E-06
.129E-05
.172E-05
.215E-05
.258E-05
.301E-05
.344E-05
.387E-05

For $Ø_0$ = 47,5° rail type section results

Vertical Diplacement

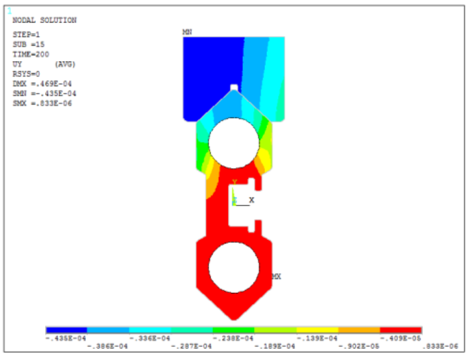

Total Displacement Sum

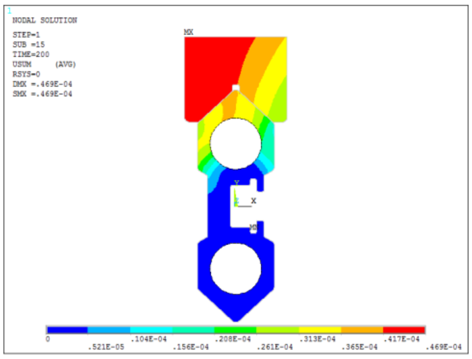

Von Mises Stress

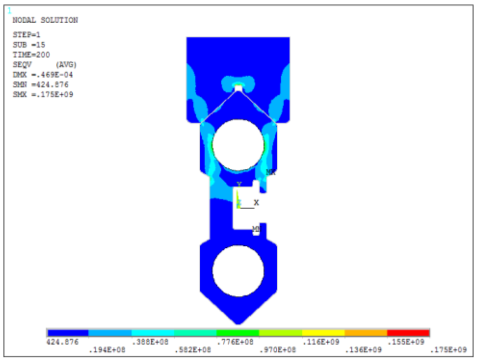

Contact Pressure

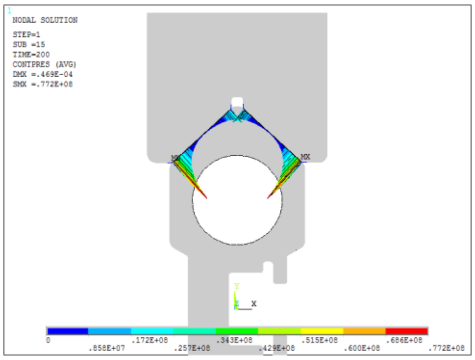

Contact Frictional Stress

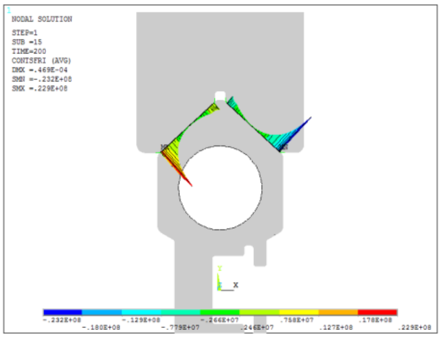

Contact Total Stress

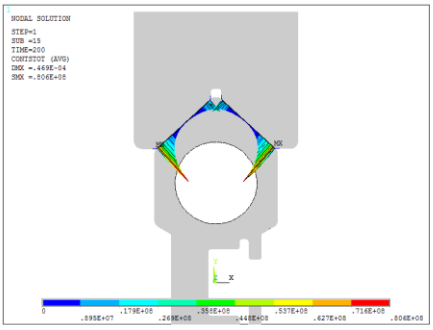

Contact Status

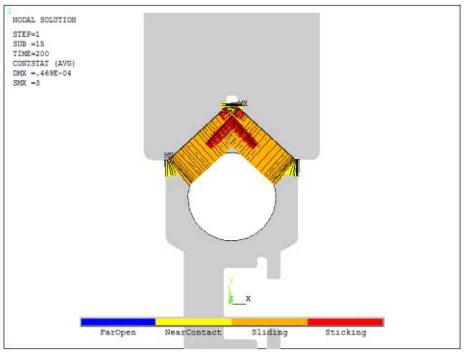

Contact Penetration

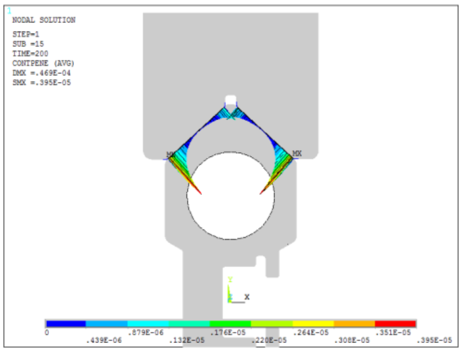

For $Ø_0 = 50^{\circ}$ rail type section results

Vertical Diplacement

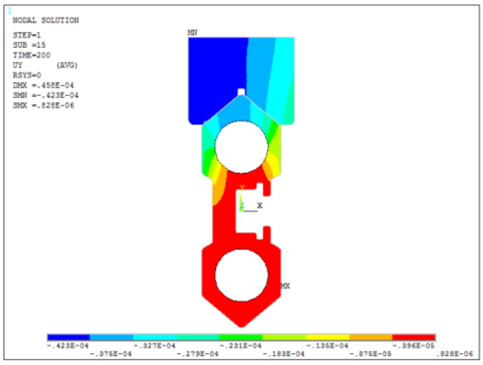
1
NODAL SOLUTION
STEP=1
SUB =15
TIME=200
UY (AVG)
RSYS=0
DMX =.458E-04
SMN =-.423E-04
SMX =.828E-06
MN
MX
Y
Z
X
-.423E-04
-.376E-04
-.327E-04
-.279E-04
-.231E-04
-.183E-04
-.135E-04
-.876E-05
-.396E-05
.828E-06

Total Displacement Sum

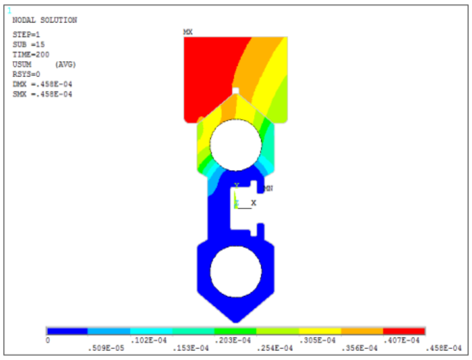
1
NODAL SOLUTION
STEP=1
SUB =15
TIME=200
USUM (AVG)
RSYS=0
DMX =.458E-04
SMX =.458E-04
MX
MN
Y
Z
X
0
.509E-05
.102E-04
.153E-04
.203E-04
.254E-04
.305E-04
.356E-04
.407E-04
.458E-04

Von Mises Stress

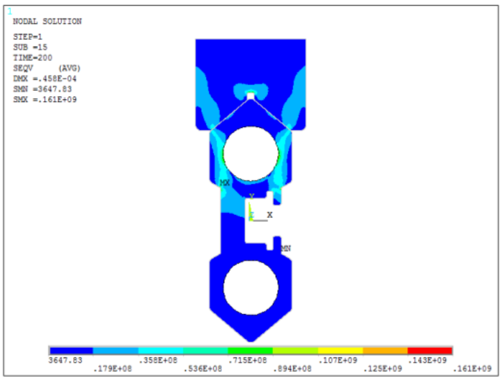
1
NODAL SOLUTION
STEP=1
SUB =15
TIME=200
SEQV (AVG)
DMX =.458E-04
SMN =3647.83
SMX =.161E+09
MX
MN
Y
Z
X
3647.83
.179E+08
.358E+08
.536E+08
.715E+08
.894E+08
.107E+09
.125E+09
.143E+09
.161E+09

Contact Pressure

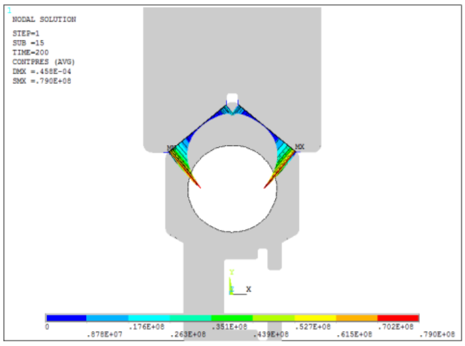
1
NODAL SOLUTION
STEP=1
SUB =15
TIME=200
CONTPRES (AVG)
DMX =.458E-04
SMX =.790E+08
MX
Y
Z
X
0
.878E+07
.176E+08
.263E+08
.351E+08
.439E+08
.527E+08
.615E+08
.702E+08
.790E+08

Contact Frictional Stress

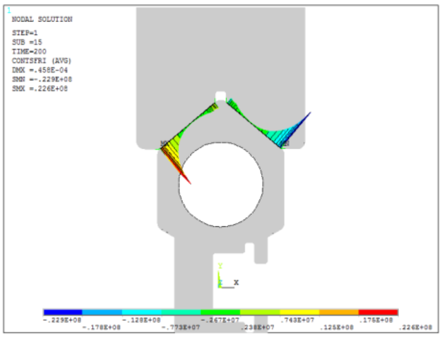
1
NODAL SOLUTION
STEP=1
SUB =15
TIME=200
CONTSFRI (AVG)
DMX =.458E-04
SMN =-.229E+08
SMX =.226E+08
Y
Z
X
-.229E+08
-.178E+08
-.128E+08
-.773E+07
-.267E+07
.238E+07
.743E+07
.125E+08
.176E+08
.226E+08

Contact Total Stress

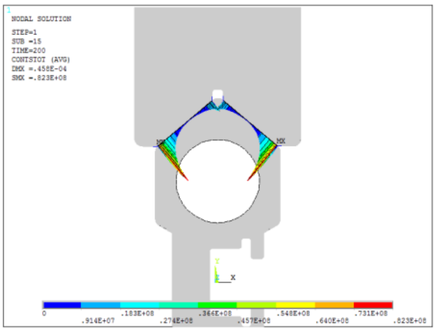
1
NODAL SOLUTION
STEP=1
SUB =15
TIME=200
CONTSTOT (AVG)
DMX =.458E-04
SMX =.823E+08
MX
Y
Z
X
0
.914E+07
.183E+08
.274E+08
.366E+08
.457E+08
.548E+08
.640E+08
.731E+08
.823E+08

Contact Status

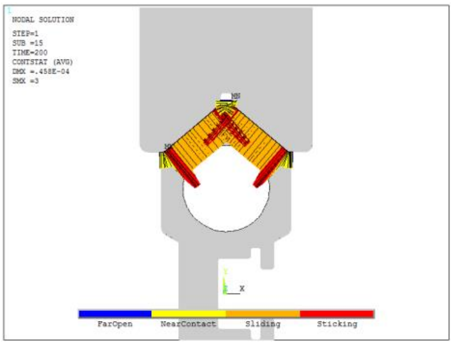
1
NODAL SOLUTION
STEP=1
SUB =15
TIME=200
CONTSTAT (AVG)
DMX =.458E-04
SMX =3
MN
Y
Z
X
FarOpen
NearContact
Sliding
Sticking

Contact Penetration

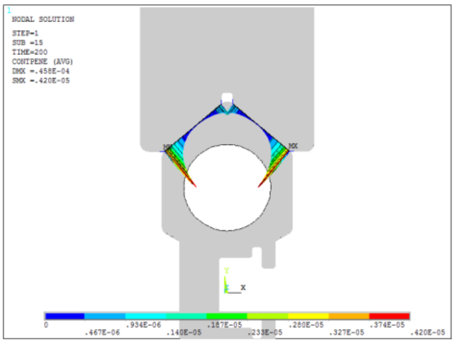
1
NODAL SOLUTION
STEP=1
SUB =15
TIME=200
CONTPENE (AVG)
DMX =.458E-04
SMX =.420E-05
MX
Y
Z
X
0
.467E-06
.934E-06
.140E-05
.187E-05
.233E-05
.280E-05
.327E-05
.374E-05
.420E-05

For $Ø_0 = 52,5^{\circ}$ rail type section results

Vertical Diplacement

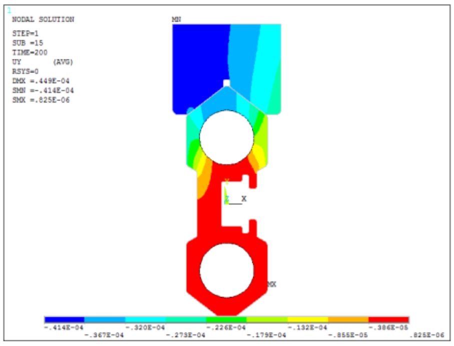

Total Displacement Sum

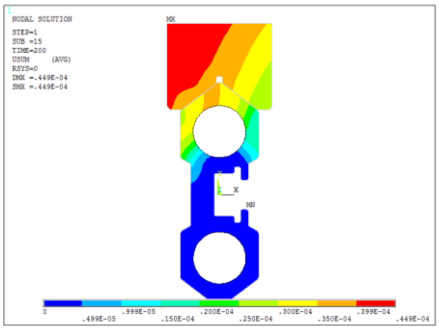

Von Mises Stress

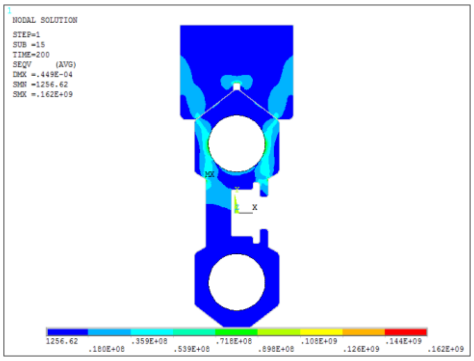

Contact Pressure

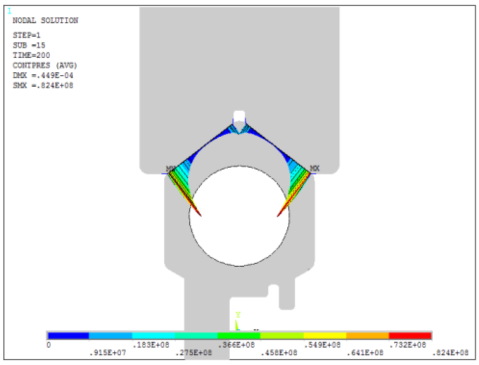

Contact Frictional Stress

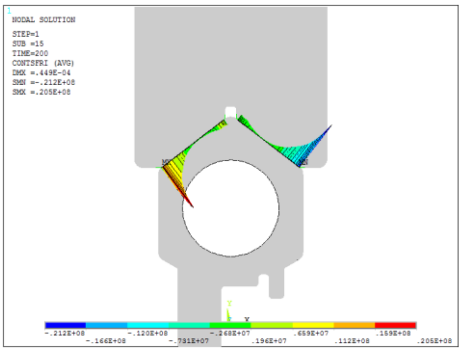

Contact Total Stress

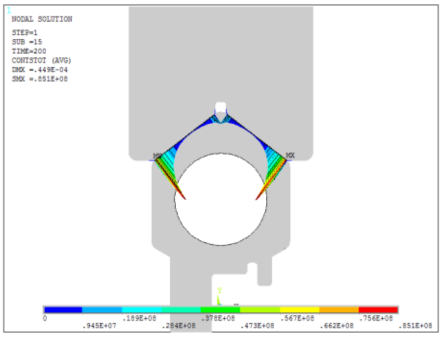

Contact Status

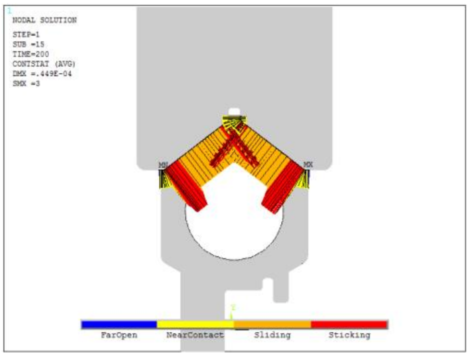

Contact Penetration

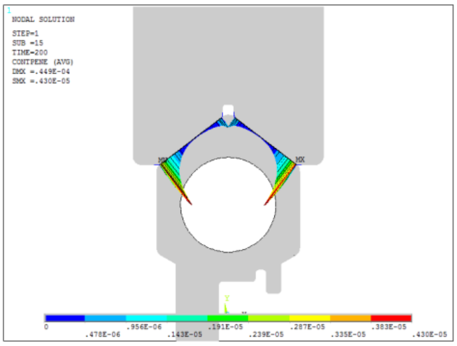

For $Ø_0 = 55^{\circ}$ rail type section results

Vertical Diplacement

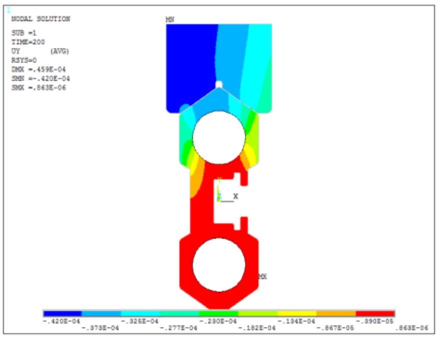
1
NODAL SOLUTION
SUB =1
TIME=200
UY (AVG)
RSYS=0
DMX =.459E-04
SMN =-.420E-04
SMX =.863E-06
MN
MX
Y
Z
X
-.420E-04
-.373E-04
-.325E-04
-.277E-04
-.230E-04
-.182E-04
-.134E-04
-.867E-05
-.390E-05
.863E-06

Total Displacement Sum

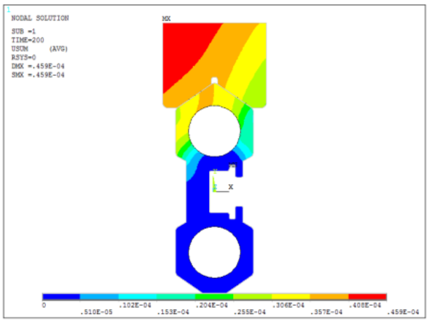
1
NODAL SOLUTION
SUB =1
TIME=200
USUM (AVG)
RSYS=0
DMX =.459E-04
SMX =.459E-04
MX
Y
Z
X
0
.510E-05
.102E-04
.153E-04
.204E-04
.255E-04
.306E-04
.357E-04
.408E-04
.459E-04

Von Mises Stress

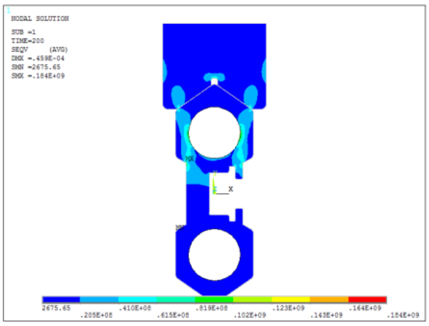
1
NODAL SOLUTION
SUB =1
TIME=200
SEQV (AVG)
DMX =.459E-04
SMN =2675.65
SMX =.184E+09
MX
MN
Y
Z
X
2675.65
.205E+08
.410E+08
.615E+08
.819E+08
.102E+09
.123E+09
.143E+09
.164E+09
.184E+09

Contact Pressure

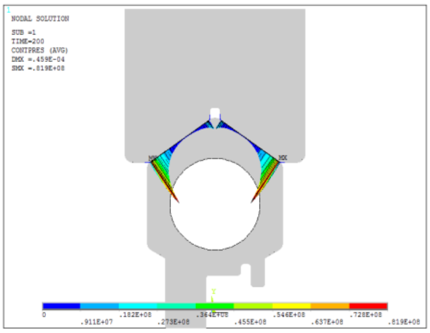
1
NODAL SOLUTION
SUB =1
TIME=200
CONTPRES (AVG)
DMX =.459E-04
SMX =.819E+08
MN
MX
Y
0
.911E+07
.182E+08
.273E+08
.364E+08
.455E+08
.546E+08
.637E+08
.728E+08
.819E+08

Contact Frictional Stress

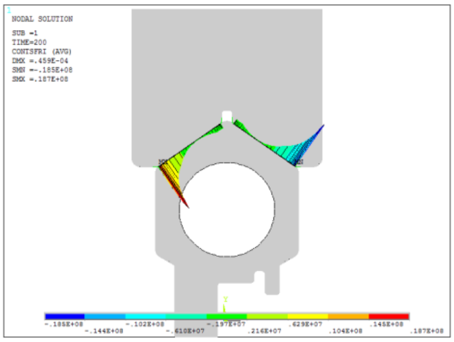
1
NODAL SOLUTION
SUB =1
TIME=200
CONTSFRI (AVG)
DMX =.459E-04
SMN =-.185E+08
SMX =.187E+08
MX
MN
Y
-.185E+08
-.144E+08
-.102E+08
-.610E+07
-.197E+07
.216E+07
.629E+07
.104E+08
.145E+08
.187E+08

Contact Total Stress

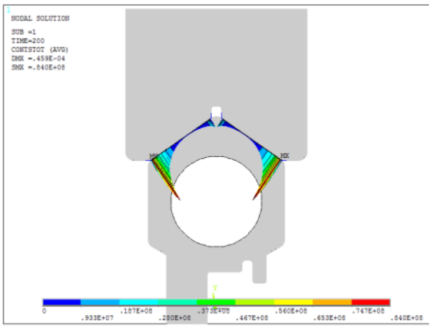
1
NODAL SOLUTION
SUB =1
TIME=200
CONTSTOT (AVG)
DMX =.459E-04
SMX =.840E+08
MN
MX
Y
0
.933E+07
.187E+08
.280E+08
.373E+08
.467E+08
.560E+08
.653E+08
.747E+08
.840E+08

Contact Status

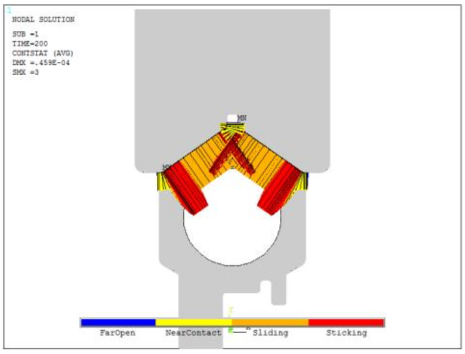
1
NODAL SOLUTION
SUB =1
TIME=200
CONTSTAT (AVG)
DMX =.459E-04
SMX =3
MN
Y
FarOpen
NearContact
Sliding
Sticking

Contact Penetration

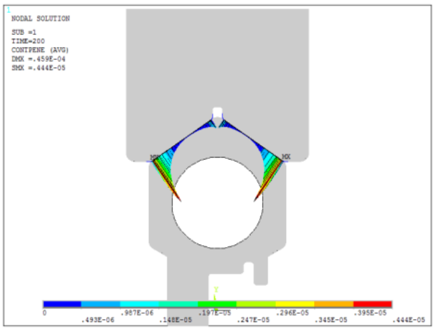
1
NODAL SOLUTION
SUB =1
TIME=200
CONTPENE (AVG)
DMX =.459E-04
SMX =.444E-05
MN
MX
Y
0
.493E-06
.987E-06
.148E-05
.197E-05
.247E-05
.296E-05
.345E-05
.395E-05
.444E-05

For $Ø_0 = 57,5^{\circ}$ rail type section results

Vertical Diplacement

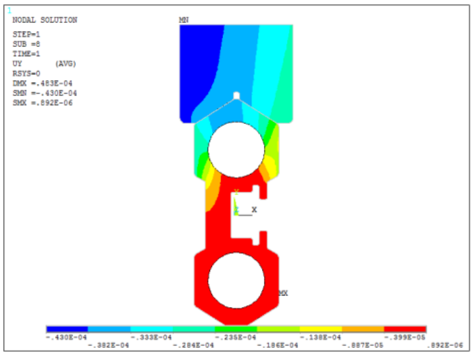

Total Displacement Sum

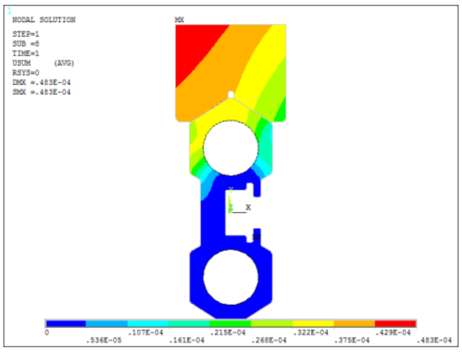

Von Mises Stress

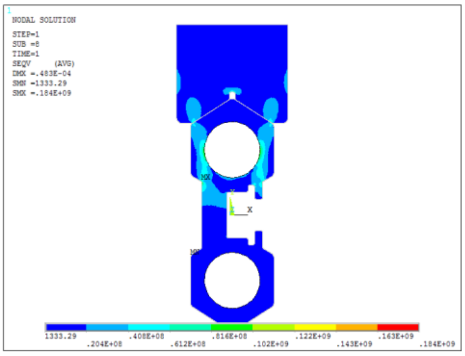

Contact Pressure

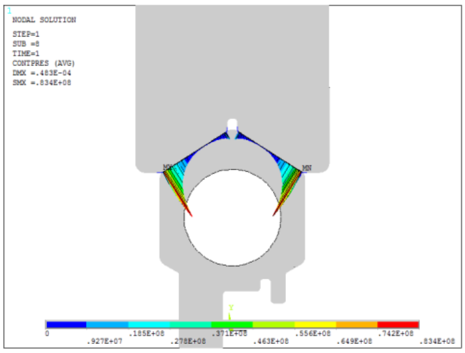

Ç

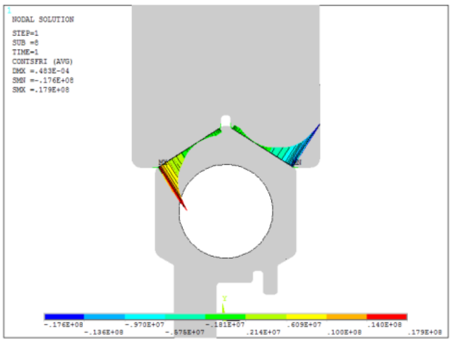

Contact Total Stress

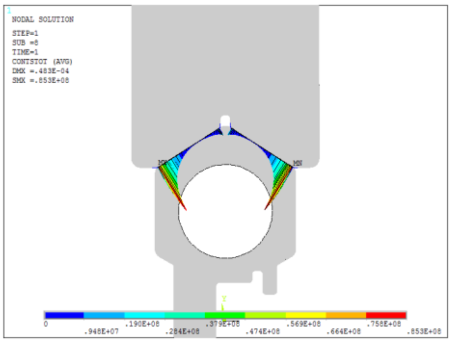

Contact Status

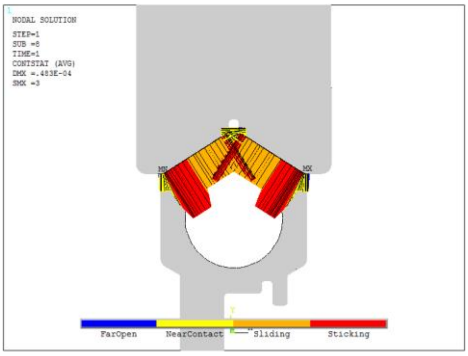

Contact Penetration

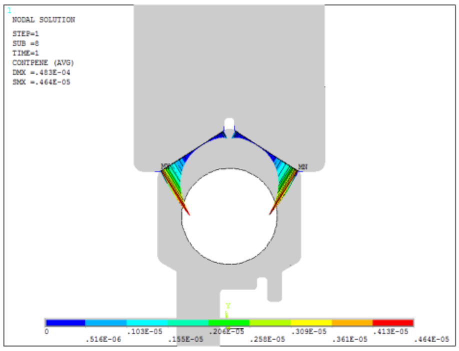

For $\varnothing_0 = 60^{\circ}$ rail type section results

Vertical Diplacement

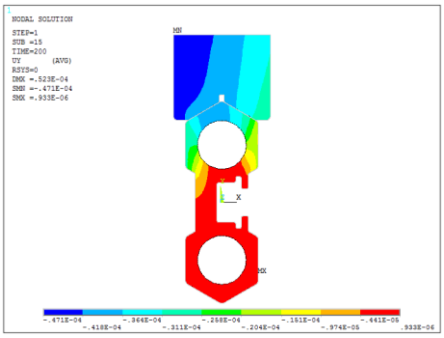

Total Displacement Sum

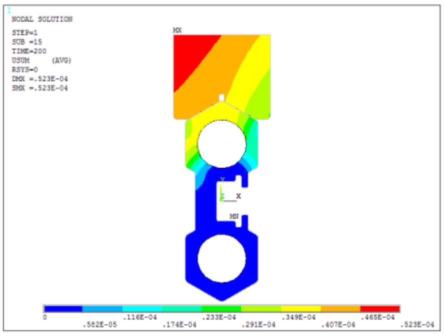

Von Mises Stress

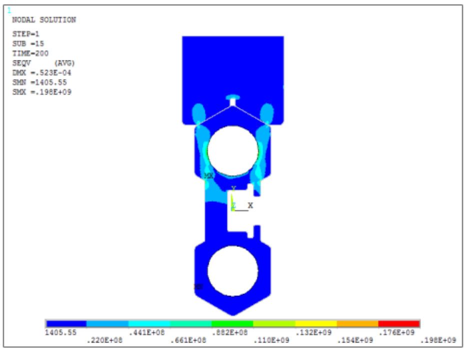

Contact Pressure

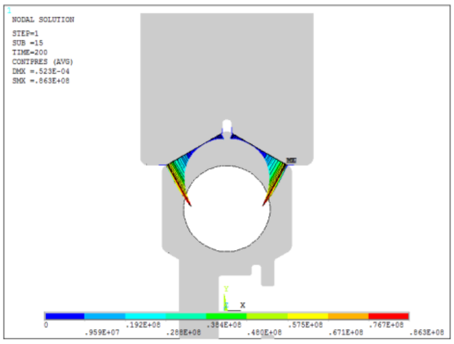

Contact Frictional Stress

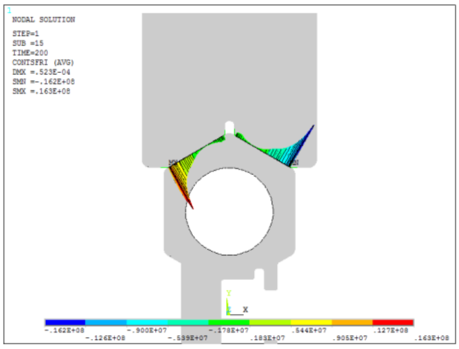

Contact Total Stress

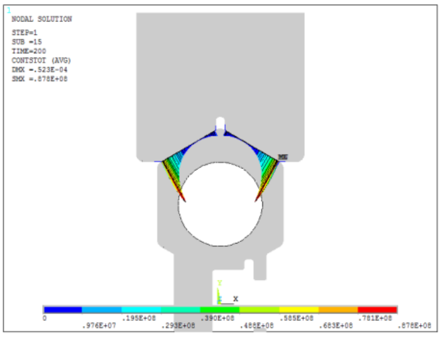

Contact Status

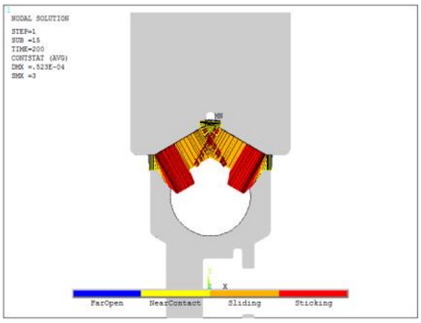

Contact Penetration

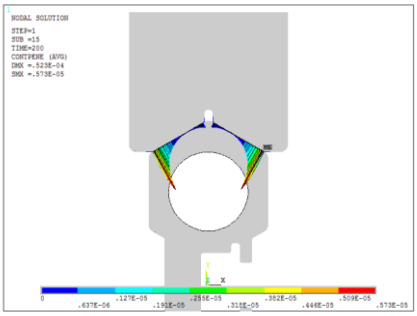

REFERENCES

[1] O.C. Zienkiewicz & R.L. Taylor, Finite Element Method, McGraw-Hill, 2000.

[2] Tirupathi R. Chandrupatla & Ashok D. Belegundu, Introduction to Finite Elements in Enginnering.

[3] Saaed Moaveni, Finite Element Analysis With Theory and Applications.

[4] Joseph E. Flaherty, Finite Element Analysis-Lecture Notes.

[5] Robert D. Cook, Finite Element Modelling for Stress Analysis, Wiley, 1995.

[6] G.R.LIU & S.S.QUEK, Finite Element Method,2003.

[7] Y. Nakasone & S. Yoshimoto - T. A. Stolarski, Enginnering Analysis with Ansys Software, Elsevier, 2006.

[8] Yves R. Talpert, Tensor Analysis and Continuum Mechanics, Kluwer, 2002.

[9] G. Thomas Mase & George E. Mase, Continuum Mechanics for Engineers, CRC, 1999.

[10] Mikhail Itskov, Tensor Algebra and Tensor Analysis for Enginners, Springer

[11] R.L.Norton, Machine Design, Pearson, 2006.

[12] R.L.Norton, Kinematics and Dynamics of Machinery, McGraw-Hill, 2013.

[13] Michael D. Greenberg,Advanced Enginnering Mathematics, 2012.

[14] Erwin Kreyszig, Advanced Enginnering Mathematics, McGraw-Hill, 2013.

[15] Richard G. Budynas & J. Keith Nisbett, Advanced Strength and Applied Stress Analysis, McGraw-Hill, 2006.

[16] Richard G. Budynas & J. Keith Nisbett ,Shigley’s Mechanical Engineering Design, McGraw-Hill, 2013.

[17] J.R. Barber, Elasticity, Springer,2012.

[18] Marc Andre Mayers & Krishan Kumar Chawla, Mechanical Behaviour of Materials, Cambridge,2009.

[19] William F. Hosford, Mechanical Behaviour of Materials, Cambridge, 2005.

[20] Michael F. Asbhy Materials Selection in Mechanical Enginnering, Elsevier, 2005.

[21] Arthur P. Boresi & Richard J. Schmidt & Omar M. Sidebottom, Advanced Mechanic of Materials, Wiley, 2005.

[22] Brian Hahn & Daniel T. Valentine, Essential Matlab For Enginners and Scientists, Elsevier, 2007.

[23] Noracon Systems-Technical manual & Kaisab Company-Technical manual

[24] Borasjyre Bmu Systems-Technical manual&Tc-American-Technical manual.

[25] Monorails and Underhung Cranes Safety Standard for Cableways, Cranes, Derricks, Hoists, Hooks, Jacks, and Slings.

[26] Premature Crane Structure Failure & Finite Element Method Analysis and Rectification, Portek Gorbel, Ceiling Mounted Brdige Cranes & Monorails.

[27] Crane Supporting Steel Structures, Design Guide, & R.A. Maccrimmon Hitachi Hoists Manual.

[28] Cranes and Derricks, Lawrence K. Shapiro - Jay P. Shapiroh.

[29] Introduction to Work Station Cranes, Gorbel.

[30] Modification and Relocation of Container Handling Cranes, Portek.

[31] Standardization of Jib Crane Design by “F.E.M. Rules” And Parametric Modeling Sandip D. Shinde PG Student Department of Production Engineering, S.G.G.S.I.E. &T. Nanded- 431 606, Maharashtra, India.

[32] Solid Modeling and Finite Element Analysis of an Overhead Crane Bridge C. Alkin, C. E. Imrak, H. Kocabas Czech Technical University in Prague Acta Polytechnica Vol. 45 No. 3/2005.

[33] Ansys-Based Accident Reconstruction on an Overhead Traveling Crane JIN Guang-zhen OUYANG Yun-hua Wuhan University of Science and Technology, Wuhan, Hubei, 430081, China.

[34] Design Evaluation of the 375 T Electric Overhead Traveling Crane Dilip K Mahanty, Satish Iyer, Vikas Manohar Tata Consultancy Services, India Dinesh Chaterjee WMI CRANES LTD., India.

[35] Crane and bunk technology report - Development of forwarder crane and bunk modules Almir Alagic Marie Allvar Kim Bladh Markus Langenoja.

[36] Specifications for Patented Track Underhung Cranes and Monorail Systems Monorail Manufacturers Association, Inc. (MMA) An Affiliated Trade Association of Material Handling Industry of America, A Division of Material Handling Industry.

[37] The Crane Manufacturers Association of America, Operational Gide for Lifting Devices.

[38] Specifications for Enclosed Track Underhung Cranes and Monorail Systems, 2003 Monorail Manufacturers Association, Inc.

[39] Design of Monorail Systems Tomas H Orihuela Jr, PE.

CURRICULUM VITAE

Credentials

Name, Surname : GÜRBÜZ YILMAZ

Place of Birth : Gönen / BALIKESIR

Marital Status : Single

E-mail : yilmaz.gurbuz88@hotmail.com

Adress: Karsıyaka Mah. 29. Sok. No:8 Gönen / BALIKESIR

Education

B.Sc. : Gazi University - 2010

B.Sc. : Kirikkale University – 2013

M:Sc.: Hacettepe University - 2014

Foreign Languages

English - German

Work Experience

Summer Practice; Küçük Pazarli Aviation Ltd. Şti (2008)

Summer Practice; Umut Medikal Ltd. Şti (2012)

Areas of Experiences

Solid Mechanics,Optimum Structural Design,Micro and Nanomanufacturing, Machine Tools and Machine Tool Design, Fatigue, Finite Element Method, Tribology, Manufacturing Processes

Projects and Budgets

This thesis has been prepared in cooperation University and Industry, 1505, with the support of TUBITAK.

Publications

Oral and Poster Presentations